UNIVERSITI TEKNOLOGI MARA

INTEGRATION OF LAND AND MARINE VERTICAL DATUMS FOR A UNIFIED HEIGHT REFERENCE SYSTEM IN PENINSULAR MALAYSIA

AFREENA NISHA BINTI MOHD ZAMRI

MSc

August 2026

UNIVERSITI TEKNOLOGI MARA

INTEGRATION OF LAND AND MARINE VERTICAL DATUMS FOR A UNIFIED HEIGHT REFERENCE SYSTEM IN PENINSULAR MALAYSIA

AFREENA NISHA BINTI MOHD ZAMRI

Thesis submitted in fulfilment
of the requirements for the degree of
Master of Science
(Built Environment)

Faculty of Built Environment

August 2026

CONFIRMATION BY PANEL OF EXAMINERS

I certify that a Panel of Examiners has met on 18 May 2026 to conduct the final examination of Afreena Nisha Binti Mohd Zamri on her Masters of Science thesis entitled "Integration of Land and Marine Vertical Datums for a Unified Height Reference System in Peninsular Malaysia" in accordance with Universiti Teknologi MARA Act 1976 (Akta 173). The Panel of Examiners recommends that the student be awarded the relevant degree. The Panel of Examiners was as follows:

Faridah Muhamad Halil, PhD
Associate Professor
Faculty of Built Environment
Universiti Teknologi MARA
(Chairperson)

Amir Sharifuddin Ab Latip, PhD
Senior Lecturer
Faculty of Built Environment
Universiti Teknologi MARA
(Internal Examiner)

Brian Bramanto, PhD
Assistant Professor
Faculty of Earth Science and Technology
Institut Teknologi Bandung, Indonesia
(External Examiner)

PROF. DR. HJH ZURAEDA BINTI IBRAHIM
Dean
Institute of Postgraduates Studies
Universiti Teknologi MARA

Date: 15 August 2026

AUTHOR'S DECLARATION

I declare that the work in this thesis was carried out in accordance with the regulations of Universiti Teknologi MARA. It is original and is the results of my own work, unless otherwise indicated or acknowledged as referenced work. This thesis has not been submitted to any other academic institution or non-academic institution for any degree or qualification.

I, hereby, acknowledge that I have been supplied with the Academic Rules and Regulations for Postgraduate, Universiti Teknologi MARA, regulating the conduct of my study and research.

Name of Student	:	Afreena Nisha Binti Mohd Zamri
Student ID. No.	:	2023402958
Programme	:	Master of Science (Built Environment) – CFAP781
Faculty	:	Built Environment
Thesis Title	:	Integration of Land and Marine Vertical Datums for a Unified Height Reference System in Peninsular Malaysia
Signature of Student	:	
Date	:	August 2026

ABSTRACT

The needs of unified vertical datum has become popular topic among geospatial and maritime authorities across the world in managing the marine spaces datasets in a more structured and sustainable manner. A fundamental challenge lies in the coexistence of disparate vertical reference systems used on land and at sea which often leads to inconsistencies and confusion especially in cases of development on land connecting to maritime areas. This highlights the need for a reliable vertical transformation model that can link the two systems under one reference. Therefore, this study is centred on the development of a vertical transformation model that provides continuity between land and marine vertical datums in Peninsular Malaysia. The geoid surface was chosen as the reference for this transformation because it is physically meaningful and globally continuous. Additionally, the Least Squares Modification of Stokes' Formula with Additive Corrections (LSMSA) offers an alternative approach to geoid modelling. It often provides higher accuracy and uses a simpler derivation process compared to other methods. Given the proprietary nature and high cost of existing national geoid models which did not employ LSMSA, this research explores the potential of the method for developing a cost-effective and high-resolution marine geoid model. In parallel, the tidal datum models specifically the Lowest Astronomical Tide (LAT) and Highest Astronomical Tide (HAT) were derived by the assimilation of multi-mission satellite altimetry with hydrodynamic modelling. This approach extended tidal data coverage up to 20 kilometres from the shoreline, where satellite altimetry is often affected by signal noise and biases. The tidal datum models were validated using tide gauge records derived from tidal harmonics processed through the UTide processing. The final computed hybrid geoid manage to achieve 4.5 cm accuracy when compared to local GNSS levelling data. This reflects a high level of accuracy comparable to the existing MyGeoid model. The vertical datum offset models were also validated against tidal datums at 9 tide gauge stations which revealed the RMSE ranging from approximately 21 cm to 51 cm. In conclusion, despite the inherent limitations which most notably the lack of GNSS observation and tidal data in open sea, the study successfully demonstrates the feasibility and advantages of employing LSMSA for marine geoid modelling and presents a foundational outline for vertical datum unification. The findings offer critical insights into the spatial variability of datum separation and provide the basis for future enhancements in vertical transformation modelling across the coastal zones of Peninsular Malaysia.

ACKNOWLEDGEMENT

Throughout this journey, I have been fortunate to meet and work with many people who have not only contributed to my academic knowledge but have also inspired, encouraged, and supported me in ways that shaped both my personal and professional growth. It is with great pleasure that I take this opportunity to express my sincere gratitude to all of them.

First and foremost, I wish to convey my deepest appreciation to my main supervisor, Dr. Muhammad Faiz Pa'suya for his invaluable guidance, encouragement, and constant support throughout this study. His patience, insightful comments, and constructive advice have been crucial in keeping me motivated and on track, ensuring that I remained dedicated to achieving the objectives of this research. I am equally indebted to my co-supervisor, Associate Professor Dr. Ami Hassan Md Din, for his generous guidance, valuable suggestions, and continuous support which have been instrumental in refining my ideas and strengthening the quality of this thesis.

I would also like to express my gratitude to Universiti Teknologi MARA (UiTM) for providing good facilities that made the completion of this research possible. Special thanks are also extended to the Department of Survey and Mapping Malaysia (DSMM) for their kind assistance in providing the gravity and GNSS levelling data, which formed a fundamental part of this study. Their contributions have been essential to the successful completion of my work.

In addition, I am thankful to the research team from Universiti Teknologi Malaysia (UTM) for their collaboration, generosity, and encouragement. The exchange of knowledge, constructive discussions, and sharing of perspectives with them have broadened my understanding and enriched the depth of this research.

A heartfelt appreciation also goes to my fellow postgraduate lab colleagues, who have been a constant source of support throughout this academic journey. Their companionship, constructive discussions, exchange of ideas, and encouragement provided not only academic stimulation but also emotional strength. The sense of companionship and teamwork within the lab environment has made this demanding journey much more manageable and fulfilling.

Finally, and most importantly, I wish to express my endless love and gratitude to my family. Their unwavering support, patience, and encouragement have been the strongest source of my motivation. Their sacrifices, prayers, and unconditional love have inspired me to persevere and complete this thesis.. To all who have played a part, directly or indirectly, in the success of this study, I extend my sincere thanks and heartfelt appreciation.

TABLE OF CONTENTS

		Page
CONFIRMATION BY PANEL OF EXAMINERS		**ii**
AUTHOR'S DECLARATION		**iii**
ACKNOWLEDGEMENT		**iv**
ABSTRACT		**iv**
TABLE OF CONTENTS		**vi**
LIST OF TABLES		**xii**
LIST OF FIGURES		**xvi**
LIST OF SYMBOLS		**xx**
LIST OF ABBREVIATIONS		**xxiii**
LIST OF NOMENCLATURE		**xxvii**
CHAPTER 1 INTRODUCTION		**1**
1.1	Research Background	1
1.2	Problem Statement	5
1.3	Research Questions	7
1.4	Research Aim and Objectives	7
1.5	Research Scope	8
	1.5.1 Study Area	8
	1.5.2 Dataset	9
	1.5.3 Data Interpretation and Analysis	15
	1.5.4 Limitation	16
1.6	Research Significance	16
1.7	Research Outline	18

CHAPTER 2 LITERATURE REVIEW **20**
2.1 Introduction 20
2.2 Components of Height 20
2.2.1 Orthometric / Normal Height 20
2.2.2 Ellipsoid 21
2.2.3 Geoid 22
2.3 Vertical Datum 23
2.3.1 Geodetic Vertical Datum 24
2.3.2 Reference Ellipsoid 26
2.3.3 Tidal Datum 27
2.3.4 Lowest and Highest Astronomical Tide 29
2.3.5 Geoid Model 30
2.3.5.1 WHU-SWPU-GOGR2022S 30
2.3.5.2 GOSG02S 30
2.3.5.3 XGM2019e 31
2.3.5.4 PMGG2020 31
2.3.6 Mean Dynamic Topography 34
2.3.6.1 DTU22MDT 35
2.3.6.2 DTUUH22MDT 36
2.3.6.3 MDOT 37
2.3.7 Mean Sea Surface 38
2.3.7.1 SDUST2020 39
2.3.7.2 DTU21 40
2.3.7.3 CNES-CLS22 41
2.4 Marine Gravity Data 42
2.4.1 DTU21GRA 42
2.4.2 Sandwell and Smith Model 43
2.4.3 SDUST2022GRA 44
2.4.4 NSOAS24 45
2.5 Tidal 47
2.5.1 Tidal Constituent 47
2.5.2 Tidal Prediction 48

2.5.3 Harmonic Analysis 50
2.6 Gravimetric Geoid Computation Method 51
2.7 Satellite Altimetry Techniques 54
2.7.1 Concepts of Satellite Altimetry Measurements 55
2.7.2 Corrections to Satellite Radar Measurements 57
2.8 Development of Vertical Transformation Model 59
2.8.1 Conceptual Relationship Between MSS and MSL 59
2.8.2 Global Realization of Unified Vertical Datum Systems 60
2.8.2.1 National Oceanic and Atmosphere Administration Vertical Datum (NOAA VDatum) 61
2.8.2.2 Vertical Offshore Reference Frame (VORF) 62
2.8.2.3 Continuous Vertical Datum for Canadian Waters (CVDCW) 64
2.8.2.4 Australian's AUSHYDROID 65
2.9 Chapter Summary 68

CHAPTER 3 RESEARCH METHODOLOGY 69
3.1 Introduction 69
3.2 Phase 1 : Data Acquisition 71
3.2.1 Gravity Data 71
3.2.1.1 Terrestrial Gravity 71
3.2.1.2 Airborne Gravity 72
3.2.1.3 Satellite – Derived Marine Gravity 74
3.2.2 Global Digital Elevation Model (GDEM) 75
3.2.3 Global Geopotential Model (GGM) 77
3.2.4 GNSS Levelling Data 78
3.2.4.1 GNSS Data at Tide Gauge Benchmark (TGBM) 79
3.2.5 Tide Gauges Records 79
3.2.6 Satellite Altimetry Data 81
3.2.7 Global Tide Model 82
3.2.8 Mean Sea Surface (MSS) Model 83
3.2.9 Mean Dynamic Topography (MDT) Model 83

3.2.10 Geoid Model 84
3.3 Phase 2 : Development of Geoid Model 85
3.3.1 Pre – Processing and Assessment of Dataset Input 85
3.3.1.1 Terrestrial Gravity Data Filtering 85
3.3.1.2 Accuracy Assessment of Input Dataset 90
3.3.2 Combine and Gridding Free Air Anomalies Data 92
3.3.3 Computation of Gravimetric Geoid Model 95
3.3.3.1 Determination of Optimum Least Square Parameters 95
3.3.3.2 Approximate Geoid 96
3.3.3.3 Additive Correction 97
3.3.3.4 Evaluation of Final Gravimetric Geoid 100
3.3.4 Development and Evaluation of Hybrid Geoid 100
3.3.4.1 Analysis of Prediction Variable 102
3.3.4.2 Evaluation of Computed Hybrid Geoid Model 102
3.4 Phase 3: Development of Marine Vertical Model 103
3.4.1 Tide Gauge Processing 103
3.4.2 Satellite Altimetry Processing 106
3.4.2.1 Formatting Mission 108
3.4.2.2 Merging Mission Class and Formation Time Series 108
3.4.2.3 Extraction Cycle 109
3.4.2.4 Moving Threshold 110
3.4.2.5 Tidal Analysis and Prediction 110
3.4.2.6 Merging Pass 111
3.4.2.7 Crossover Offset 112
3.4.3 Hydrodynamic Ocean Modelling 112
3.4.3.1 Spatial Buffer Region 112
3.4.3.2 Extraction of Tidal Data using Tide Model Driver (TMD) 113
3.4.3.3 Selection of Global Mean Sea Surface (MSS) Models 115
3.4.4 Combination and Integration of Tidal Datums 118
3.4.5 Validation of Vertical Separation Models 119
3.5 Phase 4 : Development of Vertical Transformation Model 120
3.6 Phase 5 : Conclusion and Recommendation 121

3.7 Chapter Summary 122

CHAPTER 4 RESULT AND DISCUSSION 123

4.1 Introduction 123

4.2 Computation of Geoid Model 123

4.2.1 Assessment of the Impact of Global Geopotential Models on the Geoid Model 123

4.2.2 Determination of the Optimum Least Squares Modification Parameters 127

4.2.3 Impact Assessment of Marine Gravity Data on Geoid Determination 131

4.2.4 Development of Hybrid Geoid 133

4.2.5 Final Model of Hybrid Geoid 134

4.3 Marine Vertical Separation Model 138

4.3.1 Tide Gauge Processing 138

4.3.2 Development of LAT, HAT and MSS From Altimetric Dataset 140

4.3.3 Hydrodynamic Model 143

4.3.3.1 Derivation of Tidal Data from Tide Model Driver (TMD) 143

4.3.3.2 Evaluation of Global Mean Sea Surface (MSS) Models 145

4.3.4 Modelled Tidal Datum 150

4.3.4.1 Combine and Gridded Tidal Models 150

4.4 Vertical Transformation Offset 155

4.4.1 Computation of Vertical Datum Offset 156

4.4.2 Evaluation of Vertical Datum Offset 159

4.4.3 Discussion on the Outcomes of Computed Vertical Transformation Model 167

4.5 Research Summary 168

CHAPTER 5 CONCLUSION AND RECOMMENDATION 172

5.1 Introduction 172

5.2 Research Conclusion 172

5.3 Limitation 175

5.3.1 Temporal Mismatch Between Datasets 175

5.3.2 Limitations of validation data availability and distribution 176
5.3.3 Lack of offshore validation capability 176
5.4 Recommendations for Future Research 177
REFERENCES **181**
APPENDICES **202**
AUTHOR'S PROFILE **205**

LIST OF TABLES

Tables	Title	Page
Table 1. 1	List of Gravity Anomalies Data	9
Table 1. 2	List of Global Geopotential Models	10
Table 1. 3	List of Satellite Altimeter Data	12
Table 1. 4	List of Global Mean Sea Surface Model	12
Table 1. 5	Summary of Global Mean Dynamic Topography Model	13
Table 1. 6	The List of Global Geoid Models	14
Table 1. 7	List of Tide Gauge Stations	15
Table 2. 1	Summary of Ellipsod Reference Models	27
Table 2. 2	Types of Common Tidal Datums and its Definitions (National Oceanic and Atmospheric Administration, 2000b)	28
Table 2. 3	Literature Summary of Geoid Models	33
Table 2. 4	Literature Summary of Satellite-Derived Marine Gravity Model	46
Table 2. 5	Selected Semi-Diurnal Harmonic Constituents (IHO, 2006)	47
Table 2. 6	Selected Diurnal Harmonic Constituents (International Hydrographic Organization (IHO), 2006)	48
Table 2. 7	Selected Long-Term Harmonic Constituents (International Hydrographic Organization (IHO), 2006)	48
Table 2. 8	Comparison of Accuracies between KTH and RCR Method in Geoid Computation	54
Table 2. 9	Summary of Media Corrections in Satellite Altimeter Radar	57
Table 2. 10	Summary of Geophysical Corrections in Satellite Altimeter Radar	58
Table 2. 11	Summary of Previous Studies in Development of Vertical Transformation Model	67
Table 3. 1	Properties of Terrestrial Gravity Data	72
Table 3. 2	The Summary of Satellite-Derived Marine Gravity Data	74
Table 3. 3	Properties of SRTM Model	76

Table 3. 4	Selected GGMs for Assessment of Input Dataset	77
Table 3. 5	The Summary of GNSS Levelling Data for Gravimetric Geoid Validation	78
Table 3. 6	Information of Tide Gauge Stations Obtained from DSMM	80
Table 3. 7	Properties of Selected Multi-Mission Satellites Data	81
Table 3. 8	The Summary of Global Mean Sea Surface Models	83
Table 3. 9	The Summary of Global Mean Dynamic Topography Models	84
Table 3. 10	The Summary of Global Geoid Models	84
Table 3. 11	The Summary of Tested Least Square Parameters	96
Table 3. 12	Input Format for UTide	104
Table 3. 13	The Summary of Direct MSS, Geoid and MDT Models used.	116
Table 3. 14	The Properties of Ellipsoids [Unit: Meter] (Keysers et al., 2013)	117
Table 4. 1	Statistical Analysis of Geoid Computed Using Different Geopotential Models [Unit : Metre]	125
Table 4. 2	Descriptive Statistics Between WHU-SWPU-GOGR2022S and GOSG2S [Unit: Metre]	126
Table 4. 3	Summary of Paired T-Test Results Between WHU-SWPU-GOGR2022S and GOSG2S	126
Table 4. 4	The RMSE Between 45 GNSS Derived Geometrical Geoid and Gravimetric Geoid for WHU-SWPU-GOGR2022S Using Parameter Combination of Correlation Length and Standard Deviation [Unit: Meters]	128
Table 4. 5	The RMSE Between GNSS Derived Geometrical Geoid and Gravimetric Geoid for GOSG02S Using Parameter Combination of Correlation Length and Standard Deviation [Unit: Meters]	128
Table 4. 6	The RMSE of Tested Maximum Degree (L = M) for WHU-SWPU-GOGR2022S and GOSG02S [Unit: Meters]	130
Table 4. 7	The RMSE of Gravimetric Geoids Computed Using Different Marine Gravity Model Against Varies GNSS Levelling Dataset [Unit: Meters]	132

Table 4. 8	The Statistical Properties of Final Gravimetric Geoid Model [Unit: Meters]	132
Table 4. 9	The RMSE of the Prediction Variables [Unit: Meters]	134
Table 4. 10	The Statistical Properties of Final Hybrid Geoid Model [Unit: Meters]	137
Table 4. 11	Tidal Datum for Tide Gauges Stations Using Utide	139
Table 4. 12	Statistical Analysis of Correlations Between Satellite Altimetry Mission During Crossover Adjustment [Unit: Meters]	141
Table 4. 13	The Statistical Analysis of Tidal Datum Derived From Altimetric Satellite [Unit: Meters]	142
Table 4. 14	The Statistical Analysis of Tidal Data Derived From TMD [Unit: Meter]	144
Table 4. 15	The Summary of Assessed Global MSS Models Against Local Tide Gauge Stations	147
Table 4. 16	Comparison of RMSE Values Between Hydrodynamic Only Dataset And Hydrodynamic + Satellite Altimetry Data For Tidal Datums	152
Table 4. 17	The Statistical Summary of Computed LAT and HAT Models	154
Table 4. 18	The Spatial Information of Computed Vertical Datum Offset	157
Table 4. 19	The Validation Result Between Hybrid Geoid – HAT Model Using 11 Tide Gauge Stations	160
Table 4. 20	The Validation Result Between Hybrid Geoid – LAT Model Using 11 Tide Gauge Stations	161
Table 4. 21	The Validation Result Between HAT – LAT Model Using 11 Tide Gauge Stations	161
Table 4. 22	The Validation Result Between Hybrid Geoid – HAT Model After Exclusion of Kukup and Klang Tide Gauge Stations	164
Table 4. 23	The Validation Result Between Hybrid Geoid – LAT Model After Exclusion of Kukup and Klang Tide Gauge Stations	164
Table 4. 24	The Validation Result Between HAT – LAT Model After Exclusion of Kukup and Klang Tide Gauge Stations	165

Table 4. 25 The RMSE of VDO Before and After Tide Gauge Adjustments 166

LIST OF FIGURES

Figures	Title	Page
Figure 1. 1	Relationship of Orthometric, Ellipsoidal and Geoid Heights	4
Figure 1. 2	Study Area	8
Figure 1. 3	Distribution of GNSS Levelling	11
Figure 1. 4	Distribution of Tide Gauge Stations	14
Figure 2. 1	Ellipsod Surface (Huismain & de By, 2009)	22
Figure 2. 2	The Geoid (Huismain & de By, 2009)	23
Figure 2. 3	PMGVD monument at Port Klang (Jamil, 2011)	24
Figure 2.4	Malaysia's Geoid Model Which Divided Into Two Region a) WMGEOID04 (Peninsular Malaysia) and (b) EMGEOID05 (Sabah and Sarawak)	25
Figure 2. 5	Relationship of Coastal Height Components (Sarsito et al., 2021)	34
Figure 2. 6	The DTU22 Global MDT Model (Knudsen et al., 2022)	36
Figure 2. 7	The 1992 – 2002 MDOT Model (Maximenko et al., 2009)	37
Figure 2. 8	The SDUST2020 Global MSS Model (Yuan et al., 2023)	39
Figure 2. 9	The Developed DTU21 Global MSS Model (O. B. Andersen et al., 2023)	40
Figure 2. 10	The CNES-CLS22 Global MSS Model (Schaeffer et al., 2023)	41
Figure 2. 11	Harmonic constituents in tidal prediction (National Oceanic and Atmospheric Administration, 2000a)	49
Figure 2. 13	Concept of Satellite Altimeter Measurements (Grgić & Bašić, 2021)	56
Figure 2. 14	The Relationship Between MSL and MSS Reference Surface (O. B. Andersen et al., 2018)	60
Figure 2. 15	VDatum Transformation Parameters (FIG, 2006)	62
Figure 2. 16	The Concept of VROF (Jones, 2007)	63
Figure 2. 17	The Methodology Employed in CVDCW (Nudds et al., 2016)	65

Figure 2. 18	The Concept of AUSHYDROID Heights System (Filmer et al., 2024)	66
Figure 3. 1	General Research Methodology	70
Figure 3. 2	Distribution for Terrestrial Gravity Anomalies Data	73
Figure 3. 3	Distribution of Airborne Gravity Anomalies Data	73
Figure 3. 4	Free Air Anomalies Distribution for Marine Gravity Data	75
Figure 3. 5	Global Digital Elevation Model – SRTM	76
Figure 3. 6	Distribution of GNSS Levelling Used in This Study	78
Figure 3. 7	Tide Gauges Stations in Peninsular Malaysia	80
Figure 3. 8	Combination of All Satellite Missions Employed in This Study	82
Figure 3. 9	Terrestrial Gravity Data Filtering	90
Figure 3. 10	Procedure To Compute Residual Bougeur Anomalies (Adopted from Pa'suya (2020))	93
Figure 3. 11	Combine and Gridding Using 3DLSC (Adopted from Pa'suya (2020))	94
Figure 3. 12	Overview of Geoid Modelling Using LSMSA – KTH Method	95
Figure 3. 13	The (a) Additive correction, (b) Approximate geoid, and (c) Gravimetric geoid	100
Figure 3. 14	GNSS Levelling Data for Hybrid Geoid Fitting and Validation	101
Figure 3. 15	Tidal Analysis and Tide Prediction at Tanjung Keling Using 18 Observation Period (1998 – 2015)	104
Figure 3. 16	Relationship Between the Various Surface for Computation of Offset in the Tide Reduction Determination	105
Figure 3. 17	Tidal Modelling using Satellite Altimetry Techniques	107
Figure 3. 18	Truncation of Overlapping Time Series in Merged Data (Hamden, 2022).	109
Figure 3. 19	Diagram of (a) Spatial Buffering (Red Line) Extended 20 Kilometres From Shoreline and (B) Hydrodynamic Data Points Within Buffer Region.	113
Figure 3. 20	TMD Interface (Padman et al., 2015)	114
Figure 3. 21	Sample of TMD Output	115

Figure 3. 22	Integration of Tidal Datum from (A) Hydrodynamic Data, (B) Gridded Altimetric Data and (C) Combination of Both Data	119
Figure 3. 23	Relationship Between Each Vertical Datum Offset (VDO)	120
Figure 3. 24	Illustration of Vertical Transformation Model	121
Figure 4. 1	Residual of Gravimetric Geoid Computed Using Different Geopotential Model Compared with 45 GNSS Levelling Data	124
Figure 4. 2	Difference of Geoid Height Between WHU-SWPU-GOGR2022S and GOSG2S Models	125
Figure 4. 3	The RMSE of Tested Maximum Degree in Least Square Parameters Setting for WHU-SWPU-GOGR2022S and GOSG02S Models	130
Figure 4. 4	Final gravimetric geoid model	132
Figure 4. 5	Comparative Residual Between Computed Hybrid Geoid and Wgeoid04	135
Figure 4. 6	The Spatial Distribution of Residuals Computed Hybrid Geoid and Wgeoid04 Compared to the Geometrical Geoid	136
Figure 4. 7	Final Hybrid Geoid Model	137
Figure 4. 8	Along-Track Tidal Datums Derived From Altimetric Satellite Encompassed (A) LAT, (B) MSL And (C) HAT	142
Figure 4. 9	The Sample of TMD Output	144
Figure 4. 10	Tidal Data Derived From TMD Encompassed LAT and HAT.	145
Figure 4. 11	The Comparative Assessment of Global MSS Models Against Tide Gauges Data	148
Figure 4. 12	The Comparative Assessment of Geoid Heights and MSL at Tide Gauge Stations	149
Figure 4. 13	Distribution of Tidal Data From Hydrodynamic (Yellow) and Satellite Altimetric (Blue) Data	151
Figure 4. 14	The Gridded Tidal Data From Combined Hydrodynamic and Satellite Altimetric Data	151
Figure 4. 15	The Residuals of Hydrodynamic Only and Hydrodynamic + Satellite Altimetry Data When Compared With Tide Gauges References for (A) MSL. (B) LAT and (C) HAT Tidal Models	153

Figure 4. 16	The Computed LAT Tidal Model	154
Figure 4. 17	The Computed HAT Tidal Model	155
Figure 4. 18	The VDO Model of Hybrid Geoid – HAT	157
Figure 4. 19	The VDO Model Hybrid Geoid – LAT	158
Figure 4. 20	The VDO Model of HAT – LAT	158
Figure 4. 21	The Trends of Spatial Residuals Before Tide Gauge Exclusion	162
Figure 4. 22	The Location of Tide Gauge Station at Kukup	162
Figure 4. 23	The Location of Tide Gauge Station at Klang	163
Figure 4. 24	The Trends of Spatial Residuals Before Tide Gauge Exclusion	166

LIST OF SYMBOLS

Symbols

A_i	Amplitude
w_i	Angular Frequency
ζ_P^0	Approximate Height Anomaly at Point P Computed From GGM
P	Computation Point
ρ	Crust Density Of Earth
ρ_A	Density At Sea Level
Δ	Difference
h	Ellipsoidal Height
ΔN	Geoid Height Residual
N	Geoid Separation
G	Gravitation Constant
Δg_n^{EGM}	Laplace Harmonics of Degree n Calculated from the GGM
H_n	Laplace Surface Harmonic of Degree N for the Topographic Height
Q_1	Larger Lunar Elliptic
N_2	Larger Lunar Elliptic
$\emptyset$	Latitudes
λ	Longitude

h_2	Love Number
M_f	Lunar Fortnightly
M_m	Lunar Monthly
K_2	Luni-Solar
K_1	Luni-Lunar
μ	Mean
R	Mean Earth Radius
γ	Mean Normal Gravity on the Reference Ellipsoid
ψ	Modified Strokes' Formula
Q	Moving Integration Point
N	Number of Tidal Constituents
H_p	Orthometric Height Of Point P
$\emptyset_i$	Phase of Tidal Constituents
M_2	Principal Lunar
O_1	Principle Lunar
S_2	Principal Solar
P_1	Principal Solar
J	Range
i	Row Index
a	Semi-Major Axis
S_{sa}	Solar Semi-Annual

S_a	Solar Annual
σ	Standard Deviation
Δg	Terrestrial Gravity Anomaly
t	Time
b_n	Vector of the Least Square Parameter for the Optimum Solution
δV_0^a	Zero Degree at Atmospheric Potential

LIST OF ABBREVIATIONS

Abbreviations

3DLSC	3D Least Square Collocation
BM	Benchmark
CD	Chart Datum
CVDCW	Continuous Vertical Datum for Canadian Waters
DTU	Denmark Technical University
DSMM	Department of Survey and Mapping Malaysia
DTM	Digital Terrain Model
DWC	Downward Continuation
ERS	European Remote Sensing Satellite
ESR	Earth and Space Research
FA	Free Air Anomaly
FF	Form Factor
GFO	GEOSAT Follow On
GRS80	Geodetic Reference System 1980
GDEM	Global Digital Elevation Model
GGM	Global Geopotential Model
GNSS	Global Navigation Satellite System (GNSS)
GPS	Global Positioning System

HAT	Highest Astronomical Tide (HAT)
ICFEM	International Centre of Global Gravity Field Model
FIG	International Federation of Surveyors
IHO	International Hydrographic Organization
IPCC	Intergovernmental Panel on Climate Change
KMS	Kort & Matrikelstyrensen
KTH	Kungliga Tekniska högskolan
LSMSA	Least Square Modification of Strokes formula with Additive Correction
LCL	Lower Control Limit
LAT	Lowest Astronomical Tide
MAGIC	Marine Geodetic Infrastructure in Malaysia Water
MGVD	Marine Geodetic Vertical Datum
MDT	Mean Dynamic Topography
MHW	Mean High Water
MHWN	Mean High Water Neap
MHWS	Mean High Water Spring
MLW	Mean Low Water
MLWN	Mean Low Water Neap
MLWS	Mean Low Water Spring
MSL	Mean Sea Level

MSS	Mean Sea Surface
NaN	Not a Number
NGVD	National Geodetic Vertical Datum
NOAA	National Oceanic and Atmosphere Administration
OSU	Oregon State University
OTIS	OSU Tidal Inversion Software
PMGVD	Peninsular Malaysia Geodetic Vertical Datum
RADS	Radar Altimeter Database System
RMSE	Root Mean Square Error
KTH	Royal Institutes of Technology
SBA	Simple Bouguer Anomaly
SBM	Standard Benchmark
SLA	Sea Level Anomaly
SRTM	Shuttle Radar Topography Mission
SSH	Sea Surface Height
STD	Standard Deviation
TGBM	Tide Gauge Benchmark
TMD	Tide Model Driver
UHSLC	University of Hawaii Sea Level Center
UTM	Universiti Teknologi Malaysia
UiTM	Universiti Teknologi MARA

UTide	Unified Tidal Analysis and Prediction Functions
VROF	United Kingdom Vertical Offshore Reference Frame
UCL	Upper Control Limit
VDO	Vertical Datum Offset
ZTG	Zero Tide Gauge

LIST OF NOMENCLATURE

Nomenclature

≈	Approximately Equal To
cm	Centimetre
˚	Degree
÷	Division
m	Metre
-	Minus
°	Minute
mGal	Milligal
mm	Millimetre
×	Multiplication
%	Percent
+	Plus
±	Plus or Minus
“	Second
km^2	Square Kilometre
∑	Summation

CHAPTER 1
INTRODUCTION

1.1 Research Background

Since preceding years, maritime activities have emerged as significant contributors to the economic sectors of numerous countries. a multitude of marine activities has captured the attention of not only governmental bodies but also private enterprises, seeking to leverage the ocean's potential for the advancement of welfare, community development, and regional prosperity (Binns et al., 2004). Malaysia is particularly advantageous as a maritime powerhouse due to its continent surrounded by the sea and strategically situated along one of the world's busiest shipping routes. This country boasts extensive territorial waters spanning at 65,023.4 km^2 and a substantial exclusive economic zone extending over 450,233.0 km^2 (Till & Tsjeng, 2017). This lead to the increasing recognition in driving the economic development over this region by the invaluable natural resources from oil reservoirs and natural gas deposits to the lucrative marine properties such as tourism hotspot and petroleum platforms (Zamzuri et al., 2021). Geographically, Malaysia region comprising two regions, Peninsular Malaysia (West Malaysia) and the States of Sarawak and Sabah (East Malaysia). Undeniable, the development of coastal zone along the coasts and surrounding areas of Peninsular Malaysia areas has been extensive and has a special sosio-economic and environmental significant. In fact, this region supports a large percentage of the population and it is also the center of economic activities encompassing 22 urban settlements and 12,400 rural settlements, 28 industrial estates and 54 ports located in this region (Ehsan et al.,2018).

In recent years, there has been a growing awareness among Malaysia authorities to manage marine spaces datasets in a more structured and sustainable manner for the supporting the economic development, infrastructure protection as well as maritime and coastal safety. However, the real issue today is the heterogeneous dataset over this region is referenced to different land and sea vertical datums. The concern regarding the different datums between land and marine often causes confusion in determining the appropriate datum to be applied in cases of development on land connecting to

maritime areas, such as seaside resorts or underwater buildings. Fundamentally, the application of datum in land areas is less complex compared to coastal areas. Traditionally, the land vertical datum commonly based on national levelling network constrained to historical mean sea level at specific tide gauges. In Peninsular Malaysia, the national levelling network is referenced to the mean sea level recorded at the Port Klang tide gauge station, which is defined as 3.624 meters above the zero-tide gauge (Pa'suya, Md Din, Alpay Abbak, et al., 2019). Meanwhile, in the context of modern vertical datum, development of geoid model as vertical datum over the land region become the common approach today especially to support the Global Navigation Satellite System (GNSS) derived orthometric height.

In the marine environment, the situation is more complex, with a wider variety of vertical datums being used such as Mean Sea Level (MSL), Highest Astronomical Tide (HAT), Lowest Astronomical Tide (LAT), Mean High Water (MHW), Mean Low Water (MLW), etc. All the datums are important for different aspects or purpose of coastal and marine activities, ensuring safety, planning, and risk management based on the extreme tidal conditions. For example, the depths on maritime navigation charts are referenced to the chart datum (CD), determined by the tidal height at specific port tide gauges. However, the datum presents a more intricate scenario due to environmental phenomena such as landforms, fluctuating tides, and sea level rise, which vary from one location to another. Therefore, integration of land and marine vertical datum across the littoral zone is essential to meet today's industrial and scientific requirements. It will be benefit to coastal zone management, coastal ecosystem modelling, coastal construction, and development, studying the impacts of sea level rise, storm surge inundation modelling, etc. Furthermore, it also will be benefitted to transform the heterogeneous coastal datasets referenced to different datum to a common reference frame.

Several countries have acknowledged the needs of seamless unified vertical datum between land and marine seamless coastal vertical datum and it has been the subject of international research. Some of the countries has taken an endeavour in developing a unified datum system through the implementation of projects such as National Oceanic and Atmosphere Administration's (NOAA) VDatum (National Oceanic and Atmospheric Administration, 2004), United Kingdom Vertical Offshore Reference Frame (VORF) (Iliffe et al., 2007), Continuous Vertical Datum for Canadian

Waters (CVDCW) (Robin et al., 2014), and Australian's AUSHYDROID (Filmer et al., 2024). In current age, Malaysia has gradually realized the importance of a unified different vertical datum bridging both land and marine domains. Under the Marine Geodetic Infrastructure in Malaysia Water (MAGIC) which implemented since 2013 by DSMM, one of the objectives is to develop a Marine Geodetic Vertical Datum (MGVD) as a seamless vertical reference surface for the whole area of Malaysian waters. These efforts signify Malaysia's commitment to align with global trends in geospatial data integration, aiming to enhance coordination and compatibility of datum integration across both land and marine domains. Local researchers have exemplified this recognition through their involvement in projects like the development of Geoid-based seamless vertical height datum (Abdullah & Omar, 2011) and the implementation of the Quasi-Seamless Hydrographic Separation Model (Hamden, 2022). Despite these notable efforts, a critical limitation persists as the existing studies does not focused on the seamless connection between land and marine vertical datum. There is lack of comprehensive methodologies that explicitly address the integration of heterogeneous vertical reference surfaces, such as MSL, LAT and geoid models into a unified vertical transformation framework.

In order to realize the integration between the different vertical datum at marine and land, all the datum should be referenced to the identical reference and in a continuous form. Therefore, this research prompted to provide an intensive study to integrate the land and varies marine vertical datum (HAT and LAT) over Peninsular Malaysia coastal zone through ellipsoid-based approach. From this approach, all vertical datums are referenced to a common ellipsoidal surface, specifically the Geodetic Reference System 1980 (GRS80) ellipsoid. The selection of GRS80 as the reference ellipsoid is in line with recommendations by the International Federation of Surveyors (FIG, 2006), which advocates for a unified ellipsoidal base to support consistency in geospatial referencing.

This study establishes a continuous vertical separation model that integrates both geodetic and tidal reference surfaces over the coastal zone of Peninsular Malaysia including of hybrid geoid, LAT and HAT models. A new geoid model over Peninsular Malaysia at the land and marine area were reconstructed through rigorous evaluation of multiple influencing parameters. This process involved systematic testing using various

satellite-derived global marine gravity datasets, global geopotential models (GGM), and geoid computation variables to enhance the accuracy of the marine geoid component. The computed gravimetric geoid was subsequently fitted to ground control data to produce a hybrid geoid, ensuring continuity and compatibility with national height systems that has been tied to the PMGVD. In parallel, the LAT and HAT models over the marine region were developed through the assimilation of multi-mission satellite altimetric data and a hydrodynamic model. These models were constructed based on a long-term observational dataset to ensure the temporal reliability and tidal representativeness of the computed tidal datums. Prior to the construction of the vertical transformation model, the LAT and HAT models were validated against in-situ tide gauge observations. Subsequently, comprehensive vertical datum offsets for each model were computed to facilitate the development of a transformation model. This step is essential to enable a seamless integration between geoids and tidal datums, where conceptual relationship among these height components and their respective vertical datums is illustrated in Figure 1. 1. The developed transformation models represent the principal outcome of this research, contributing to the overarching objective of unifying the vertical datum across land and marine domains.

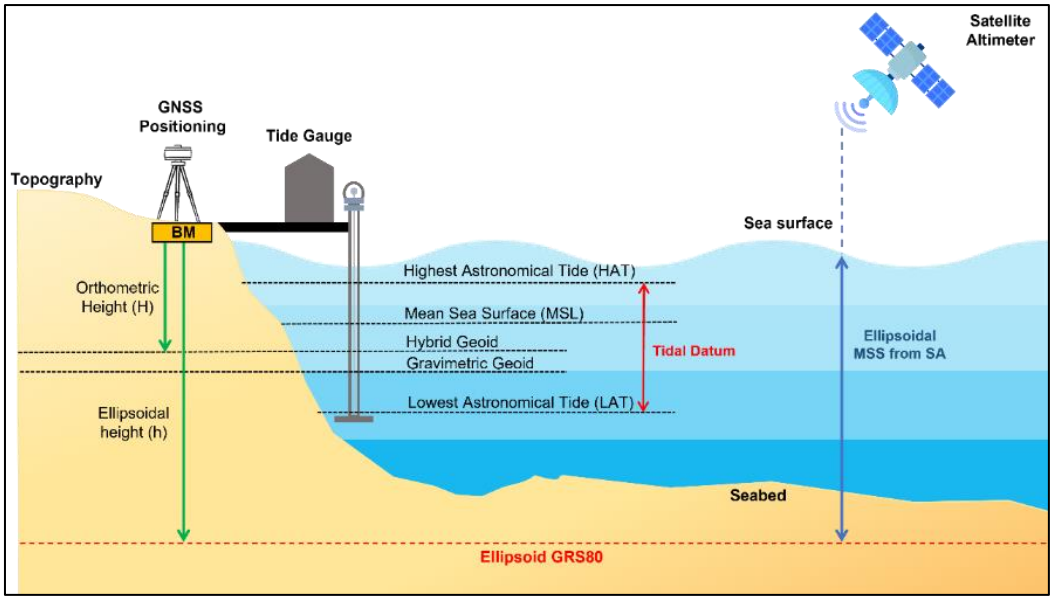


Figure 1. 1 Relationship of Orthometric, Ellipsoidal and Geoid Heights

1.2 Problem Statement

The integration of land and marine vertical datums has become increasingly important for hydrographic surveying, coastal mapping, navigation, and coastal zone management. Traditionally, terrestrial and marine height systems have been established independently using different observation techniques and reference surfaces. Land elevations are commonly referenced to the Land Survey Vertical Datum (LSVD), whereas marine depths are referenced to Chart Datum (CD). The use of different vertical reference systems creates inconsistencies in height and depth information, making it difficult to integrate geospatial datasets across the land–sea interface and limiting coastal applications, including marine cadastre, coastal infrastructure development, and geophysical studies (Abdullah & Omar, 2011; Binns et al., 2004; Cui et al., 2019; Steudler, 2014; Yusof Hussaini & Alias, 2023; Zamzuri & Hassan, 2021; Filmer et al., 2024). Consequently, the development of an integrated vertical datum transformation framework has become an important research priority (Parker, 2002; Parker et al., 2003).

One of the key components of a unified vertical datum is an accurate geoid model. Malaysia has made significant progress in geoid modelling through the development of WMGeoid04 under the MyGeoid project and its subsequent refinement through the Marine Geodetic Infrastructure (MAGIC) project (Cob et al., 2022; Jabatan Ukur dan Pemetaan Malaysia, 2005). Numerous studies have further improved geoid modelling in Malaysia using different gravimetric approaches (Forsberg, 2005; Sulaiman et al., 2014; Pa'Suya et al., 2018; Pa'suya, Din, et al., 2019; Pa'suya et al., 2022; Zamri et al., 2024). Nevertheless, the existing national geoid model was primarily developed for terrestrial applications and does not adequately represent marine regions. Moreover, recent advances in satellite-derived marine gravity, Global Gravity Models (GGMs), Digital Elevation Models (DEMs), and satellite altimetry have created new opportunities to improve marine gravimetric geoid determination (Abbak et al., 2012; O. B. Andersen et al., 2023; D. Sandwell et al., 2014; Sukma & Leni, 2024). However, these newly available datasets have not been comprehensively evaluated for Peninsular Malaysia, limiting the accuracy of the marine geoid required for vertical datum integration.

Another essential component is the establishment of continuous tidal datum surfaces. In Peninsular Malaysia, tidal datums such as the Lowest Astronomical Tide (LAT) and Highest Astronomical Tide (HAT) are primarily derived from tide gauge observations through harmonic analysis (Jabatan Ukur dan Pemetaan Malaysia, 2024). Although tide gauges provide reliable long-term observations, they are limited by sparse spatial coverage, local vertical land movement, inconsistent reference systems, and reduced reliability when tidal information is extrapolated away from the observation sites (Abd Rahman et al., 2024; Adebisi et al., 2021). Satellite altimetry provides continuous sea surface observations over the open ocean (Ardalan & Hashemifaraz, 2024), while hydrodynamic models improve tidal information within coastal regions where altimetry accuracy decreases (Hamden, 2022). Despite their complementary strengths, these datasets have not yet been integrated to establish continuous tidal datum surfaces for Peninsular Malaysia.

The absence of an accurate marine gravimetric geoid together with continuous tidal datum surfaces has limited the development of a unified vertical datum transformation model for Malaysia. Existing vertical reference systems, including the geoid, Mean Sea Level (MSL), Lowest Astronomical Tide (LAT), and Highest Astronomical Tide (HAT), remain referenced to different vertical surfaces, creating inconsistencies in height transformation and reducing the interoperability of terrestrial and marine geospatial datasets. Therefore, there is a need to develop an integrated framework that combines an improved marine gravimetric geoid, continuous tidal datum surfaces, and a unified vertical datum transformation model referenced to the GRS80 ellipsoid. Such a framework would establish explicit relationships among these vertical reference surfaces, enabling seamless height transformation and supporting hydrographic surveying, coastal engineering, navigation, marine cadastre, and integrated coastal zone management in Peninsular Malaysia

1.3 Research Questions

The research questions underscore the central focus and summarize the key elements related to this study. The formulation of these inquiries is pivotal in delineating the scope of investigation and providing a brief overview of the research objectives which the questions are as stated:

i) What is the optimal combination of datasets to enhance the accuracy of marine geoid model over Peninsular Malaysia?

ii) How can tidal datums be precisely derived?

iii) How can vertical separation models be effectively integrated to establish a unified vertical datum between the land and marine domains?

1.4 Research Aim and Objectives

This research aims to establish the vertical datum unification over land and marine areas in Peninsular Malaysia. In order to achieve the research aim, the following research objectives are addressed:

i) To refine geoid model in marine regions through the evaluation of input datasets for seamless land–marine height integration.

ii) To develop tidal models of the Lowest Astronomical Tide (LAT) and Highest Astronomical Tide (HAT) through the integration of multi-mission satellite altimetry and hydrodynamic modelling.

iii) To establish a series of vertical transformation models aimed at harmonizing multiple vertical datums across both land and marine regions.

1.5 Research Scope

This section offers a concise yet comprehensive overview of the research scope, encompassing key aspects such as the delineation of the study area and the composition of the dataset used throughout the research process.

1.5.1 Study Area

The study area selected for this research is strategically positioned to encompass the geographical expanse of Peninsular Malaysia, extending towards the coastal zones within clearly defined spatial boundaries. The computational models employed in this study were delineated by geographic coordinates ranging from 1˚N to 7˚N latitude and from 99˚E to 105˚E longitude as illustrated in Figure 1. 2.

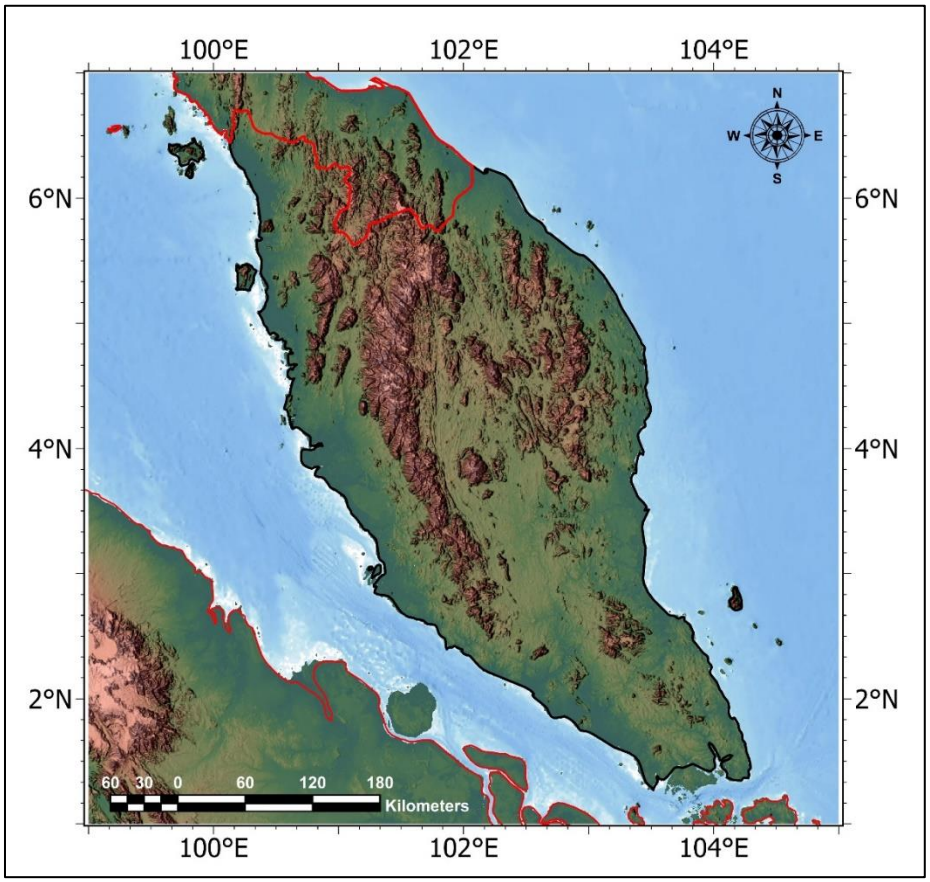


Figure 1. 2 Study Area

1.5.2 Dataset

Data presents the most critical parts prior to the execution of this research as the final outcome developed from the integration of various datasets. Preceding this research, the dataset is categorized into two distinct implementations in which dataset to compute geoid model and dataset to compute tidal datums from multi-mission satellite altimetry, hydrodynamic model. Detailed descriptions of all datasets are provided within the respective subsections.

i) Gravity Anomalies Data

Prior to this research, the gravity data in the form of free air anomalies values are crucial as primary data for the computation of gravimetric and hybrid geoid models over Peninsular Malaysia. It involved with the integration of three distinct gravity data encompassed terrestrial, airborne, and satellite-derived marine gravity data. The terrestrial and airborne gravity data were officially obtained from the Department of Survey and Mapping Malaysia (DSMM). Satellite-derived marine gravity was added to the computation to provide gravitational data that covers the marine region. In this study, four different satellite-derived marine gravity were assessed to find the optimal models that fits Peninsular Malaysia regions in the computation of accurate marine geoid model. The gravity data were acquired from various sources of dataset as listed in Table 1. 1.

Table 1. 1
List of Gravity Anomalies Data

Gravity Data	Year	No.of Data/ Resolution	Sources
Terrestrial	2019	9916	Department of Survey and Mapping Malaysia (DSMM)
Airborne	2019	24855	Department of Survey and Mapping Malaysia (DSMM)
Sandwell (V32)	2014	1 arc-minute	Sandwell & Smith
DTU21	2021	1 arc-minute	Technical University of Denmark (DTU Space).
SDUST2020	2020	1 arc-minute	Shandong University of Science and Technology
NSOAS24	2024	1 arc-minute	National Satellite Ocean Application Service (NSOAS)

ii) Global Geopotential Model (GGM)

The datasets associated with Global Geopotential Models (GGMs) are openly accessible through the official platform of the International Centre for Global Gravity Field Models (ICGEM) website at https://icgem.gfz-potsdam.de/home. Prior to the computation of a refined geoid, a comprehensive evaluation will be conducted on five GGMs that have been most recently published between the years 2019 and 2023. The selected models include both satellite-only and combined GGMs, where A represents altimetry, S represents satellite data (e.g., GRACE, GOCE, and LAGEOS), G represents ground-based observations such as terrestrial, shipborne, and airborne gravity data, while T denotes topographic information. Details about these GGMs are provided in Table 1. 2. A comparative analysis was subsequently performed to determine the GGM that exhibits the highest compatibility with the regional geoid characteristics of Peninsular Malaysia. This evaluation is essential for selecting the most suitable model to support accurate and reliable geoid modelling within the study area.

Table 1. 2
List of Global Geopotential Models

Type	No.	Model	Year	Type of Data
Satellite Only	1	WHU-SWPU-GOGR2022S	2023	S (GOCE), S (GRACE)
	2	GOSGO2S	2023	S (GOCE)
	3	Tongji-GMMG2021S	2022	S (GOCE), S (GRACE)
Combined	4	SGG-UGM-2	2020	A, EGM2008, S (GOCE), S (GRACE)
	5	XGM2019e-2159	2019	A, G, S(GOCO06s), T

iii) Global Navigation Satellite System (GNSS) Levelling

This research utilized Global Navigation Satellite System (GNSS) levelling data obtained from DSMM for three purposes: i) Geoid validation (ii) Hybrid geoid fitting and (iii) Ellipsoid-based tide conversion. The dataset comprising GNSS positioning at 11 tide gauges benchmark from GNSS Campaign 2019, 173 and 45 data from DSMM scattered across Peninsular Malaysia. The distribution of GNSS levelling data is illustrated in Figure 1. 3

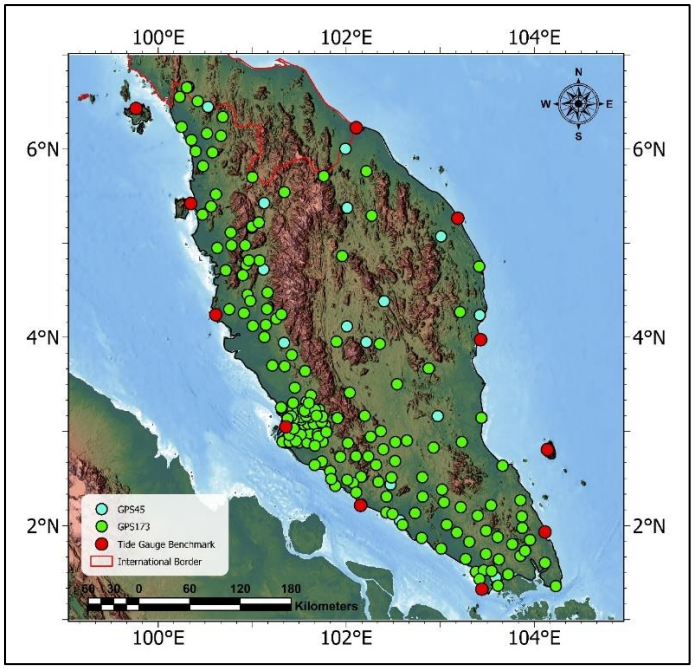


Figure 1. 3 Distribution of GNSS Levelling

iv) Satellite Altimetry Data

Satellite altimetry data served as the principal dataset for the derivation of tidal datums specifically the LAT and HAT. This investigation integrated observations from six distinct satellite altimetry missions, including TOPEX/Poseidon A and B, Jason-1A/B, Jason-2A/B, Jason-3A, Sentinel-6A, and GFO. The temporal coverage of the dataset extends from 1992 through 2024, as detailed in Table 1. 3. All datasets were sourced from the Radar Altimeter Database System (RADS) and subjected to rigorous preprocessing to derive precise along-track Sea Surface Height (SSH) measurements for subsequent analysis.

Table 1. 3
List of Satellite Altimeter Data

Satellite	Phase	Cycle	Date
Topex	A	305 - 327	13/10/2016 - 17/05/2017
	B	000 - 227	12/02/2016 - 7/4/2022
Jason 1	A	001 - 364	25/9/1992 -10/8/ 2002
	B	369 - 481	20/9/2002 - 8/10/2005
Jason 2	A	001 - 260	17/01/2002 - 26/1/2009
	B	262 - 374	12/02/2009 - 03/03/2012
Jason 3	A	000 - 303	4/07/2008 - 2/10/2016
Sentinel - 6A	A	004 - 117	19/12/2020 - 18/1/2024
GFO	A	037 - 202	8/1/2000 - 25/9/2007

v) Mean Sea Surface Model

In this study, global Mean Sea Surface (MSS) models are crucial component in the derivation of tidal datums specifically LAT and HAT, which were computed based on tidal amplitudes generated by the hydrodynamic model through the Tide Model Driver (TMD) processing. As the TMD yields LAT and HAT values relative to the MSS, it becomes essential to incorporate additional MSS models to facilitate the transformation of these tidal datums into ellipsoidal-based vertical reference surfaces. Accordingly, three contemporary global MSS models are summarized in Table 1. 4 and these models were systematically assessed to identify the most appropriate model that best represents the regional sea surface characteristics surrounding Peninsular Malaysia.

Table 1. 4
List of Global Mean Sea Surface Model

MSS Model	Resolution	Ellipsoid Reference	Obs. Period
SDUST2020	$1' \times 1'$	GRS80	1993 - 2019
DTU21	$1' \times 1'$	GRS80	1993 - 2021
CNES-CLS22	$1' \times 1'$	GRS80	1993 - 2021

vi) Mean Dynamic Topography Model

The Mean Dynamic Topography (MDT) model was incorporated into this study to complement and diversify the analysis of the MSS by evaluating the composite surface generated through the summation of MDT and global geoid model. This approach enables the reconstruction of an alternative MSS representation, thereby allowing a comparative assessment against established MSS datasets. In this context, three contemporary global MDT models as listed in Table 1. 5 were employed in this study with the aim of determining the most regionally representative solution for the coastal domains of Peninsular Malaysia.

Table 1. 5
Summary of Global Mean Dynamic Topography Model

MDT Model	MSS	Geoid	Period
DTU22	DTU21MSS	XGM2019e	1993-2012
DTUUH22	DTU21MSS	XGM2019e	1993-2012
MDOT Hawaii	Drifter-derived AVISO Satellite Altimetry	GRACE	1992-2012

vii) Global Geoid Model

The global geoid models incorporated in this study perform a parallel role to the MDT models, as previously outlined in Subsection 0, by facilitating the reconstruction of alternative mean sea surface representations through their integration with tidal datums. These geoid datasets were sourced from the ICGEM, a publicly accessible repository which available at https://icgem.gfz-potsdam.de/home. Table 1. 6 is the list of specific global geoid models that has been adopted in this study.

Table 1. 6
The List of Global Geoid Models

Geoid Model	Year	Ellipsoid Reference	Tide-System
WHU-SWPU-GOGR2022S	2023	GRS80	Tide free
GOSG02S	2023	GRS80	Tide free
XGM2019e	2019	GRS80	Tide free

viii) Tide Gauges Data

Tide gauges data in this study used as validation references to evaluate the performance of global MSS models and vertical separation models computed herein. The datasets were acquired from DSMM repositiory via University of Hawaii Sea Level Center (UHSLC) website. A total of 11 tide gauges stations sparsed along coastal regions of Peninsular Malaysia were utilized as depicted in Figure 1. 4 and listed in Table 1. 7. The corresponding tidal datums for these coastal locations were derived from 18 years observation of sea level records processed using harmonic analysis in UTide Processing. A comprehensive explanation of the methodology is provided in Chapter 3.

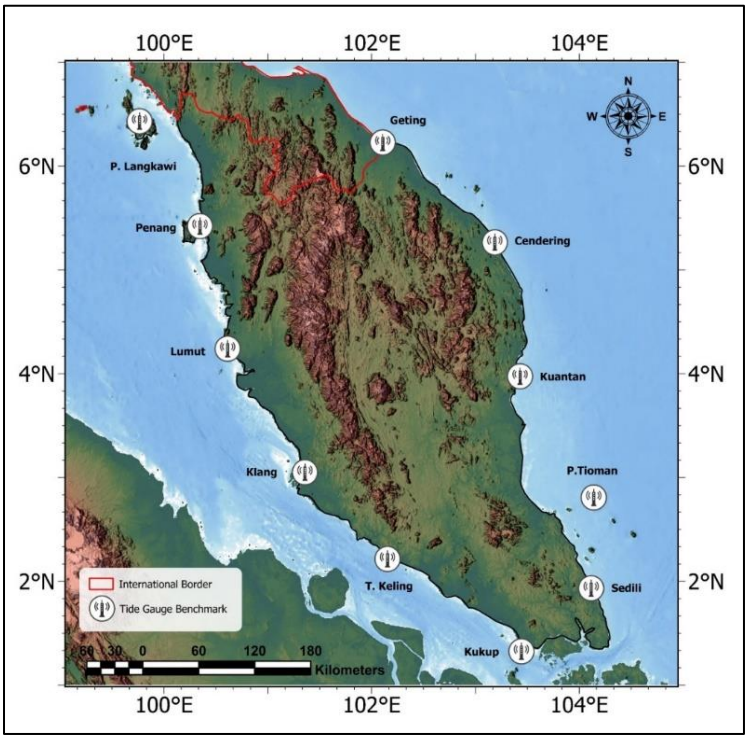


Figure 1. 4 Distribution of Tide Gauge Stations

Table 1. 7
List of Tide Gauge Stations

Station	TGBM	Latitude	Longitude	Observation Period
Klang	B0169	3˚ 03' 00 "N	101˚ 21' 29 "E	1998–2015
Tanjung Keling	M0331	2˚ 12' 54 "N	102˚ 09' 11 "E	1998–2015
Pulau Langkawi	K0172	6˚ 25' 55 "N	99˚ 45' 54 "E	2001–2018
Lumut	A0401	4˚ 14' 24 "N	100˚ 36' 47 "E	1998–2015
Penang	P0379	5˚ 25' 19 "N	100° 20' 49" E	1998–2015
Cendering	T0283	5˚ 15' 54 "N	103° 11' 13" E	1998–2015
Kuantan	C0331	3˚ 58' 30 "N	103° 25' 48" E	1998–2015
Pulau Tioman	C0501	2˚ 48' 25 "N	104° 08' 24" E	1998–2015
Sedili	J0888	1˚ 55' 55 "N	104° 06' 54" E	1998–2015
Kukup	J5328	1˚ 19' 30 "N	103° 26' 35" E	1998–2015
Geting	D0354	6˚ 13' 37 "N	102° 06' 25" E	1998–2015

1.5.3 Data Interpretation and Analysis

The scope of analysis in this study is limited to the following:

i) Analysis of GGMs, satellite-derived marine gravity dataset, and the determination of optimal parameters for gravimetric geoid computation using the KTH method.

ii) Analysis of hybrid geoid model derived through kriging interpolation and its validation against local GNSS levelling datasets.

iii) Analysis of tidal datum modelling over the coastal waters of Peninsular Malaysia through the integration of multi-mission satellite altimetry and hydrodynamic approaches using harmonic analysis.

iv) Analysis of vertical separation offsets between geoid model, MSL, HAT and LAT using tidal datums derived from local tide gauges dataset.

1.5.4 Limitation

The study is subject to limitations related to the availability of validation data, particularly in offshore regions. While reliable GNSS levelling and tide gauge datasets are available on land and along coastal zones, there is a complete absence of direct validation data in open sea areas. As a result, the vertical separation offsets derived for offshore regions cannot be independently verified using in-situ observations. Consequently, the assessment of offshore vertical datum transformation relies on model consistency and indirect geodetic inference rather than direct observational validation. This limitation is particularly important in open sea environments, where no physical height control points are available to confirm the accuracy of the transformed vertical reference surfaces. Although the developed model remains physically consistent within the geodetic framework, the lack of offshore validation data introduces higher uncertainty in open sea regions compared to coastal and inland areas.The tidal datum analysis is also constrained by the availability and distribution of tide gauge stations.

1.6 Research Significance

The significance of this research lies in the development of a seamless unified datum that connecting the land and marine through the development of separation vertical surface models. The separation models between each surface allows the any transformation of height become possible via the adoption of GNSS-derived height, which primarily benefits the geomatics community. This research also holds further significance in the following aspects:

1. The first objective of this research centred on the formulation of a refined hybrid geoid model particularly within the Peninsular Malaysia marine region. The methodology employed included a rigorous evaluation of geoid parameters using the KTH approach which has widely practices by worldwide geodesists due to its simpler and accurate geoid modelling outcomes. The significance of this effort lies in its potential to provide empirical guidance to Malaysian geodesists and survey agencies as practical benchmark for improving the precision of geoid-based height system in Malaysia. Furthermore, the

development of a more accurate marine geoid model aligns with broader international geodetic goals, including the pursuit of a universal 1 cm geoid accuracy as advocated by global initiatives such as the International Association of Geodesy (IAG). In this regard, the present study not only supports national geospatial advancement but also positions Malaysia to contribute meaningfully to global efforts in achieving high-precision vertical referencing, thereby enhancing the reliability of geospatial information across marine and coastal domains.

2. This research involved with the development of several vertical references surface encompassed the hybrid geoid, LAT, and HAT by utilizing the gravity anomalies, satellite altimetry and hydrodynamic ocean model. The integration of these data capable to provide transformation parameters of specific vertical reference surface which benefit to the ease of hydrographers. The significant applications of these models are in forecasting the sea level rise and coastal inundation which are the critical aspect for coastal risk management (Rashidi et al., 2021). Thus, it may provide a valuable insight to assist the organization such as Intergovernmental Panel on Climate Change (IPCC) Coastal Management Subgroup and Response Strategies Working Group in managing the coastal domain.

3. The seamless integration of datum across land and marine domains resulting from this research holds immense benefits for the marine cadastre environment. Researchers have long underscored the challenges posed by discontinuities in datum between these realms as highlighted in Binns et al. (2004), Mohd Amsyar & Abdullah Hisam (2011), Nor Ainn Alfatihah et al. (2021) and Yusof Hussaini & Alias (2023). An effective implementation of this research may foster significant advancement of consistency and accuracy in spatial data management in both land and maritime environment.

1.7 Research Outline

The outline of this research was structured into five chapters with each section closely connected to the others and the information built upon in the previous chapter is essential for grasping the following ones.

Chapter One : Introduction

This chapter emphasis on providing a concise overview of the study. It outlines the issues that prompted the research, including the research background, problem statement, aim and objectives, research scope, and research significance.

Chapter Two : Literature Review

This chapter highlighted the literature review that provide further theoretical information related to the definitions and terms frequently used across this study. Topic such as datum, vertical surfaces, models, constituents and etc. were briefly discussed in this chapter to provide a deeper understanding of the research that has been carried out.

Chapter Three : Research Methodology

This chapter highlighted the methodologies starting from preparation of data until the completion of the final output in a sequential manner. The flow of methodologies in this study were spilt into three based on each objective since each objective involved in development of different types of output. The first methodology for the first objective highlighted the data preparation (data acquisition, filtering, and cross validation), reconstruction of gravity data, evaluation of parameters and computation of gravimetric and hybrid geoid model. The methodology for second objective were also break down in detail on how tidal datums were derived from the assimilation of multi-mission satellite altimetry and hydrodynamic modelling. The third objective involved with the development of vertical transformation model aimed to mitigate the data from one datum to another. The process included were the computation of vertical datum offset from each vertical datum models by standardizing the origin to ellipsoid surface.

Chapter Four : Result and Discussion

This chapter presents an in-depth examination of the research findings, systematically organized according to each research objectives. The outcomes were critically analyzed to provide a clear understanding of the methodologies employed and the significance of the results obtained. The supplementary analyses were included to reinforce the validity of the methodological approaches and to demonstrate the robustness of the implemented techniques. Collectively, this chapter offers a comprehensive presentation of results and discussions aimed to provide deeper insight into the implications of the outcomes within both geodetic and marine contexts.

Chapter Five : Conclusion and Recommendation

Chapter Five is the final chapter that concluded the research in overall. All of the hypothesis and outcomes were briefly summarized to highlight the novelty of this research. Moreover, the limitations discerned throughout this research are thoughtfully integrated into the recommendations, thereby underscored as avenues for potential future inquiries.

CHAPTER 2
LITERATURE REVIEW

2.1 Introduction

This chapter provides an in-depth review of essential literature to refine the research methodology, covering the theoretical components of height, the concept of datum, tidal phenomena, and employed methods. It begins by explaining the theoretical components of height and highlighting their interrelationships, offering insights into how these concepts are foundational to the study. The discussion then moves to the concept of datum, emphasizing its significance and the theoretical information related to tidal constituents and prediction. Furthermore, this chapter delves into tidal phenomena, examining key studies and findings. Additionally, the methods utilized throughout this study are meticulously detailed to enhance understanding of the rationale behind the chosen methodologies.

2.2 Components of Height

In geodetic measurement, the parameter of height is divided into three which are the orthometric or normal height (H), ellipsoidal height (h), and geoid height (N). These components are interdependent, forming the basis for deriving any height at a specific point on Earth's topographical surface. This relationship is crucial for various applications, particularly those related to surveying and construction.

$$H = h - N \tag{2.1}$$

2.2.1 Orthometric / Normal Height

The classical definition by Heiskanen & Moritz (1967), defined the orthometric or normal height as a distance that measured positive outward along the plumb line from geoid to topographical surface of Earth. This concept is pivotal in geodetic calculations, especially for determining precise height measurements, which are considered true elevations on the Earth's surface. Orthometric height is typically derived from

prolonged observations of MSL, where the average sea level between the highest and lowest sea level recorded at specific tide gauges is computed and disseminated in the form of standard benchmarks (SBM) or benchmarks (BM). There are two methods on which the surveyor can obtained the orthometric height, which is by traditional levelling or GPS positioning derived height (Jabatan Ukur dan Pemetaan Malaysia, 2005), However, since levelling is unpractical for a long-distance observation and time consuming, the utilization of GPS/GNSS observation has become increasingly necessary for accurately acquiring the positions on ground. The orthometric height can be derived using the formula as previously stated in Equation (2.1).

2.2.2 Ellipsoid

An ellipsoid is a mathematically simplified representation of Earth's shape, essential for various geodetic and geographic computations (Roman, 2007). It is a simple geometric shape that looks like a slightly flattened sphere and mathematically defined by two parameters, encompassed the semi-major/minor axis and flattening as depicted in **Error! Reference source not found.** (Mills & Dodd, 2014). Theoretically, s urface of the Earth is undulated due to the gravitational force which led to a complex mathematical derivation related to any measurements. However, an ellipsoid reference was computed to provide an ease to a simpler mathematical derivation related to any determination of geographic (latitude, longitude, and height) positions through the formula stated in Equation (2.1). Basically, ellipsoidal height is the difference of the vertical distance between a point on the Earth's topographical surface to the ellipsoid. In current age, the utilization of GNSS technology has adopted the ellipsoid-reference based height in the observation, enabling a consistent and precise framework for measuring and recording geographic positions. The efficiency and reliability of GNSS have made ellipsoid-referenced height measurements the standard in geodetic practices. However, it is crucial to acknowledge the limitations of the ellipsoid model. While it provides a generalized shape for the Earth, it excludes the undulating topographical variations caused by gravitational anomalies. These undulations are significant for high-precision applications such as geoid modelling and advanced geodetic surveys.

Therefore, an additional vertical reference surface known as the geoid, is required to complement the ellipsoid.

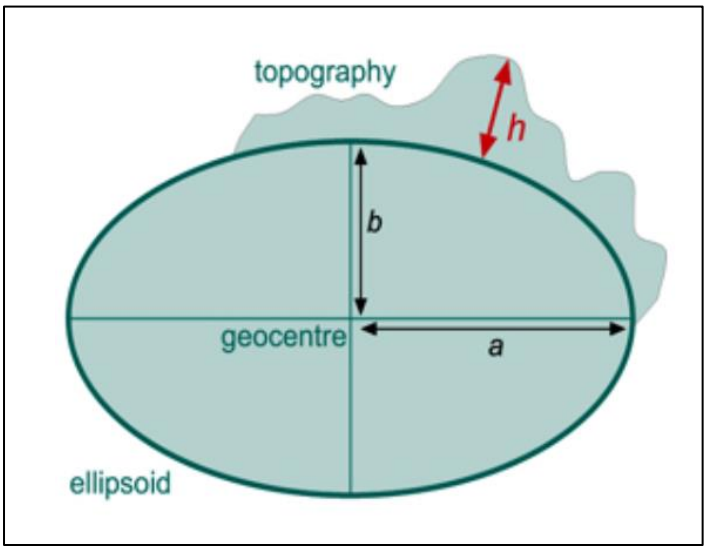


Figure 2. 1 Ellipsod Surface (Huismain & de By, 2009)

2.2.3 Geoid

In reality, the Earth's shape, and surface exhibit undulations due to the gravitational forces exerted by its land masses, which is called the geoid as illustrated in Figure 2. 2 (Heiskanen & Moritz, 1967). Due to the undulated surface, the mathematical derivation related to physical measurements became complex, in which the researchers since preceding years have taken a measure in developing a model that can accurately derived the elevation of the geoid. Basically, geoid height is the separation value between geoid and ellipsoid surface (Jabatan Ukur dan Pemetaan Malaysia, 2005) . The value of geoid height is pivotal in determination of orthometric height subjected to the observation carried out using GPS/GNSS instruments. The value of geoid height is obtained from the product of geoid model computed by integrating the gravity anomalies data with the global reference of geopotential model and digital elevation model. In current age, numerous countries have developed their own local geoid models to enhance the precision of geoid height measurements, ensuring they are well-suited to the specific geographical elevations of their regions.

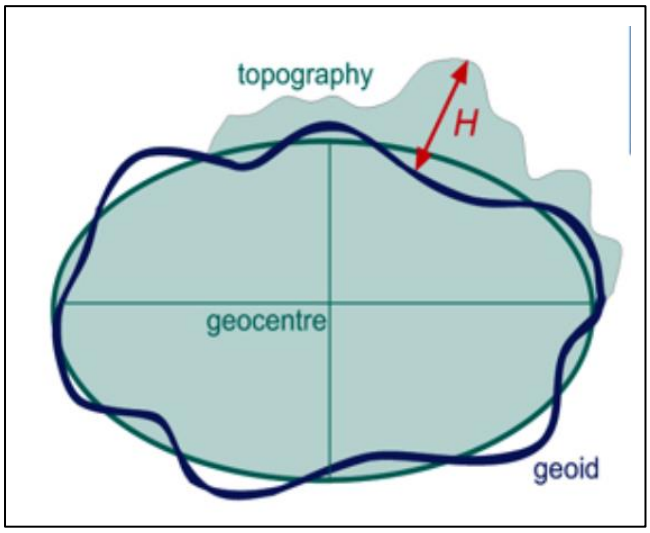


Figure 2. 2 The Geoid (Huismain & de By, 2009)

2.3 Vertical Datum

Datum is one of critical parameter in the matter related to measurement to be done on land or coastal area. According to National Oceanic and Atmospheric Administration (NOAA) (2021), datum is an abstract coordinate system with a reference surface that serves as a starting location to begin survey or map creation. It holds a paramount position within the realm of geodetic applications in every country which subjected to facilitate multitude of activities and disciplines especially in surveying, navigation, natural resources management and environmental monitoring (Véronneau et al., 2006). In the context of height derivation using GNSS, vertical datum is pivotal. Fundamentally, vertical datum is defined as an equipotential surface derived by a geopotential value, W_0 that serves as the reference surface of physical height (Amjadiparvar et al., 2016). Vertical datum can fundamentally define as a precise reference surface denoting a zero-height elevation. This foundational concept serves as the cornerstone upon which geodetic measurements and spatial referencing systems are built, providing a standardized framework for vertical positioning in geospatial analysis, engineering, and other fields. In Malaysia, the utilization of vertical datum is different between the land and coastal area. The vertical datum for land adopted the height referenced to the Peninsular Malaysia Geodetic Vertical Datum (PMGVD) while the coastal adopted heights via the continuous observation tidal datums consists of MSL, LAT, and HAT (Sulaiman et al., 2012).

2.3.1 Geodetic Vertical Datum

Early in 1980s, Malaysia has implemented a measure to improvise the National Geodetic Vertical Datum (NGVD) which involved with the projects of i) Tidal observation, ii) Precise levelling, and iii) Gravity survey. Due to the geographical division of Malaysia's landmasses into two distinct regions of Peninsular and Sabah Sarawak, the computation of the NGVD was conducted separately for each region. The first project involved with the establishment of NGVD were derived by the tidal observation for about a decade. In the case of Peninsular Malaysia, observations were conducted between 1984 and 1993, focusing on the tide gauge located in Port Klang. Similarly, Sabah and Sarawak conducted observations at Kota Kinabalu's tide gauge from 1988 to 1997(Jabatan Ukur dan Pemetaan Malaysia, 2005). In 1994s, Department of Survey and Mapping Malaysia (DSMM) has established a levelling network by transferring the MSL at Port Klang to PMGVD station as shown in Figure 2. 3. The PMGVD monument was erected within the DSMM building in Kuala Lumpur, serving as the principal reference point for the geodetic vertical datum in Peninsular Malaysia. This datum was established at a value of 3.624 meters above zero tide gauge from MSL at Port Klang, determined through precise levelling survey (Jamil, 2011).



Figure 2. 3 PMGVD monument at Port Klang (Jamil, 2011)

The third project involved with gravity surveys that were carried out prior to develop a precise geoid model of Malaysia back in 2002 and 2003. During that time, DSMM has embarked with the utilization of airborne gravity by the collaboration with a Danish Company known as Kort & Matrikelstyrensen (KMS). This endeavour was deemed more practical to increase the density of gravity data due to Malaysia's topographical surface, which is predominantly mountainous, especially in the central region of Peninsular Malaysia making ground gravimeter surveys become limited. Through the present of terrestrial and airborne gravity data, DSMM has successfully established hybrid geoid model for both Peninsular and Sabah Sarawak known as MyGEOID which consists of two hybrid geoid model which is WMGEOID04 (Peninsular) and EMGEOID05 (Sabah and Sarawak) as illustrated in Figure 2.4. WMGEOID05 geoid model was fitted to the PMGVD at Port Klang while EMGEOID05 was fitted to Sabah Datum 1997. This development was aimed at complementing and strengthening the existing geodetic infrastructure for the utilization of GNSS services (Jamil, 2011).

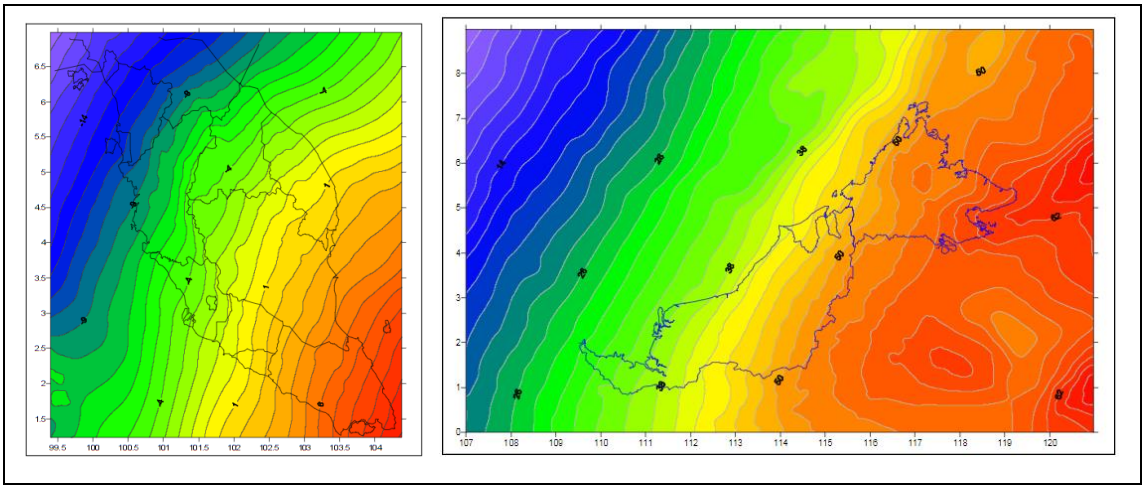


Figure 2.4 Malaysia's Geoid Model Which Divided Into Two Region a) WMGEOID04 (Peninsular Malaysia) and (b) EMGEOID05 (Sabah and Sarawak)

2.3.2 Reference Ellipsoid

A reference ellipsoid is a mathematically defined, idealized surface used to approximate the Earth's shape. It serves as a geometrically smooth, rotationally symmetric model of the Earth, designed to closely represent mean sea level on a global scale. This model intentionally excludes local irregularities caused by transient phenomena such as tides, atmospheric pressure variations, ocean currents, and wave activity, which would otherwise introduce complexity into geodetic calculations (EarthScope Consortium, 2011). In geodetic and oceanography applications, the reference ellipsoid functions as a fundamental component for establishing vertical and horizontal datums. The implementation is not limited only GNSS-based positioning, but also extends to spaceborne systems, particularly in satellite radar altimetry. The implementation of an ellipsoidal reference is crucial for translating raw positional data into meaningful geographic coordinates and for referencing sea surface height measurements collected by satellite altimeters.

Among the numerous ellipsoidal models introduced over time, the Geodetic Reference System 1980 (GRS80) and the World Geodetic System 1984 (WGS84) remain the most widely adopted globally. The GRS80 was formally defined by the International Association of Geodesy (IAG) and is frequently used within global and regional geodetic frameworks, including the International Terrestrial Reference Frame (ITRF). In parallel, the WGS84 was developed by the United States Department of Defence, primarily for global navigation and military applications and has become the standard for most GNSS and mapping systems. In the context of satellite altimetry, many missions such as TOPEX/Poseidon, Jason-1/2/3, and Sentinel-6 utilized the TOPEX/Poseidon ellipsoid as their reference surface. This should explained on how altimetric data products has resulted in most MSS and MDT models being produced in the TOPEX/Poseidon ellipsoid framework to maintain internal consistence (AVISO+, 2024).

Although numerous ellipsoids have been introduced for geodetic applications, this study focuses on GRS80, WGS84, and TOPEX/Poseidon due to their direct relevance to the datasets and processing workflow employed. The GRS80 ellipsoid is adopted as the common reference surface for the development of the vertical datum

transformation models. However, several input datasets used in this study, particularly satellite altimetry products and hydrodynamic datasets, are originally referenced to either the WGS84 or TOPEX/Poseidon ellipsoid. Therefore, a clear understanding of the characteristics and relationships among these three ellipsoids is necessary to ensure a consistent transformation of all datasets into a common reference frame. While the differences between GRS80, WGS84, and TOPEX/Poseidon are relatively small, each ellipsoid is defined by slightly different semi-major axis, flattening, and eccentricity parameters. These differences can introduce systematic offsets when datasets referenced to different ellipsoids are integrated without proper transformation. The fundamental parameters of the three ellipsoids are summarized in Table 2. 1.

Table 2. 1
Summary of Ellipsod Reference Models

Properties	**GRS80**	**WGS84**	**TOPEX/Poseidon**
flattening	$\frac{1}{298.257222101}$	$\frac{1}{298.257223563}$	$\frac{1}{298.257}$
Semi - major axis (a)	6378137.0 m	6378137.0 m	6378136.3 m
Semi - minor axis (b)	6356752.3141 m	6356752.3142 m	6356751.6 m
Eccentricity² (e^2)	0.00669438002290	0.00669437999014	~ 0.00669438

2.3.3 Tidal Datum

In the marine environment, tidal datum is a critical issue due to the dynamic nature of ocean surfaces that changing over time, unlike the relatively stable geodetic datums on land. Therefore, a specialized datum is needed to provide accurate elevation values in marine regions, which known as tidal datum. The characteristics of tidal datums vary from one place to another depending on the tidal predictions of sea behaviour over time. Since tidal datums are considered local datums, those from a specific area should not be extended into areas with differing hydrographic characteristics without supporting measurements. (Palmer et al., 2023). Since tidal datums play an essential role in defining state sovereignty boundaries over maritime

areas (Palmer et al., 2023), there are numerous efforts by countries across the world in developing a high accuracy of tidal datum for effective management of maritime applications. The establishment of the local tidal datums that can integrate with geodetic datums are encouraged to create a unified reference frame for height measurements worldwide, leverage technologies like the ellipsoid and GPS. Theoretically, tidal datum is defined by the periodic variations in water levels associated with ocean tides over a long period of tidal phase observations (National Oceanic and Atmospheric Administration, 2000a). The determination of tidal datums usually requires at least 18.6 years observation period, accounting for the modulation of lunar constituents marked by the complete cycle of the moon's regression to its nodes (Abd Rahman et al., 2024; Hamden, 2022). The tidal datums are not confined on a single datum but there are various types of it as listed in Table 2. 2, which the application of it may vary from one project to another.

Table 2. 2
Types of Common Tidal Datums and its Definitions (National Oceanic and Atmospheric Administration, 2000b)

Abb.	Tidal Datum	Descriptions
MSL	Mean Sea Level	Average water level usually derived over 19 years observation period.
HAT	Highest Astronomical Tide	Highest predicted astronomical tide expected to occur at a specific tide station over the time period.
LAT	Lowest Astronomical Tide	Lowest predicted astronomical tide expected to occur at a specific tide station over the time period.
MHW	Mean High Water	Average elevation of all high tides recorded over a specific period, typically a Metonic cycle of 19 years.
MHWN	Mean High Water Neap	Average elevation of high tides during neap tides, which are characterized by the smallest tidal ranges. Neap tides occur about twice a month when the moon and sun's gravitational forces are at right angles.
MHWS	Mean High Water Spring	Average elevation of high tides during spring tides, which have the largest tidal ranges. Spring tides occur about twice a month when the gravitational forces of the moon and sun are aligned.
MLW	Mean Low Water	Average elevation of all low tides recorded over a specific period, typically 19 years.
MLWN	Mean Low Water Neap	Average elevation of low tides during neap tides.
MLWS	Mean Low Water Spring	Average elevation of low tides during spring tides, indicating the lowest typical tidal ranges.

2.3.4 Lowest and Highest Astronomical Tide

The Lowest Astronomical Tide (LAT) and Highest Astronomical Tide (HAT) represent the minimum and maximum predicted sea levels, respectively, under average meteorological conditions and purely astronomical influences within a specific temporal window. These tidal datums correspond to the extreme vertical limits of tidal fluctuations, measured from the seabed to the sea surface over a period. Tidal phenomena are primarily driven by the gravitational interactions of the Earth-Moon-Sun system. Therefore, a complete and stable representation of LAT and HAT requires an observational period of at least 18.6 years, corresponds to a full lunar nodal cycle, which is period it takes for the Moon's orbital plane to complete its regression around the Earth once (Abd Rahman et al., 2024; Hamden, 2022). This full cycle is necessary to capture the influence of modulating tidal constituents, including those that occur infrequently but significantly affect the amplitude and timing of tidal extremes.

In geodetic and oceanographic practice, these tidal datums are derived through harmonic analysis, which decomposes sea level observations into a series of tidal constituents with varying frequencies and amplitudes (Pugh et al., 2015). These tidal constituents exhibit a wide range of frequencies, from high-frequency diurnal and semidiurnal components to low-frequency, long-period constituents (refer subsection 2.5.1). As such, a short-term sea level record may not capture the full spectrum of constituents especially the low-frequency constituents leading to inaccurate estimations of these respective datums (International Hydrographic Organization (IHO), 2020). Nevertheless, within the discipline of hydrography, short-term observations are often employed pragmatically when long-term data are not available. According to the International Hydrographic Organization (IHO) standards, provisional LAT and HAT values can be accepted if derived from temporary tide gauge deployments and correlated with nearby long-term stations or harmonic predictions (International Hydrographic Organization (IHO), 2020). This approach is commonly adopted in hydrographic surveys to establish interim vertical references, particularly for bathymetric mapping, nautical charting, and safe navigation, where immediate operational needs outweigh the limitations of long-term datum stability.

2.3.5 Geoid Model

In this study, global geoid models and existing local geoid models are incorporated as complementary datasets together with Mean Dynamic Topography (MDT) models to reconstruct the Mean Sea Surface (MSS) model. The combined model configurations are assessed to identify the optimal MSS solution for facilitating the transformation of hydrodynamic data into the GRS80 ellipsoidal reference frame.

2.3.5.1 WHU-SWPU-GOGR2022S

The WHU-SWPU-GOGR2022S model is a satellite only gravity field model derived by the combination of data from GOCE and GRACE missions. Given this model provide a complete up to 300 spherical harmonic degree and order, it allows a representation of moderately fine spatial variations of Earth's gravity field with approximately 67 km resolution on the Earth's surface (Zhao et al., 2023). In this study, the WHU-SWPU-GOGR2022S model was selected due to its recent released and demonstrated performance that indicated a consistent geoid height derivation with those obtained from other established gravity field models (Azmin et al., 2024; Mphuthi, 2025).

2.3.5.2 GOSG02S

The GOSG02S is a satellite only gravity field model which derived from Satellite Gravity Gradiometry (SGG) data and Satellite-to-Satellite Tracking (SST) observations from the GOCE mission. The model employs the least squares adjustment method to derive the spherical harmonic coefficients representing the global gravity field. This rigorous statistical approach minimizes residuals between observed and computed quantities to estimate the most probable field solution (Xu et al., 2023). Similar to the WHU-SWPU-GOGR2022S model, GOSG02S also provide the dataset using spherical harmonic order and degree of 300 which was released in 2023 through ICGEM.

2.3.5.3 XGM2019e

The XGM2019e is a combined global gravity field which incorporates the GOCO06s satellite-only solution for long-wavelength gravity information (up to degree/order 300), combined with a 15′ global ground gravity grid and 1′ topographic and altimetric enhancements to capture shorter-wavelength details. It is computed using spheroidal harmonic expansions and provides coefficients up to degree and order 5399, corresponding to a spatial resolution of approximately 4 km. XGM2019e is particularly useful in coastal and oceanic regions due to its improved geoid representation, with performance validated through comparisons with independent MDT datasets such as DTU17MDT (Zingerle et al., 2020).

2.3.5.4 PMGG2020

The PMGG2020 is a local gravimetric geoid model developed by Pa'suya et al. (2022), who a Malaysian researcher actively engaged in geoid modelling. The model was computed through the integration of local gravity anomalies data from DSMM, which are the terrestrial and airborne data. The derivation of gravity field on marine region was covered by DTU V.17 which is a satellite-derived marine gravity data. For the computation of the gravimetric geoid, the KTH method was employed by utilizing the Tandem-X Digital Elevation Model (DEM) for topographic corrections and the GO_CONS_GCF_2_SPW_R4 satellite gravity model for the long-wavelength components. Validation of PMGG2020 was conducted using 173 GNSS levelling data across Malaysia. The model demonstrated good agreement with the observed data, achieving a standard deviation of approximately 0.058 m which indicates a high-accuracy of geoid model.

Table 2. 3 summarizes the characteristics of the selected geoid models. The WHU-SWPU-GOGR2022S and GOSG02S models represent recent satellite-only solutions that provide consistent long- to medium-wavelength gravity information. In contrast, XGM2019e incorporates both satellite and terrestrial gravity data, enabling a higher spatial resolution and improved representation of short-wavelength gravity signals. PMGG2020 differs from the global models as it was specifically developed for Malaysia using local gravity datasets and has been independently validated against

GNSS levelling observations. Consequently, the selected models provide a combination of global and local gravity field representations that are suitable for evaluating the optimal MSS reconstruction and vertical datum transformation framework adopted in this study.

Table 2. 3
Literature Summary of Geoid Models

Author	Model	Year	Type	Data Source	Key Characteristics
Zhao et al.(2023)	WHU-SWPU-GOGR2022S	2023	Satellite Only	• GOCE • GRACE	• Recent satellite-only gravity field model providing consistent representation of medium-wavelength gravity signals.
Xu et al.(2023)	GOSG02S	2023	Satellite Only	• GOCE	• Developed using least-squares adjustment to estimate global gravity field coefficients.
Zingerle et al.(2020)	XGM2019e	2019	Combined Dataset	• GOCO06s • Ground gravity data • Topographic data • Satellite altimetry	• Combines satellite and terrestrial gravity information with high-degree harmonic expansion. • Provides improved short-wavelength gravity signals, particularly in coastal and marine areas.
Pa'suya et al.(2022)	PMGG2020	2020	Combined Dataset	• Local gravity anomalies • DTU17 marine gravity • DEM: TanDEM-X • GGM: GO_CONS GCF_2_SPW_R4	• Developed specifically for Malaysia using local gravity observations and KTH method. • Validated using 173 GNSS levelling points with a standard deviation of approximately 0.058 m.

2.3.6 Mean Dynamic Topography

The Mean Dynamic Topography (MDT) is fundamentally important in geodesy and physical oceanography in deriving the geodetic vertical datum and understanding the ocean circulation pattern related to mean sea level tilt (Higginson et al., 2015; Huang, 2017). MDT represents the deviation between the averaged sea surface height and the geoid that capture the steady-state component of ocean circulation (Knudsen et al., 2024). Two common approaches to derive the MDT is by oceanographic or geodetic method. The oceanographic method calculates the MDT through the temporal averaging of ocean circulation model outputs over a specific time window that effectively smoothing the short-term sea level variation (Huang, 2017). Conversely, the geodetic approach determines MDT as different between MSS and Geoid as stated in equation (2.1) and the relationship of height components in coastal domain are as illustrated in Figure 2. 5.

$$MDT = MSS - Geoid \tag{2.1}$$

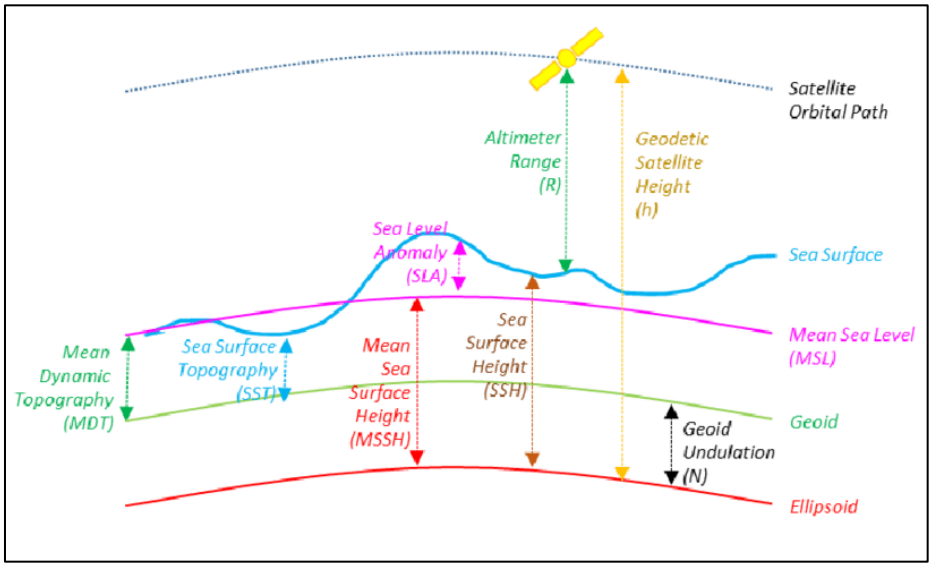


Figure 2. 5 Relationship of Coastal Height Components (Sarsito et al., 2021)

However, the computation of the MDT is not straightforward since there are factors in need for consideration related to the reference ellipsoid and tide-system used for both MSS and geoid model (Filmer et al., 2024). Direct computation of MDT only

possible when both models are in the same reference. While conceptually straightforward, this approach can be challenging due to the difference in resolution between the MSS and geoid model especially near the coast, which may lead to the omission errors in MDT estimation (Bingham & Haines, 2006). However, the advancement of global MDT model developed by several worldwide agencies has greatly helpful to geodesist without the need to manually derived the MDT. DTU is among the active agency that has continuously developed not only MSS models but also MDT models. Their latest releases include the DTU22MDT and its enhanced version namely DTUUH22MDT, which integrates mean drifter velocity fields to improve the model's spatial resolution and dynamic consistency, particularly in coastal and marginal seas (Knudsen et al., 2022). In this study, various global MDT models are employed with the objective of diversifying the analysis of the MSS by combining them with different global geoid models. This approach facilitates a comparative assessment of the performance of each MDT and geoid pairing, aimed to identify the most suitable combination for representing sea surface height variations across coastal regions of Peninsular Malaysia.

2.3.6.1 DTU22MDT

The DTU22MDT was developed to provide an updated geodetic MDT by integrating a new MSS model and an enhanced geoid model. According to Knudsen et al. (2022), the geodetic MDT was calculated using the combined XGM2019e geoid, which incorporates satellite altimetry-derived marine gravity data to minimize the unresolved components of the geoid up to spherical harmonic degree 2160. Furthermore, DTU22MDT utilized the refined DTU21MSS model which was constructed from over two decades of multi-mission altimetry observations (O. B. Andersen et al., 2023). A significant advancement in DTU22MDT stems from improvements in the DTU21MSS, particularly in its filtering techniques. Unlike earlier versions that applied Gaussian filters with variable width and anisotropy, DTU21MSS adopted a less aggressive filtering strategy to better preserve short-wavelength geoid signals that are typically unrecovered by GRACE and GOCE missions. In coastal zones, where conventional filtering often struggles due to land proximity, an optimal filter was

applied to enhance the accuracy of the ocean signal recovery. In this study, the model for both DTU22MDT and DTUUH22MDT were downloaded from DTU space website at (https://data.dtu.dk/articles/dataset/The_DTU_2022_Mean_Dynamic_Topography_models/26947894) in grid format.

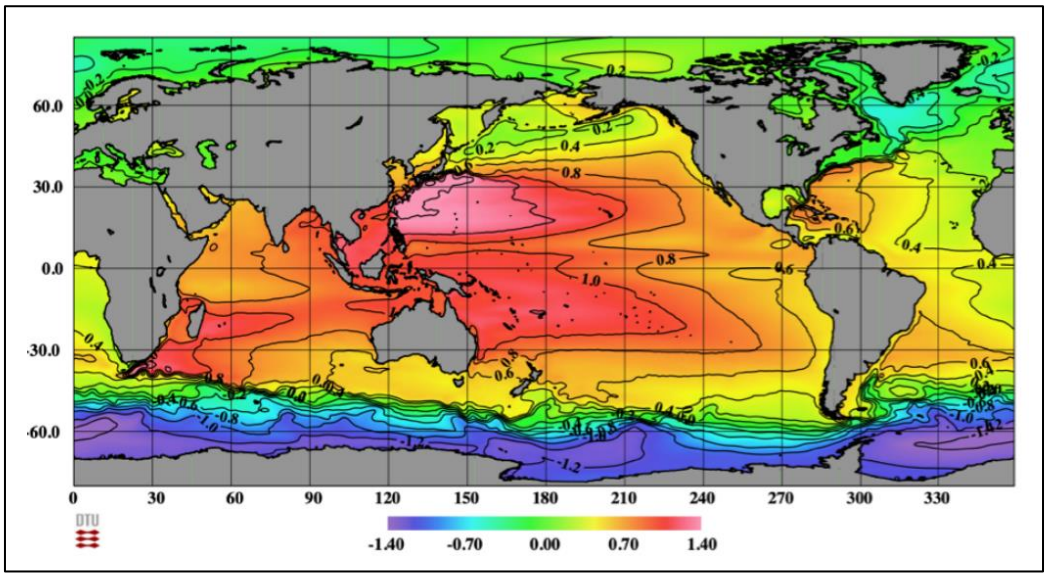


Figure 2. 6 The DTU22 Global MDT Model (Knudsen et al., 2022)

2.3.6.2 DTUUH22MDT

Building upon the development of DTU22MDT, a new MDT model known as DTUUH22MDT was introduced by incorporating mean drifter velocity data into the modelling process (Knudsen et al., 2022). This model was generated using a finite difference approach that allowed for the integration of both MDT heights and mean ocean currents. To minimize noise and better represent spatial variability, the model applied minimum variance and minimum slope constraints. Additionally, special boundary conditions were imposed at coastlines to prevent unrealistic current flows across land. The resulting DTUUH22MDT model includes geostrophic surface currents derived from this enhanced approach. While the general structure of the geodetic and combination models is similar, notable differences can be observed in finer details indicating improved resolution of dynamic changes near the coastline.

2.3.6.3 MDOT

The MDOT model was developed by Nikolai Maximenko of the International Pacific Research Center (IPRC) and Peter Niiler from the Scripps Institution of Oceanography (SIO) and represents a major step forward in understanding global ocean surface circulation (Maximenko et al., 2009). This model provides an estimate of the mean sea surface height relative to the geoid by combining a wide range of observations collected between 1992 and 2022. The dataset includes satellite altimetry, drifter-derived surface currents, wind data from the National Centers for Environmental Prediction (NCEP), and gravity field data from the GRACE mission (Maximenko, 2006; Maximenko et al., 2009). One of the key establishments of MDOT lies in its integration of multiple data sources, which improves accuracy in regions where satellite observations alone may fall short, particularly near boundary currents and in equatorial areas where ocean dynamics are more complex (Rio & Hernandez, 2004). The model was obtained from the official Asia-Pacific Data-Research Center (APDRC) via (https://apdrc.soest.hawaii.edu/projects/DOT/).

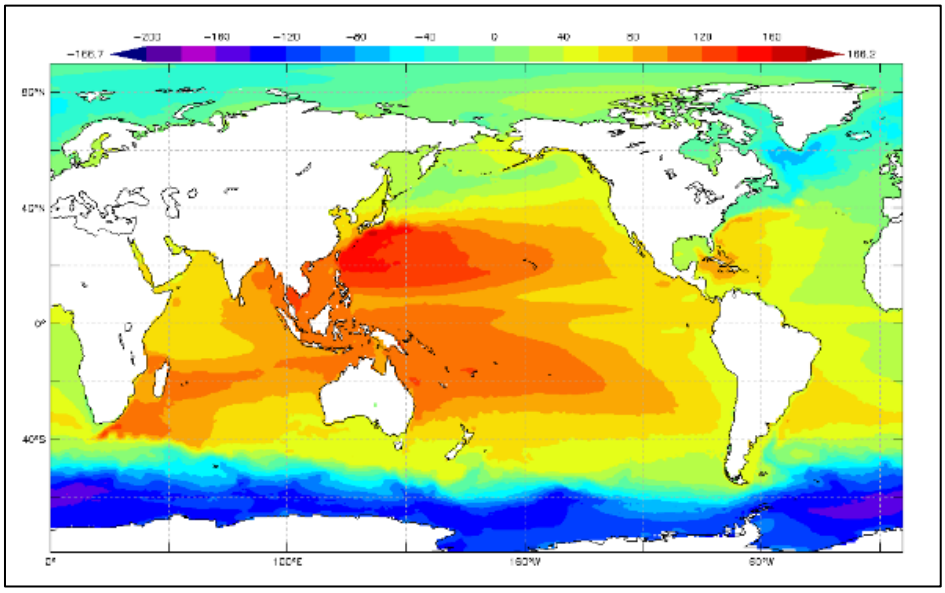


Figure 2. 7 The 1992 – 2002 MDOT Model (Maximenko et al., 2009)

2.3.7 Mean Sea Surface

Since the advent of the first altimetric satellite back in 1975, known as Geodynamics and Earth Ocean Satellite (Geos-3), new avenue of both regional and global Mean Sea Surface (MSS) modelling was expanded (Stanley, 1979). Advancements in MSS modelling using multi-mission satellite altimetry has substantially propelled, beginning with missions such as TOPEX/Poseidon, ERS-1/2, Jason series (Jason-1/2/3) and extending to the most recent SWOT mission. These altimetric satellites have provided a globally consistent, high-resolution, and temporally coherent MSS through the continuous measurement of sea surface height (SSH) for decades (Schaeffer et al., 2012). The MSS constitutes a fundamental geophysical parameter that represents the long-term average SSH measured with respect to a defined reference ellipsoid. It plays an essential role in understanding and monitoring sea level rise, ocean circulation, and climate variability (Guo et al., 2022; Pujol et al., 2018). According to Vestøl et al. (2025), the basis of the MSS model that has been developed were derived from the simple formulation of assimilation of geoid height relative to the ellipsoid (HREF) and mean dynamic topography (MDT) as stated in (2.2).

$$MSS = Geoid + MDT \tag{2.2}$$

At present, several agencies worldwide are still actively engaged in the development and continuous refinement of their altimetric-based MSS products. Among the leading contributors are the Space Research Center at the Technical University of Denmark (DTU), the Centre National d'Études Spatiales and Collecte Localisation Satellites (CNES-CLS) and Shandong University of Science and Technology (SDUST). Currently, DTU has made significant advancements in MSS modelling, with successive versions including DTU10, DTU15, DTU18 and the latest release which is DTU21 as illustrated in **Error! Reference source not found.** (O. A ndersen et al., 2015; O. B. Andersen et al., 2023). Similarly, CNES-CLS has officially released four series of global MSS models: CNES-CLS11, CNES-CLS15, CNES-CLS18, and CNES-CLS22 presented in **Error! Reference source not found.** (Pujol et a l., 2018; Schaeffer et al., 2012, 2023). In parallel, the research team at China specifically

the Shandong University of Science and Technology has released SDUST2020 global MSS model as depicted in Figure 2. 8, following the successful development of an MSS model for the China Seas (Yuan et al., 2023).

2.3.7.1 SDUST2020

SDUST2020 was constructed using a 19-year moving average method, incorporates multi-mission satellite altimetry data, including observations from HY-2A, Jason-3, and Sentinel-3A (Yuan et al., 2023). The model's accuracy was enhanced through a series of advanced processing techniques, such as colinear adjustment of Exact Repeat Mission (ERM) data, ocean variability corrections, multi-satellite crossover adjustments, and least squares collocation (LSC) for gridding. These refinements were implemented during the model's development to enhance its accuracy prior to its official release in early 2023. The SDUST2020 model was acquired online via website (https://zenodo.org/records/6555990) and the data was given in .nc format.

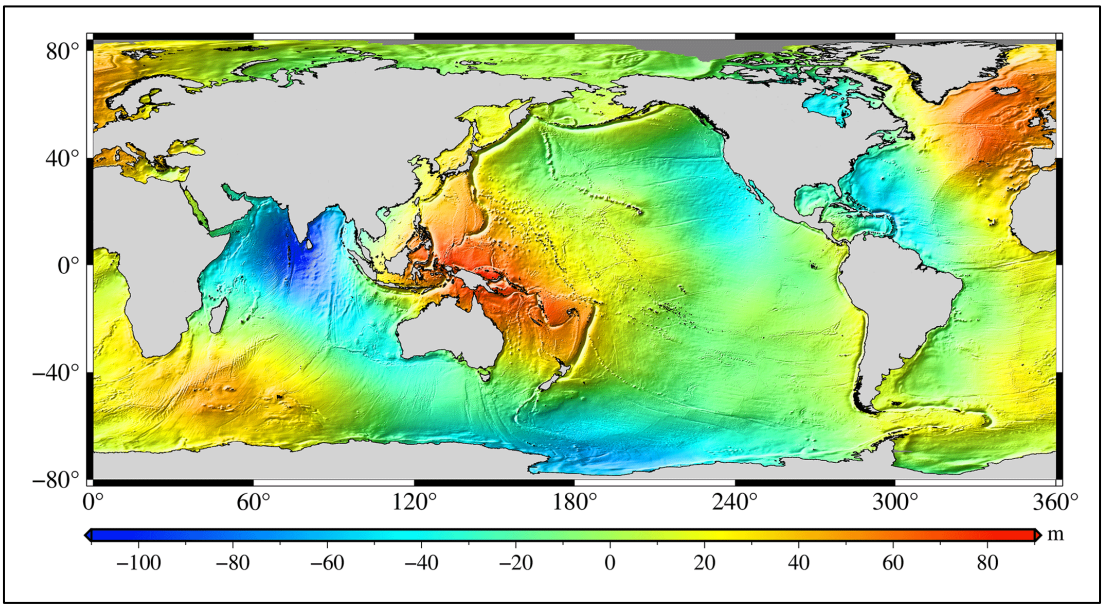


Figure 2. 8 The SDUST2020 Global MSS Model (Yuan et al., 2023)

2.3.7.2 DTU21

The DTU21 model was officially released in 2022 which developed by the Technical University of Denmark as a significant advancement over its predecessors, DTU15 and DTU18 (O. B. Andersen et al., 2023). This model was specifically designed to enhance spatial coverage, data processing, and methodological accuracy. DTU21 integrates over 15 years of satellite altimetry data, including contributions from geodetic missions such as CryoSat-2, Jason-2 LRO, and SARAL/AltiKa, as well as from exact-repeat missions like TOPEX and Jason-1/2. Key improvements include the use of 2 Hz altimetry data, the implementation of advanced two-pass waveform retracking, and refined processing techniques in coastal and polar regions using the SAMOSA+ physical retracker, all of which contribute to its superior performance compared to previous DTU models. The DTU21 model was acquired from DTU space official website at (https://data.dtu.dk/articles/dataset/DTU21_Mean_Sea_Surface/19383221), where the data is in ASCII format.

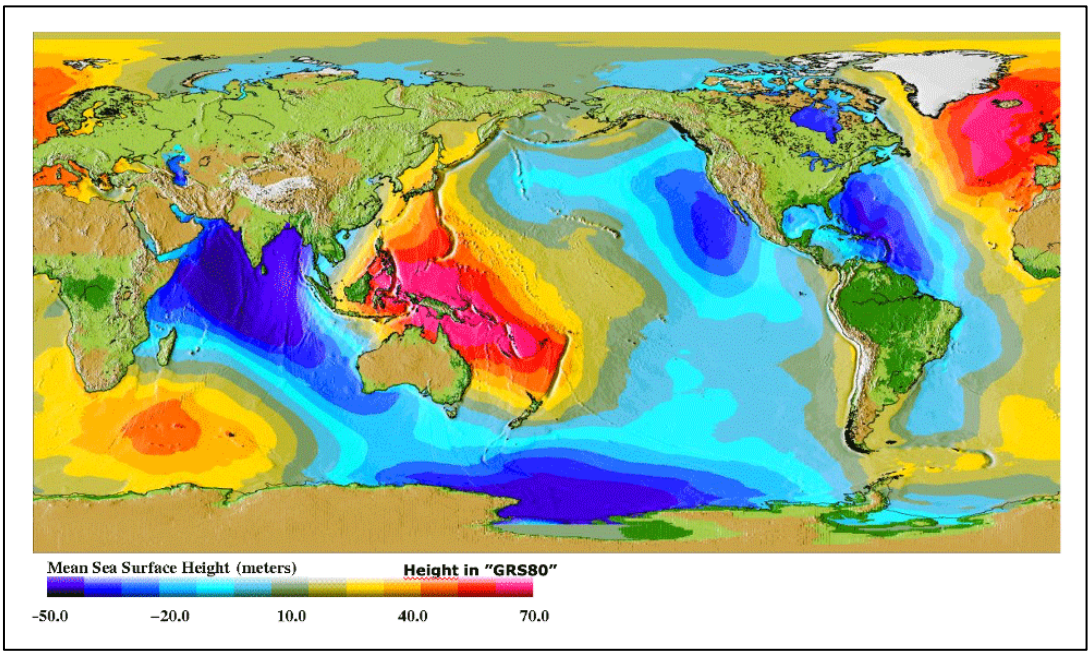


Figure 2. 9 The Developed DTU21 Global MSS Model (O. B. Andersen et al., 2023)

2.3.7.3 CNES-CLS22

The CNES-CLS22 model is a high-resolution MSS product aimed at improving the representation of short-wavelength sea surface features through the incorporation of high-frequency altimetric data. This model employed several advanced techniques, including filtered full-rate altimetry, least squares collocation, corrections for ocean variability and sea surface slope, and the integration of lead-based sea surface height estimates to enhance Arctic coverage (Schaeffer et al., 2023). Validation against Sentinel-3A and ICESat-2 demonstrated that the CNES-CLS22 model reduces short-wavelength MSS errors by up to 40% and improved sea level estimation accuracy by approximately 6% in coastal regions when compared to its predecessor, CNES-CLS15. The CNES-CLS22 model obtained in .nc format through the +AVISO website (https://www.aviso.altimetry.fr/en/data/products/auxiliary-products/mss/mss-global-cnes-cls/mss-cnes-cls2022-description.html).

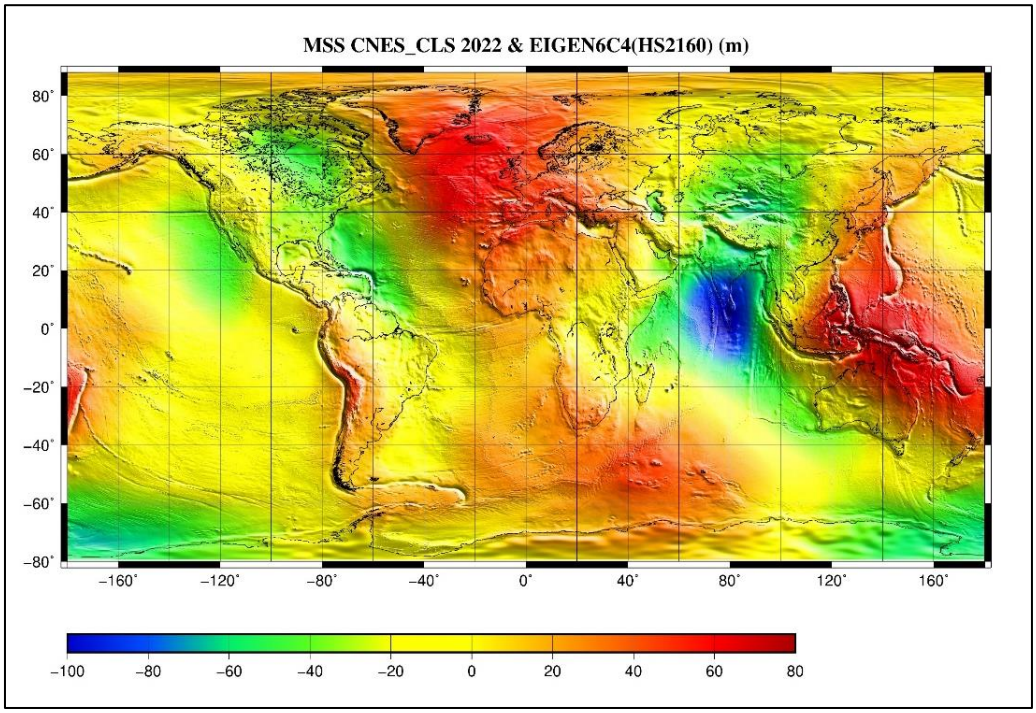


Figure 2. 10 The CNES-CLS22 Global MSS Model (Schaeffer et al., 2023)

This research investigates the feasibility of utilizing those global MSS models to derive tidal datums specifically the LAT and HAT that referenced to the ellipsoid. Referencing tidal datums to the ellipsoid can significantly improves the spatial continuity and consistency of vertical datums across the land-sea interface where the existence of MSS models makes the computation easier (Mills & Dodd, 2014). However, the performance of each MSS model may vary geographically, as regional differences in oceanographic conditions and data coverage can influence the model accuracy. Therefore, it is essential to evaluate the compatibility of each MSS model within the specific study region to determine the most suitable option. This necessity arises from the fact that MSS models are developed using different methodologies, reference frames, and correction strategies, which may not capture the actual sea surface characteristics uniformly across all regions (International Hydrographic Organization (IHO), 2020).

2.4 Marine Gravity Data

2.4.1 DTU21GRA

Since 1997, Technical University of Denmark (DTU) under leadership of Andersen and Knudsen has played a pioneering role in the development of global marine gravity field models derived from satellite altimetry as part of a project known as KMS96 (O. B. Andersen et al., 2005). Over time, new models such as DTU13GRA, DTU15GRA and DTU17GRA were developed by the including additional satellite altimetry data from Cryo-Sat2 and used EGM2008 as a reference field model to increase the accuracy and precision of the models (Abdallah et al., 2022b). The improvements in temporal coverage, spatial resolution, and filtering techniques progressively enhanced the fidelity of marine gravity anomalies particularly in areas with sparse shipborne gravity coverage. The most recent model released namely DTU21GRA, integrates five additional years of Sentinel-3A observations, three years of Sentinel-3B data, and reprocessed CryoSat-2 data, all contributing to improved accuracy in both open ocean and coastal regions (Y. Wu et al., 2022).

2.4.2 Sandwell and Smith Model

The Sandwell and Smith global marine gravity model was first developed in 1997, introduced a method for deriving marine gravity anomalies from satellite altimetry by analysing sea surface slopes (D. Sandwell & Smith, 1997). Since then, the model has undergone substantial refinement. The early versions such as V21 and V22 focused on integrating ERS-1 and Geosat data to produce 1-minute global grids of free-air gravity anomalies (D. T. Sandwell & Smith, 2009). Subsequent versions have incorporated data from additional satellite missions, improved waveform retracking algorithms, and more sophisticated filtering and masking techniques. The latest version is Grav 32.1 which has been released in 2022 incorporates over a decade of enhancements and includes 12 additional months of AltiKa, CryoSat-2 LRM/SAR and Sentinel-3A/B data (D. Sandwell et al., 2014). Several key improvements distinguish this version from its predecessors:

i) Waveform retracking was applied to reduce significant wave height (SWH) noise by decreasing the smoothing filter scale from 45 km to 30 km.
ii) Sea state bias corrections were optimized for all altimeters.
iii) A refined land/ocean mask was implemented to eliminate data within 3 km of coastlines, minimizing land contamination.
iv) Low-pass filters were updated, with east and north vertical deflection components smoothed using a 10 km filter (previously 16 km), enhancing resolution, and preserving short-wavelength gravity features.

This model represents a continued effort to refine satellite-derived gravity anomaly datasets, offering improved accuracy for applications in oceanography, geophysics, and marine geodesy. As satellite altimetry technology continues to evolve, future versions will likely yield even greater accuracy and resolution, which aligns with the objectives of this study in investigating dataset in refining the geoid model over marine regions.

2.4.3 SDUST2022GRA

The SDUST2022GRA is a marine gravity anomaly developed by Shandong University of Science and Technology (SDUST) in 2024. The uniqueness of this model lies in its derivation method that uses radar and ICESat-2 laser altimetry in determination of the gravity anomalies data, which previously underutilized in global gravity recovery efforts (Li et al., 2024). Traditionally, marine gravity anomalies have been inferred from radar altimetry by exploiting along-track SSH gradients to estimate deflections of the vertical (DOV). While radar altimetry offers broad ocean coverage, it suffers from directional bias due to the predominantly north–south orientation of satellite orbits, leading to an imbalance between the northward and eastward DOV components (D. Sandwell & Smith, 1997; Hwang et al., 2002). This anisotropy limits the accuracy of gravity anomaly recovery, particularly in coastal and high-latitude regions where radar observations are sparse or degraded due to surface roughness, sea-ice contamination, and reduced orbital coverage. In order to overcome those limitations, SDUST2022GRA introduced an innovative cross-track geoid gradient (GG) retrieval scheme using ICESat-2 multiple-beam laser altimetry. This configuration not only enriches spatial sampling but also enhances coverage in challenging environments. Methodologically, the model employs least-squares collocation (LSC) to fuse geoid gradients from multiple satellite missions, weighting each dataset based on empirically derived error variances. Additionally, SDUST2022GRA also benefits from rigorous pre-processing of ICESat-2 ATL12 data which includes re-referencing ocean tide corrections using the high-resolution FES2014 model to ensure consistency across altimeter datasets. Notably, this model demonstrated a RMSE of 4.43 mGal to 5.07 mGal when validated against seven million global shipborne observations (Li et al., 2024). In summary, SDUST2022GRA represents a new generation of marine gravity models that is developed from the hybridization of radar and laser altimetry which underscores the strategic importance of ICESat-2 in addressing historical deficiencies in global gravity datasets especially across previously neglected or problematic regions. Therefore, this model is adopted in this study to assess its performance on refining the marine geoid model in Peninsular Malaysia.

2.4.4 NSOAS24

National Satellite Ocean Application Service (NSOAS24) is marine gravity product which was recently released by China in 2024. NSOAS24 represents a significant advancement that addresses the limitation of its predecessor known as NSOAS22, in terms of boundary discontinuity and noise amplification in coastal and high-latitude regions (Zhang et al., 2025). Unlike the earlier model that relied heavily in legacy of satellite data, NSOAS24 integrates high resolution SSH and DOV derived from multi mission satellite altimetry including HY-2A/B, CryoSat-2. SARAl/AltiKa and Jason series (X. Chen et al., 2024). These datasets were meticulously processed through waveform retracking, resampling, filtering and quality control measures before being gridded into 1′×1′ resolution using a Green's function-based interpolation method. One of the core innovations in NSOAS24 lies in its spline-based Green's function method, which effectively minimizes signal noise through directional gradients and tension constraints. This approach enhances the spatial continuity and smoothness of the gravity field in complex and nearshore environments. The performance of NSOAS24 has been rigorously evaluated against benchmark gravity models such as DTU21 and Scripps/SIO V32.1, as well as independent shipborne gravity datasets from various sources. Based on the evaluation results, NSOAS24 indicated a better accuracy than its predecessor (NSOAS22) with reduction of standard deviation of marine gravity anomalies by up to 1.2 mGal in some areas. Notably, the accuracy of NSOAS24 is comparable to other satellite-derived marine gravity dataset such as DTU21 and making it a reliable for option as marine gravity data in geoid computation (Zhang et al., 2025).

The comparison of satellite-derived marine gravity datasets stated in Table 2. 4 is representing different generations of satellite-derived gravity modelling techniques, ranging from established benchmark products to more recent solutions with improved altimetry coverage and processing methods. The comparison provides a basis for assessing their consistency, resolution, and suitability for marine geoid refinement in Peninsular Malaysia.

Table 2. 4
Literature Summary of Satellite-Derived Marine Gravity Model

Author	Model	Institution	Year	Data Source	Methodology	Main Strengths	Limitations
Y. Wu et al. (2022)	DTU21GRA	DTU Space, Denmark	2021	Sentinel-3A/B, CryoSat-2, previous altimetry missions	Marine gravity anomalies derived from multi-mission satellite altimetry using improved retracking and processing techniques	Improved coastal and open-ocean gravity recovery through incorporation of recent altimetry observations. Long development history and extensive validation.	Performance may decrease in regions with complex coastal morphology and limited altimeter coverage.
D. Sandwell et al. (2014)	Sandwell and Smith V32.1	Scripps Institution of Oceanography (SIO)	2022	AltiKa, CryoSat-2, Sentinel-3A/B, Geosat, ERS series	Gravity anomalies estimated from sea surface slopes and vertical deflections derived from satellite altimetry	Considered the benchmark global marine gravity model. Improved waveform retracking, sea-state bias correction, coastal masking, and shorter filtering scales enhance short-wavelength gravity recovery.	Radar-altimetry-derived gravity may exhibit directional bias due to orbit geometry.
Li et al. (2024)	SDUST2020 GRA	Shandong University of Science and Technology (SDUST), China	2024	Radar altimetry and ICESat-2 laser altimetry	Fusion of geoid gradients and deflections of the vertical using Least Squares Collocation (LSC)	First global marine gravity model integrating ICESat-2 laser altimetry. Improved performance in coastal, high-latitude, and poorly surveyed regions. RMSE of approximately 4.43–5.07 mGal against shipborne gravity observations.	Relatively new product with limited application and validation in Southeast Asian waters.
Zhang et al. (2025)	NSOAS24	National Satellite Ocean Application Service (NSOAS), China	2024	HY-2A/B, CryoSat-2, SARAL/AltiKa, Jason series	Spline-based Green's function interpolation using SSH and DOV observations	Improved spatial continuity and reduced noise compared to NSOAS22. Demonstrates accuracy comparable to DTU21 and SIO V32.1, particularly in coastal regions.	Long-term performance and independent validation remain limited due to recent release.

2.5 Tidal

2.5.1 Tidal Constituent

Tidal constituents refer to parameters of periodic components, which can be their frequencies, amplitudes, phases, or speeds (National Oceanic and Atmospheric Administration, 2000a). Each tidal constituent symbolizes a periodic change or fluctuation of water level resulting from gravitational interactions relative to the position of Earth, Moon, and Sun. The derivation of tide prediction usually requires three types of constituents: semi-diurnal constituents, diurnal constituents, and long-term constituents (Annunziato & Probst, 2016). These comprehensive elements are crucial for precise tidal modelling and forecasting, especially in areas characterized by intricate coastal geometries and bathymetry. This research, however, implemented four constituent parameters for each type of constituents as tabulated in Table 2. 5, Table 2. 6, and Table 2. 7.

Table 2. 5
Selected Semi-Diurnal Harmonic Constituents (IHO, 2006)

Abb.	Constituent	Solar Period (Hours)	Descriptions
M_2	Principal Lunar	12.42	The semi-diurnal constituent dominated by fictitious gravitational pull of the moon, which moves in a circular orbit in the plane of the equator.
S_2	Principal Solar	12.00	The semi-diurnal constituent dominated by the gravitational pull of mean sun, which moves in a circular orbit in the plane of the equator.
N_2	Larger Lunar Elliptic	12.66	The semi-diurnal constituent that modulated the M2 components due to the elliptical orbit of the moon in the plane of the equator.
K_2	Luni-Solar	11.97	The semi-diurnal constituents that combined gravitational force of the moon and sun due to the shared frequency between Solar K_2 and Lunar K_2, modulated by the S_s.

Table 2. 6
Selected Diurnal Harmonic Constituents (International Hydrographic Organization (IHO), 2006)

Abb.	Constituent	Solar Period (Hours)	Descriptions
K_1	Luni-Lunar	23.93	The major diurnal constituent modulated the M_2 in converting the orbit from the plane of the equator into the mean plane of the real moon.
O_1	Principle Lunar	25.82	The diurnal constituents dominated by fictitious moon which has a fixed circular orbit in the mean plane of the real moon.
P_1	Principal Solar	24.07	The diurnal constituent that dominated by the fictitious sun which has a circular orbit in the ecliptic plane to facilitate diurnal tidal pattern.
Q_1	Larger Lunar Elliptic	26.87	The diurnal constituents that modulated the K_1 and O_1 due to the ecliptic orbit of the moon.

Table 2. 7
Selected Long-Term Harmonic Constituents (International Hydrographic Organization (IHO), 2006)

Abb.	Constituent	Solar Period (Hours)	Descriptions
M_f	Lunar Fortnightly	327.9	The long-term lunar constituents with a fortnight period due to the moon's orbit around the earth that accounts for the departure from the sinusoidal declination.
M_m	Lunar Monthly	661.3	The long-term lunar constituent due to the monthly lunar cycle and accounts for the irregularities in the rate of change of distance and speed.
S_{sa}	Solar Semi-Annual	4383	The long-term solar constituent due to the earth's orbit around the sun approximately about six months accounts the variability in the declination factor.
S_a	Solar Annual	8766	A long-period solar constituent related to Earth's annual orbit and varying distance from the Sun. It has small amplitude and indistinguishable from mean sea level changes caused by winds and monsoon effects.

2.5.2 Tidal Prediction

Tidal prediction usually based upon the derivation of harmonic tidal constituents over a specific period of time. According to Schureman (1994), tides are a system that exists due to the astronomical phenomena primarily driven by the gravitational cycle and motion of the earth, sun, and moon. However, although linear superpositions of harmonic constituents can represent the elemental tidal force, the reality is more

complex due to physical phenomena such as coastlines' shape or ocean depth. In order to cater for the nonlinear nature of the tidal system, the process of tidal prediction adopted various frequencies consisting of the sums, differences, and harmonic to approximate the actual behaviour of tides for more accurate prediction of the tides (Schureman, 1994). The illustration as depicted in Figure 2. 11 is the example of tidal prediction that was derived from varies major constituents defined by differing frequencies to facilitate more accurate tide prediction (National Oceanic and Atmospheric Administration, 2000a). Tidal predictions can be customized to suit different durations depending on the needs of various applications whether they be monthly, annual, or long-term prediction. Monthly tidal predictions are predominantly utilized to aid activities in navigation, fisheries, and aquaculture sectors, where accurate short-term data is crucial for operational planning and safety. Annual tidal predictions, on the other hand, play a significant role in broader and more strategic areas such as climate change studies, tourism planning, and coastal management. Researchers investigating climate patterns and their impacts on sea levels and coastal ecosystems benefit from annual data to observe trends and make predictions. Long-term tidal predictions, derived from observations exceeding 18.6 years, are essential for the computation and development of tidal datums.

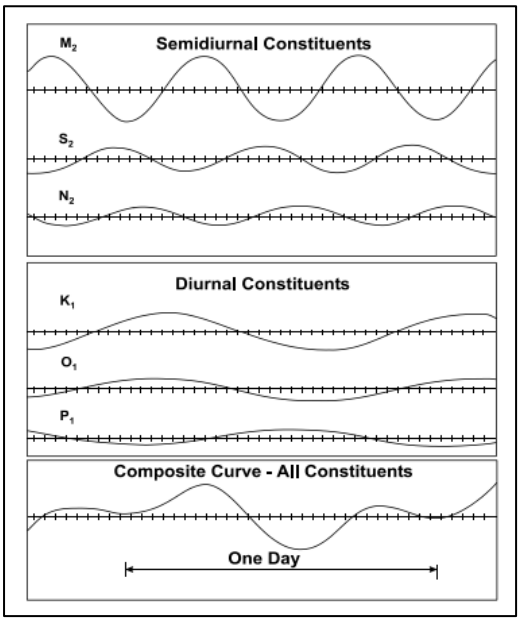


Figure 2. 11 Harmonic Constituents in Tidal Prediction (National Oceanic and Atmospheric Administration, 2000a)

2.5.3 Harmonic Analysis

Harmonic analysis is a fundamental mathematical process that decomposes complex signals into simpler components to study periodic phenomena. In the context of tidal derivation, the classical definition, according to Boon & Kiley (1978) indicates that harmonic analysis involves identifying and quantifying the principal harmonic constituents that contribute to the observed tidal behaviour. It can also define as the mathematical method used to break down the observed tide or tidal current at a given location into fundamental harmonic components (International Hydrographic Organization (IHO), 2006). Historically, the method of tide reduction using harmonic was first devised by an Irish physician and mathematician known as Sir William Thomson (Lord Kelvin) in 1867 (Schureman, 1994). The process of harmonic analysis involves the process of interpreting the signals or frequencies from various periodic components of tides referred to as harmonic tidal constituents, as previously listed in Table 2. 5, Table 2. 6, and Table 2. 7. It is essential for distinguishing the various periodic components of tides to simulate the astronomical tide accurately. Each of these components represents a specific frequency and amplitude, capturing different periodic influences on the tides reflects a particular aspect of these forces, such as the lunar day or solar day cycle used to predict the height and timing of tides for future periods (Boon & Kiley, 1978). This research uses this method to derive the tidal datum encompassing the LAT and HAT for Peninsular Malaysia through satellite altimetry and hydrodynamic modelling. Subsequently, the basis computation of harmonic analysis derived from the formula stated in Equation (2.2).

$$X(t) = H_n \, COS \, (\sigma_n t - \, g_n) \tag{2.2}$$

In this context, X represents the value of a variable quantity at a specific time t. The term H_n indicates the amplitude of oscillation, while g_n refers to the phase lag. Additionally, σ_n denotes the angular speed. The process of analysis determines the amplitudes and phase lags, which are crucial parameters for defining the tidal regime at the particular location being observed. These parameters provide a comprehensive understanding of how the tides behave over time at that specific site.

2.6 Gravimetric Geoid Computation Method

Over the years, several approaches have been developed for gravimetric geoid determination, including the Remove-Compute-Restore (Forsberg, 1991), Stokes-Helmert Scheme (Vaníček & Martinec, 1994), Ellipsoidal Bruns' Formula (Ardalan & Grafarend, 2001) and Least Square Modification of Strokes formula with Additive Correction (LSMSA)(Sjöberg, 2003b, 2005). Among these methods, the RCR and LSMSA approaches have gained widespread application in geoid modelling studies worldwide, including in Malaysia due to their adaptability to heterogeneous data environments and compatibility with modern global geopotential models and high-resolution terrain data. This adaptability is particularly important in regions where gravity observations are unevenly distributed and where data quality may vary between land, marine, and satellite-derived sources.

The RCR technique has become one of the most established methodologies for regional gravimetric geoid and quasi-geoid determination. The fundamental principle of the method involves removing the long-wavelength component represented by a GGM and the short-wavelength terrain effects from the gravity observations. The residual gravity field is then used in the geoid computation process, which subsequently restoring the removed components to obtain the final geoid model (Forsberg, 1991). This strategy reduces spectral inconsistencies between datasets and enables a more efficient integration of gravity observations at different spatial scales. Due to its robustness and proven performance, the RCR approach has been extensively employed in regional geoid modelling projects worldwide, including applications in Malaysia (Jamil et al., 2017), Kuwait (Al-Ajami et al., 2022), Korea (Lee & Kwon, 2022), Sudan (Osman & Anjasmara, 2023), Greece (Fotopoulos et al., 1999) and Albania (Natsiopoulos et al., 2026).

Least Squares Modification of Stokes' Formula with Additive Corrections (LSMSA) also known as KTH method was developed at the Royal Institute of Technology (KTH), Sweden. This method is mainly advantageous in terms of the simplicity of the combined topographic effect of geoid without having to be concerned about the involvement of any related terrain effect, whether direct or indirect. This method implements the use of least squares to reduce the influence of ambiguity of error sources for such data of gravity, GGM and GDEM (Sjöberg, 2003c). Fundamentally,

the KTH method applies to using unreduced gravity anomalies to produce approximate geoid height, which is not influenced by the reduction of the earth's topographic masses (Ssengendo, 2015). According to L. Sjöberg (2003b) , the removal or reduction of topographic masses is not strictly specified but relatively independently free of choice of the technique due to the application of addictive correction in this method to obtain final geoid height. Owing to these advantages, KTH has gained considerable recognition as an alternative approach for gravimetric geoid determination and has been successfully implemented in numerous countries, including New Zealand (Abdalla & Tenzer, 2011), Latvia (Janpaule, 2014), Uganda (Sjöberg et al., 2015a), India (Goyal et al., 2021), East Malaysia (Othman et al., 2024), West Malaysia (Talib & Sulaiman, 2016; Pa'Suya et al., 2018; Azmin et al., 2024; Zamri et al., 2025), Kazakhstan (Shoganbekova et al., 2025) and Indonesia (Oktavia & Heliani, 2026).

In Malaysia, the current official national geoid model is primarily based on the RCR framework (Cob et al., 2022). However, despite its successful application, the RCR method addresses major error sources such as truncation errors, gravity anomaly errors, and GGM omission errors individually rather than optimising them simultaneously within a single framework. In contrast, KTH method provides a more rigorous alternative from a theoretical perspective. It explicitly incorporates a least-squares optimisation strategy that simultaneously balances truncation errors, gravity data errors, and GGM errors in a unified formulation, leading to a statistically optimal solution for geoid height estimation (Ssengendo, 2015). While the RCR method continues to serve as the foundation of the current Malaysian national geoid because of its well-established workflow and widespread application, recent studies have highlighted the advantages of the KTH approach. The KTH method is recognised for its ability to manage multiple error sources more effectively and provide greater numerical stability, particularly in regions with limited gravity data coverage or varying data quality.

A number of studies have compared the performance of the KTH and RCR approaches in the computation of their regional geoid model as summarized in Table 2. 8. Early investigations by Abbak et al. (2012) in Turkey and Yildiz et al. (2012) in the Auvergne region reported that the KTH method achieved lower geoid height discrepancies than the RCR approach, indicating improved modelling accuracy. Similar

findings were later reported in Northeast China by Zhong et al. (2024), where both the traditional and modified implementations of the RCR method were evaluated against the KTH solution. The results indicates that KTH method able to produce slightly superior results against traditional RCR and similar accuracy with the modified RCR. Studies conducted in Southeast Asia also demonstrated the potential of the KTH approach. A study in Klang Valley, Malaysia by Ming et al. (2021) and in East Kalimantan, Indonesia by Sukma and Leni (2024) reported that the KTH method significantly outperformed the RCR method.

However, the superiority of one method over the other is not universal. The study in Republic of Croatia (Varga et al., 2018) and in Jilin Province, China (Wu et al., 2020), recorded that the RCR method produced marginally better results than the KTH approach. Similarly, Prijatna et al. (2024) reported a slight advantage of the RCR method over the KTH method for geoid determination across Java Island, Indonesia. These contrasting findings suggest that the performance of both methods is influenced by factors such as gravity data quality, terrain characteristics, data coverage, and the selection of computational parameters. Overall, the majority of comparative studies indicate that the KTH method is capable of achieving accuracy that is comparable to or better than the RCR approach, particularly when dealing with heterogeneous gravity datasets and complex topographic conditions. Given that the current Malaysian national geoid was developed using the RCR method, further investigation of the KTH approach is warranted to assess its suitability and potential advantages for future geoid refinement in Malaysia.

Table 2. 8
Comparison of Accuracies between KTH and RCR Method in Geoid Computation

Author	Region	KTH	RCR
Abbak et al. (2012)	Turkey	6.7 cm	9.8 cm
Yildiz et al. (2012)	Auvergne	2.4 cm	3.0 cm
Varga et al. (2018)	Republic of Croatia	3.9 cm	3.5 cm
Wu et al. (2020)	Jilin Province, China (Plain Area) (Mountain Area)	 2.9 cm 2.4 cm	 2.5 cm 2.0 cm
Ming et al. (2021)	Klang Valley, Malaysia	0.7 cm	3.1 cm
Zhong et al. (2024)	Northeast China	2.3 cm	3.6 cm (Traditional) 2.2 cm (Modified)
Sukma & Leni, (2024)	East Kalimantan, Indonesia	5.3 cm	7.8 cm
Prijatna et al. (2024)	Java Island, Indonesia	9.2 cm	8.4 cm

2.7 Satellite Altimetry Techniques

Fundamentally, derivation of tidal datums were made based on the sea level observation recorded at tide gauges. However, the limitation exists as tide gauge stations are limited has a small coverage as the derivation of tidal datum can only be made accurately within specific distance, approximately 10 kilometres due to the changes of sea characteristics (Abd Rahman et al., 2024). In a broader range of tidal datum determination, other alternative should be adopted. In regards with the limitations, the technology of satellite altimetry radar has shed the lights for its capability to deliver a global, continuous, and remotely precise measurements of sea level referenced to a specific geodetic reference frame across different time periods and using various altimeter sensors. (Grgić & Bašić, 2021). A variety of altimeter satellite missions have consistently provided reliable and accurate sea level data and the implementation of this technology has facilitate numerous applications in fields such as

geodesy, oceanography, and climate research. The advent of satellite altimetry has revolutionized the observation of global ocean tides, especially in the open ocean. Enhanced techniques for precise orbit determination, alongside improved instrumental and geophysical corrections, have significantly increased the accuracy of sea surface height (SSH) measurements since the launch of the TOPEX/Poseidon mission (Fok, 2012).

2.7.1 Concepts of Satellite Altimetry Measurements

The history of the satellite altimeter (SALT) mission was first laid during the 1969 NASA's Williamstown Conference on Solid Earth and Ocean Physics (Kaula, 1966). It was subsequently developed through experimental missions such as Skylab (G. S. Brown, 1977), the Geodynamics Experimental Ocean Satellite 3 (GEOS-3) (Stanley, 1979), and the SEAfaring SATellite (SEASAT) (Shum et al., 1993). The successful implementation of the experiments has led to rapid advancements in the launch of SALT. The concept of SALT measures the sea surface height (SSH) based on the travel time of the microwave signal emitted by the satellite to the sea surface and back, combined with known microwave power (Hamden, 2022). This data, along with the satellite's three-dimensional position relative to a geocentric coordinate system obtained through independent tracking methods allows for calculating sea level profiles relative to the ellipsoid. The primary measurements from SALT include the range of the satellite above the water surface and its altitude relative to the ellipsoid, known as orbital height. The altimeter on the satellite emits short pulses of radiation and measures the travel time of the signal reflected from the sea surface to determine sea surface height accurately (Fok, 2012). According to Grgić and Bašić (2021), the measurement to derive the distance between the satellite and the sea surface can be expressed through the formula as expressed in Equation (2.3).

$$\hat{R} = \frac{ct}{2} \tag{2.3}$$

where $\hat{R}$ is typically the range from the round-trip time travel without accounted with the refraction and c is the speed of light in vacuum. After applying the corrections to the measurements, the basic equation can be modified to present the corrected range R using the following Equation (2.4):

$$R = \hat{R} = \sum_j \Delta R_j = \hat{R} - \left(\Delta R_{tropoD} + \Delta R_{tropoW} + \Delta R_{iono} + \cdots\right) \quad (2.4)$$

where the $\Delta R_j, j = 1, \ldots$ is the sum of atmospheric and technology corrections applied to the signal pulse, ΔR_{tropoD} is the dry tropospheric correction, ΔR_{tropoW} denotes the wet tropospheric correction, ΔR_{iono} represents the ionospheric correction and other sequences of the corrections as listed in. Additionally, the accuracy of determining sea SSH depends directly on the accuracy of these corrections applied to $\hat{R}$. If the atmospheric correction values are not precise, the calculated sea surface height will be less accurate. Subsequently, direct derivation of SSH with respect to the ellipsoid surface as be computed using the Equation (2.5).

$$SSH = h_{OR} - R = h_{OR} - \hat{R} + \sum_j \Delta R_j \quad (2.5)$$

where h_{OR} is the pre-defined orbit of satellite that computed using a fixed coordinate relative to reference ellipsoid from the measured range R. Figure 2. 12 is the illustration of the measurement concept of satellite altimeter data in remotely capturing the SSH.

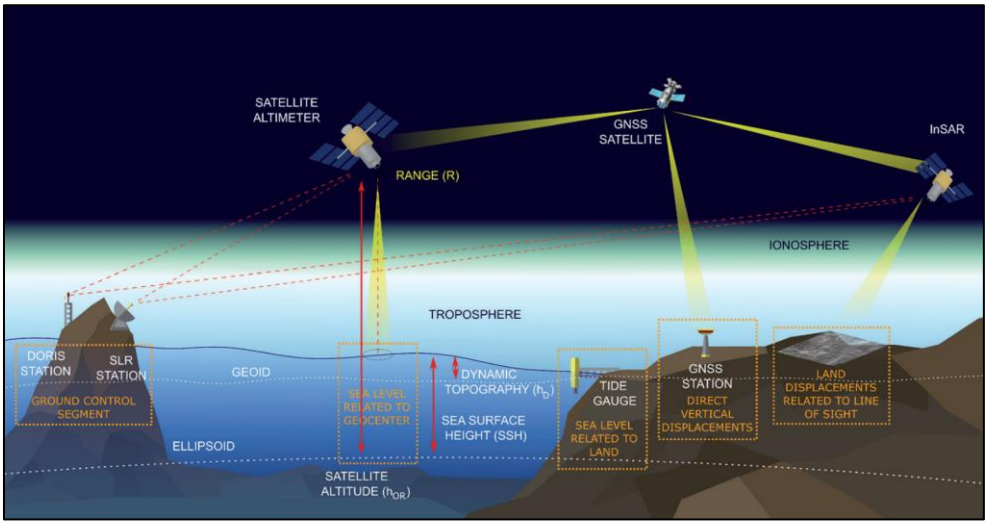


Figure 2. 12 Concept of Satellite Altimeter Measurements (Grgić & Bašić, 2021)

2.7.2 Corrections to Satellite Radar Measurements

Direct altimetry measurement from earth orbiting platform required several corrections to achieve the desirable sea surface or land surface topography measurements. According to Tapley and Rosborough (1985), orbit's error is the most significant source of error in satellite altimetry. Thus, correcting the orbit errors is crucial to accurately determine the satellite's altitude relative to the Earth's surface (above the reference ellipsoid). These corrections ensure that the altitude measurements are precise before deriving SSH free from the bias. It is essential to apply both media corrections to correct for measurement and environmental factors and geophysical corrections to adjust for Earth system dynamics. These corrections ensure that the altimeter height measurements reflect true variations in sea surface height rather than being affected by systematic errors or environmental influences. Table 2. 9 and Table 2. 10 is the information of corrections applied in the satellite altimetry data.

Table 2. 9
Summary of Media Corrections in Satellite Altimeter Radar

Media Correction	
Dry Troposphere	The dry troposphere correction addresses the delay in radar signals resulting from the presence of dry atmospheric gases, primarily nitrogen and oxygen. This delay is directly related to atmospheric pressure and can be accurately corrected using models like the one developed by (Saastamoinen, 1972). The formula of the dry troposphere correction is as follow: $\Delta h_{dry} = -0.2277 P_0 (1 + 0.0026 \cos 2\emptyset)$ (2.6) The variable P_0 is the sea level pressure in hector Pascal (hPa), $\emptyset$ denotes the latitude for standard gravity at the observation point to account for the earth's oblateness.
Wet Troposphere	The wet tropospheric correction is an adjustment made to account for the effects of water vapor in the troposphere on satellite altimeter measurements. According to Tapley and Rosborough (1985), water vapor can cause delays in the radar signals used by the altimeter, which need to be corrected using formula as expressed in (2.7): $\Delta h_{wet} \approx 636 \left(\frac{cm^3}{g}\right) \int \sigma_{vap}(z) dz$ (2.7) where $\sigma_{vap}(z)$ is the vertical integration of water vapour density in g/cm^3.

Ionosphere	The ionosphere delay is a frequency-dependent correction affecting satellite altimeter measurements due to the ionized layer of the atmosphere, the ionosphere. This layer impacts radar signals differently depending on their frequency which can range from 5 cm to 20 cm in the frequency domains around 14 Hz (Lorell et al., 1982). The correction for this delay can be computed using the following formula in Equation (2.8). $$\Delta R_{ion} = \frac{kTEC}{f^2} \quad (2.8)$$ where ΔR_{ion} is the ionospheric correction, k is a fixed od 0.40250 GHz^2 per unit of TEC. TEC represents the total number of free electrons integrated along the path of the radar signal and f denotes the radar frequency.
Sea State Bias	Sea state bias correction addresses the influence of ocean surface roughness on radar signal reflection, encompassing factors such as wave height and wind speed that affect the altimeter's readings. A progressive parametric model incorporating four parameters has been developed to define the SSB correction using the expressed Equation (2.9). $$\Delta h_{SBB} = SWH\ (a_1 + a_2 U + a_3 U^2 + a_4 SWH) \quad (2.9)$$ where SWH represents the wave height, U is the derived wind speed from backscatter coefficient and a_1, a_2, a_3, a_4 represent the set of coefficients.

Table 2. 10
Summary of Geophysical Corrections in Satellite Altimeter Radar

Geophysical Correction	
Atmosphere Barotropic	Atmosphere Barotropic correction, also referred to as the inverse barometer effect, adjusts for fluctuations in sea level caused by changes in atmospheric pressure. The correction is applied to eliminate the influence of ocean surface deformation caused by atmospheric loading (Ponte, 2006). The correction can be estimated from surface pressure using Equation (2.10). $$\Delta h_{DAC} \approx -0.99484\ (P_0 - P_{ref}) \quad (2.10)$$ where P_0 is the dry tropospheric correction, P_{ref} and represents the global mean pressure.
Solid Earth Tide	Solid Earth tide correction compensates for the deformation of the Earth's crust caused by gravitational forces from the moon and the sun (Munk & MacDonald, 1961). The correction for ocean tides in satellite altimetry accounts for the elastic deformation of the Earth, assuming a uniform mass density. This deformation is characterized using Love numbers, which describe how the Earth responds to tidal forces. Despite tidal forces causing changes in sea level amplitude, these variations typically amount to less than 1 mm is considered negligible in altimetry measurements that aim for precision levels better than 2 cm (Fok, 2012).

2.8 Development of Vertical Transformation Model

2.8.1 Conceptual Relationship Between MSS and MSL

Theoretically, MSL and MSS hold a similar concept but they are derived from different observations system and therefore do not represent identical physical surfaces. The geodetic approach provides an effective means of determining the long-term sea level surface by integrating satellite observations, GNSS measurements, and tide gauge observation. Within this framework, the sea surface can be represented either by a MSS model derived from satellite altimetry or by MSL observations obtained from tide gauge stations (O. B. Andersen et al., 2018). When tide gauge measurements are combined with co-located GNSS observations, the local MSL can be expressed as an ellipsoidal height and directly related to global geodetic reference systems. The relationship between MSL and MSS is as illustrated in Figure 2. 13.

Satellite altimetry determines the sea surface height by measuring the distance between an orbiting satellite and the ocean surface. After applying the necessary corrections, repeated observations collected over an extended period are averaged to produce an MSS model (Yuan et al., 2023). In contrast, MSL is obtained from continuous water-level measurements recorded at tide gauge stations and represents the average sea level at a specific coastal location over a defined time period (Adebisi et al., 2021). Although MSS and MSL originate from different observation techniques, both describe the long-term average value of the sea surface. Once referenced to a common ellipsoid and tide system, MSS and MSL can be considered equivalent representations of mean sea level (O. B. Andersen et al., 2018). Consequently, MSS is frequently adopted in regional and global studies where spatially continuous sea-level information is required.

The selection of MSS is further supported by the characteristics of the hydrodynamic dataset employed in this research. The tidal datums incorporated within the hydrodynamic model are derived from global ocean tide models, which are themselves developed using long-term satellite altimetry observations combined with numerical ocean modelling and other auxiliary datasets (Shoganbekova et al., 2025). Although MSS and MSL are not strictly identical due to the influence of local coastal processes, ocean circulation, and dynamic topography,both quantities describe the long-

term average position of the sea surface. When referenced to the same ellipsoid and tide system, MSS can serve as a practical approximation of MSL, particularly in regional studies where extensive tide gauge observations are unavailable. Given the limited availability of MSL observations in Malaysia and the ellipsoidal nature of the hydrodynamic datasets employed, the use of MSS provides a more practical, spatially complete, and internally consistent solution. Therefore, the adoption of MSS in place of MSL is considered appropriate and justified for the development of the ellipsoid-based hydrodynamic model presented in this study.

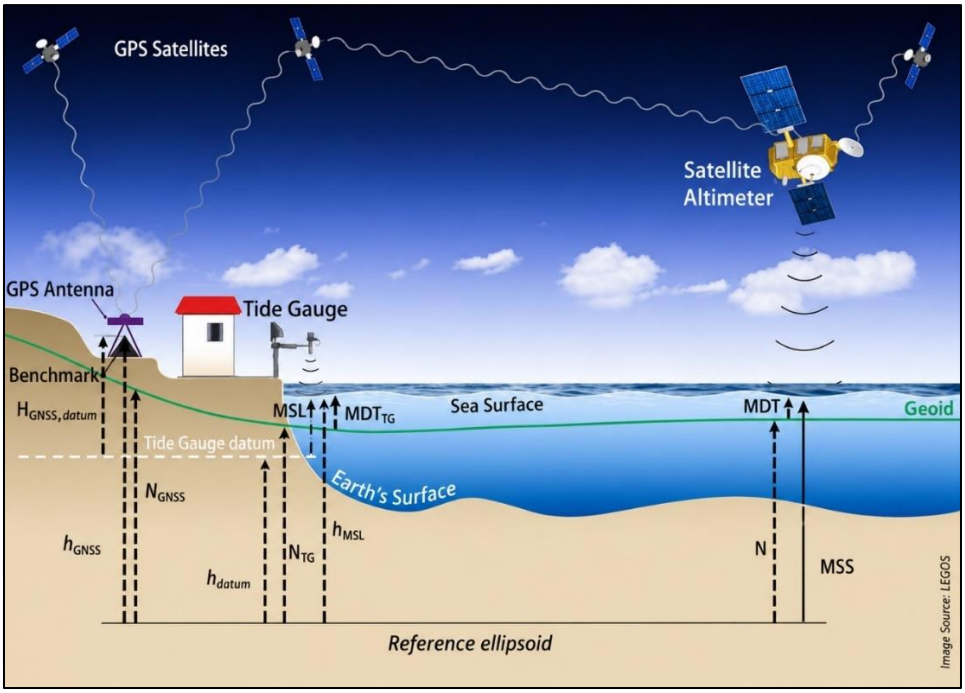


Figure 2. 13 The Relationship Between MSL and MSS Reference Surface (O. B. Andersen et al., 2018)

2.8.2 Global Realization of Unified Vertical Datum Systems

The realization of unified vertical datum bridging across the land and marine has increasing gaining attention among geodetic and hydrographic worldwide. Numerous countries have recognized the importance of establishing a seamless unified vertical datum to improve the consistency of elevation information when integrating data in both land and marine domains. This necessity arises from the growing demand for accurate and consistent elevation data to support coastal zone management,

engineering, flood modelling, sea level monitoring, and climate change adaptation and 3D marine cadastre management (Abdullah & Omar, 2011; Sánchez & Sideris, 2017; IHO, 2020). In response, several nations have undertaken dedicated efforts to develop a unified vertical reference frameworks tailored to their national geospatial and maritime needs.

2.8.2.1 National Oceanic and Atmosphere Administration Vertical Datum (NOAA VDatum)

VDatum is a vertical datum transformation tool that enables reference conversion among different vertical surfaces. The development of VDatum was originated from challenges addressed in merging datasets from two different domains of land and marine that has been collected independently in Tampa Bay, Florida (Gesch & Wilson, 2001). The core objective of VDatum is to eliminate datum discrepancies that hinder the seamless merging of datasets from multiple sources, format, projection, resolution, accuracy, and datums. It is developed by the American through the collaboration of NOAA's National Ocean Service (NOS), National Geodetic Survey (NGS), Office of Coast Survey (OCS) and Center for Operational Oceanographic Product and Services (CO-OPS) (Gesch & Wilson, 2001). The VDatum tool capable of handling more than 30 transformations across three major vertical datum classes which is tidal, orthometric, and ellipsoidal as displayed in Figure 2. 14. It employed a methodology that combines hydrodynamic modelling, geoid modelling, and spatial interpolation techniques to enable accurate conversions between datums such as MLLW (Mean Lower Low Water), NAVD88 (North American Vertical Datum of 1988), and NAD83(86) (North American Datum 1983 (National Oceanic and Atmospheric Administration, 2004). The key application of VDatum lies in the creation of a National Bathymetric Database, where historical and newly acquired depth data are transformed to a common chart datum, enabling the production of electronic navigational charts (ENCs) and improved support for coastal hazard modelling, marine spatial planning, and boundary delineation (National Oceanic and Atmospheric Administration, 2013b). The success of VDatum underscores the importance of geodetic coherence across land-sea interfaces and represents a transformative advancement in the field of coastal

geodesy. It has laid the foundation for similar vertical unification projects globally and continues to serve as a benchmark for nations aspiring to harmonize their elevation frameworks across diverse vertical datums.

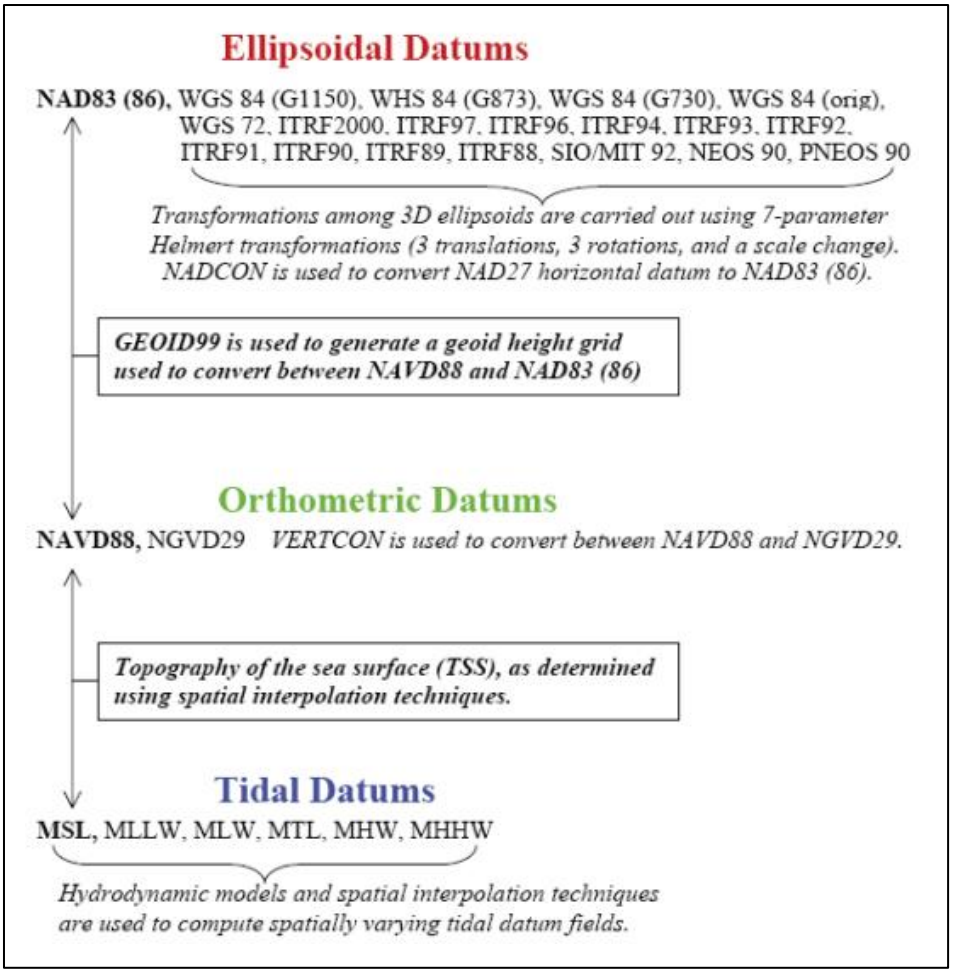


Figure 2. 14 VDatum Transformation Parameters (FIG, 2006)

2.8.2.2 Vertical Offshore Reference Frame (VORF)

The Vertical Offshore Reference Frame (VORF) represents a suite of high-resolution surface models designed to support hydrographic surveying and charting within United Kingdom (UK) waters. VORF serves as a computational framework that facilitates the transformation of positional and mapping data across multiple vertical reference surfaces. These surfaces were specifically developed to address critical challenges in the offshore domain, including the latency and complexity of integrating

onshore and offshore operations, discrepancies in tidal chart accuracy, and inconsistencies arising from the use of multiple vertical datums (Jones, 2007). The development of VORF involved the assimilation of a diverse array of geospatial and oceanographic datasets such as tide gauge data, GPS data, satellite altimetry, gravity field models and tidal model (Iliffe et al., 2007). Its functionality extends beyond basic datum transformations to include robust error estimation, interactive data visualization, detection of transformation anomalies, and support for both single-point and batch-mode processing. Furthermore, it is capable of managing complex spatial scenarios, such as inland waterways and impounded tidal zones, while enabling rapid data retrieval and processing (Jones, 2007). All VORF surfaces are referenced to the GRS80 ellipsoid in order to ensure the compatibility of VORF in conjunction with high precision GNSS techniques (FIG, 2006). This ellipsoidal referencing is crucial for enabling seamless integration between ellipsoidal, orthometric, and tidal height systems in coastal and offshore geospatial applications. In summary, the schematic concept of VORF height system is as presented in Figure 2. 15.

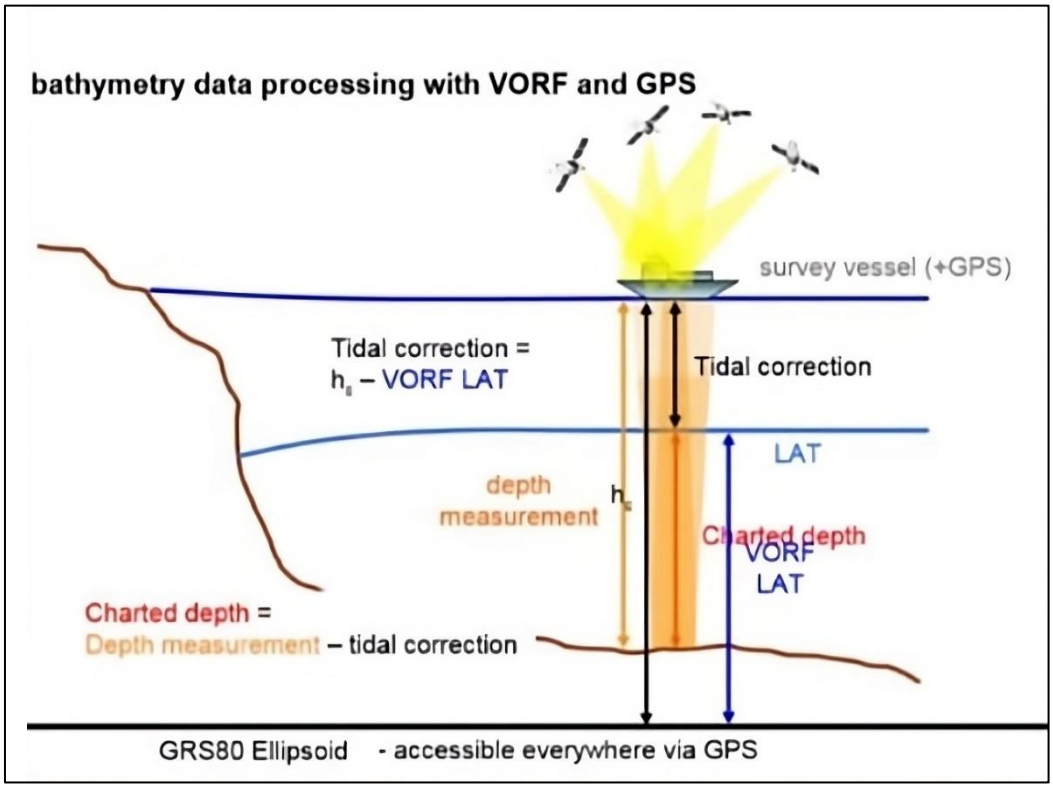


Figure 2. 15 The Concept of VROF (Jones, 2007)

2.8.2.3 Continuous Vertical Datum for Canadian Waters (CVDCW)

Since 1883, the Canadian Hydrographic Service (CHS) has played a pivotal role in advancing hydrographic science to ensure the safe and efficient navigation of Canada's waterways. Its core responsibilities include the execution of bathymetric surveys, the production of nautical charting products, the mapping of oceanic and freshwater environments, and the identification of coastal hazards (Robin et al., 2016). With the advent of GNSS technology, CHS has been able to modernize its operational procedures, particularly through the adoption of "through-the-ellipsoid" bathymetric reduction methods. This approach allows depths to be referenced directly to a global reference ellipsoid, streamlining hydrographic workflows, and improving the spatial accuracy of marine datasets. The pursuit of this innovation led to the development of the Continuous Vertical Datum for Canadian Waters (CVDCW) which designed to define seamless vertical separation models across Canada's marine domain. Initiated in the early 2010s, the CVDCW project reached significant stages of implementation between 2014 and 2016 (Nudds et al., 2016). The CVDCW framework is referenced to the GRS80 ellipsoid to support the transformation between ellipsoidal heights and tidal or chart datums within the NAD83 (CSRS) reference frame and Canada's geoid model called CGG2013 (Natural Resources Canada, 2025). The underlying methodology of CVDCW is based on a layered decomposition of vertical separation components. These include the geoid (ellipsoid to equipotential surface), dynamic ocean topography (geoid to mean water level), and the tidal component that relates mean water level to the target datum, such as Lower Low Water Large Tide (LLWLT). As illustrated in Figure 2. 16, the integration of these components relies on a wide range of geospatial and oceanographic datasets, including tide gauge records, GNSS observations, satellite altimetry, high-resolution hydrodynamic models, and tidal constituent simulations (Nudds et al., 2016). The development of CVDCW reflects an increasing global emphasis on the importance of vertical datum unification, particularly in the context of coastal zone management, marine infrastructure planning, and climate change adaptation. Its role in supporting coastal management, marine infrastructure, and climate adaptation underscores the need for accurate, consistent vertical referencing to ensure maritime safety, data interoperability, and long-term coastal resilience.

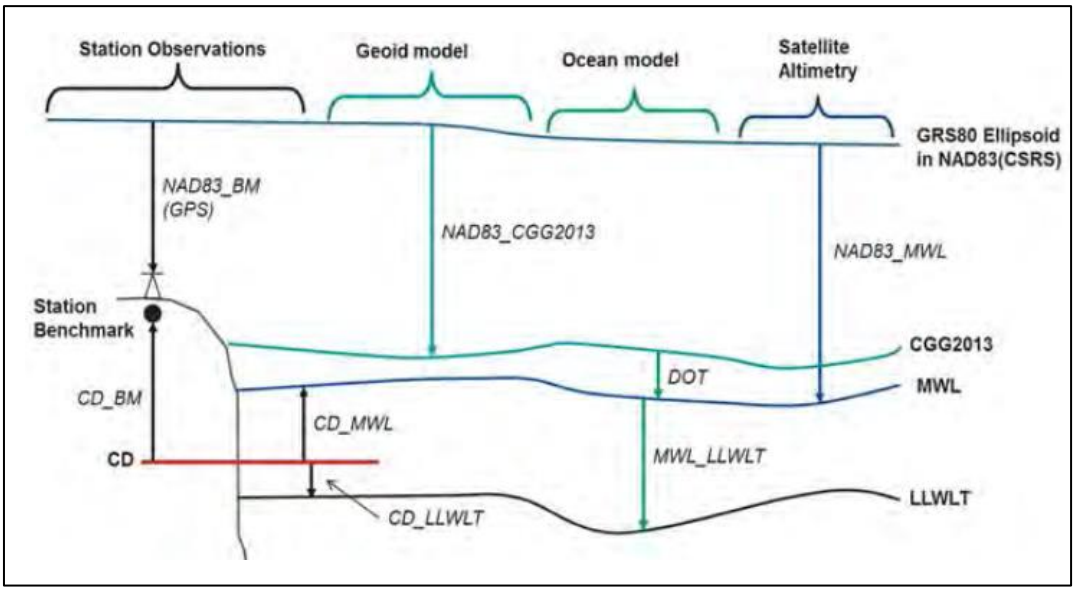


Figure 2. 16 The Methodology Employed in CVDCW (Nudds et al., 2016)

2.8.2.4 Australian's AUSHYDROID

The development of AUSHYDROID represents a pivotal advancement in Australia's geodetic infrastructure by addressing the long standing challenge of integrating disparate land and sea vertical datums across the coastal interface. Historically, vertical datums for land and marine environments have been independently defined by national levelling networks inland while tidal datums such as the LAT or CD used in marine domain. The AUSHYDROID working group has been established under the auspice of the inter-Governmental Committee for Survey and Mapping (ICSM) and leadership of Australian Hydrographic Office (AHO). The motivation of the development of AUSHDROID is due to the increasing importance of Australia's coastal and offshore region for economic, security, maritime safety, and environmental consideration (Filmer et al., 2024). The model serves as the maritime counterpart to AUSGeoid, representing the vertical separation between the reference ellipsoid and LAT, thereby facilitating the transformation of GNSS-derived heights into charted marine depths (Turner et al., 2010; Featherstone et al., 2011). The development of AUSHYDROID integrate multiple geospatial dataset such as MSS, MDT, geoid models and ocean tide model (OTM) as illustrated in Figure 2. 17. In short, AUSHYDROID stands as a forward-looking initiative that integrate the geodesy,

oceanography, and geospatial data in the creation of unified vertical reference for Australia's coastal and marine areas. As Australia continues to confront challenges from the rising sea levels, coastal inundation, and growing demands for maritime safety, having a consistent vertical datum like AUSHYDROID is both timely and necessary (Keysers et al., 2015).

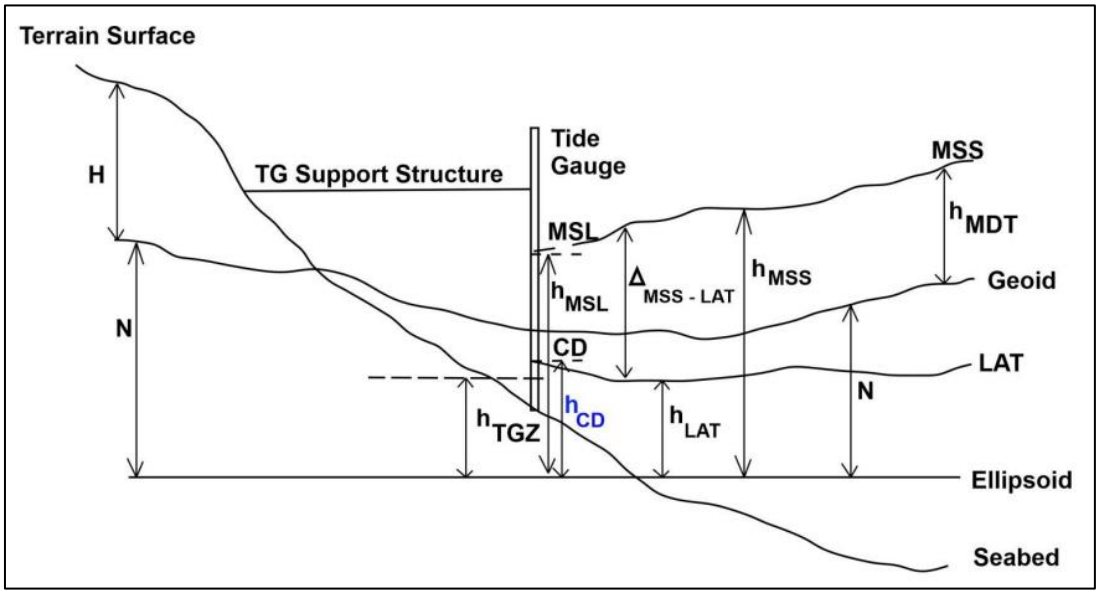


Figure 2. 17 The Concept of AUSHYDROID Heights System (Filmer et al., 2024)

Table 2. 11
Summary of previous studies in development of vertical transformation model

Author	System / Country	Purpose / Objective	Key Methodology	Data Input	Reference Frame / Datums Involved	Key Applications
Gesch et al. (2001)	NOAA VDatum (USA)	To enable seamless transformation between different vertical datums across land and marine environments and eliminate datum inconsistencies	• Combines hydrodynamic modelling, geoid modelling, and spatial interpolation • Supports more than 30 transformation types	• Tide gauge data • Gravity field models • GNSS • Bathymetry • Coastal datasets	• Tidal datums (e.g., MLLW) • Orthometric datum (NAVD88) • Ellipsoidal datum (NAD83)	• National Bathymetric Database • Electronic navigational charts (ENCs) • Coastal hazard modelling • Marine spatial planning • Boundary delineation
Iliffe et al. (2007)	VORF (UK)	To support hydrographic surveying and unify vertical reference surfaces for UK waters	• High-resolution surface modelling • Datum transformation framework with error estimation and anomaly detection	• Tide gauges • GNSS • Satellite altimetry • Gravity field models • Tidal models	• GRS80 ellipsoid reference integrating tidal, orthometric, and ellipsoidal heights	• Offshore navigation • Hydrographic charting • Inland waterway management • Spatial data integration
Nudds et al. (2016)	CVDCW (Canada)	To create seamless vertical separation models across Canadian marine regions for modern hydrographic operations	• Layered decomposition of vertical separation (geoid, dynamic ocean topography, tidal components) • GNSS-based “through-the-ellipsoid” approach	• Tide gauges • GNSS • Satellite altimetry • Hydrodynamic models • Tidal constituents	• GRS80 ellipsoid • NAD83 (CSRS) • CGG2013 geoid • Tidal datums (e.g., LLWLT)	• Bathymetric reduction • Coastal zone management • Marine infrastructure planning • Climate adaptation
Filmer et al. (2024)	AUSHYDROID (Australia)	To integrate land and marine vertical datums for coastal and offshore applications	• Integration of geoid, MSS, MDT, and ocean tide models (OTM)	• GNSS • MSS • MDT • Geoid models • Ocean tide models	• Relationship between ellipsoid and LAT • AUSGeoid	• GNSS-based depth conversion • Maritime safety • Coastal infrastructure planning • Sea level rise studies

2.9 Chapter Summary

This chapter has outlined the fundamental concepts and existing studies related to vertical reference systems and their transformation. It begins with the basic principles of height determination, where orthometric and normal heights are defined in relation to the geoid and reference ellipsoid. These components form the basis for understanding how vertical positions are expressed in geodetic practice and how different height systems can be related through consistent reference surfaces. The discussion continues with the concept of vertical datums, including geodetic vertical datums and tidal-based references. Particular attention is given to tidal datum definitions and review of several global geoid and geopotential models such as WHU-SWPU-GOGR2022S, GOSG02S, XGM2019e, and PMGG2020, which provide improved representations of the Earth's gravity field and support more consistent height system integration. In addition, marine-related height reference surfaces are examined through Mean Sea Surface and Mean Dynamic Topography products. Models such as DTU22MDT, DTUUH22MDT, SDUST2020, DTU21, and CNES-CLS22 are discussed due to their role in bridging oceanographic observations with geodetic height frameworks. These datasets are essential for understanding sea surface variability and for linking ocean height information with terrestrial reference systems.

The chapter further reviews marine gravity datasets, which includes DTU21GRA, Sandwell and Smith, SDUST2022GRA, and NSOAS24 are highlighted for their contribution to improving gravity field resolution and geoid accuracy. The tidal section explains the importance of tidal constituents, harmonic analysis, and prediction methods in separating temporal ocean signals from geodetic measurements. Gravimetric geoid computation methods and satellite altimetry techniques are also discussed. The chapter then reviews the development of vertical transformation models, particularly the relationship between Mean Sea Surface and Mean Sea Level, along with established systems such as NOAA VDatum, VORF, CVDCW, and AUSHYDROID. Overall, this chapter brings together the main theoretical and methodological aspects required for the study. It shows that vertical datum unification involves the integration of geoid modelling, tidal modelling, and transformation frameworks.

CHAPTER 3
RESEARCH METHODOLOGY

3.1 Introduction

The research methodology in this study was structured into six phases. The first phase involved data acquisition, which included the collection of various datasets such as gravity anomalies, Global Geopotential Models (GGMs), GNSS levelling data, tide gauge records, satellite altimetry data, global Mean Sea Surface (MSS) models, global Mean Dynamic Topography (MDT) models, and global geoid models. The second phase focused on the computation of geoid models, beginning with the pre-processing and accuracy assessment of various datasets and least square parameters, followed by the combination and gridding of gravity anomalies, and the computation of both gravimetric and hybrid geoids. The third phase was dedicated to developing the marine vertical separation model, which integrated satellite altimetry, hydrodynamic modelling, and tide gauge data processing. The fourth phase involved the development of a vertical transformation model through the estimation of vertical datum offsets. The fifth phase comprised the conclusion and recommendations. This phase addressed the limitations and gaps identified throughout the research and integrated these insights into recommendations to guide future studies. The research workflow designed to achieve the study's aims and objectives is illustrated in Figure 3. 1.

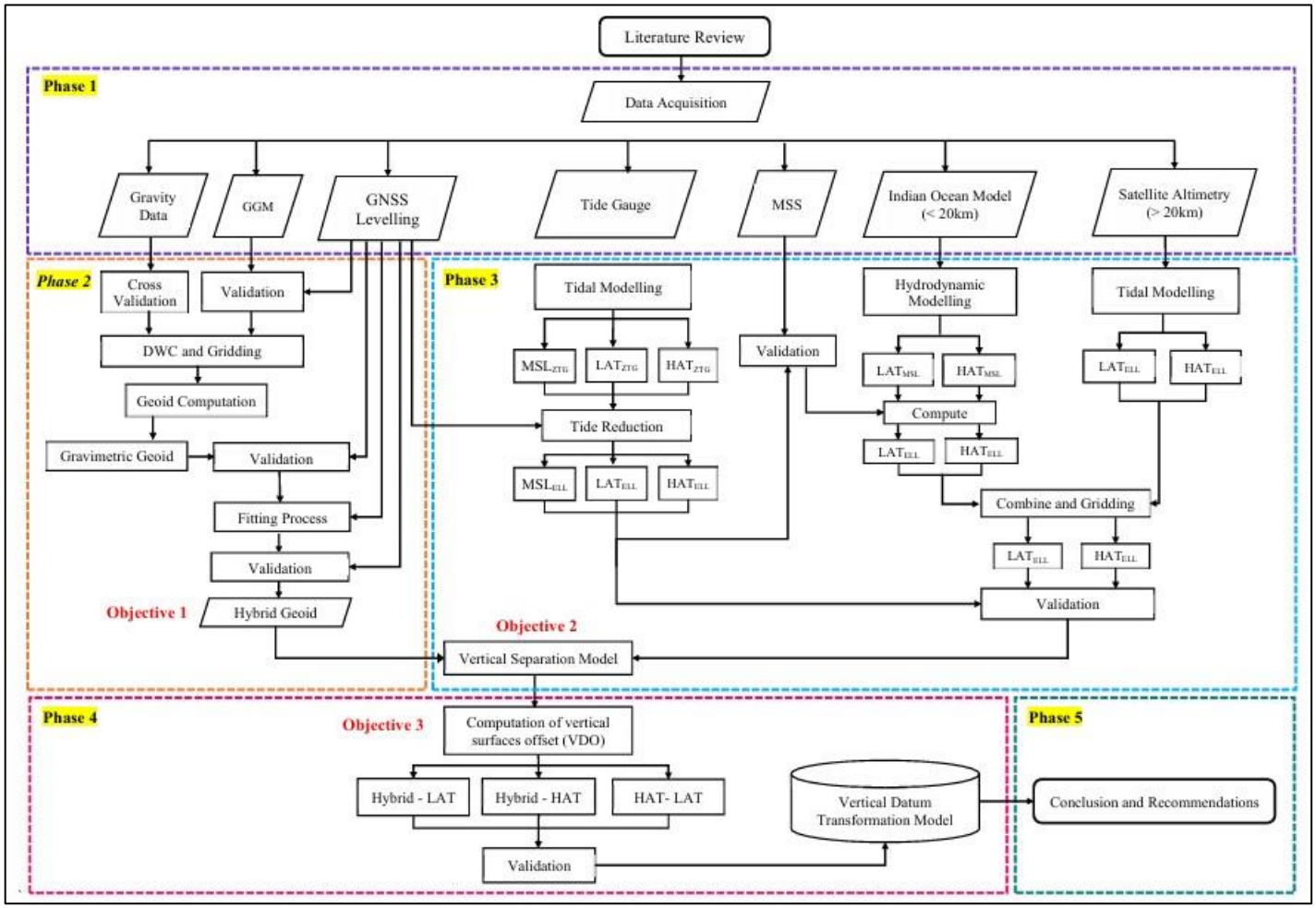


Figure 3. 1 General Research Methodology

3.2 Phase 1 : Data Acquisition

The computation of the geoid model, vertical separation models, and vertical transformation model necessitates the utilization of a comprehensive series of data as primary inputs. The data acquisitions involved in this research were gravity anomalies, GGMs, Global Navigation Satellite System (GNSS) levelling data, tide gauge records, satellite altimetry, MSS models, MDT models and global geoid models. This section further clarifies the detailed information and sources of each data utilized in this study.

3.2.1 Gravity Data

The gravity data served as the foundational input for the computation of the geoid model, which was derived from free-air anomalies data. In this research, three types of gravity anomalies data were utilized in the computation of gravimetric geoids which encompassed the terrestrial, airborne, and satellite-derived marine gravity.

3.2.1.1 Terrestrial Gravity

Terrestrial gravity data constitutes one of the fundamental inputs in the computation of high-precision geoid models. It plays a critical role in capturing short- to medium-wavelength gravitational variations over land that enable an accurate interpretation and refinement of regional geoid heights, particularly in complex terrains in Peninsular Malaysia. In this study, terrestrial gravity observations were sourced from the DSMM through the Peninsular Malaysia Gravity Standardization Net 1989 (PMGSN89) Project (Jabatan Ukur dan Pemetaan Malaysia, 2005). This extensive gravity survey provides highly accurate terrestrial gravity measurements with reported uncertainties ranging between 0.03 and 0.10 mGal. A total of 9916 terrestrial gravity anomalies data were employed in the geoid modelling process in this study. These data serve as a high-resolution foundation for gravity anomaly gridding and geoid height determination. The statistical summary and spatial metadata of the terrestrial gravity dataset are presented in Table 3. 1 the distribution of the terrestrial gravity data is as illustrated in Figure 3. 2.

3.2.1.2 Airborne Gravity

Airborne gravity data serves as a vital supplementary dataset, particularly in regions that are logistically inaccessible to terrestrial gravimetry such as highland or forested areas where conventional ground-based surveys are either impractical or unfeasible. In Malaysia, airborne gravity data acquisition has been conducted on three separate occasions. The first campaign was carried out by DSMM in 2002 to 2003 as part of the MyGeoid Project aimed at enhancing national geoid modelling accuracy. The second airborne survey mapping was carried out in 2019 to 2022 through MAGIC IV project to extend the marine gravity data over the South China Sea and further to the Malacca Straits through the third project called MyMarineGI Project Phase I in year 2021 to 2022 (Cob et al., 2022). This initiative aimed to provide a denser dataset that encompasses the coastal areas, including the Malacca Straits and the South China Sea with accuracy within 1 to 2 mGal (Jabatan Ukur dan Pemetaan Malaysia, 2021). However, due to data availability constraints, this study was limited to using airborne gravity data exclusively from the first campaign (2002–2003). This limitation is acknowledged as a factor that may affect the accuracy of the resulting geoid model. In total, 24855 airborne gravity anomaly values were utilized in the geoid computations. Detail regarding the information and spatial distribution of the dataset are presented in Table 3. 1 following by illustrated in Figure 3. 2 and Figure 3. 3 respectively.

Table 3. 1
Properties of terrestrial gravity data

Data Type	Terrestrial Gravity	Airborne Gravity
Year	2019	2019
Accuracy	0.03 – 0.10 mGal	1 – 2 mGal
Number of Data	9916	24855
Source of Data	DSMM	DSMM

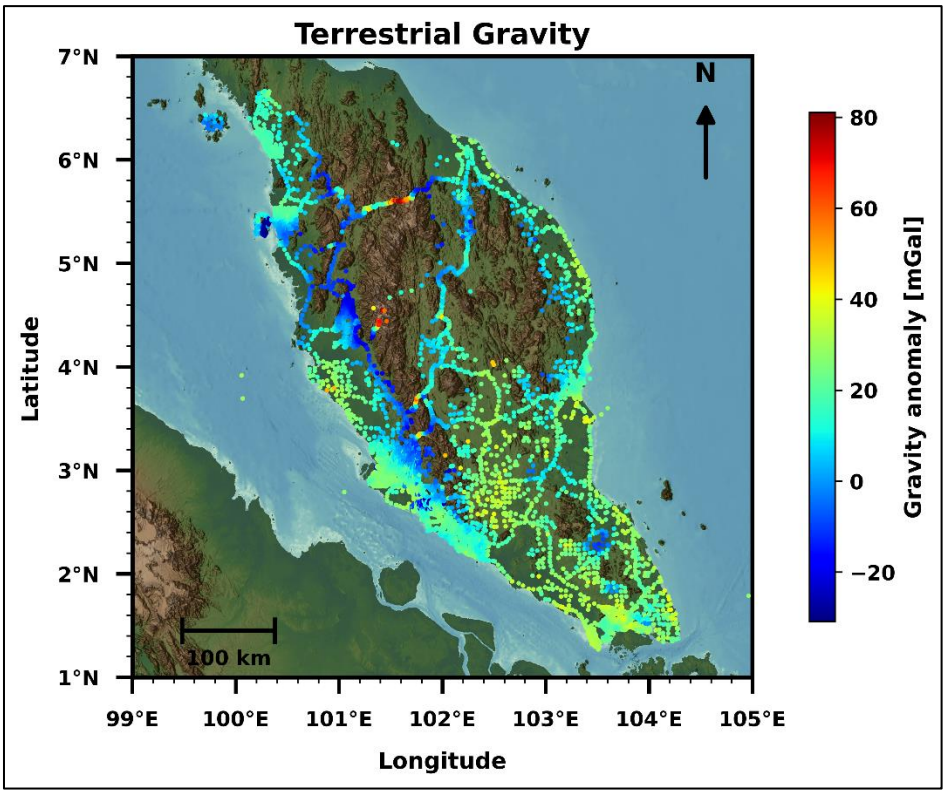


Figure 3. 2 Distribution for Terrestrial Gravity Anomalies Data

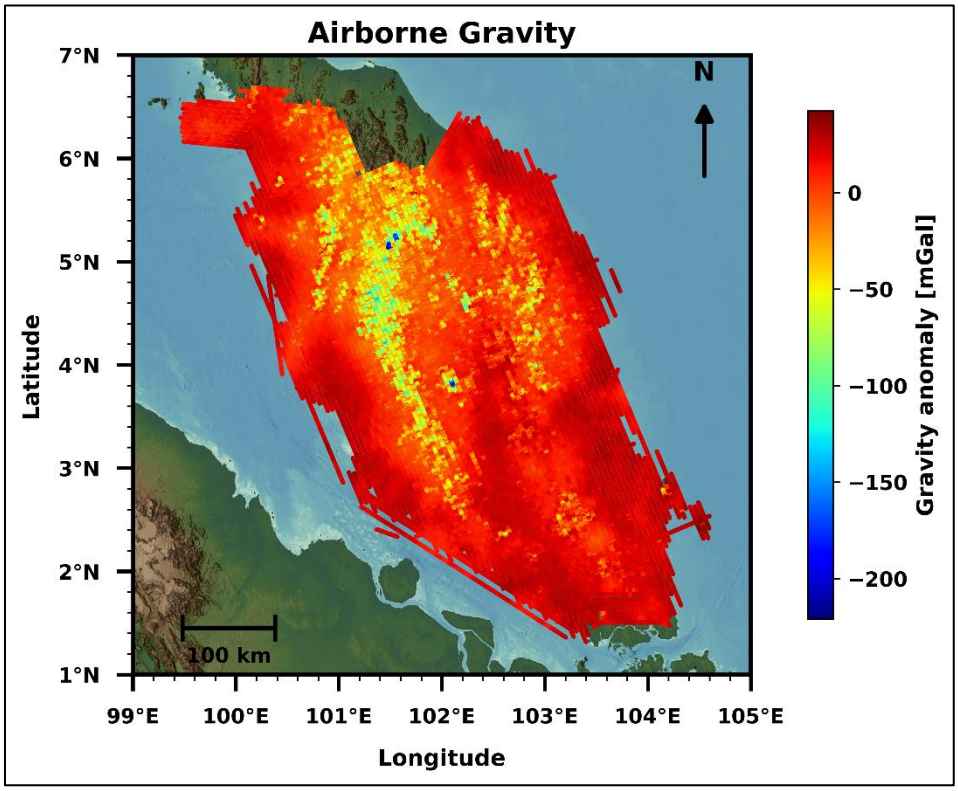


Figure 3. 3 Distribution of Airborne Gravity Anomalies Data

3.2.1.3 Satellite – Derived Marine Gravity

In geoid computation, additional gravity anomalies data were compulsory to provide a data on marine area. Commonly, the satellite-derived marine gravity data is adopted as to cover the marine region due to its global coverage. Apparently, there are many agencies that provide the global coverage of marine gravity data derived from the altimetric satellite. In this study, four models were utilized to investigate the most suitable model that fit the regional Peninsular Malaysia. The models used are the common model that has been widely used by most of the geoid modelers which is Sandwell and Smith – Grav 32.1 model (D. T. Sandwell & Smith, 2009) and DTU21GRA model (O. B. Andersen et al., 2010). Additionally, the other two models were the recent satellite-derived marine gravity models released by China in 2024 which is the SDUST2022GRA (Li et al., 2024) and NSOAS24 (Zhang et al., 2025). Detail spatial information these models were displayed in Table 3. 2 and illustrated in Figure 3. 4.

Table 3. 2
The Summary of Satellite-Derived Marine Gravity Data

Data Type	Year	Resolution	Source of Data	Reference
DTU21	2021	1′ x 1′	Denmark Technical University (DTU)	(O. B. Andersen & Knudsen, 2020)
GRAV 32.1	2022	1′ x 1′	Sandwell and Smith	(D. Sandwell et al., 2014)
SDUST2022GRA	2024	1′ x 1′	Shandong University of Science and Technology (SDUST)	(Li et al., 2024)
NSOAS24	2024	1′ x 1′	National Satellite Ocean Application Service (NSOAS)	(Zhang et al., 2025)

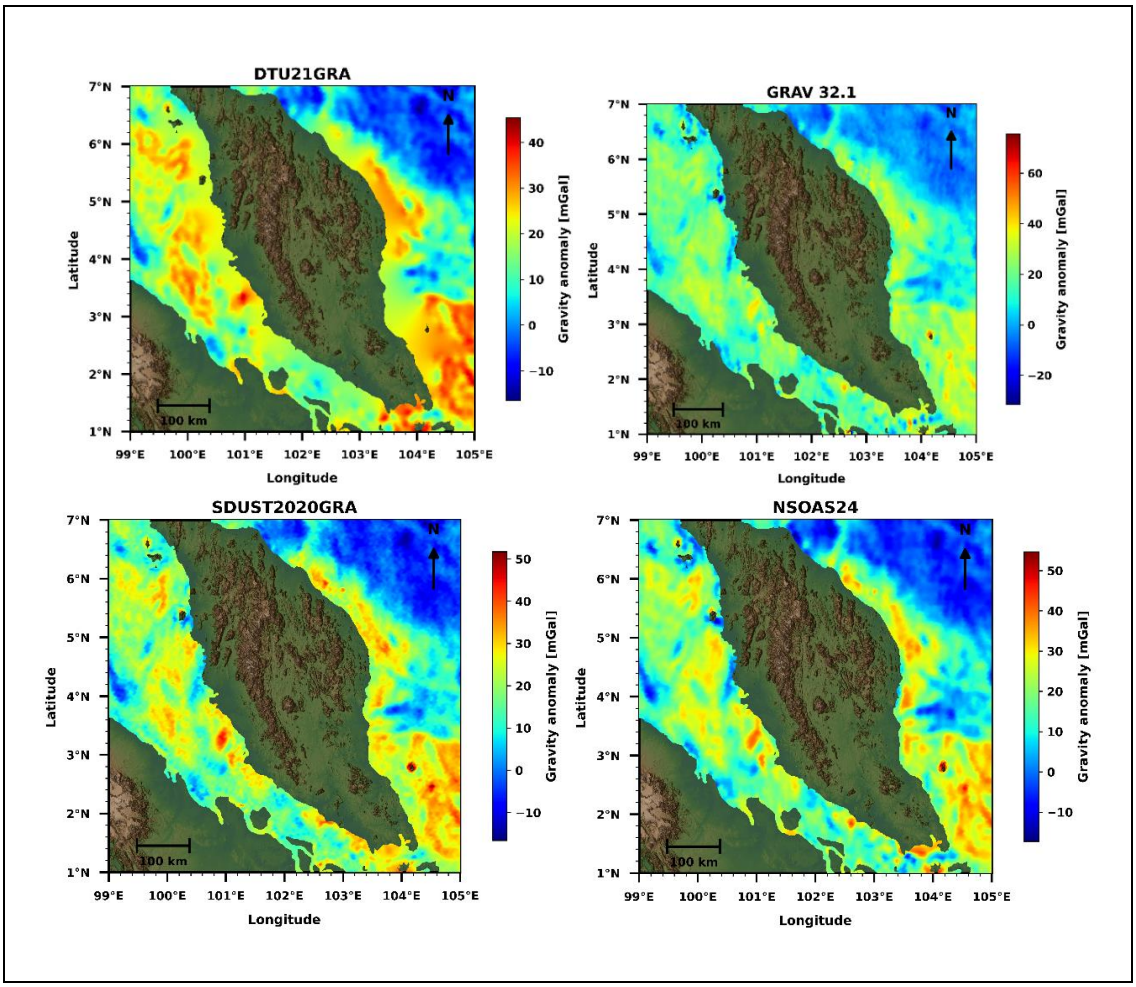


Figure 3. 4 Free Air Anomalies Distribution for Marine Gravity Data

3.2.2 Global Digital Elevation Model (GDEM)

In geoid computation, global digital elevation model (GDEM) played pivotal role subjected to the derivation of height on land region. The data were utilized to compute the topographic correction and downward continuation correction. These corrections are crucial steps in the geoid computation process in considering the influence of the Earth's topography on the gravity measurements allowing for more accurate determination of the geoid's shape and height. In this study, Shuttle Radar Topography Mission (SRTM) was adopted in the geoid computation. The SRTM model was included as the reference models for elevation to be evaluated since the existing geoid model for Malaysia utilized SRTM in its computation. The SRTM model boasts a resolution of 1 arc-second, equating to approximately 30 meters, ensuring

comprehensive global coverage. This model was acquired through the official website via (https://www.usgs.gov/centers/eros/science/usgs-eros-archive-digitalelevationshuttle-radar-topography-mission-srtm-1), which is the publisher of SRTM data (Earth Resources Observation and Science (EROS), 2019). Detailed information regarding the SRTM model and the map is provided in Table 3. 3 and Figure 3. 5 respectively.

Table 3. 3
Properties of SRTM Model

Version	SRTM V3
Released Date	November 2018
Projection	Geographic (Latitude and Longitude)
Resolution	1 arc-second (~30 meters)
Raster Tile	1˚ × 1˚
Reference	Earth Resources Observation and Science (EROS) (2019)
Source	https://www.usgs.gov/centers/eros/science/usgs-eros-archive-digital-elevationshuttle-radar-topography-mission-srtm-1

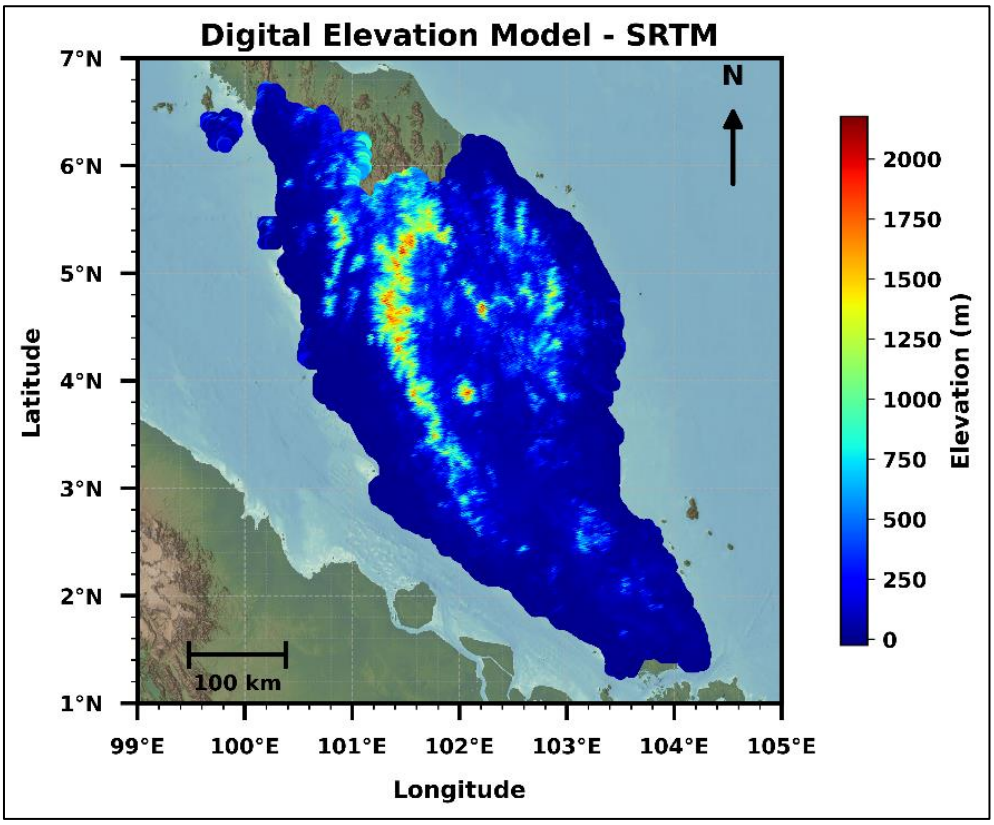


Figure 3. 5 Global Digital Elevation Model – SRTM

3.2.3 Global Geopotential Model (GGM)

The application of global geopotential model (GGM) is vital in computation of geoid model to accurately interpolate the geoid height that closely represent the undulation of earth gravitational model locally and globally. Computation of geoid model in Peninsular Malaysia using a globally recognized model can ensures compatibility with other geoid models and geodetic data on a global scale. This higher resolution allows for a more detailed representation of the earth's gravitational field and thus leads to better accuracy of geoid model interpolation. Prior to the assessment of the input dataset in geoid modelling, five recent GGMs consists of three satellite only and two combined model were acquired from ICGEM official website via (https://icgem.gfz-potsdam.de/tom_longtime). The details of each GGMs were as listed in Table 3. 4.

Table 3. 4
Selected GGMs for Assessment of Input Dataset

	Model	Year	Degree	Data Type	Reference
Satellite Only	WHU-SWPU-GOGR2022S	2023	300	S (GOCE), S (GRACE)	Zhao et al.(2023)
	GOSGO2S	2023	300	S (GOCE)	Xu et al. (2023)
	Tongji-GMMG2021S	2022	300	S (GOCE), S (GRACE)	Chen et al. (2022)
Combined	SGG-UGM-2	2020	2190	A, EGM2008, S (GOCE), S (GRACE)	Liang et al. (2020)
	XGM2019e_2159	2019	2159	A, G, S (GOCO06s), T	Zingerle et al. (2020)

3.2.4 GNSS Levelling Data

In this study, the GNSS data were acquired for multiple purposes such as to validate the accuracy of gravimetric geoid, for geoid fitting procedure to compute hybrid geoid to calculate the tide reduction for verification of tidal datum along coastal region of Peninsular Malaysia. A total of 45 and 173 point of GNSS levelling data were acquired from DSMM while another 11 GNSS observation at tide gauge stations were acquired from GNSS Campaign in 2019 (Pa'suya, 2020). The information of the data is listed in Table 3. 5 and spatial distribution of the data are as illustrated in Figure 3. 6.

Table 3. 5
The Summary of GNSS Levelling Data for Gravimetric Geoid Validation

Dataset	Number of Station	Source
GPS-45	45	DSMM
GPS-173	173	DSMM
TGBM	11	2019 GNSS Campaign
Combine All	229	DSMM + 2019 GNSS Campaign

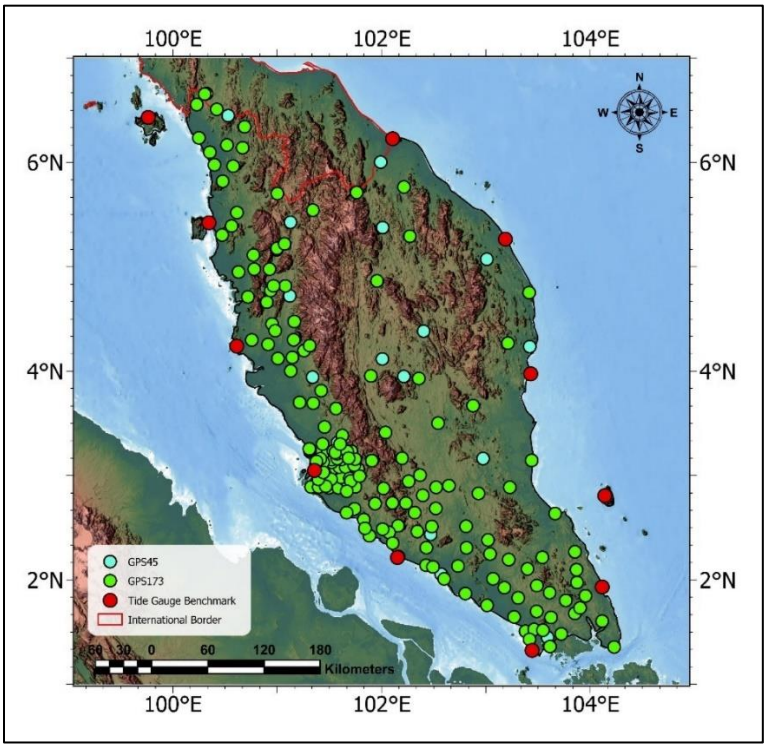


Figure 3. 6 Distribution of GNSS Levelling Used in This Study

3.2.4.1 GNSS Data at Tide Gauge Benchmark (TGBM)

The GNSS data observed on the tide gauge benchmark (TGBM) are required to transform the tidal height specifically the LAT and HAT datum with respect to the GRS80 ellipsoid reference. In this study, the GNSS observation at tide gauge stations across Peninsular Malaysia were adopted from the Tide Gauge GNSS Campaign 2019 which has been carried out through a joined collaboration of Universiti Teknologi MARA (UiTM) and Universiti Teknologi Malaysia (UTM) in 2019 (Hamden, 2022). The campaign was conducted at 11 TGBM sites and each GNSS session conducted at the TGBM has lasted between 5 to 6 hours and utilized the same receiver type which was Trimble 5700 that equipped with dual-frequency capabilities. The cut-off angle for the satellite signals was set at 15° to minimize the impact of low-angle signals, which can be more prone to errors due to atmospheric interference and multipath effects. The data sampling rate was configured at 1", allowing for high-resolution data collection that captures detailed variations in the GNSS signals (Pa'suya, 2020).

3.2.5 Tide Gauges Records

The tide gauge data utilized in this study served as supplementary observational input for the validation of the vertical separation models consists of LAT and HAT which were derived through the assimilation of multi-mission satellite altimetry and hydrodynamic modelling. These tidal observations were obtained from the DSMM and accessed via the University of Hawaii Sea Level Center (UHSLC) data repository (https://uhslc.soest.hawaii.edu/network/). A total of 11 tide gauge stations were employed in the analysis as listed in Table 3. 6 with their spatial distribution depicted in Figure 3. 7. The dataset comprises long-term records of sea level measurements spanning observation periods ranging from 30 to 33 years, covering the time frame from 1984 to 2016. From the data, the tidal datum of LAT and HAT values at each station were derived using harmonic analysis approach through UTide processing techniques (Codiga, 2011). Subsequently, the tidal datums derived from local tide gauge data underwent a series of tidal reduction procedures to transform the heights referenced to the GRS80 ellipsoid, prior to conducting comparative assessments with other computed tidal models in this study.

Table 3. 6
Information of Tide Gauge Stations Obtained from DSMM

Location	Latitude	Longitude	TGBM	Period	Duration (year)
Klang	3˚ 03' 00 "N	101˚ 21' 29 "E	B 0169	1984 - 2016	33
T. Keling	2˚ 12' 54 "N	102˚ 09' 11 "E	M 0331	1985 - 2016	32
P. Langkawi	6˚ 25' 55 "N	99˚ 45' 54 "E	K 0172	1986 - 2016	31
Lumut	4˚ 14' 24 "N	100˚ 36' 47 "E	A 0401	1985 – 2016	32
Penang	5˚ 25' 19 "N	100° 20' 49" E	PP 0379	1985 - 2016	32
Cendering	5˚ 15' 54 "N	103° 11' 13" E	T 0283	1985 - 2016	32
Kuantan	3˚ 58' 30 "N	103° 25' 48" E	C 0331	1984 – 2016	33
P. Tioman	2˚ 48' 25 "N	104° 08' 24" E	C 0501	1986 – 2016	31
Sedili	1˚ 55' 55 "N	104° 06' 54" E	J 0801	1987 – 2016	30
Kukup	1˚ 19' 30 "N	103° 26' 35" E	J 5328	1986 – 2016	31
Geting	6˚ 13' 37 "N	102° 06' 25" E	D 0354	1987 - 2016	30

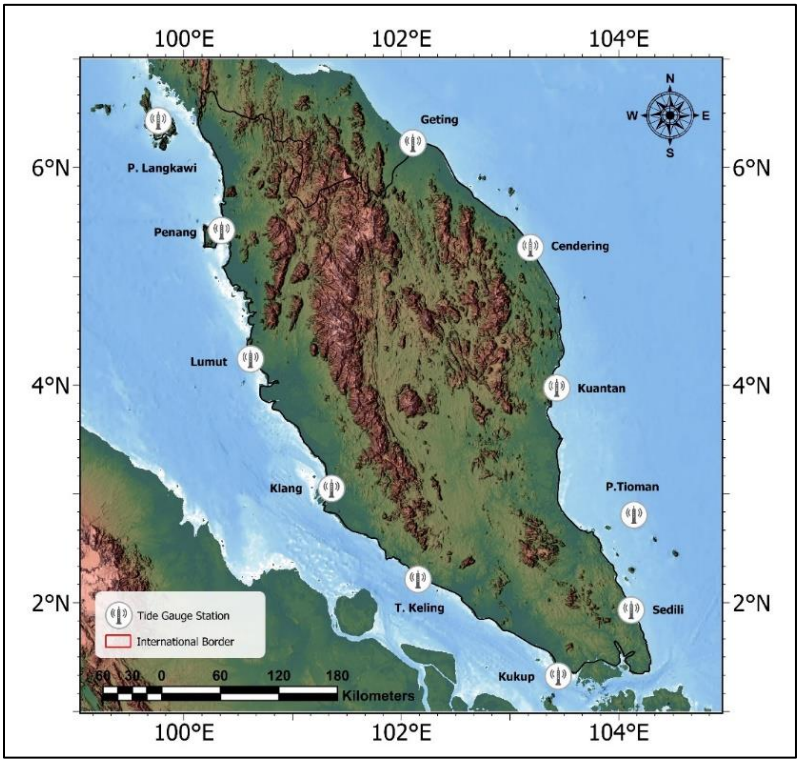


Figure 3. 7 Tide Gauges Stations in Peninsular Malaysia

3.2.6 Satellite Altimetry Data

The data acquisition for satellite altimetry data involved with extraction process from multi-mission satellite altimeter database known as Radar Altimetry Satellite System (RADS). A total of six satellite missions consists of TOPEX, Jason series, GEOSAT Follow On (GFO), Sentinel-6A utilized in this research. The temporal scope of the dataset spans from 1992 to 2024 which approximately implemented the 32 years observation period through integration of varies satellite missions as tabulated Table 3. 7. In this research, the satellite altimetry data were extracted according to the study area to standardize with the boundaries limit of geoid model. Figure 3. 8 illustrates the combination of each along-track mission satellite altimetry data utilized in this study.

Table 3. 7
Properties of Selected Multi-Mission Satellites Data

Mission	Phase	Repeated Period (days)	Date	Cycle
TOPEX	A	9.9156	25/09/1992 -10/8/ 2002	001 - 364
	B		20/09/2002 - 08/10/2005	369 - 481
Jason 1	A	10	17/01/2002 - 26/01/2009	001 - 260
	B		12/02/2009 - 03/03/2012	262 - 374
Jason 2	A	10	04/07/2008 - 02/10/2016	000 - 303
	B		13/10/2016 - 17/05/2017	305 - 327
Jason 3	A	10	12/02/2016 - 07/04/2022	000 - 227
Sentinel 6A	A	10	19/12/2020 - 18/01/2024	004 - 117
GFO	A	17	08/01/2000 - 25/09/2007`	037 - 202

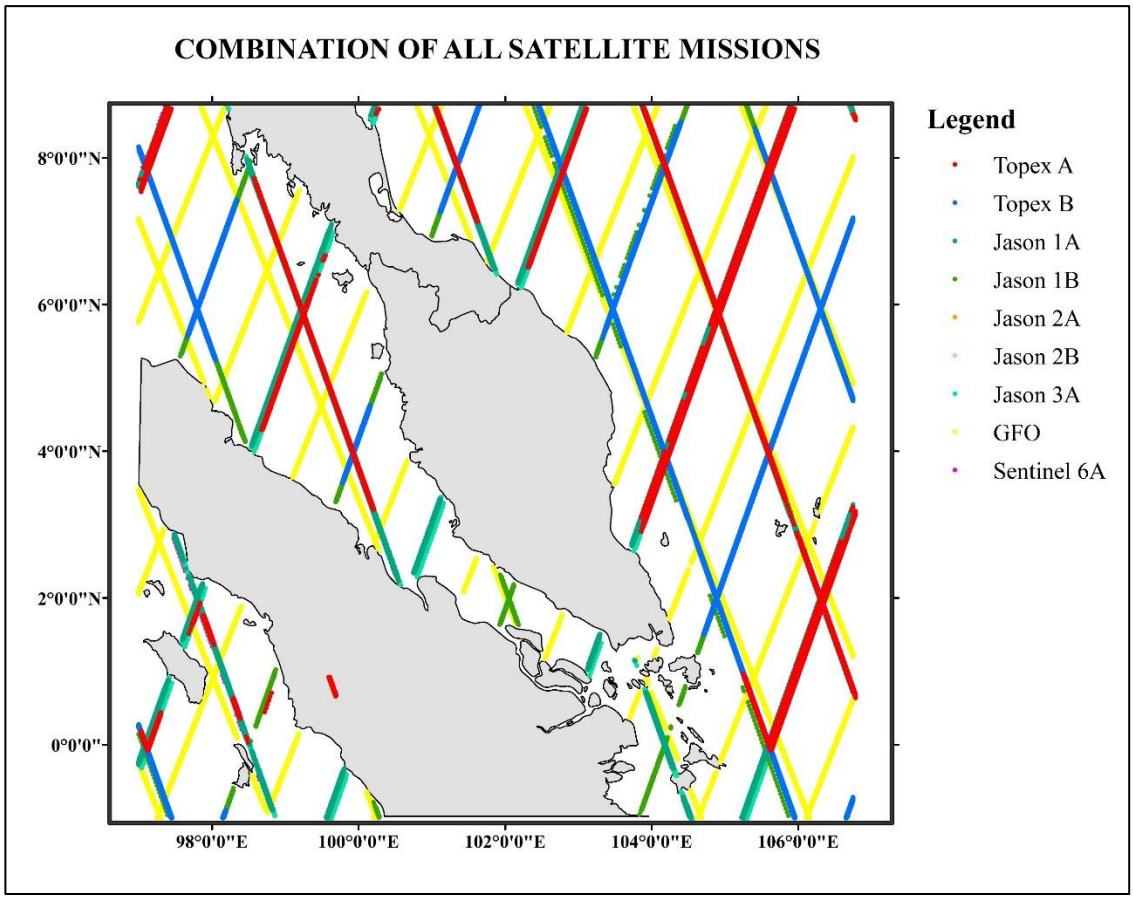


Figure 3. 8 Combination of All Satellite Missions Employed in This Study

3.2.7 Global Tide Model

The Indian Ocean Model was acquired for this research to reference the global tide model for hydrodynamic modelling. The model was developed by Oregon State University (OSU), one of the most advanced and widely utilized model providers for tidal prediction (Egbert & Erofeeva, 2002). The Peninsular Malaysia region has also been included in the Indian Ocean Model, which provides the global tide model up to 1/12° or approximately 5 km accuracy. The regional models at 1/12° are still considerably good enough to derivate tidal data in the deep ocean. The model can be obtained through the official OSU TPXO website at https://www.tpxo.net/regional.

3.2.8 Mean Sea Surface (MSS) Model

The mean sea surface (MSS) model was required as a supplementary dataset to support the hydrodynamic approach adopted in this study. This is due to the fact that the LAT and HAT derived from hydrodynamic modelling using the Tide Model Driver (TMD) software are referenced to the MSL/MSS. Therefore, in order to convert the LAT and HAT to an ellipsoid-based reference frame, the integration of a global MSS model was necessary. The selection of the most suitable MSS model was based on a comparative analysis against tidal datums derived from local tide gauge stations with the model exhibiting the lowest RMSE being selected. Three recent global MSS models evaluated in this study include SDUST2020, DTU21, and CNES-CLS22 which has been summarized in Table 3. 8.

Table 3. 8
The Summary of Global Mean Sea Surface Models

MSS Model	**SDUST2020**	**DTU21**	**CNES-CLS22**
Year	2020	2021	2022
Resolution	$1' \times 1'$	$1' \times 1'$	$1' \times 1'$
Ellipsoid	TOPEX	TOPEX	TOPEX
Obs. Period	1993 - 2019	1993 - 2021	1993 - 2021
Reference	(Yuan et al., 2023)	(O. B. Andersen et al., 2023)	(Schaeffer et al., 2023)
Source of Data	https://essd.copernicus.org	https://data.dtu.dk	https://www.aviso.altimetry.fr/en/home.html

3.2.9 Mean Dynamic Topography (MDT) Model

The global mean dynamic topography (MDT) models were acquired with the objective of diversifying the analysis of the MSS by combining them with different global geoid models. This approach facilitates a comparative assessment of the performance of each MDT and geoid pairing which aimed to identify the most suitable combination for representing sea surface height variations across coastal regions of Peninsular Malaysia. Three global MDT models utilized in this study are DTU22MDT, DTUUH22MDT and the 1992-2002 MDOT which has summarized in Table 3. 9.

Table 3. 9
The Summary of Global Mean Dynamic Topography Models

MSS Model	DTU22MDT	DTUUH22MDT	MDOT
Year	2022	2022	2002
Geoid	XGM2019e	XGM2019e	Drifter-derived AVISO Satellite Altimetry
Ellipsoid	DTU21MSS	DTU21MSS	GRACE
Obs. Period	1993-2012	1993-2012	1992 - 2012
Reference	(Knudsen et al., 2022)	(Knudsen et al., 2024)	(Maximenko et al., 2009)
Source of Data	https://data.dtu.dk	https://data.dtu.dk	https://apdrc.soest.hawaii.edu

3.2.10 Geoid Model

In this study, three global geoid model which are WHU-SWPU-GOGR2022S, GOSG02S and XGM2019e were obtained from the ICGEM database and another local geoid model was acquired from Pa'suya et al. (2022). These geoid models were utilized by pairing with the MDT models to derive the MSS. The objective was to evaluate the performance of the MSS by applying various model combinations aiming to identify the most suitable model that closely represents the sea level variations around Peninsular Malaysia coastal region. For this study, the model was downloaded from the ICGEM database in the GRS80 reference ellipsoid and tide-free system. The summary of the geoid model is as listed in Table 3. 10, where A represents altimetry, S represents satellite data (e.g., GRACE, GOCE, and LAGEOS), G represents ground-based observations such as terrestrial, shipborne, and airborne gravity data, while T denotes topographic information.

Table 3. 10
The Summary of Global Geoid Models

Geoid Model	Year	Data	Reference
WHU-SWPU-GOGR2022S	2023	S (GOCE), S (GRACE)	(Zhao et al., 2023)
GOSG02S	2023	S (GOCE)	(Xu et al., 2023)
XGM2019e	2019	A, G, S(GOCO06s), T	(Zingerle et al., 2020)

3.3 Phase 2 : Development of Geoid Model

This section delves into the intricate processes underlying the computation of the geoid model. It begins with the pre-processing and assessment of dataset input, then combine and gridding of free air anomalies and proceeds to the calculation of the gravimetric geoid model. Subsequently, the computed gravimetric geoid underwent fitting procedure to GNSS levelling data for the computation of hybrid geoid model. This phase concisely outlines the theoretical process, definitions and formulas utilized in this study.

3.3.1 Pre – Processing and Assessment of Dataset Input

The primary aim of first research objective involved with the computation of hybrid geoid using the optimal input dataset in improvising the accuracy of geoid model in coastal region. Prior to geoid computation, several procedures of data preparation, data execution and evaluation need to be properly executed to ensure accurate and reliable results.

3.3.1.1 Terrestrial Gravity Data Filtering

Terrestrial gravity undeniably contributes significantly to produce a high-accuracy geoid model on land regions due to its high-precision data. Previously, the position of gravity data was derived from various methods, including measurements from topographic maps, handheld GPS devices, and Real Time Kinematic (RTK) GPS systems, which reflect the technological capabilities of different eras. Therefore, direct utilization of the raw data was impractical as there was a possibility that the outlier or problematic points were included in the dataset. The data underwent the data filtering process to eliminate and filter the outliers using two methods, which is the visual inspection and cross-validation method.

a) Visual Inspection

Visual inspection is a simple filtering process where the outliers are easily identified due to their unusual data values. This inspection was conducted using two methods. In the first method, outliers were removed from the interpolated GDEM points. Typically, points with a height value of -9999 indicated that the terrestrial point was incorrectly positioned in the coastal region. These points were deemed illogical and were removed from the dataset. The second method involved sorting and filtering the data in Microsoft Excel. Latitude and longitude data were sorted in ascending and descending order to detect duplicate entries or data points outside the study area's boundaries. This approach was particularly effective in identifying and roughly eliminating problematic data or outliers.

b) Cross - validation

The second method is the process where the raw terrestrial gravity anomalies data that has been acquired underwent the editing and filtering process known as cross-validation method (Geisser & Eddy, 1979). It is a method to identify the outliers such as redundant point, unusual value, or incorrect format of data that involved with a series of filtering and removing of outliers during the process as depicted in Figure 3. 9. Numerous researchers such as (Danila, 2012; Miyahara et al., 2014; Ssengendo, 2015; Pa'suya et al., 2019) has implemented this cross-validation process in refining their data for precise computation of geoid model. Before the computation of cross-validation, the first procedure involved with the reduction of terrestrial gravity data on the earth's surface to the gravity anomaly's surface. Fundamentally, the definition of gravity anomaly on earth's surface divided into two which is the classical and modern definitions. The classical definition defined that the gravity anomaly refers to the difference between g_{P_0} at point P_o on the geoid and normal gravity γ_Q at point Q on the reference ellipsoid as expressed in Equation (3.1) and (3.2).

$$\Delta g = g_{P_0} - \gamma_Q \tag{3.1}$$

$$g_{Po} = g_P + F \tag{3.2}$$

where F denotes the free air reduction, which adjusts the gravity measurement from the surface, g_P to the geoid surface assuming no masses exist above the geoid. This reduction can be accomplished by following this Equation based on Hofmann-Wellenhof & Moritz (2006) expressed in Equation (3.3).

$$F = -\frac{\partial \gamma}{\partial H_P} = 0.03086\, H_P \tag{3.3}$$

Although the H_P represents the orthometric height, the classical gravity anomaly influenced by the density ρ of the masses between the geoid and topographical surface. Therefore, Molodensky (1945) has formulated the identification of the Earth's surface using gravity (g) and the geopotential (w) leading to the concepts of normal height and corresponding surfaces such as the telluroid and quasigeoid (Hofmann-Wellenhof & Moritz, 2006). Subsequently, the modern definition of gravity anomaly could be defined as the difference between the gravity value at point P and the normal gravity on the telluroid γ_T using the following Equation (3.4).

$$\Delta g = g_P - \gamma_T \tag{3.4}$$

where

$$\gamma_{T=}\gamma - (0.3087691 - 0.0004398\, sin^{\,2}\phi) H_P^N \tag{3.5}$$

The variable γ represents the normal gravity on the reference ellipsoid (GRS80), which can be calculated using the Somigliana formula (Moritz, 1980).

$$\gamma = \gamma_e \frac{1 + k\, sin^2\varphi}{\sqrt{1 - e^2\, sin^2\varphi}} \tag{3.6}$$

Where γ_e is the gravity on the equator, k is the constant, e^2 is the first eccentricity and φ is the geodetic latitude. The numerical value of γ can be determined through the linear Equation as expressed:

$$\gamma = 9.9.780326771\, (1 + a_2\, sin^2\varphi + a_4\, sin^4\varphi + a_6\, sin^6\varphi + a_8\, sin^8\varphi \tag{3.7}$$

where

$$a_2 = 5.279\,0414 \times 10^{-3}, a_4 = 2.327\,18 \times 10^{-5}, \quad a_4 = 1.262 \times 10^{-7} \text{ and } a_4 = 7 \times 10^{-10} \tag{3.8}$$

$$H_P^N = H + (H_P - \zeta_P) \tag{3.9}$$

H represents the orthometric height of the gravity points, while the $(H_P - \zeta_P)$ indicated the geoid to quasigeoid separation, which could be computed based on the approximate formula according to the (Heiskanen & Moritz, 1967).

$$H_P - \zeta_P = \frac{\Delta g_B}{\gamma} H \tag{3.10}$$

where Δg_B is the Simple Bougeur Anomaly (SBA) and can be expressed as:

$$\Delta g_B = g_P - \gamma_Q + 0.1967H \tag{3.11}$$

Subsequently, the terrestrial gravity anomalies were compared with the GGM. However, GGM data lack short-frequency information, which predominantly originates from topographic masses. Consequently, according to Hofmann-Wellenhof and Moritz (2006), the impact of the topography or Residual Terrain Model (RTM) must be removed using the Simple Bouguer reduction to get a more accurate residual gravity anomalies using following Equation (3.12) and (3.13).

$$\Delta g = \Delta g_{FA} - \Delta g_{RTM} - \Delta g_{GGM} \tag{3.12}$$

where

$$\Delta g_{RTM} = 2\pi G \rho H \tag{3.13}$$

where G denotes the universal gravitational constant ($6672.59 \times 10 - 14\ m^3\ s^{-2}\ kg^{-1}$) and ρ denotes the density of earth's crust ($2.67\ gcm^{-3}$). H represent the height of point extracted from GDEM. Subsequently, the cross validation of the dataset was computed using kriging interpolation method. The kriging interpolation method were implemented as it poses better result compared to the IDW and Nearest Neighbour

method (Pa'suya, 2020). Then, the histogram is drawn based on the estimated residual from the cross-validation output from surfer. The plotted histogram used as indicator to set the tolerance in detecting the outliers in the dataset. These residuals were analysed using a histogram to evaluate their statistical distribution and identify potential outliers.

In this study, outliers refer to gravity anomaly observations exhibiting unusually large residuals relative to the overall dataset, which may arise from measurement errors, data recording mistakes, or local inconsistencies in the gravity field. The detection of outliers was carried out using the three-sigma (3σ) criterion, whereby observations with residuals exceeding ±3 standard deviations from the mean residual were considered anomalous and subsequently removed from the dataset. This approach assumes that the residuals follow an approximately normal distribution, in which about 99.7% of valid observations are expected to fall within the ±3σ interval as adopted from Montgomery & Runger (2018), using equation as expressed in Equation (3.14).

$$\mu - 3\sigma \leq r_i \leq \mu + 3\sigma \tag{3.14}$$

Where μ denotes the mean residuals, σ is standard deviation of residuals and r_i is the residual of i observation.

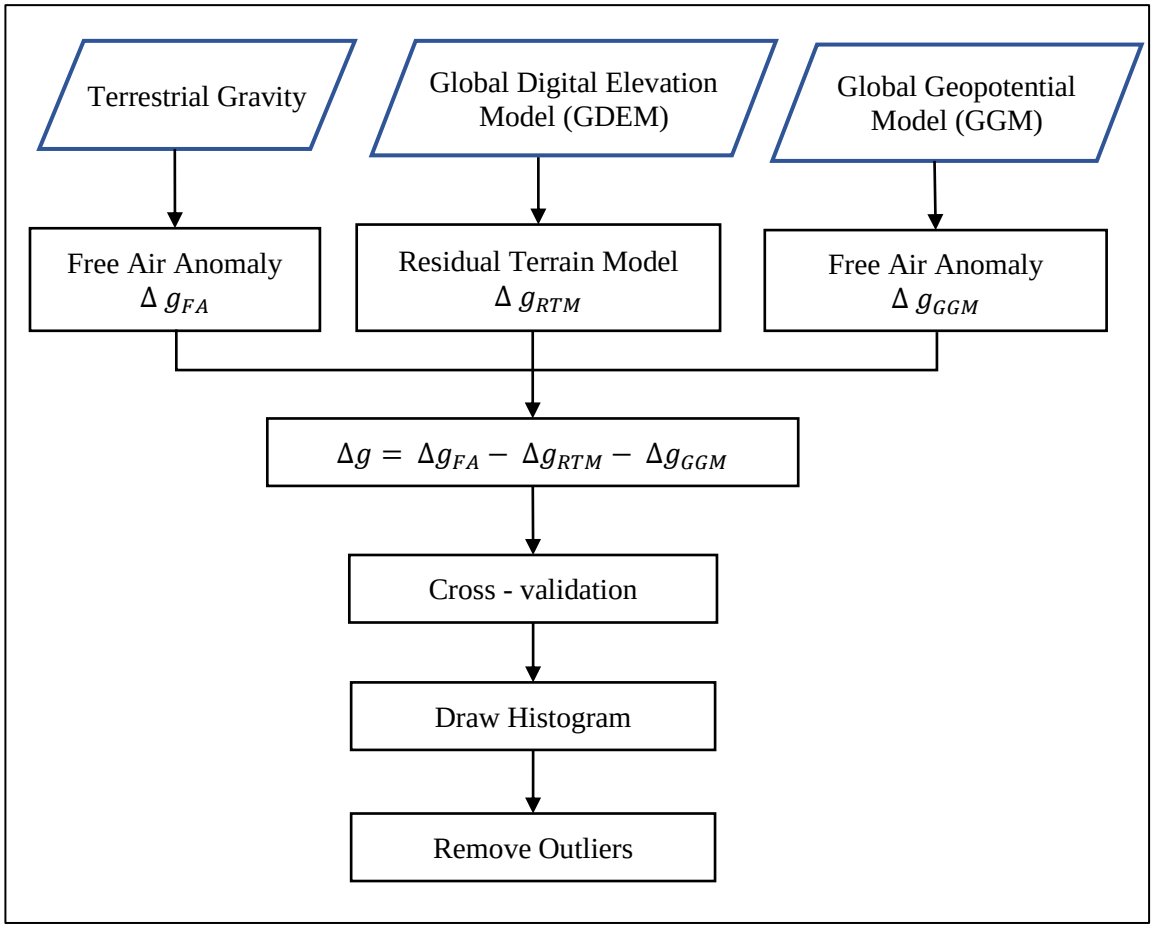


Figure 3. 9 Terrestrial Gravity Data Filtering

3.3.1.2 Accuracy Assessment of Input Dataset

In the pursuit of producing a highly accurate geoid model, a series of meticulous evaluations have been incorporated into the process to ensure the acquisition of the optimal input dataset. This comprehensive evaluation process includes the assessment of GGMs, least square parameters and marine gravity data. Each of these factors played a critical role in refining the input data, thereby enhancing the precision and reliability of the resulting geoid model in coastal region.

a) Evaluation of Global Geopotential Model

The selection of optimum GGM was pivotal in geoid computation using the LSMSA method, where the GGM model was utilized with terrestrial gravity data in the

combined solution (Ssengendo, 2015). In this research, five recent GGMs (as listed in Table 3. 4) were evaluated to find the best-fit GGM model for Peninsular Malaysia's region. In order to ensure consistent comparison and minimize biases arising from variations in reference ellipsoid, tide conventions, and geoid reference in all utilized GGMs were standardized into the tide-free system and employ GRS80 as the normal field (Vergo s et al., 2014). The choice of optimum GGM was determined based on the lowest standard deviation between the GGM and GNSS/levelling geoid heights. Geoid determination using the modified Stokes formula requires selecting an appropriate GGM and integrating it with local gravity data for a comprehensive solution. The evaluations were executed by comparing GGM derived geoid heights with values derived from GNSS/levelling data using the expressed formula in Equation (3.15).

$$\Delta N_i = N_i^{GPS} - N_i^{GGM} = h_i - H_i^{N-O} - N_i^{GGM} \tag{3.15}$$

where h denotes the ellipsoidal height, H_i^{N-O} indicates the normal orthometric height, and N_i^{GGM} represents the geoid height obtained from the GGM. However, it is widely recognized that GNSS levelling data comprehensively represent the entire geoid spectrum, whereas GGMs are constrained by their maximum degree and thus susceptible to omission errors and biases from GNSS and levelling data. To mitigate the impact of these systematic biases, absolute differences (ΔN_i) can be adjusted using parametric models fitted through least squares methods (Kiamehr & Sjöberg, 2005; Kotsakis & Sideris, 1999; Sansò & Sideris, 2013). The absolute differences are computed using a four-parameter models as derived:

$$\Delta N_i = a_i^T x + v_i \tag{3.16}$$

Where

$$x = [x_1\ x_2\ x_3\ x_4\ ]^T \tag{3.17}$$

$$a_i = [1\ cos\,\varphi_i\, cos\,\lambda_i \quad cos\,\varphi_i\, sin\,\lambda_i \quad sin\,\varphi_i]^T \tag{3.18}$$

The variable x denotes for a vector of unknown parameter, a_i represents a vector of predetermined coefficients that rely on the latitude (φ_i) and longitude (λ_i) of the points. v_i is mx1 vector of residuals where m signifies the count of GNSS levelling points.

b) Evaluation of Marine Gravity Model

As the initiative of refining the accuracy of geoid model particularly in coastal region, four recent marine gravity models were evaluated to select the best model that suits Peninsular Malaysia's region. The model includes DTU21GRA (O. B. Andersen & Knudsen, 2020), Sandwell and Smith (D. Sandwell et al., 2014), SDUST2020GRA (Li et al., 2024) and NSOAS24 (Zhang et al., 2025). These models were selected based on their temporal currency, spatial resolution, and regional applicability. Different marine gravity models were included during combine and gridding of gravity anomalies data, together with the airborne and terrestrial gravity dataset. After constructing the gravimetric geoid from each dataset combination, the models were validated against GNSS levelling data collected throughout Peninsular Malaysia. The evaluation process provided insights into the performance of different marine gravity datasets to identify the model that offered the most reliable representation of the geoid for the study area.

3.3.2 Combine and Gridding Free Air Anomalies Data

Prior to the computation of geoid model, the gravity anomalies data encompassed the terrestrial, airborne, and satellite-derived marine gravity data required to be presented in combined and gridded form. The anomalies in free air are closely linked to the altitude of observation, making direct interpolation impractical. To minimize interpolation errors, these anomalies are typically converted to simple Bouguer anomalies, which exhibit smoother characteristics compared to free air anomalies, before undergoing interpolation and gridding. Several researchers, including Featherstone and Kirby (2000), Kiamehr (2007), Yang (2013) and McCubbine et al. (2018). have suggested various approaches for combining and gridding gravity anomaly data. In this study, the method for combining and gridding gravity data follows the approach proposed by McCubbine et al. (2018). The method involved with the use of residual bouguer anomaly as stated in Equation (3.19).

$$\Delta\, g_{RB} = \delta g_B - \Delta g_{GGM} \tag{3.19}$$

where $\Delta\, g_{BA}$ represents the residual bouguer anomaly, Δg_{GGM} denotes the long wavelength of GGM gravity signal from bouguer anomaly data and δg_B is the bouguer's plate reduction. Subsequently, the gridded residual gravity anomaly after the interpolation process was added by the gridded δg_B and Δg_{GGM} to yield a final grid of surface gravity anomalies as expressed in Equation (3.20). The workflow of computation of residual bouguer anomaly is as illustrated in Figure 3. 10.

$$\Delta\, g_{gridded} = g_{r(gridded)} + g_{GGM(gridded)} + \delta g_{B(gridded)} \tag{3.20}$$

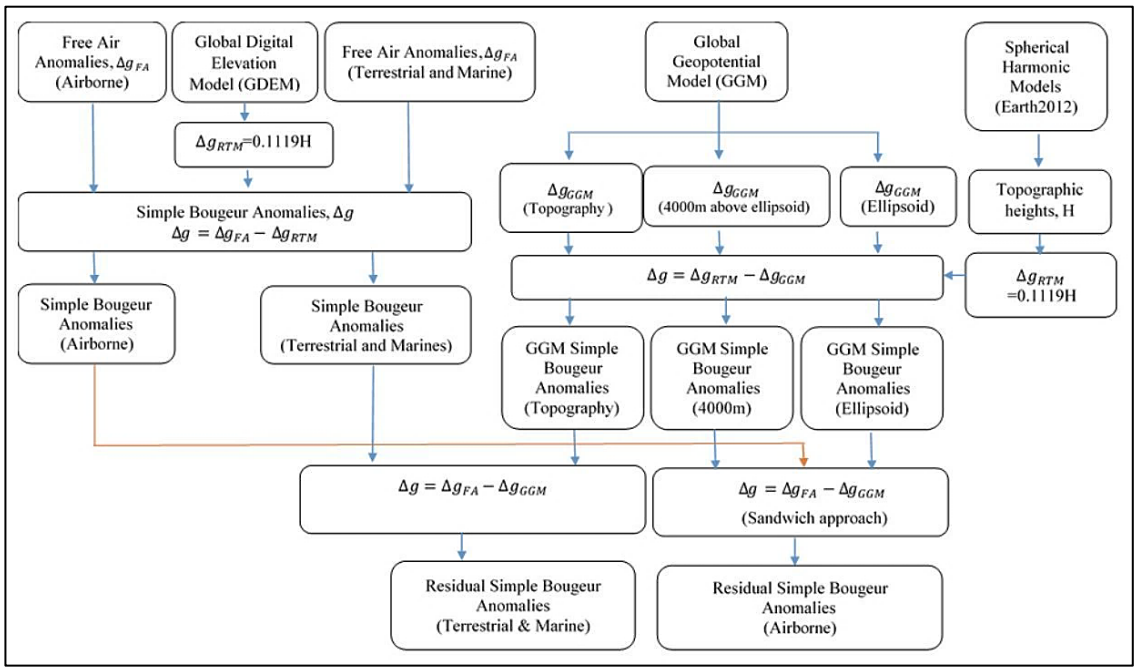


Figure 3. 10 Procedure To Compute Residual Bougeur Anomalies (Adopted from Pa'suya (2020))

After the computation of residual bouguer anomalies, the data were combined and gridded using 3D least square collocation (3DLSC) method. Although there are several regularisations technique to downward continuation (DWC) of airborne data, the 3DLSC was chosen for its ability to simultaneously combine, downward and gridding the gravity anomalies datasets encompassed the terrestrial, airborne, and

marine in a single procedure. The planar logarithmic covariance term for the LSC process is adopted from Forsberg (1987).

$$C\left(g_{1,}, g_2\right) = -f \sum_{k=0}^{3} \alpha_k \, log \; (D_k + \sqrt{r^2 + (D_k + h_1 + h_2)^2}) \tag{3.21}$$

where

$$f = C_0 \, log \left(\frac{(D+T)^3 (D+3T)}{D\,(D+2T)^3} \right) \tag{3.22}$$

The variable r is the planar distance between gravity observation sites (g_1 and g_2), (h_1 and h_2) are the heights, α_k = [1, -3, 3, -1], C_0 is the variance of the measurements g and D_k = D + kT and T are analytical parameters fitted to the g empirical spatial covariance. Figure 3. 12 is the workflow to combine and gridding the residual gravity anomalies data.

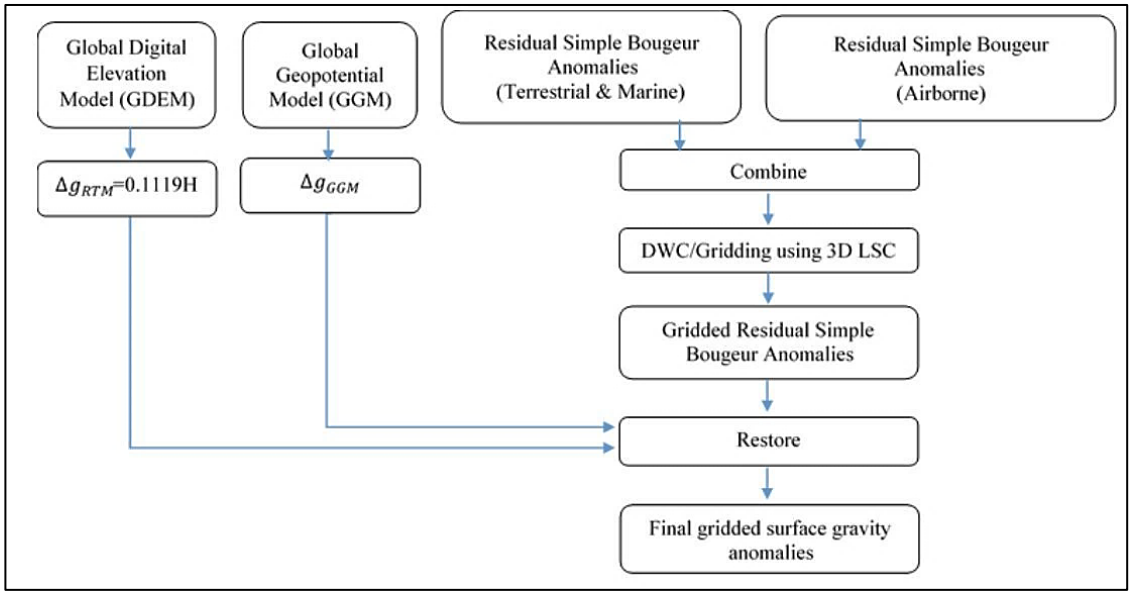


Figure 3. 11 Combine and Gridding Using 3DLSC (Adopted from Pa'suya (2020))

3.3.3 Computation of Gravimetric Geoid Model

The computation of gravimetric geoids in this study implements the KTH method developed at the Royal Institute of Technology (KTH) (Sjöberg, 2003b, 2003a, 2005, 2020). Figure 3. 12 illustrates the overview of KTH method with the implementation of Least Square Modification of Stokes's Formula with Addictive Correction (LSMSA).

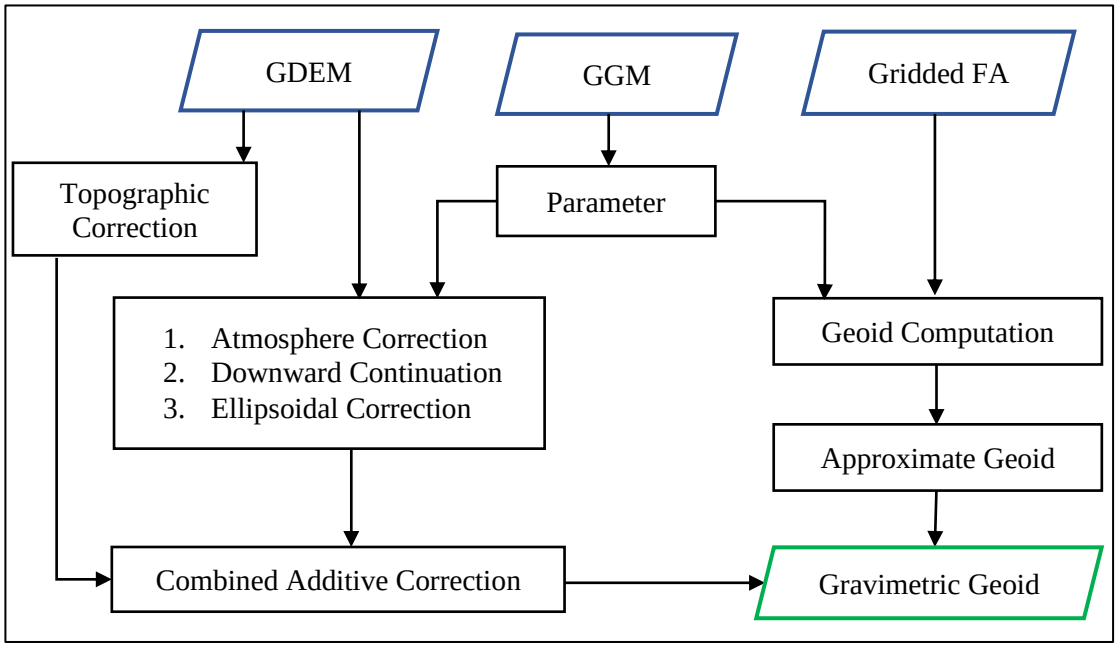


Figure 3. 12 Overview of Geoid Modelling Using LSMSA – KTH Method

3.3.3.1 Determination of Optimum Least Square Parameters

In geoid determination, the classical Stokes' formula often requires modification to minimize truncation errors, which arise primarily from the limited availability of terrestrial gravity data near the computation point. Since gravity data is often incomplete or unevenly distributed, the integration over the Stokes' kernel is typically confined to a spherical cap with a radius of only a few hundred kilometres. To address this challenge, stochastic modifications to Stokes' formula in Equation (3.23) have been introduced by (Sjöberg, 1991, 2003b). These approaches involve the incorporation of arbitrary modification coefficients denoted as S_n and b_n which are tailored to reduce the influence of data errors from both the terrestrial gravity observations and the GGM.

$$\bar{N} - \frac{c}{2\pi}\iint_{\sigma_0} S^L(\psi)\Delta g d\sigma + c\sum_{n=2}^{M} b_n \Delta g_n^{GGM} \tag{3.23}$$

From the formula, $S^L(\psi)$ represent the modified stokes kernel, Δg is the gravity anomlies and g_n^{GGM} refers to the spherical harmonic coefficients of GGM. The selection of S_n and b_n depends on several factors. This study emphasizes on the investigation of the correlation length of gravity field (ψ), standard deviation of the gravity anomaly errors ($\sigma_{\Delta g}$), maximum spherical harmonic degree (L) and upper degree of GGM (M) as summarized in Table 3. 11. Choosing appropriate values for these parameters is essential for improving the computational efficiency and ensuring stable geoid estimates, especially in regions with sparse gravity coverage. This necessitates rigorous numerical experiments to determine the optimal configuration of parameters and derive reliable modification coefficients for the geoid computation process.

Table 3. 11
The Summary of Tested Least Square Parameters

Parameter	Range
Correlation length of gravity field (ψ),	0.1˚ - 0.6˚
Standard deviation of the gravity anomaly errors ($\sigma_{\Delta g}$)	1 mGal – 6 mGal
Spherical harmonic degree (L) and upper degree of GGM (M) M = L	20 - 300

3.3.3.2 Approximate Geoid

The approximate geoid is important in deriving geoid height based on GGM data. Prior to the approximate geoid computation in this study, the GGM was integrated with gridded free air anomalies computed from the first and second strategies. According to L. Sjöberg (2003b), the approximate geoid is added with the combined additive correction for final gravimetric geoids computation using the formula in Equation (3.24).

$$\widetilde{N} = \frac{C}{2\pi}\iint_{\sigma_0} S^L(\psi)\Delta g d\sigma + C\sum_{n=2}^{L} b_n \Delta g_n^{EGM} \tag{3.24}$$

where $C = \frac{R}{2\gamma}$, R is the mean earth radius, γ is the mean normal gravity on the reference ellipsoid, Δg is the terrestrial gravity anomaly, b_n is the vector of the least square parameter for the optimum solution, $b_n = (Q_n^L + S_n^*)\frac{c_n}{c_n + dc_n}$ for $2 \leq n \leq M, \Delta g_n^{EGM}$ is the Laplace harmonics of degree n calculated from the GGM (Heiskanen & Moritz, 1967).

3.3.3.3 Additive Correction

ix) Topographic Correction

In KTH method, topographic correction is computed to remove the topographic effect due to the undulation of terrains or mountainous areas, particularly in Perak and Pahang states of Peninsular Malaysia. It is solved by a mathematical model in Equation (3.25), which is the combination of formula zero and first degree of direct and indirect topographic effects (Ssengendo, 2015).

$$\delta N_{comb}^{T}(P) \approx -\frac{2\pi\mu}{\gamma}\left(H^2(P) + \frac{2}{3}\frac{H^3(P)}{R}\right) \tag{3.25}$$

Where ρ is the crust density of earth, R is earth radius, H is the topographic elevation, P is the computation point and γ is the normal gravity on reference ellipsoid.

x) Downward Continuation

The Downward Continuation (DWC) correction is determined using the integration of optimum result of GGM model and its maximum degree parameter. Following Ssengendo (2015) computation is performed using Equation (3.26), (3.27), (3.28) and (3.29).

$$\delta N_{dwc}^{L} = \delta N_{dwc}^{B,L} + \delta N_{dwc}^{te,L} \tag{3.26}$$

where

$$\delta N_{dwc}^{B,L} = \delta N_{dwc}^{B,} + c \sum_{n=2}^{\infty} \left[\left(\frac{R}{r_p} \right)^{n+1} - 1 \right] (s_n^* + Q_n^L) \, \Delta g_n \tag{3.27}$$

$$\delta N_{dwc}^{B} \approx \frac{H_P \Delta g_n}{\gamma_0} + 3 \frac{H_P}{r_0} \zeta_P - \frac{H_P^2}{2\gamma_0} \left(\frac{\partial \Delta g}{\partial H_P} \right) \tag{3.28}$$

$$\delta N_{dwc}^{te,L} \approx \frac{R}{4\pi\gamma_0} \iint S^L(\psi) \left(H_P - H_Q \right) \left(\frac{\partial \Delta g}{\partial H_P} \right)_Q d\sigma_Q \tag{3.29}$$

From the Equation, ζ_P^0 is the approximate height anomaly at point P computed from GGM, $r_p = R + H_p$ is spherical radius where H_p is the orthometric height of point P and Q that represent moving integration point, and ψ is the modified strokes' formula.

xi) Atmospheric Correction

The atmosphere must be removed or minimized in condition where masses outside the geoid are removed from gravity anomalies, in order to fulfil the strokes' boundary condition (Danila, 2012). Following the Equation, combined atmospheric correction is as expressed in Equation (3.30) and (3.31).

$$\begin{aligned} \delta N_{comb}^{atm}(P) = {} & \frac{\delta V_0^a}{\gamma} - \frac{2\pi R \rho_A}{\gamma} \sum_{n=2}^{M} \left(\frac{2}{n-1} - s_n - Q_n^M \right) H_n(P) \\ & - \frac{2\pi R \rho_A}{\gamma} \sum_{n=M+1}^{\infty} \left(\frac{2}{n-1} - \frac{n+1}{2n+1} Q_n^M \right) H_n(P) \end{aligned} \tag{3.30}$$

where

$$H_n(P) = \sum_{m=-n}^{n} H_{nm} \bar{Y}_{nm}(P) \tag{3.31}$$

From the Equation, δV_0^a is the term of zero degree at atmospheric potential, ρ_A is the density at sea level, which is approximately equal to 1.23 e^{-1} (g /cm^3), γ is the mean normal gravity on ellipsoid reference, and H_n is the Laplace surface harmonic of degree n for the topographic height.

xii) Ellipsoidal Correction

The modified version of Strokes' formula that combine terrestrial gravity anomalies and GGM around computation point are commonly used to determine the final gravimetric geoid (Sjöberg et al., 2015b). This is because, when GGM correctly applied at sea level, the remaining ellipsoidal correction for Strokes' formula is limited to the integration capsize. The correction for ellipsoidal is derived using Equation (3.32) as follows:

$$\delta N_e(P) = \frac{R}{2\gamma}\sum_{n=2}^{\infty}\left(\frac{2}{n-1} - s_n^* - Q_n^M\right)\left(\frac{a-R}{R}\,\Delta g_n^{GGM}(P) + \frac{a}{R}\,(\delta g_e)_n\right) \quad (3.32)$$

where $s_n^* = s_n$ if $2 \leq n \leq M$ and $s_n^* = 0$, R is earth radius, P is the computation point, a is the semi-major axis, and γ is the normal gravity on reference ellipsoid. The final gravimetric geoids have been obtained by adding all the additive correction.

xiii) Final Gravimetric Geoid

In this research, the final gravimetric geoids were produced using several data sources which include gravity data that consist of marine, terrestrial, and airborne gravity data. In the KTH computation, the computation of final gravimetric geoid involved with adding the additive corrections to the approximate geoid that has been computed (as stated in Equation (3.33) to interpolate new geoid model which is the final gravimetric geoid as illustrated in Figure 3. 13.

$$N = \widetilde{N} + [\,\delta N_{comb}^{T} + \delta N_{dwc}^{L} + \delta N_{comb}^{atm} + \delta N_e] \quad (3.33)$$

Where $\widetilde{N}$ is the approximate geoid, δN_{comb}^{T} is the topographic correction, δN_{dwc}^{L} is the downward continuation, δN_{comb}^{atm} is the atmospheric correction and δN_e is the ellipsoidal correction.

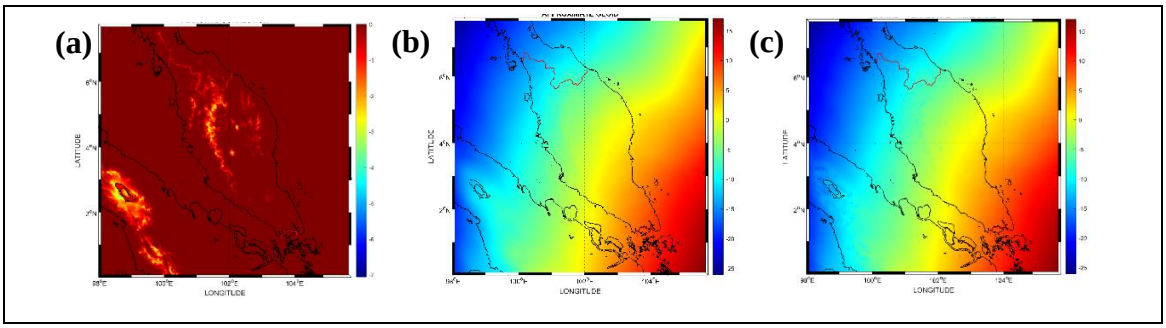


Figure 3. 13 The (a) Additive correction, (b) Approximate geoid, and (c) Gravimetric geoid

3.3.3.4 Evaluation of Final Gravimetric Geoid

The final computed gravimetric geoid was subsequently evaluated to determine the accuracy and reliability of the derived model. This evaluation was carried out by comparing the gravimetric geoid with local geometrical geoids obtained from a total of 45 GNSS levelling datasets, as previously illustrated in Figure 1. 4. The comparison enabled a direct assessment of the agreement between the two geoid representations at the selected control points. The accuracy of the gravimetric geoid model was quantified using the root mean square error (RMSE). The RMSE value was determined using the simple mathematical expression given in Equation (3.34). This involved computing the residuals between the geometrical geoid heights derived from GNSS levelling observations and the corresponding geoid heights interpolated from the computed gravimetric geoid model. The resulting RMSE value reflects the overall magnitude of the residuals and provides a clear measure of the performance and reliability of the developed gravimetric geoid.

$$RMSE = N_{geometrical} - N_{gravimetric} \tag{3.34}$$

3.3.4 Development and Evaluation of Hybrid Geoid

After acquiring the optimal gravimetric geoid, the developed gravimetric geoid model then underwent a fitting process prior to derive a new hybrid geoid model. Tthe hybrid geoid was generated by fitting the computed gravimetric geoid to the local GNSS/levelling data. This adjustment process was essential to minimize systematic

discrepancies and enhance the consistency between the gravimetric model and the national vertical control network. The computed hybrid geoid forms a crucial component of the vertical transformation datum, as it closely conforms to the official height system currently adopted in Malaysia's surveying practices.

The process of deriving the hybrid geoid was made by fitting the optimally computed gravimetric geoid in the preceding phase of this study to a total of 153 GNSS levelling data as illustrated in Figure 3. 14 marked with blue points. The fitting process was computed using the SURFER. A trend surface removal method specifically a 4 – parameter datum shift model was utilized in order to account the systematic differences between the gravimetric geoid and the GNSS levelling height. This method was applied to eliminate large scale biases and datum inconsistency as it implemented three shifts in the X, Y, and Z directions and one regional tilt component in the computation. The prediction method of interpolation was modelled using collocation, which also known as kriging method. This statistical interpolation technique accounts for both the spatial correlation structure of the residuals and the stochastic properties of the data, enabling the estimation of local corrections with minimized interpolation errors (Moritz, 1980).

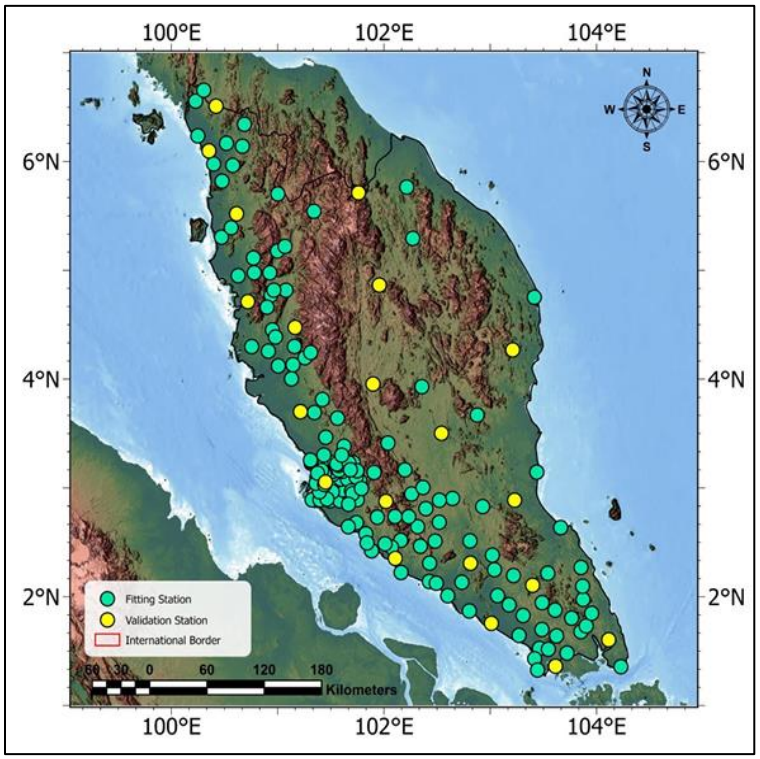


Figure 3. 14 GNSS Levelling Data for Hybrid Geoid Fitting and Validation

3.3.4.1 Analysis of Prediction Variable

Following the configuration of trend surface removal and prediction method, an additional sensitivity analysis was conducted in this study to determine the most appropriate prediction parameters related to the half correlation distance and RMS of data noise. The analysis involved a systematic variation of five distinct values for each parameter. According to Tscherning et al. (1992), the selection of an appropriate correlation distance should be informed by the spatial distribution of GNSS levelling data. Typically, correlation distances in the range of 50 km to 100 km are considered standard as they capture the local to regional variations in the gravity field while avoiding over smoothing. However, due to the relatively good amount and uniform distribution of GNSS levelling benchmarks across Peninsular Malaysia, this study extended the test range to include shorter correlation distances. Specifically, values from 20 km to 100 km were assessed at 20 km intervals. The inclusion of shorter distances such as 20 km and 40 km aim to better preserve the high-frequency geoid variations that closely align with the PMGVD. This approach helps to minimize the introduction of artificial biases and avoids excessive smoothing or shifting of the geoid surface, thereby ensuring that the fitted hybrid geoid remains realistic to the actual vertical reference system. Similarly, the data noise parameter, representing the stochastic error associated with the observational data was varied from 0.02 to 0.10 in increments of 0.02. This range reflects the typical signal-to-noise ratio observed in terrestrial and airborne gravity data when processed for regional geoid modelling. It is to identify the optimal setting that minimizes prediction error and enhances the reliability of the hybrid geoid.

3.3.4.2 Evaluation of Computed Hybrid Geoid Model

After completion of the fitting process in the development of the new hybrid geoid, the model was validated using 20 GNSS levelling data as depicted in yellow markes in Figure 3. 14. The GNSS dataset was carefully selected to ensure a well distributed spatial coverage so that the performance of the model could be evaluated fairly over the entire study area. In addition, the final hybrid geoid was compared with the existing hybrid geoid produced by DSMM namely WGeoid04, to investigate

whether the newly computed hybrid geoid provides an improvement in accuracy relative to the existing model.

3.4 Phase 3: Development of Marine Vertical Model

This section outlines the methods and procedures applied in the development of vertical separation models. The work draws on three main approaches including the analysis of coastal tide gauge records, processing of satellite altimetry data and the application of hydrodynamic modelling. Each approach is described in the following subsections providing a thorough breakdown of how these approaches were employed to fulfil the second objective of this study.

3.4.1 Tide Gauge Processing

Tide gauges data in this research utilized to for the purpose of validating the vertical separation models computed from assimilations of satellite altimetry and hydrodynamic modelling. In this study, tidal datums were derived using harmonic analysis approach through Unified Tidal Analysis and Prediction Functions (UTide) which is a tidal analysis tools developed by Codiga (2011). It includes enhancements that allow for the effective treatment of multi-year records with irregular temporal sampling. In harmonic analysis, the tidal time series is viewed as a combination of multiple cosine waves to estimate the tidal signal. The harmonic analysis coefficient parameters are used to determine the amplitude and phase of the primary tidal constituents (Hamden, 2022). For this research, tidal observations from tide gauges across Peninsular Malaysia were analysed using 35 harmonic constituents available in the system.

Prior to that, the required tidal time series were obtained from the DSMM via the UHSLC data repositories. Since the raw data from UHSLC were not in a format directly compatible with the processing software, a data preparation stage was necessary. This involved reformatting the tide gauge records into the input structure specified in Table 3. 12 to ensure smooth execution of the software. Once prepared, the analysis proceeded with the derivation of tidal datums specifically the LAT and HAT. These values were computed based on the highest and lowest predicted tides over a

period of approximately 18 years, corresponding to a full regression cycle of the lunar nodes as illustrated in Figure 3. 15.

Table 3. 12
Input Format for UTide

Year	Month	Day	Hour	Minute	Second	Sea level (mm)
1998	1	1	0	0	0	3540

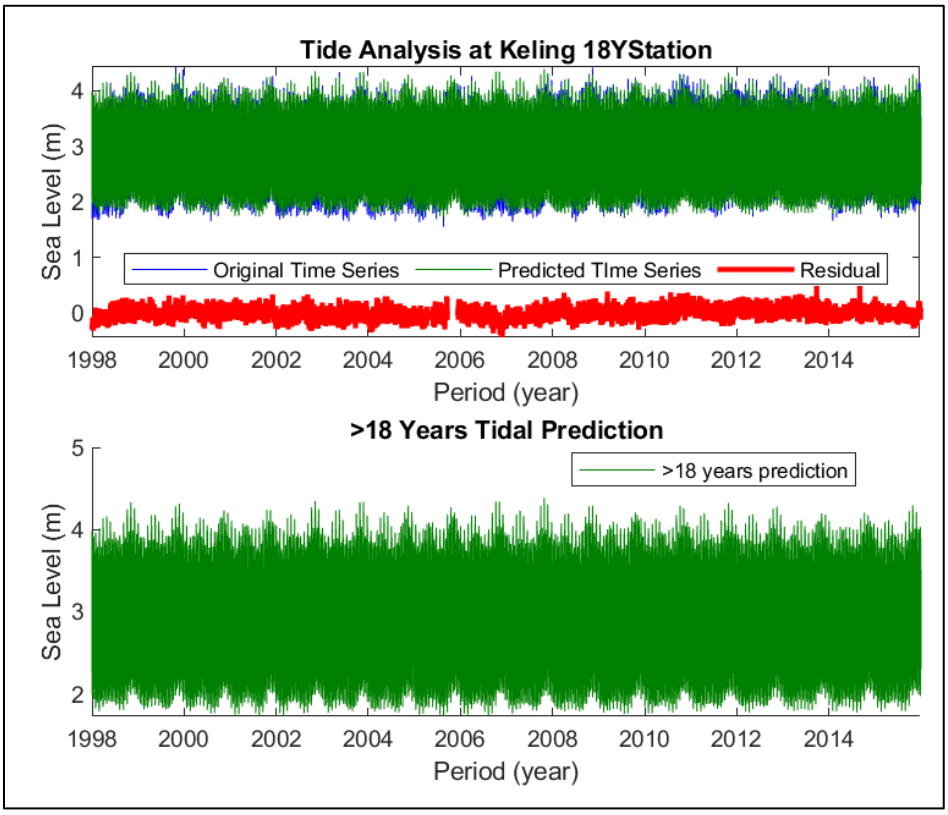


Figure 3. 15 Tidal Analysis and Tide Prediction at Tanjung Keling Using 18 Observation Period (1998 – 2015)

The UTide processing provides output of derived tidal datums with respect to the zero tide gauge. Since this study adopted an ellipsoid-based reference, a tide reduction procedure was carried out. The needs of same reference frame are pivotal for the integration process with other tidal datum from satellite altimetry and hydrodynamic data that derived the tidal based on ellipsoid surface. The procedure to reduce the tidal datum from tide gauges to ellipsoid can be realized through the GNSS levelling observation that has been carried out at every TGBM stations through the Tide Gauge

GNSS Campaign in 2019. The result of GNSS observation on each TGBM was then used to estimate the offset from each vertical surface to GRS80 ellipsoid as illustrated in Figure 3. 16. Subsequently, the formula as stated in Equation (3.36 is used to transform from zero tide gauge to GRS80 ellipsoid surface.

$$H_{LAT} = h_{GNSS} - H_{LEV} \tag{3.35}$$

In this context, H_{LAT} is the LAT value derived from UTide that refer to the zero tide gauge. The h_{GNSS} represent the ellipsoidal height at tide gauge benchmark acquired from GNSS observation and H_{LEV} corresponds to the height difference between the arbitrary tide gauge zero surface and the benchmark as provided by DSMM.

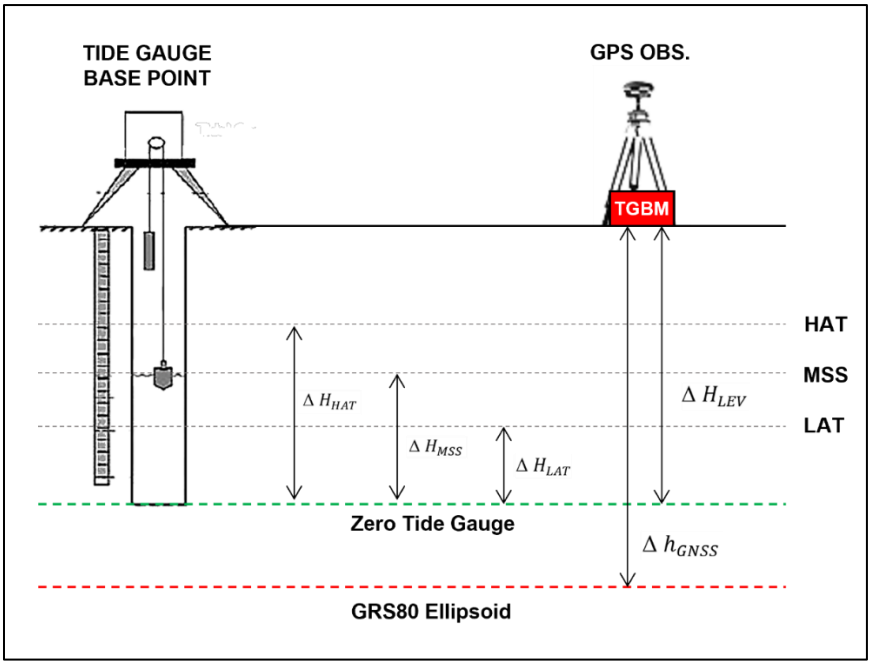


Figure 3. 16 Relationship Between the Various Surface for Computation of Offset in the Tide Reduction Determination

3.4.2 Satellite Altimetry Processing

Before the advent of satellite altimetry technologies, tide gauges were the sole source of data for ocean tide modelling. These instruments, primarily located along coastlines, provide highly accurate measurements of ocean tides and sea level variations. Tide gauges have been instrumental in our understanding of tidal behaviours, coastal processes, and sea over time. However, due to the sparse distribution of tide gauges around the globe, particularly in remote and deep-sea areas, their data could offer more insight into the spatial properties of ocean tides in the open ocean (Hamden et al., 2021). Coastal tide gauges, by their nature, are confined to the peripheries of landmasses and cannot capture the full complexity of that occur 10 kilometres further from shore (Abd Rahman et al., 2024).

In contrast, satellite altimetry offers extensive spatial coverage over the open ocean and has become an important source of sea surface and tidal information. Nevertheless, conventional satellite altimetry measurements within approximately 20 km of the coastline are often flagged as unreliable and excluded from analysis, as reported by Gommenginger et al. (2011), Cipollini et al. (2017), and Abd Rahman et al. (2024). The degradation in measurement quality in coastal regions is primarily attributed to land contamination of radar waveforms, inaccuracies in coastal tidal corrections, increased sea surface variability, and loss of altimeter tracking caused by interference from nearby land reflectors (Abdallah et al., 2022a) Despite these limitations, satellite altimetry remains the most effective approach for obtaining tidal information over offshore and open-ocean regions due to its wide spatial coverage and consistent observations. Consequently, complementary approaches are required to compensate for the reduced availability and accuracy of altimetric data in the nearshore zone, thereby ensuring a continuous and reliable representation of sea level from the coastline to the open sea. In this section, the processing steps for tidal modelling for satellite altimetry data were broken down as illustrated in Figure 3. 17.

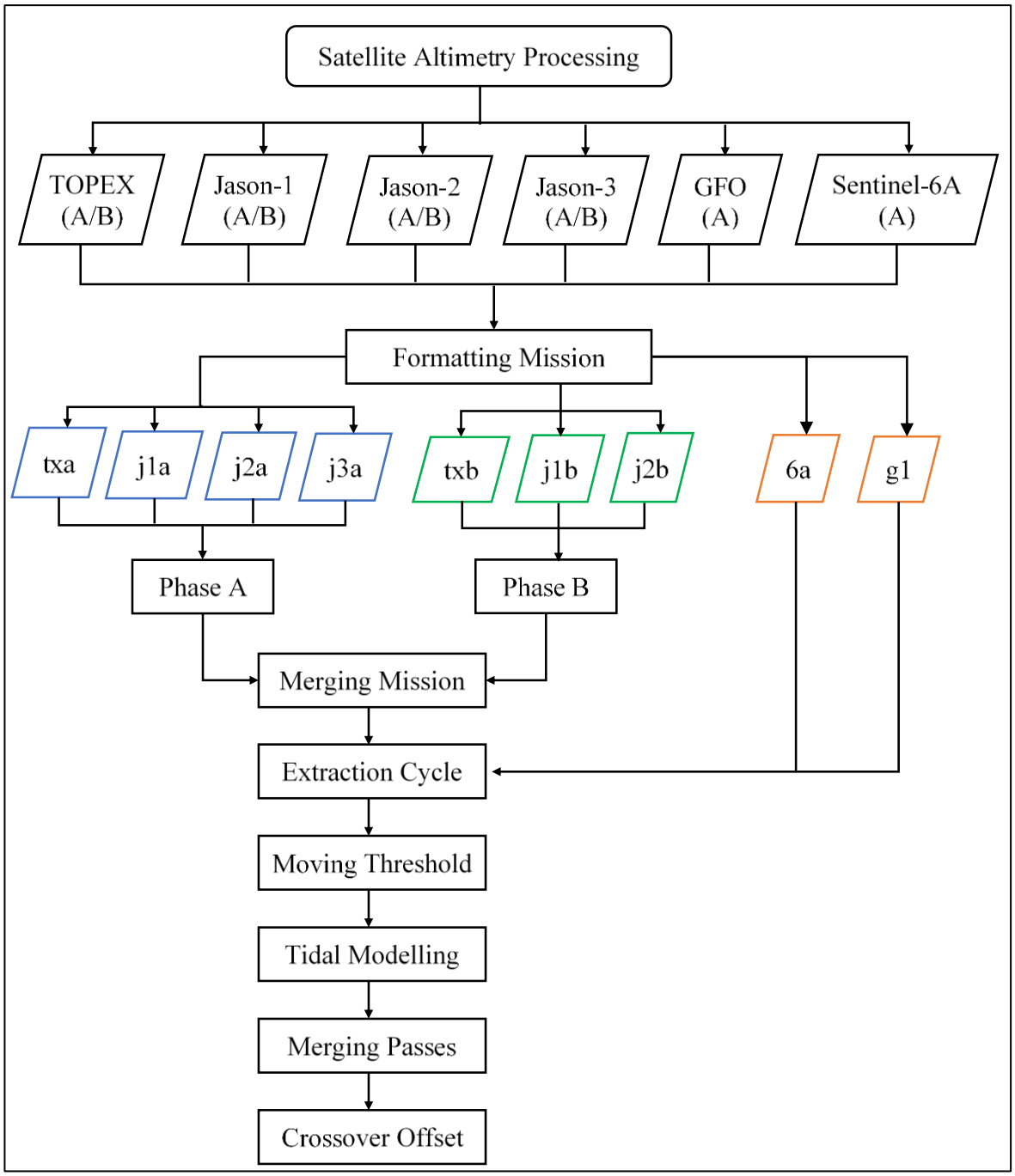


Figure 3. 17 Tidal Modelling using Satellite Altimetry Techniques

3.4.2.1 Formatting Mission

The first processing step in formatting mission involved with the computation of Sea Surface Height (SSH) that has been extracted from RADS system to compute the regional tidal datum. The computation of sea surface height has been carried out from six satellite mission consists of TOPEX, Jason-1, Jason-2, Jason-3, GFO, and Sentinel-6A. The SSH data utilized in this study spanning approximately 32 years from combined TOPEX class, GFO and additional Sentinel-6A that provide recent and denser SSH observation up to year 2024 data.

3.4.2.2 Merging Mission Class and Formation Time Series

After the formatting mission was complete, the data from satellite missions with the same phase and repeat period were merged into a single dataset. In this research, the TOPEX satellite mission was merged with Jason-1, Jason-2, and Jason-3 because they all have a repeat period of 10 days to return to their original position after orbiting the Earth. During this phase, careful attention to the arrangement of the data was crucial to ensure correct data merging, as the observation data must be in chronological order. For the merging of TOPEX class Phase A, the sequence of the data is as follows: TOPEX (25/09/1992 - 10/08/2002), Jason-1 (17/01/2002 - 26/01/2009), Jason-2 (04/07/2008 - 02/10/2016), and Jason-3 (12/02/2016 - 07/04/2022). This sequence shows that TOPEX began its mission in September 1992 and concluded in August 2002. Jason-1 then took over in January 2002 and operated until January 2009. Subsequently, Jason-2, launched in July 2008, replaced Jason-1, and continued until October 2016. Jason-3 followed, starting its mission in February 2016, and ending in April 2022. The overlapping date in SSH time series that existed between two adjacent mission was truncated to preserve the seamless uniform time intervals between the missions as illustrated in Figure 3. 18. Furthermore, the GFO and Sentinel-6A missions function independently and do not have overlapping time series with other missions, which prevents their SSH data from being merged with data from other satellites.

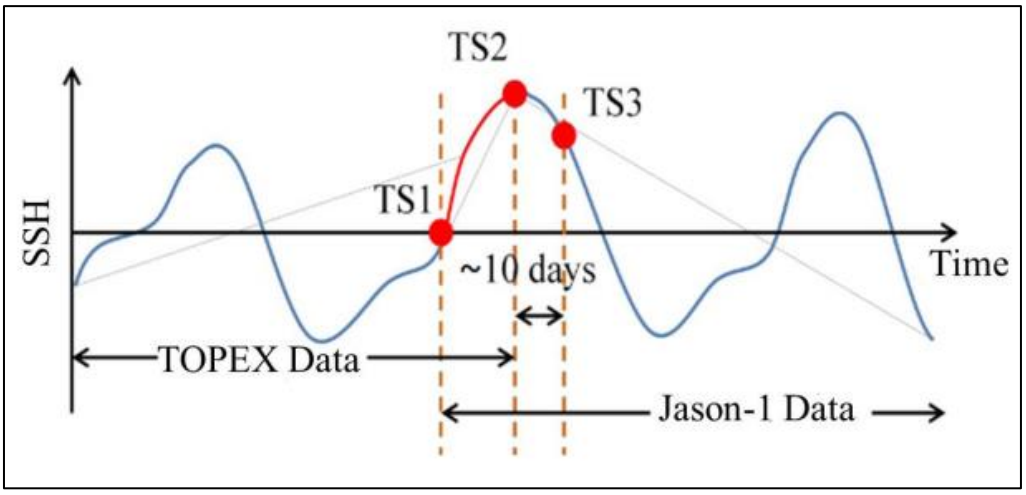


Figure 3. 18 Truncation of Overlapping Time Series in Merged Data (Hamden, 2022).

3.4.2.3 Extraction Cycle

The next process involved with the extraction of combined mission data based on the cycle and time periods to synchronizes the data. In the execution of extraction cycle system, the data from different satellite mission were extracted based on the specific time range and input of the pass number by having the TOPEX satellite mission as the reference point. For each reference point in TOPEX data, the closest point in other datasets is identified and store together in a merged file consists of a combined mission from older date to newer. The distance between the reference points and observation points uses the Haversine formula stated in Equation (3.36).

$$d = 2r \times \left(\sqrt{sin^2\left(\frac{\Delta\, \emptyset}{2}\right)} + cos(\emptyset_1) \times\ sin^2\left(\frac{\Delta\lambda}{2}\right) \right) \tag{3.36}$$

where $\Delta\emptyset$ is the difference in latitudes, $\Delta\lambda$ denotes the difference in longitude, and r is the earth's radius which is 6371 km.

3.4.2.4 Moving Threshold

Following the extracted data from the extraction cycle, the moving threshold process is applied to remove or set any data points to NaN beyond a specified distance threshold set at 7 kilometres (Hamden, 2022). This procedure is accounted to filter out erroneous or less reliable data points that could affect the accuracy of the derived measurements. The identification of threshold was derived from the Equation (3.37)

$$A\,[i,j] = \begin{cases} A[i,j] & if\ A[i,j] < 7 \\ NaN & if\ A[i,j] \geq 7 \end{cases} \tag{3.37}$$

where i is the row index and j ranges from 2 to 7, in which the column to be set to NaN if the distance condition is met.

3.4.2.5 Tidal Analysis and Prediction

The following processing step involved the tidal analysis and prediction derived from the harmonic constituents' amplitudes and phases. The tide prediction used the harmonic approach by interpreting the SSH times series from the TOPEX class, GFO and Sentinel-6A mission. During the process, the dataset was filtered by the implementation Upper Control Limit (UCL) of 3σ rule to remove the outliers using the formula stated in Equation (3.38).

$$UCL = \mu + 3\sigma \tag{3.38}$$

where the mean (μ) and standard deviation (σ) is computed to set the control limit, where data that exceed the limit will be replaced as NaN. The tidal prediction and classification were computed using Form Factor (F) method to identify the type of tides through the interpretation of amplitudes and phases from harmonic constituents. Apparently, four tidal constituents namely K1, O1, M2, and S2 indicated as the most dominant tidal characteristic in Peninsular Malaysia. Thus, these constituents were denoted in the Equation (3.39) to derive the tidal types.

$$F = \frac{K1 + O1}{M2 + S2} \tag{3.39}$$

The type of tide was classified based on the value of F as follows: diurnal if F > 3.0, semi-diurnal if F ≤ 0.25, mixed - predominantly diurnal if 1.5 < F ≤ 3.0, and mixed - predominantly semi-diurnal if 0.25 < F ≤ 1.5. Subsequently, the tidal analysis to derive the HAT, LAT, and MSL based on the principle of harmonic analysis, where the sea level is represented as a sum of sinusoidal functions corresponding to different tidal constituents. The computation of tidal sea level at time, SL (t) and following HAT, LAT, and MSL are as stated in Equation (3.40), (3.41), (3.42), and (3.43).

$$SL\ (t) = \sum_{i=1}^{N} A_i\ cos\ (w_i t + \emptyset_i) \tag{3.40}$$

$$HAT = Max\ [SL(t)] \tag{3.41}$$

$$LAT = Min\ [SL(t)] \tag{3.42}$$

$$MSL = \frac{1}{N} \sum_{i=1}^{N} SL(t) \tag{3.43}$$

where, N is the number of tidal constituents, A_i represents the amplitude, w_i is the angular frequency, $\emptyset_i$ is the phase of tidal constituents and t is the time which the sea level is calculated.

3.4.2.6 Merging Pass

After acquiring the tidal datum from the previous tidal analysis output, the LAT-MSL-HAT (LMH) information is consolidated into a single comprehensive file. This file integrates the essential tidal parameters, providing a consolidated resource for the last processing steps involved with the crossover offset.

3.4.2.7 Crossover Offset

The final stages of satellite altimetry processing focus on determining the crossover offset between two missions. This step is crucial for facilitating comparative analysis and quality assessment of data collected from different missions. The process includes calculating the Upper Control Limit (UCL) and Lower Control Limit (LCL) using 3σ as stated in Equation (3.38) and (3.44). Once the crossover offset is applied to the data, it undergoes conversion from the TOPEX Ellipsoid to the WGS84 Ellipsoid reference surface to produce the final output.

$$LCL = \mu - 3\sigma \tag{3.44}$$

3.4.3 Hydrodynamic Ocean Modelling

Hydrodynamic modelling is one of the alternatives to acquired vertical separation on coastal area as limitation existed in if the tidal datum were to fully dependent from the tide gauges or satellite altimetry data. As for tide gauges, the tidal datum can only be produced in a smaller scale not further that 10 kilometres from the buffer distance of tide gauge station due to the changes in sea behaviours (Abd Rahman et al., 2024). At the same time, satellite altimetry data is advantageous to provide tide prediction on a larger scale. However, the satellite-derived SSH data within 20 kilometres from coastal are known to be problematic and often excluded in the tidal computation (Hart-Davis et al., 2023). In order to cater with those limitations, hydrodynamic approach is taken as supplementary data to fill the loophole 20 kilometres along coastal area of Peninsular Malaysia with sea level data. The hydrodynamic data were derived through the tidal prediction using Tide Model Driver (TMD).

3.4.3.1 Spatial Buffer Region

The first steps required the needs to create a spatial grid point for the study area. First, spatial grid points were generated within the enclosed boundaries of the study area

using interval 0.09 which is approximately equal to 10 km. This grid and the shapefile for Peninsular Malaysia's boundaries were imported into Global Mapper software for further editing and buffering. Using Global Mapper's buffer tools, a 20-kilometer buffer zone around Peninsular Malaysia was created, as depicted in Figure 3. 19 (a). Grid points located outside this buffer zone were then removed, leaving only the points within the buffered region. This process resulted in a total of 541 grid points within the buffer zone shown in Figure 3. 19 (b), which were subsequently exported into a .txt file which facilitated subsequent data extraction and analysis.

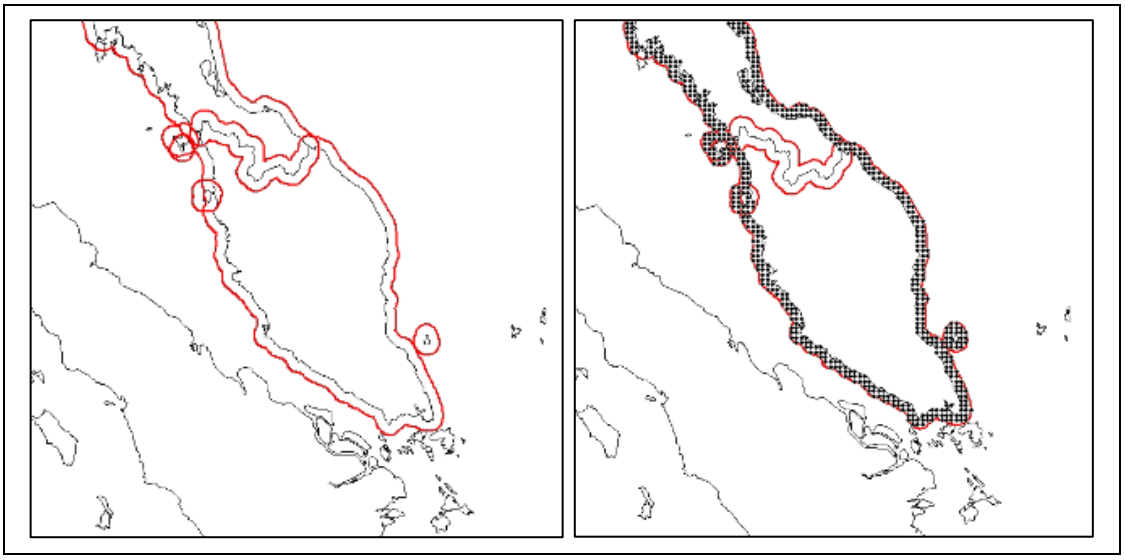


Figure 3. 19 Diagram of (a) Spatial Buffering (Red Line) Extended 20 Kilometres From Shoreline and (B) Hydrodynamic Data Points Within Buffer Region.

3.4.3.2 Extraction of Tidal Data using Tide Model Driver (TMD)

The data extraction for tidal data were extracted from Indian Ocean Model using Tide Model Driver (TMD) software. It is a system developed by Oregon State University (OSU) and Earth and Space Research (ESR) to derive the harmonic constituents for tidal modelling (Padman et al., 2015). The system is a MATLAB based toolbox which provide the scripts to access the tidal fields and prediction, and a geographical user interface enable user to browse and select the fields for specific prediction variables. The interface of the TMD system is as depicted in Figure 3. 20. Before the data extraction can be made, each point that has been exported from Global

Mapper were sorted into separate individual file and arranged according to TMD's specified input format. The arrangement format of the data input is [lat long yy mm dd hh mi sec dt_min TSLength]. The value of dt_min represents the interval of data in minutes and the TSLength determined by the calculation of specific duration tide prediction using formula stated in Equation (3.45).

$$24\ hours\ \times 365\ days\ \times Duration\ of\ tide\ prediction \tag{3.45}$$

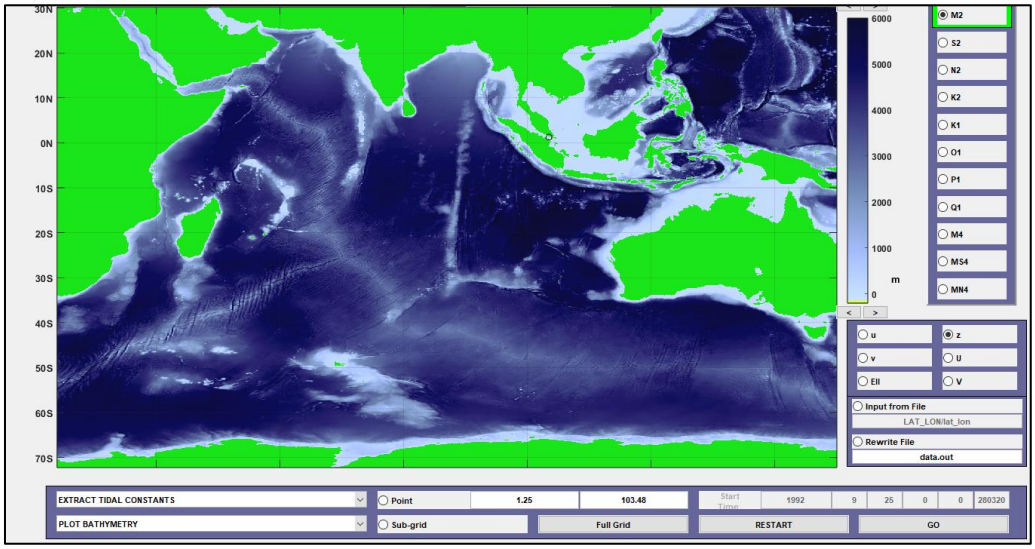


Figure 3. 20 TMD Interface (Padman et al., 2015)

In the processing, the reference model was user's preference. In this research, the tide prediction was derived from the Indian Ocean Model downloaded from the repository website at (https://www.tpxo.net/regional). The Indian Ocean Model is one of the global ocean models that provide the regional coverage for Malaysia which facilitate the extraction of data from it. The tidal prediction in TMD is derived using harmonic analysis based in specified harmonic constituents. It involved with the interpretation of amplitudes derived from harmonic constituents consist of the M2, S2, N2, K2, K1, O1, P1, Q1, M4, MS4, and MN4. After a successful derivation of the point, the output will come out as depicted in Figure 3. 21. Subsequently, the time series data underwent a sorting and computation process to derive the HAT, LAT, and MSS. The indicator of HAT and LAT were interpreted by sorting the sea level data from highest to lowest, and vice versa. The highest recorded data is noted as the HAT and the lowest

recorded data indicated as LAT. The value of MSS acquired by computing the average of the recorded value from data derived for 32 years observation period starting from 1992 to 2024.

```
Lat:     1.2500, Lon:   103.4800, Parameter: z(m)
Depth (m):      26.19
Constituents included: m2  s2  n2  k2  k1  o1  p1  q1  m4  ms4 mn4
Time start: 00:00,  9.25.1992
Time step (min):      60.00
Time Series length (hours):280320
25-Sep-1992 00:00:00    -0.3628
25-Sep-1992 01:00:00    -0.0464
25-Sep-1992 02:00:00     0.2434
25-Sep-1992 03:00:00     0.4261
25-Sep-1992 04:00:00     0.4678
25-Sep-1992 05:00:00     0.3795
```

Figure 3. 21 Sample of TMD Output

3.4.3.3 Selection of Global Mean Sea Surface (MSS) Models

In this phase, a global MSS model was required to transform the hydrodynamic outputs from the TMD into the GRS80 ellipsoid reference surface. The selection of the appropriate model was based on accuracy assessments against local tide gauge data. Several global MSS models were considered, including both direct models and replicated versions derived from combinations of geoid models and MDT models. This stage was particularly important because different models are defined with varying reference surfaces and tidal systems. To address this, a detailed inspection was undertaken to identify models that required additional processing in order to standardize their spatial metadata and minimize potential error propagation. Filmer et al. (2024) highlighted the importance of this step, noting that replicated models need particular attention as the ellipsoid reference and tidal system used for MDT models must align with those of the original MSS models to ensure accurate representation of MSS values as summarized in Table 3. 13.

Table 3. 13
The Summary of Direct MSS, Geoid and MDT Models used.

	Model	Ellipsoid Reference	Tide System
MSS	SDUST2020	TOPEX	Mean Tide
	DTU21	TOPEX	Mean Tide
	CNES-CLS22	TOPEX	Mean Tide
Geoid	WHU-SWPU-GOGR2022S	GRS80	Tide free
	GOSG02S	GRS80	Tide free
	XGM2019e	GRS80	Tide free
	PMGG2022	GRS80	Tide free
	Gravimetric geoid (Computed)	GRS80	Tide free
		MSS	**Geoid**
MDT	DTU22	DTU21MSS	XGM2019e
	DTUUH22	DTU21MSS	XGM2019e
	MDOT Hawaii	Drifter-derived AVISO	GRACE

It is known that GNSS observations provide heights that are referenced to a reference ellipsoid, most commonly GRS80 or WGS84 (Moritz, 2000). In geodetic practice, many global and regional geoid models are computed based on the parameters of the GRS80 ellipsoid (Filmer et al., 2024). In contrast, most MSS models are referenced to the TOPEX/Poseidon ellipsoid as these MSS products were originally derived from multi-mission satellite altimetry observations (O. B. Andersen et al., 2018). It is important to note that each reference ellipsoid is defined by its unique set of geometric parameters, including the semi-major axis (a), semi-minor axis (b), flattening (1/f), and eccentricity (e) as listed in Table 3. 14. These parameters determine the mathematical surface of the ellipsoid and directly affect how geodetic coordinates (latitude, longitude, and ellipsoidal height) are represented. This study chooses to standardize all geoid and MSS models to the GRS80 ellipsoid to ensure the consistency across the integration. This harmonization allows GNSS-derived ellipsoidal heights to be directly compared and integrated with the vertical models. Furthermore, the use of a single reference ellipsoid is essential for the practical implementation of vertical

transformation models in field surveys to avoid systematic errors in height determination due to the mismatch ellipsoid reference.

Keysers et al. (2013) stated that the conversion from TOPEX/Posidon ellipsoid to GRS80 ellipsoid can be converted by simply subtracting a constant value from MSS models. The difference between these ellipsoids usually between -70 cm to -71.36 cm at equator and pole respectively. This aligned with study by Filmer et al. (2024) and (O. B. Andersen et al., 2018), which indicated that the difference is approximately -70.4 cm. Therefore, this study adopted the similar constant value of -70.4 cm to transform all models into GRS80 based reference.

Table 3. 14
The Properties of Ellipsoids [Unit: Meter] (Keysers et al., 2013)

Properties	**GRS80**	**WGS84**	**TOPEX/Poseidon**
Semi-major axis (a)	6378137.0000	6378137.0000	6378136.3000
Semi-minor axis (b)	6356752.3141	6356752.3142	6356751.6006
Flattening (1/f)	298.2572	298.2572	298.2570
Eccentricity (e)	0.08181919	0.08181919	0.08181922

Another parameter considered in this study is the tide system used in each model. The permanent tide of the Earth is caused by the gravitational pull of the Sun and Moon which creates a small deformation of the Earth especially near the equator. Depending on whether this effect is kept or removed, different tide systems are defined. The mean-tide system keeps the effect of the permanent tide in the Earth's shape, while the tide-free system removes it. There is also a zero-tide system, where the permanent tide is removed but its indirect influence on gravity is still kept (Mäkinen, 2021). In most cases, GNSS heights are given in the tide-free system, while many global MSS models are provided in the mean-tide system. If these two systems are used together without adjustment, small but important errors can occur. Therefore, all models in this study were converted into the tide-free system to avoid accumulation of errors and to match with the GNSS observations. The conversion was done using the formula given by Petit & Luzum (2010), as shown in Equation (3.46).

$$h_{TF} = h_{MT} - A_0 h_2 \tag{3.46}$$

Where A_0 is D $(\frac{1}{3} - Sin^2\phi)$ with ϕ latitude and $D = 29.767$ cm. h_2 is the love number equal to 0.6078.

3.4.4 Combination and Integration of Tidal Datums

The integration of tidal datum is essential to obtain a unified tidal datum based on the satellite altimetry derived tide models and hydrodynamic model derived from TMD into a single seamless model for HAT and LAT. Before the integration can be happened, the satellite altimetry data were gridded using kriging interpolation method in surfer software. The interpolation process is meant to acquire a uniform dataset that share the same interval as the geoid model subjected to calculate vertical datum offset in the development of vertical transformation model. The interval of the gridded satellite altimetric data is set to be the same as the computed hybrid geoid which is 1-minute spacing, equivalent to 1.8 kilometres. The gridded altimetric data on land region and 20 kilometres beyond the shoreline were eliminated as the tidal data only meant for the coastal area and the altimetry data are problematic unreliable along the shoreline (Pa'suya et al., 2023). Figure 3. 22 is the visualization on data integration between the gridded altimetric data and hydrodynamic data. Subsequently, total of three vertical separation models consist of LAT, and HAT are computed.

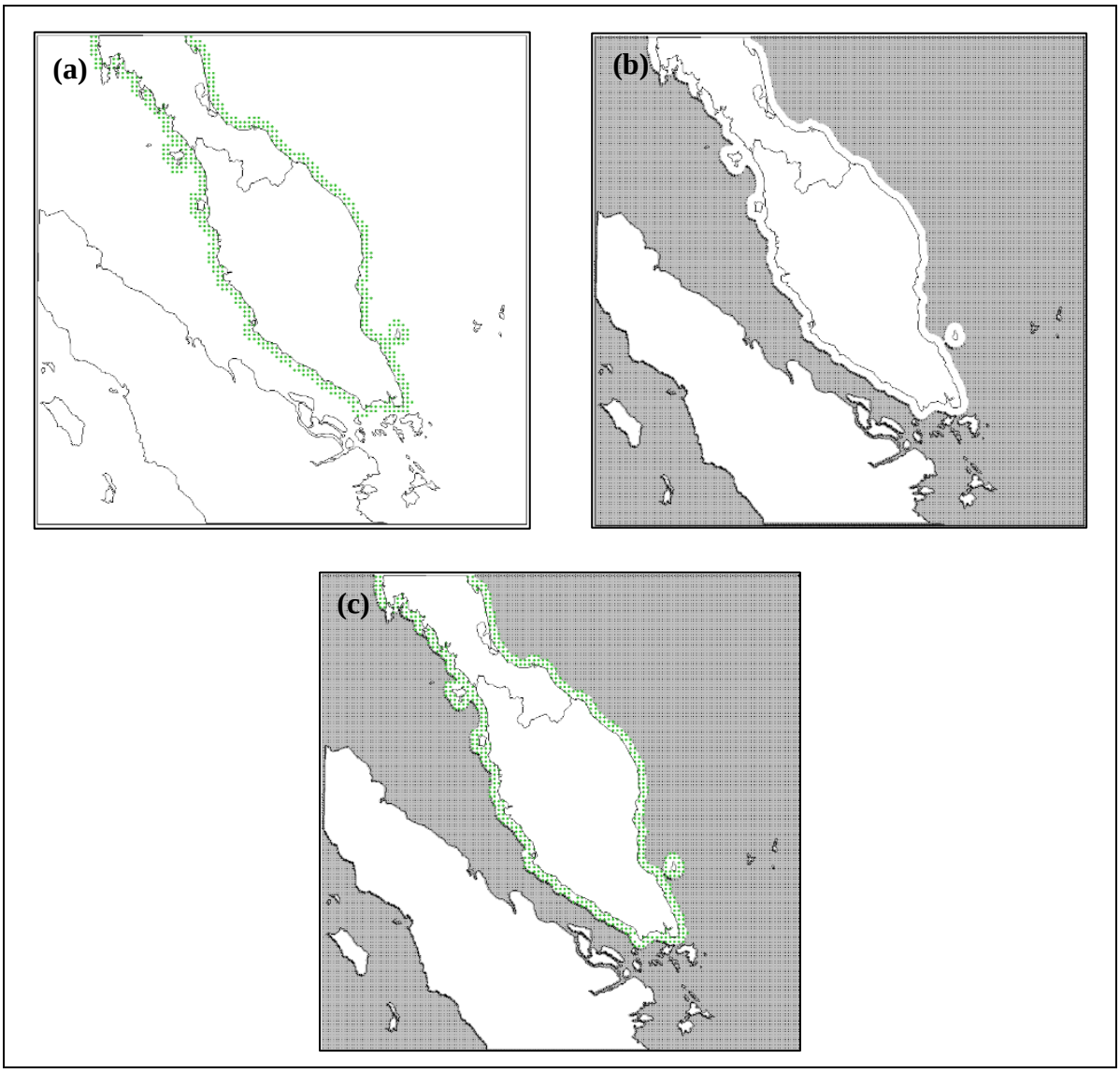


Figure 3. 22 Integration of Tidal Datum from (A) Hydrodynamic Data, (B) Gridded Altimetric Data and (C) Combination of Both Data

3.4.5 Validation of Vertical Separation Models

Validation of the developed vertical separation models can be performed by comparing the models with tidal datum from tide gauge stations. Total of eleven tide gauges as listed in Table 3. 6 was utilized to compute the difference and RMSE from tidal datum derived from tide gauge and satellite altimetry data using formula expressed in Equation (3.47) and (3.48) respectively. However, the limitation existed as the number of tide gauges are too little considering the vast study area covering the Peninsular Malaysia and the reliability of validation can only be ensured within 10

kilometres buffer zone of the tide gauge location. This is because the characteristic of the sea varies from one location to another. Thus, validation for data exceeding 10 kilometres from the tide gauge is considered as inaccurate.

$$\Delta\, LAT \;=\; LAT_{TG} - \; LAT_{model} \tag{3.47}$$

$$\Delta\, HAT \;=\; HAT_{TG} - \; HAT_{model} \tag{3.48}$$

3.5 Phase 4 : Development of Vertical Transformation Model

This research adopted an ellipsoid-based approach, wherein all respective models encompassed the hybrid geoid, LAT and HAT utilized a uniform reference surface specifically the GRS80 ellipsoid surface as zero origin. The computation of vertical datum offsets (VDO) was conducted specifically for three different models as illustrated in Figure 3. 23 and Figure 3. 24. The methodology for deriving these offsets involved a straightforward mathematical Equation as expressed in Equation (3.49).

$$\Delta\, Offset \;=\; Model\,1 - \; Model\,2 \tag{3.49}$$

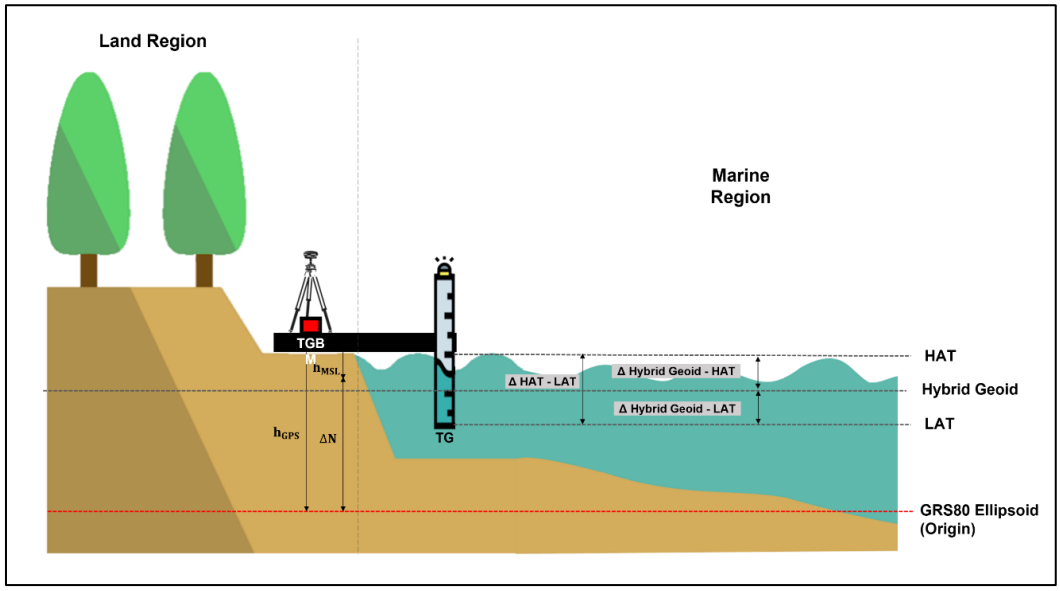


Figure 3. 23 Relationship Between Each Vertical Datum Offset (VDO)

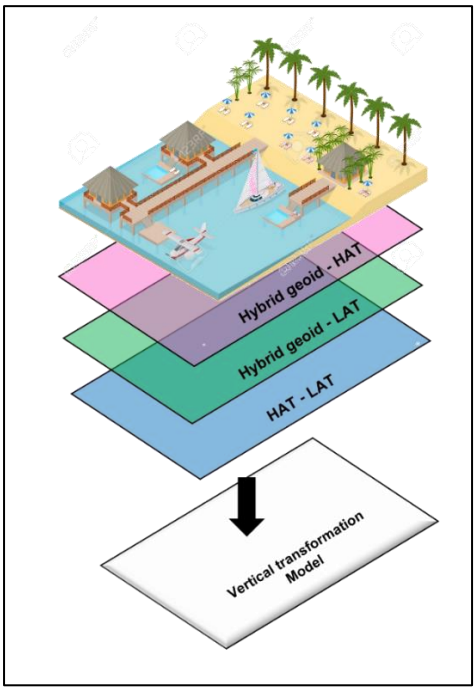


Figure 3. 24 Illustration of Vertical Transformation Model

The computed VDOs were then validated once again using offset value derived from tidal datum at the tide gauge stations to access the accuracy of computed transformation models in this study.

3.6 Phase 5 : Conclusion and Recommendation

The final phase focused on drawing conclusions from the results of the vertical transformation model and providing recommendations for future work. At this stage, the study also identified the main constraints and challenges faced during the research. These limitations were carefully analysed and used to shape recommendations that can guide future studies toward more complete and reliable outcomes. The recommendations highlighted the need for a multidisciplinary approach, as vertical transformation models involve knowledge from different scientific fields. Encouraging collaboration across disciplines will help to improve both the accuracy and the applicability of future research. In this way, the findings of this study can serve as a foundation for further investigations, allowing future work to refine, expand, and strengthen the understanding of vertical transformation in geodetic applications.

3.7 Chapter Summary

Chapter 3 outlines the methodology adopted in this study, which is organised into a series of structured phases to ensure a consistent and systematic workflow in developing the geoid model, marine vertical model, and vertical transformation framework. The chapter begins with an overview of the research design, followed by Phase 1, which covers data acquisition from multiple sources. These include terrestrial, airborne, and satellite-derived marine gravity data, as well as Global Digital Elevation Models (GDEM), Global Geopotential Models (GGM), GNSS levelling observations, tide gauge records, satellite altimetry products, global tide models, Mean Sea Surface (MSS), and Mean Dynamic Topography (MDT). Each dataset is incorporated to support different aspects of the modelling process and to ensure a comprehensive geodetic and oceanographic representation.

Phase 2 describes the development of the gravimetric geoid model. This stage involves initial data screening and pre-processing, including filtering of terrestrial gravity observations, assessment of input data quality, and the integration and gridding of free-air anomaly data. The geoid computation is then carried out using a least squares approach, followed by the derivation of an approximate geoid surface and the application of additive corrections. The resulting gravimetric geoid is evaluated, and a hybrid geoid is subsequently developed by incorporating additional prediction variables to improve model consistency and performance.

Phase 3 focuses on the development of the marine vertical model. This phase includes the processing of tide gauge records and satellite altimetry data, covering mission standardisation, time series generation, cycle extraction, data filtering, tidal analysis and prediction, merging pass, and crossover adjustment. In parallel, hydrodynamic modelling is performed through spatial buffering, extraction of tidal data using the Tide Model Driver (TMD), and assessment of selected MSS models. The outputs are then combined to establish consistent tidal datums, which are subsequently validated. Phase 4 describes the development of the vertical transformation model, which integrates outputs from both the geoid and marine vertical components to establish a unified vertical reference framework. Finally, Phase 5 summarises the study and presents concluding remarks together with recommendations for future work.

CHAPTER 4
RESULT AND DISCUSSION

4.1 Introduction

This chapter presents the outcomes of the vertical transformation model developed from various vertical reference surfaces to achieve the unification of land and marine vertical datums. The first objective focused on the computation of a refined marine gravimetric geoid and the construction of a corresponding hybrid geoid model. Subsequently, the discussion proceeds to the second objective which involved the derivation of tidal datums using satellite altimetry data, hydrodynamic model, and processed coastal tide gauge observations. The vertical transformation offsets derived from the integration of models in the first and second objectives represent the final outputs of this research. Furthermore, all results obtained in this study are systematically analysed and further discussed throughout this chapter.

4.2 Computation of Geoid Model

4.2.1 Assessment of the Impact of Global Geopotential Models on the Geoid Model

As elaborated in previous section, the GGM constitutes a fundamental input necessary for geoid determination. Therefore, to assess their suitability, five contemporary GGMs were included in the geoid computation, with model accuracy evaluated against 45 GNSS levelling benchmarks within the study area (refer to Figure 3.7). The statistical outcomes of this validation, including minimum, maximum, mean geoid height, root mean square error (RMSE), are summarized in Table 4. 1. Among the tested models, WHU-SWPU-GOGR2022S and GOSG02S exhibits the lowest RMSE of 0.040 m indicating the highest agreement with the reference GNSS levelling data. However, despite having identical RMSE values, the geoid surfaces derived from WHU-SWPU-GOGR2022S and GOSG02S are not identical. This is evident from the variation in their respective minimum, maximum, and mean geoid heights. WHU-

SWPU-GOGR2022S produced a mean value of -4.462 m, while GOSG02S yielded a nearly symmetrical 4.439 m.

Although the results show that all models exhibit a similar degree of spatial variability in geoid height, the actual spatial distribution of the geoid values varies across models. This means that while the extent of variation is consistent, the geographic patterns such as where the highest or lowest values occur are differ significantly. These spatial differences are illustrated in Figure 4. 1. This inversion suggests that although both models achieve similar levels of accuracy in terms of absolute height differences, they represent different systematic offsets in the regional gravity field. The remaining models which are Tongji-GMMG2021S, SGG-UGM-2 and XGM2019e_2159 exhibited slightly higher RMSE values ranging from 0.044 m to 0.046 m which indicated a marginally lower accuracy. Notably, the mean geoid heights derived from Tongji-GMMG2021S and XGM2019e_2159 are both approximately -4.4 m, which aligns closely with WHU-SWPU-GOGR2022S. In contrast, SGG-UGM-2 displays a positive mean geoid height of approximately 4.4 m, mirroring the pattern observed in GOSG02S. These differences in mean values show that each model has its own built-in systematic vertical bias even though their standard deviations and RMSE are quite similar. Such offsets often arise from differences in model development strategies, such as the selection of vertical datum, the choice and weighting of satellite or gravity datasets, and the model processing methodologies (Liu et al., 2024).

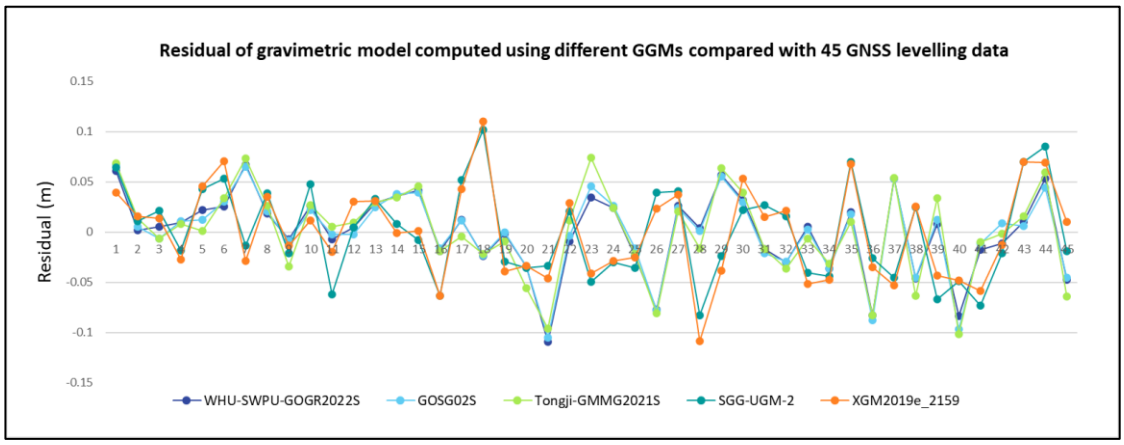


Figure 4. 1 Residual of Gravimetric Geoid Computed Using Different Geopotential Model Compared with 45 GNSS Levelling Data

Table 4. 1
Statistical Analysis of Geoid Computed Using Different Geopotential Models [Unit : Metre]

GGM	Min	Max	Mean	RMSE
WHU-SWPU-GOGR2022S	-26.136	17.116	-4.462	0.040
GOSG02S	-26.192	17.096	4.439	0.040
Tongji-GMMG2021S	-26.169	17.122	-4.406	0.044
SGG-UGM-2	-26.109	17.152	4.407	0.046
XGM2019e_2159	-26.137	17.136	-4.407	0.046

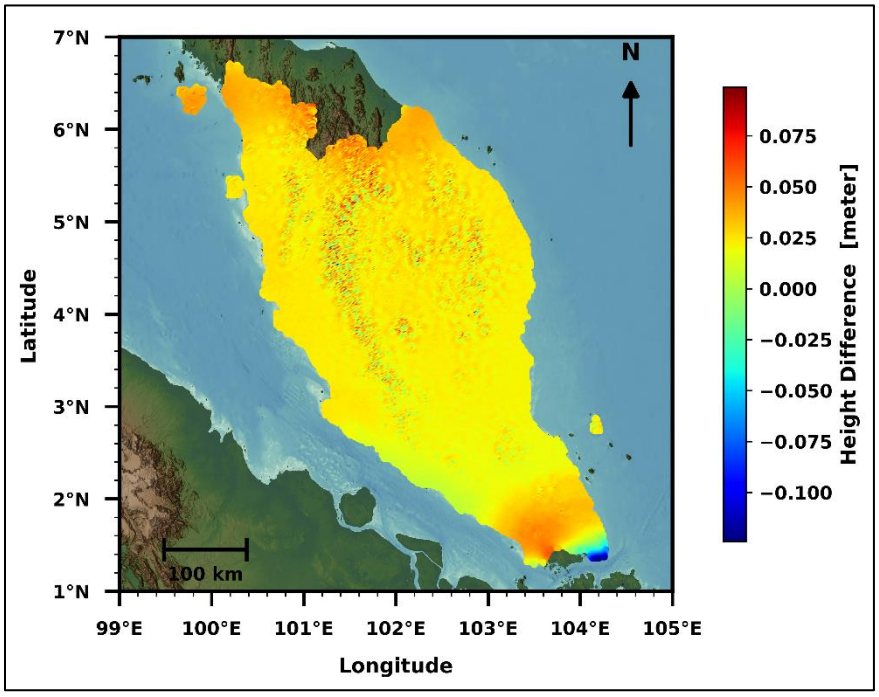


Figure 4. 2 Difference of Geoid Height Between WHU-SWPU-GOGR2022S and GOSG2S Models

Another paired t-test analysis was performed to further evaluate the distinction between WHU-SWPU-GOGR2022S and GOSG02S. The descriptive statistics of both models are presented in Table 4. 2, where a total of 45 paired observations were assessed for each dataset. The results indicate that the mean values of WHU-SWPU-GOGR2022S and GOSG02S are -1.962 m and -1.986 m, respectively, showing only a minor difference between the two datasets. The standard deviation (SD) values are 6.618 m and 6.619 m, which are nearly identical and suggest a very similar spread of data for both models. In addition, the standard error of the mean (SEM) is consistent for

both datasets at 0.987 m, indicating comparable levels of uncertainty in the estimated means. Overall, the descriptive statistics demonstrate that both models exhibit highly similar statistical characteristics in terms of central tendency and dispersion.

The results for the paired t-test are summarized in Table 4. 3. The result shows that the mean difference in geoid heights between the two models is 0.024 m, with a 95% confidence interval ranging from 0.022 m to 0.026 m. This narrow interval reflects a high level of precision in estimating the difference, implying that the offset is consistent across all measurement points. From a statistical perspective, the t-value of 21.218 is exceptionally high, and the two-tailed p-value of < 0.0001 indicates that there is less than a 0.01% chance that this difference occurred by random chance alone. In other words, the difference between the two models is real, consistent and statistically very strong, not just random noise in the data. In practical terms, even though both models achieved the same RMSE value (0.040 m), this analysis revealed a systematic vertical offset between them. Such an offset, though seemingly small in magnitude but can have implications in high-precision geodetic applications, particularly where absolute vertical referencing is critical.

Table 4. 2
Descriptive Statistics Between WHU-SWPU-GOGR2022S and GOSG2S [Unit: Metre]

GGM	N	Mean	SD	SEM
WHU-SWPU-GOGR2022S	45	-1.962	6.618	0.987
GOSG02S		-1.986	6.619	0.987

Table 4. 3
Summary of Paired T-Test Results Between WHU-SWPU-GOGR2022S and GOSG2S

Description	Result
Mean Difference (WHU – GOSG02S)	0.024 m
95% Confidence Interval	0.022 m – 0.026 m
t-value	21.218
Degree of freedom (df)	44
Standard error of difference	0.001
p-value (two-tailed)	< 0.0001
Significance	Statistically significant

4.2.2 Determination of the Optimum Least Squares Modification Parameters

In this study, the correlated model was applied to compute the least squares modification parameters. The analysis evaluates how these parameters respond to different assumed standard deviations of terrestrial gravity data and to variations in the correlation length within the reciprocal-distance correlation function for both WHU-SWPU-GOGR2022S and GOSG02S. This step was necessary to determine the optimal parameter settings before finalizing the model to be applied in the geoid computation. In this study, two key parameters were evaluated in combination of the correlation length of gravity field (ψ) and standard deviation of the gravity anomaly errors ($\sigma_{\Delta g}$). The correlation length and standard deviation were tested over the range 0.1° to 0.6° and 1.0 mGal to 6.0 mGal respectively. Through this systematic testing of different parameters combinations, the pairing with minimum RMSE between the GNSS derived geometrical geoid and the computed gravimetric geoid can be identified. In this study, the geometrical geoid were derived from 45 GNSS levelling data to test those parameters.

The RMSE results for WHU SWPU GOGR2022S and GOSG02S are shown in Table 4. 4 and Table 4. 5 respectively. Across all parameter combinations, the RMSE values ranging from approximately 3.8 cm to 5.1. However, both models recorded their lowest RMSE when the correlation length was 0.1° and the standard deviation was 1.0 mGal. This recurring pattern suggests that a shorter correlation length combined with a lower noise assumption allows the model to better capture the local gravity signal variability. As a result, the fitting between the GGM-derived geoid and the reference data becomes more stable and precise under this parameter configuration. In contrast, the highest RMSE values are observed when the correlation length is increased to the range of 0.4° to 0.6° combined with a higher standard deviation of 6.0 mGal. This suggests that overly smooth spatial correlation assumptions and increased noise levels reduce the model's ability to represent finer-scale gravity variations, leading to reduced fitting performance.

Overall, the results indicate that both GGMs exhibit optimal performance under the same parameter setting (0.1° and 1.0 mGal), highlighting a consistent optimal configuration for minimizing geoid height discrepancies. The close similarity in RMSE

patterns further supports the conclusion that both models demonstrate comparable reliability and performance in geoid determination applications. Therefore, this combination was adopted into the least square computation in geoid derivation.

Table 4. 4
The RMSE Between 45 GNSS Derived Geometrical Geoid and Gravimetric Geoid for WHU-SWPU-GOGR2022S Using Parameter Combination of Correlation Length and Standard Deviation [Unit: Meters]

WHU-SWPU-GOGR2022S		Standard Deviation (mGal)					
		1.0	**2.0**	**3.0**	**4.0**	**5.0**	**6.0**
Correlation Length (°)	**0.1**	0.0380	0.0413	0.0435	0.0449	0.0461	0.0473
	0.2	0.0389	0.0429	0.0446	0.0462	0.0476	0.0491
	0.3	0.0399	0.0434	0.0453	0.0467	0.0483	0.0501
	0.4	0.0404	0.0438	0.0453	0.0470	0.0487	0.0506
	0.5	0.0406	0.0439	0.0454	0.0470	0.0488	0.0507
	0.6	0.0409	0.0439	0.0453	0.0469	0.0486	0.0507

Table 4. 5
The RMSE Between GNSS Derived Geometrical Geoid and Gravimetric Geoid for GOSG02S Using Parameter Combination of Correlation Length and Standard Deviation [Unit: Meters]

GOSG02S		Standard Deviation (mGal)					
		1.0	**2.0**	**3.0**	**4.0**	**5.0**	**6.0**
Correlation Length (°)	**0.1**	0.0382	0.0412	0.0435	0.0450	0.0460	0.0472
	0.2	0.0389	0.0427	0.0448	0.0461	0.0476	0.0490
	0.3	0.0398	0.0435	0.0452	0.0467	0.0483	0.0502
	0.4	0.0403	0.0438	0.0454	0.0470	0.0487	0.0508
	0.5	0.0406	0.0438	0.0455	0.0470	0.0487	0.0508
	0.6	0.0408	0.0438	0.0453	0.0469	0.0486	0.0507

Another optimum parameter evaluated in this study was the maximum spherical harmonic degree (L) together with the upper degree of the GGM (M), with the results summarised in Table 4. 6. Initially, both WHU-SWPU-GOGR2022S and GOSG02S provide a maximum available degree of 300. Hence, the evaluation was conducted by testing both models at regular intervals of 20 degrees, starting from degree 20 up to degree 300, in order to assess the effect of spectral resolution on RMSE performance. The results show a clear reduction in RMSE as the degree increases from low values, where the highest RMSE is observed at degree 20 with a value of 0.2479 m for both models. This relatively large error is attributed to the limited capability of low-degree spherical harmonic expansions, which only represent long-wavelength components of the Earth's gravity field (Pavlis et al., 2012). Consequently, finer spatial variations of the geoid are not adequately captured, leading to larger residuals.

A continuous improvement in accuracy is observed as the degree increases, with a significant reduction in RMSE up to approximately degree 100. Beyond this point, the RMSE values continue to decrease gradually and begin to stabilise, indicating that the inclusion of higher-degree harmonics progressively enhances the representation of medium and short wavelength gravity signals (Pavlis et al., 2012). The analysis further reveals that both WHU-SWPU-GOGR2022S and GOSG02S achieve their lowest RMSE at degree 240, with values of 0.0379 m and 0.0381 m, respectively. At this level, both models demonstrate an optimal balance between signal representation and noise contribution, resulting in the most accurate geoid performance. Additionally, both models exhibit almost identical RMSE behaviour across the range from degree 100 to 300, as illustrated in Figure 4. 3, with only minimal deviations observed between them. This similarity indicates that both GGMs have comparable spectral characteristics and perform consistently across increasing harmonic degrees.

Although the differences in RMSE are generally negligible across most degrees, the selection of the optimal configuration was made by prioritising the parameter set that produces the lowest error. Accordingly, the WHU-SWPU-GOGR2022S model with both spherical harmonic degree (L) and upper GGM degree (M) set to 240 was adopted as the final configuration for geoid computation using the LSMSA method.

Table 4. 6
The RMSE of Tested Maximum Degree (L = M) for WHU-SWPU-GOGR2022S and GOSG02S [Unit: Meters]

Degree (L= M)	RMSE	
	WHU-SWPU-GOGR2022S	GOSG02S
20	0.2479	0.2479
40	0.1353	0.1353
60	0.0777	0.0778
80	0.0782	0.0782
100	0.0548	0.0548
120	0.0453	0.0452
140	0.0488	0.0489
160	0.0417	0.0420
180	0.0433	0.0432
200	0.0439	0.0434
220	0.0393	0.0390
240	0.0379	0.0381
260	0.0382	0.0383
280	0.0381	0.0381
300	0.0380	0.0382

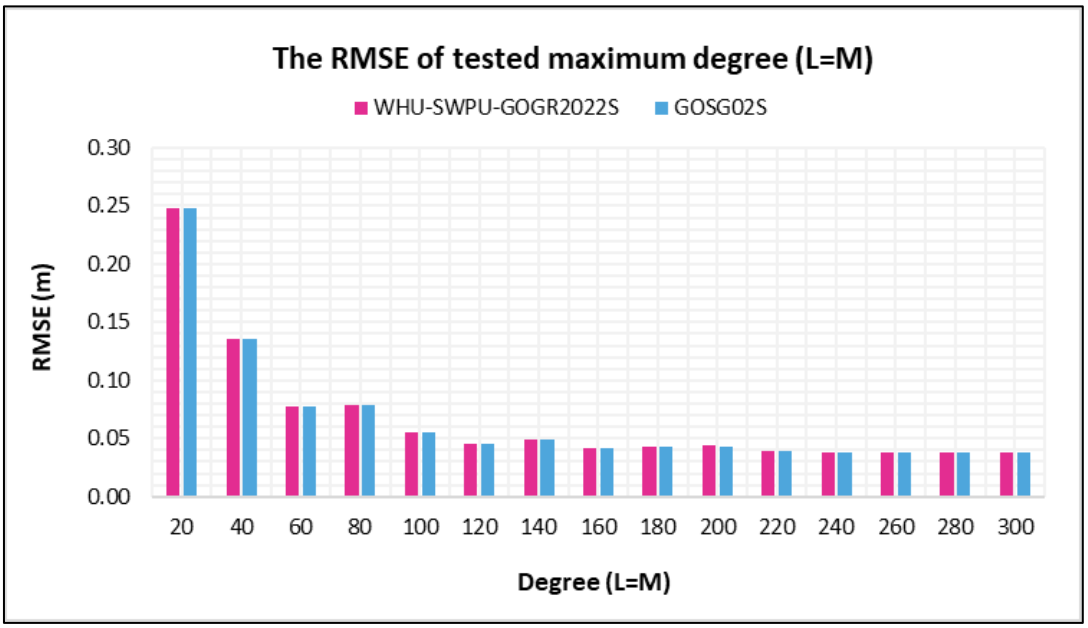


Figure 4. 3 The RMSE of Tested Maximum Degree in Least Square Parameters Setting for WHU-SWPU-GOGR2022S and GOSG02S Models

4.2.3 Impact Assessment of Marine Gravity Data on Geoid Determination

As an effort to refine the geoid model in marine region, assessment of four different global satellite-derived marine gravity data were tested encompassed the model from Sandwell and Smith, NSOAS24, SDUST2020 and DTU21. The resulting models were then validated using several independent GNSS levelling datasets including 45 points and 173 points of GNSS levelling dataset acquired from DSMM and 10 GNSS dataset acquired from 2019 GNSS Campaign as previously mentioned in subsection 3.2.4.1. The RMSE values from the validation are summarised in Table 4. 7. The findings show that the Sandwell and Smith model yield the smallest RMSE when compared to the separate 45 points and 173 points of GNSS dataset which are 0.036 m and 0.056 m respectively. However, when tested against the GNSS levelling dataset located at tide gauge stations, the Sandwell and Smith model exhibited a slightly higher RMSE (0.043 m) compared to NSOAS24 (0.033 m) and DTU21 (0.039 m).

The results suggested that the latter two datasets may offer marginally improved accuracy near the shoreline with differences of approximately 1 cm relative to the Sandwell and Smith model. This difference could be attributed to the resolution and calibration methods employed in NSOAS24 and DTU21 which have been optimised for high precision coastal altimetry applications (O. B. Andersen et al., 2023; Zhang et al., 2025). When all GNSS datasets were combined into a single validation set, the Sandwell and Smith model still emerged as the most overall accurate model which achieved a RMSE of 0.062 m. While the numerical differences between the models were relatively small, this consistent performance across datasets supports the use of the Sandwell and Smith dataset as the preferred marine gravity input for the final geoid model in this study. In conclusion, although NSOAS24 and DTU21 showed competitive or superior performance in certain coastal locations, the overall validation indicates that the Sandwell and Smith dataset provide more reliable representation of gravity anomalies distribution across land and coastal domains of Peninsular Malaysia.

Table 4. 7
The RMSE of Gravimetric Geoids Computed Using Different Marine Gravity Model Against Varies GNSS Levelling Dataset [Unit: Meters]

Marine Gravity Model	RMSE			
	GPS 45	GPS 173	GPS TG	Combine
Sandwell and Smith	0.036	0.056	0.043	0.062
NSOAS24	0.040	0.057	0.033	0.064
SDUST2020	0.047	0.066	0.050	0.070
DTU21	0.040	0.057	0.039	0.063

The statistical properties of the final gravimetric geoid model utilized in this study are summarised in Table 4. 8 and the spatial distribution of the computed geoid heights is illustrated in Figure 4. 4. The model exhibits a minimum geoid height of -32.792 m, a maximum of 21.017 m, and a mean value of -5.234 m.

Table 4. 8
The Statistical Properties of Final Gravimetric Geoid Model [Unit: Meters]

Model	Min	Max	Mean
Gravimetric Geoid	-32.792	21.017	-5.234

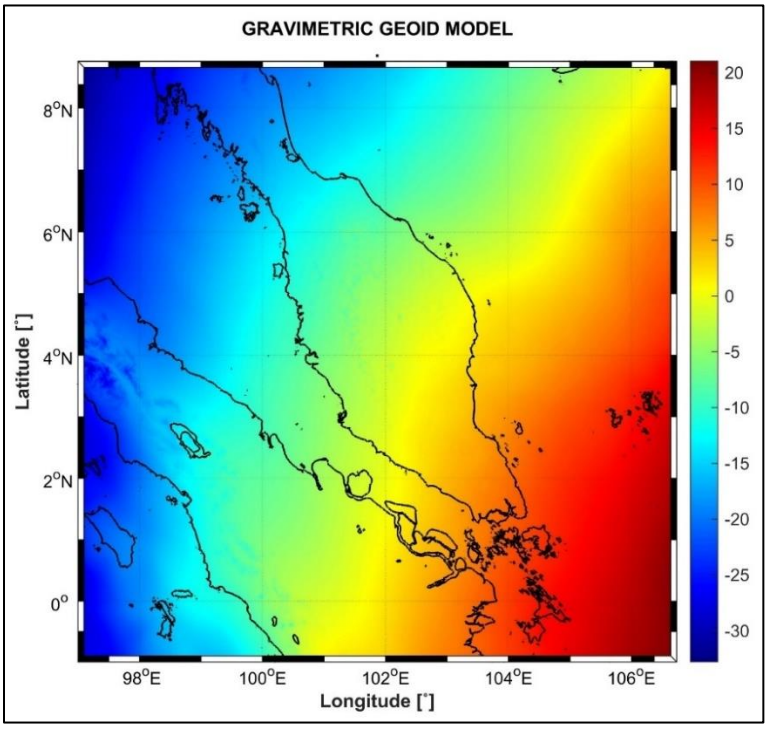


Figure 4. 4 Final gravimetric geoid model

4.2.4 Development of Hybrid Geoid

In this study, the hybrid geoid was generated by fitting the computed gravimetric geoid to the local GNSS/levelling data. Table 4. 9 presents the RMSE value obtained from testing various configurations of prediction variables (correlation distance and RMS of data noise) when validated against 20 GNSS levelling data. The result reveal that the optimal configuration yielding the lowest RMSE of 0.0445 m was corresponded to a correlation distance of 40 km and a data noise RMS of 0.040 m. This configuration appears to provide the most appropriate balance between modelling the spatial characteristics of the gravity field and accounting for observational uncertainties. A correlation distance that is too short may not adequately represent the spatial covariance structure, while an excessively long distance can over-smooth local geoid variations. Therefore, the correlation length should match the dominant wavelength of the gravity field to achieve optimal prediction accuracy (Moritz, 1980). The superior performance obtained at 40 km suggests that this distance is sufficiently long to model the regional gravity field while preserving local variations represented by the terrestrial and airborne gravity observation.

Conversely, the highest RMSE of 0.0502 m was recorded for the combination of a 20 km correlation distance and a data noise RMS of 0.100 m. This result indicates that the adopted parameters were less suitable for representing the covariance structure of the gravity field. The relatively short correlation distance limits the spatial influence of neighbouring gravity observations, reducing the effectiveness of the collocation prediction. At the same time, the high noise RMS assumes larger uncertainties in the input data, causing the observations to be down-weighted during the estimation process. As a result, the predicted geoid surface becomes less constrained by the actual gravity measurements and exhibits poorer agreement with the GNSS levelling validation data.

For all tested correlation distances, the RMSE tends to increase when the RMS of data noise exceeds 0.040 m. This suggests that assigning excessively large observational uncertainties weakens the contribution of gravity observations in the collocation solution. Likewise, the results show that increasing the correlation distance beyond 40 km does not lead to further improvements, with RMSE values gradually increasing to approximately 0.046 m - 0.048 m. This behaviour indicates that longer

correlation distances may smooth out short-wavelength gravity signals that contribute to local geoid variations. Therefore, the combination of a 40 km correlation distance and a 0.040 m data noise RMS provides the most realistic representation of both the spatial correlation and noise characteristics of the gravity data within the study area, resulting in the highest agreement with the GNSS-levelling observations.

Table 4. 9
The RMSE of the Prediction Variables [Unit: Meters]

		RMS of Data Noise				
		0.02	**0.04**	**0.06**	**0.08**	**0.10**
Distance (km)	**20**	0.0450	0.0457	0.0471	0.0488	0.0502
	40	0.0463	0.0445	0.0450	0.0461	0.0474
	60	0.0467	0.0451	0.0453	0.0460	0.0471
	80	0.0473	0.0461	0.0459	0.0463	0.0472
	100	0.0479	0.0464	0.0461	0.0466	0.0474

4.2.5 Final Model of Hybrid Geoid

The final hybrid geoid model was evaluated by comparing geoid heights derived from 20 GNSS levelling stations with both the computed hybrid geoid and the existing WGeoid04 model developed by DSMM. The residuals obtained from both models are presented in Figure 4. 5, while their spatial distribution is illustrated in Figure 4. 6. Based on the graph, the residual values for both models are distributed around zero, indicating that the predicted geoid heights are in reasonable agreement with the geometrical geoid derived from GNSS-levelling observations. Residuals that are centred close to zero suggest the absence of significant systematic bias and demonstrate that both models are capable of representing the local vertical datum with acceptable accuracy. Nevertheless, the computed hybrid geoid exhibits a slightly better agreement with the reference data as the maximum residual produced by the computed hybrid geoid does not exceed 0.010 m, whereas the residuals of WGeoid04 reach approximately 0.016 m. The smaller residual range indicates that the computed hybrid

geoid provides a more consistent representation of the local geoid surface and reduces discrepancies between the gravimetric geoid and the geometrical geoid observations.

The spatial distribution of residuals shown in Figure 4. 6 further supports this observation. The computed hybrid geoid demonstrates generally lower residual value, particularly along the coastal regions of the study area. Coastal zones are often characterised by complex gravity field variations due to the transition between land and marine environments, which may introduce modelling uncertainties in geoid determination (Y. Liu et al., 2026). The reduction of residuals in these areas suggests that the computed hybrid geoid is better able to accommodate local gravity field characteristics and vertical datum distortions. Although the improvement relative to WGeoid04 is modest, it indicates that the refinement procedure has enhanced the representation of the geoid surface, especially in regions where accurate height transformation is critical.

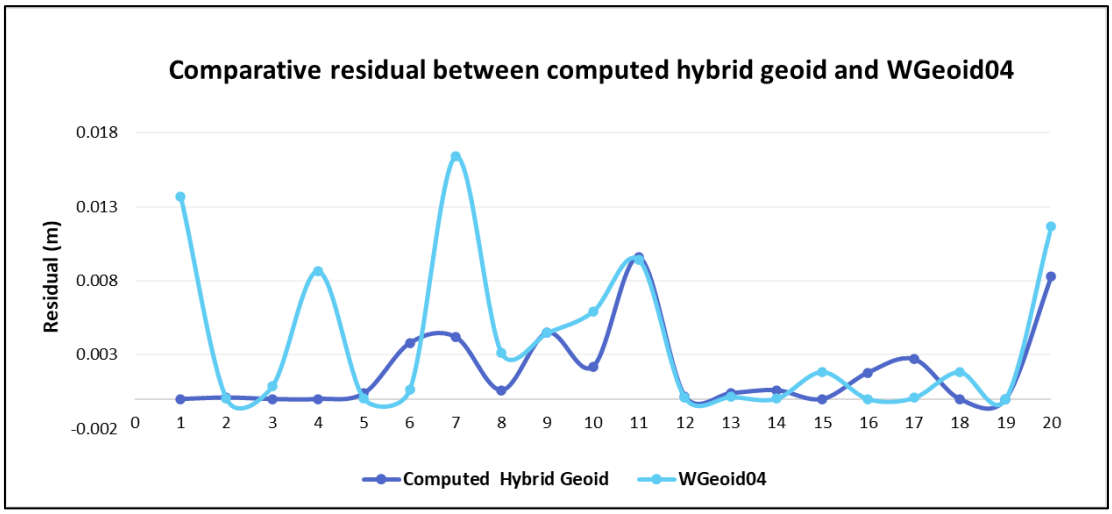


Figure 4. 5 Comparative Residual Between Computed Hybrid Geoid and Wgeoid04

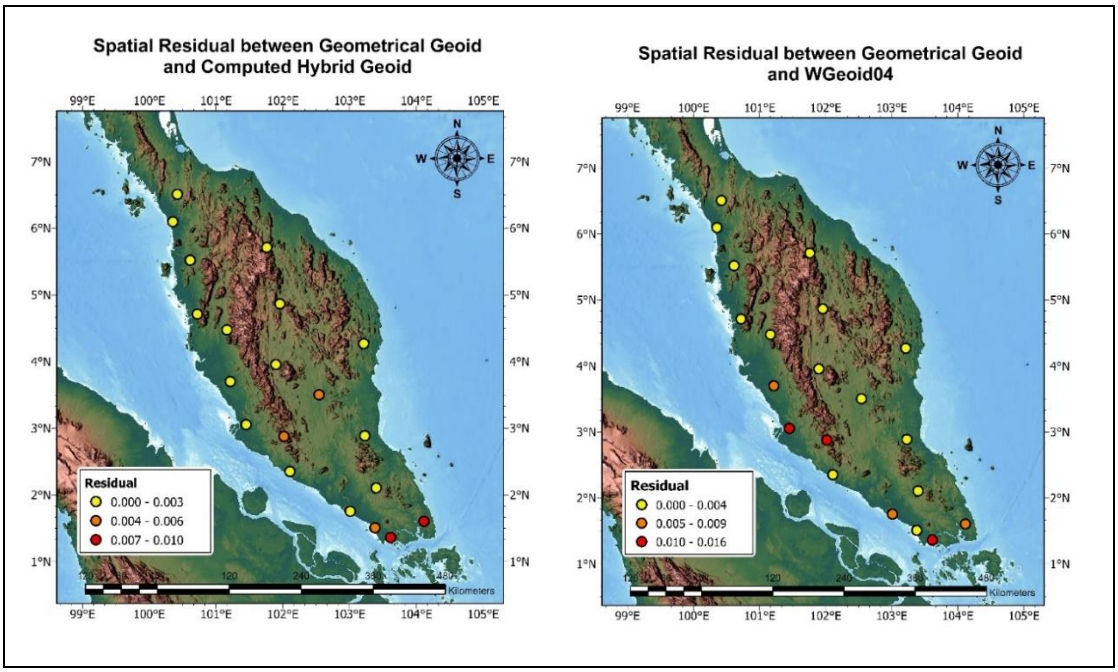


Figure 4. 6 The Spatial Distribution of Residuals Computed Hybrid Geoid and Wgeoid04 Compared to the Geometrical Geoid

The statistical properties of both models are summarised in Table 4. 10. The computed hybrid geoid achieved an RMSE of 0.044 m, compared to 0.063 m for WGeoid04. This corresponds to an improvement of approximately 30%, demonstrating a noticeable enhancement in agreement with the GNSS levelling data. The lower RMSE reflects a reduction in the overall prediction error and indicates that the hybrid geoid provides a more accurate approximation of the true geoid surface within the study area. The statistical results therefore demonstrate that the computed hybrid geoid offers superior performance compared to WGeoid04. While both models are capable of representing the geoid surface reasonably well, the lower residuals and reduced RMSE achieved by the computed hybrid geoid indicate that the inclusion of local control data has improved the compatibility between ellipsoidal and orthometric heights. Consequently, the final hybrid geoid model provides a more reliable surface for height transformation applications and serves as an improved local representation of the vertical reference framework within the study area. The final hybrid geoid model is illustrated in Figure 4. 7.

Table 4. 10
The Statistical Properties of Final Hybrid Geoid Model [Unit: Meters]

Model	Min	Max	Mean	RMSE
Hybrid Geoid	-20.179	13.530	3.241	0.044
WGeoid04	-22.317	13.745	-2.566	0.063

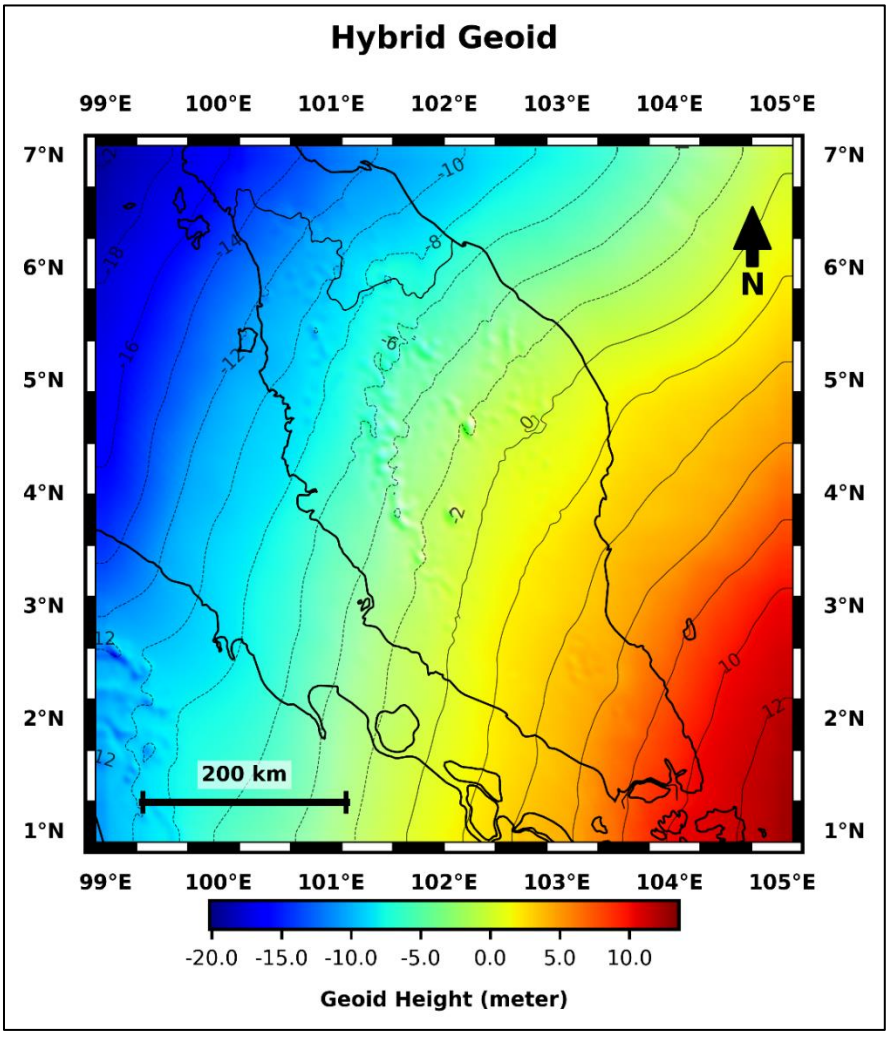


Figure 4. 7 Final Hybrid Geoid Model

4.3 Marine Vertical Separation Model

The derivation of the vertical separation model in this objective includes the computation of tidal datum specifically the Lowest Astronomical Tide (LAT) and Highest Astronomical Tide (HAT) through the assimilation of satellite altimetry mission and hydrodynamic model. An assessment of several global MSS models was conducted to provide essential input for the hydrodynamic tidal data relative to the ellipsoidal reference surface. In parallel, long term sea level observations from coastal tide gauge stations were independently processed to derive tidal datums, which were subsequently used to validate the modelled vertical separation values. All results obtained throughout this study are further analysed and discussed in this section.

4.3.1 Tide Gauge Processing

Tide gauge records of sea level observations were employed to derive the tidal datums specifically MSL, LAT and HAT. These data are important to validate the computed marine vertical separation models in this study. These data were processed using UTide software which integrates harmonic analysis techniques to extract tidal characteristics. The analysis was conducted for eleven selected tide gauge stations as illustrated in Figure 3.10. The MSL were determined by averaging hourly sea level measurements over a long-term observation period where the minimum and maximum sea surface value were extracted through harmonic decomposition which quantifies the amplitudes and phase lags of the dominant tidal constituents to derive the LAT and HAT. As the UTide-derived tidal datums are referenced to the zero tide gauge, a transformation to the ellipsoidal height reference frame was necessary by using Equation (3.32). This conversion ensures consistency with the reference frame of the modelled tidal datum computed from the assimilation of multi-mission satellite altimetry data and hydrodynamic model for seamless comparison between the data. The tidal datums derived from tide gauge data were subsequently used as independent validation benchmarks to evaluate the accuracy and performance of the LAT and HAT model. The results of the tidal datums derived from the UTide for the eleven stations are summarized in Table 4. 11.

Table 4. 11
Tidal Datum for Tide Gauges Stations Using Utide

Station	Latitude	Longitude	Respect To ZTG			H_{ZTG}	h_{GNSS}	Respect to Ellipsoid		
			LAT	MSL	HAT			LAT	MSL	HAT
Klang	3.050	101.358	0.529	3.673	6.468	7.494	0.608	-6.357	-3.213	-0.418
Tanjung Keling	2.215	102.153	1.725	2.885	4.386	6.427	4.336	-0.366	0.794	2.295
Pulau Langkawi	6.432	99.765	0.441	2.248	4.007	5.545	-12.655	-17.759	-15.952	-14.193
Lumut	4.240	100.613	0.399	2.230	3.841	5.685	-4.893	-10.179	-8.348	-6.737
Penang	5.422	100.347	1.043	2.724	4.139	4.962	-9.222	-13.141	-11.460	-10.045
Cendering	5.265	103.187	0.789	2.240	3.836	4.688	1.969	-1.930	-0.479	1.117
Kuantan	3.975	103.430	0.918	2.838	4.775	6.496	6.790	1.212	3.132	5.069
Pulau Tioman	2.807	104.140	0.926	2.863	4.659	6.586	11.839	6.179	8.116	9.912
Sedili	1.932	104.115	0.712	2.429	3.881	4.468	11.417	7.661	9.378	10.830
Kukup	1.325	103.443	2.274	4.044	6.079	6.880	10.207	5.601	7.371	9.406
Geting	6.227	102.107	1.595	2.324	3.378	5.964	-3.211	-7.580	-6.851	-5.797

4.3.2 Development of LAT, HAT and MSS From Altimetric Dataset

The derivation of tidal datums particularly the LAT and HAT was accomplished through the processing of multi-mission satellite altimetry data. The satellite missions incorporated in this study include TOPEX/Poseidon A/B, Jason-1 A/B, Jason-2 A/B, Jason-3A, GEOSAT Follow-On (GFO), and Sentinel-6A. These missions were selected due to their extensive temporal coverage and high-resolution SSH measurements (Vignudelli et al., 2019). In this study, harmonic tidal analysis was performed using a standard set of 12 major tidal constituents namely M2, S2, N2, K2, K1, O1, P1, Q1, MF, MM, SSA, and SA to derive the tidal datum.

Table 4. 12 is the statistical analysis of correlations between satellite altimetry mission during crossover adjustment when merging different phases of datasets. In this study, two crossover adjustments were carried out to merge the combined altimetric satellite dataset from (a) Phase A to Phase B and (b) Phase A to GFO. From the process, the error estimations of the minimum, maximum, mean, and overall RMSE for each tidal datums encompassed the LAT, MSL and HAT were computed. It can be seen from the table that the correlation RMSE between the Phase A and Phase B are 0.151 m (LAT), 0.142 m (MSL) and 0.148 m (HAT). Subsequently, the correlation RMSE between the Phase A and GFO are 0.145 m (LAT), 0.110 m (MSL) and 0.150 m (HAT). The overall precision ranges from 0.110 m to 0.151 m which indicates similar levels of consistency across both merged datasets. These patterns are consistent with the physical behaviour of the datums where the MSL shows the lowest RMSE in both correlation outputs. The MSL shows lower errors because it represents an averaged sea surface that smoothest out the short-term fluctuations while LAT and HAT are based on tidal extremes that are more affected by local coastal dynamics and complex conditions which led to slightly higher discrepancies. However, small differences between the LAT and HAT errors which only about millimetre to centimetre scale suggested that the remaining biases are spatially stable and not dominated by time-related systematic effects (Fan et al., 2025).

Table 4. 12
Statistical Analysis of Correlations Between Satellite Altimetry Mission During Crossover Adjustment [Unit: Meters]

Correlation	Phase A – Phase B			Phase A - GFO		
Tidal Datum	LAT	MSL	HAT	LAT	MSL	HAT
Minimum Error	-0.331	-0.261	-0.299	-0.269	-0.266	-0.299
Maximum Error	0.271	0.274	0.268	0.341	0.209	0.288
Mean Error	0.023	0.014	0.026	0.070	-0.022	0.054
RMSE	0.151	0.142	0.148	0.145	0.110	0.150

Following the satellite altimetry processing, the derived tidal datums were transformed from the TOPEX/Poseidon ellipsoid to the GRS80 reference ellipsoid using the formulation outlined by (O. B. Andersen et al., 2018; Keysers et al., 2015). This transformation was essential as satellite altimetry missions commonly adopted TOPEX/Poseidon ellipsoid in its altimetric datasets. In contrast, this study adopts the GRS80 ellipsoid as the standard reference surface to ensure consistency with the International Terrestrial Reference Frame (ITRF), which forms the foundation of modern GNSS positioning systems. By expressing all tidal datum information within a common reference frame, direct comparisons with geoid models, GNSS observations, and vertical reference surfaces can be performed without introducing additional reference system biases.

The statistical properties of the altimetry-derived tidal datums are summarised in Table 4. 13 and its spatial distributions are illustrated in Figure 4. 8 The results indicate that LAT ranges from -32.429 m to 20.315 m with a mean value of -2.823 m, while MSL ranges from -31.292 m to 21.544 m with a mean value of -1.654 m. HAT exhibits the highest values, ranging from -30.125 m to 22.710 m and producing a mean value of -0.667 m. These results are consistent with the theoretical relationship among tidal datums, where LAT represents the lowest tidal level, MSL represents the average sea level condition, and HAT corresponds to the highest tidal level. Consequently, the mean values increase progressively from LAT to MSL and subsequently to HAT. The standard deviation values of 13.860 m, 14.006 m, and 14.080 m for LAT, MSL, and HAT, respectively, indicate substantial spatial variability throughout the study area. The similar standard deviation values obtained for all three tidal datums suggest that they

are influenced by a common underlying sea surface structure, while the differences in their mean values primarily reflect the tidal range represented by each datum.

Table 4. 13
The Statistical Analysis of Tidal Datum Derived From Altimetric Satellite [Unit: Meters]

Tidal Data	Minimum	Maximum	Mean	STD
LAT	-32.429	20.315	-2.823	13.860
MSL	-31.292	21.544	-1.654	14.006
HAT	-30.125	22.710	-0.667	14.080

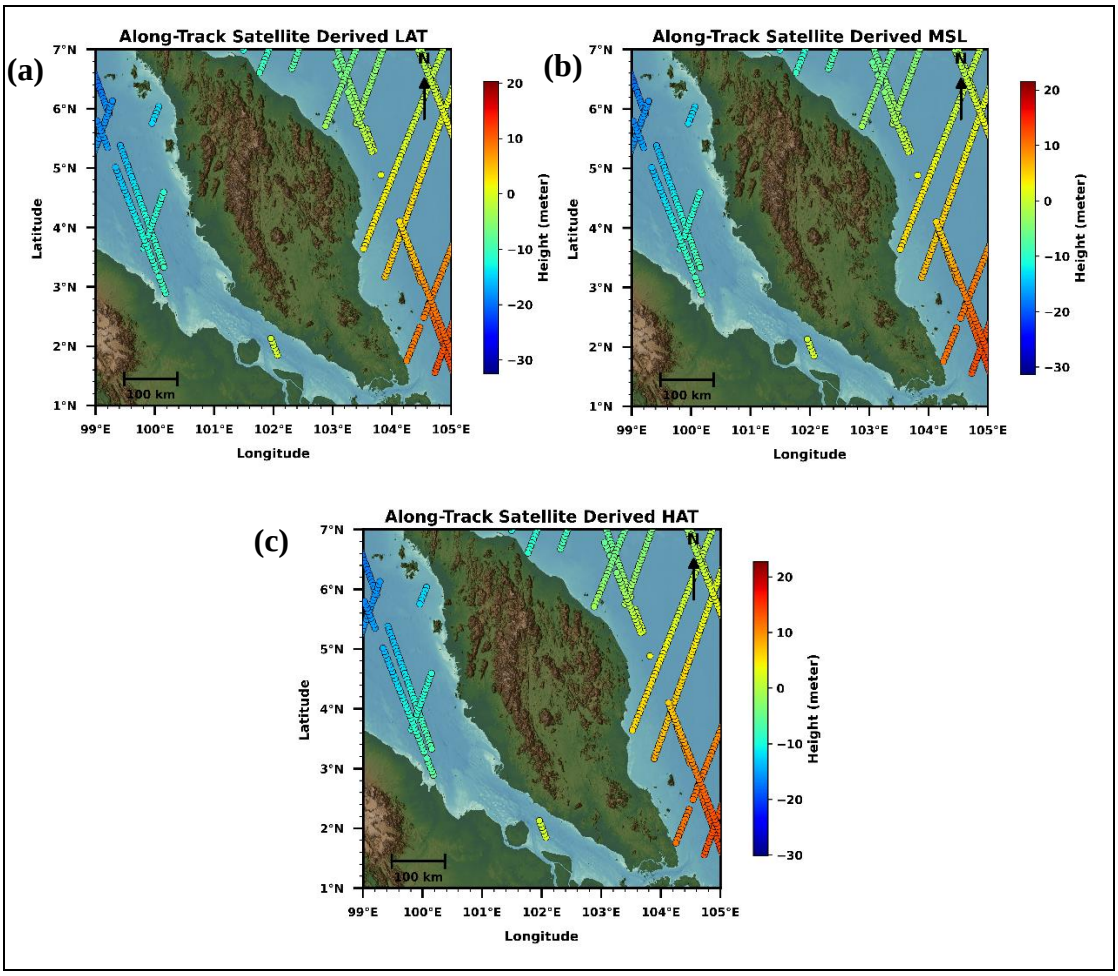


Figure 4. 8 Along-Track Tidal Datums Derived From Altimetric Satellite Encompassed (A) LAT, (B) MSL And (C) HAT

4.3.3 Hydrodynamic Model

Hydrodynamic model in this study was utilized to compensate for the absence of satellite altimetry data within a 20 km buffer zone from the shoreline, where altimetric measurements are commonly excluded due to land contamination effects and signal degradation in the coastal zone (O. B. Andersen & Knudsen, 2016; Gommenginger et al., 2011; Y. Liu et al., 2026; Vignudelli et al., 2019). Specifically, null grids were generated using a spatial resolution of 5 arc-minutes which corresponds to approximately 10 kilometers at the equator. This resolution was selected based on the assumption that tidal characteristics remain relatively stable within a 10 km coastal buffer and exhibit significant variability only beyond this threshold, where deeper water dynamics and open-sea influences begin to dominate (Abd Rahman et al., 2024). Additionally, several global MSS models were evaluated with the purpose of converting the hydrodynamic data from TMD into ellipsoid based reference.

4.3.3.1 Derivation of Tidal Data from Tide Model Driver (TMD)

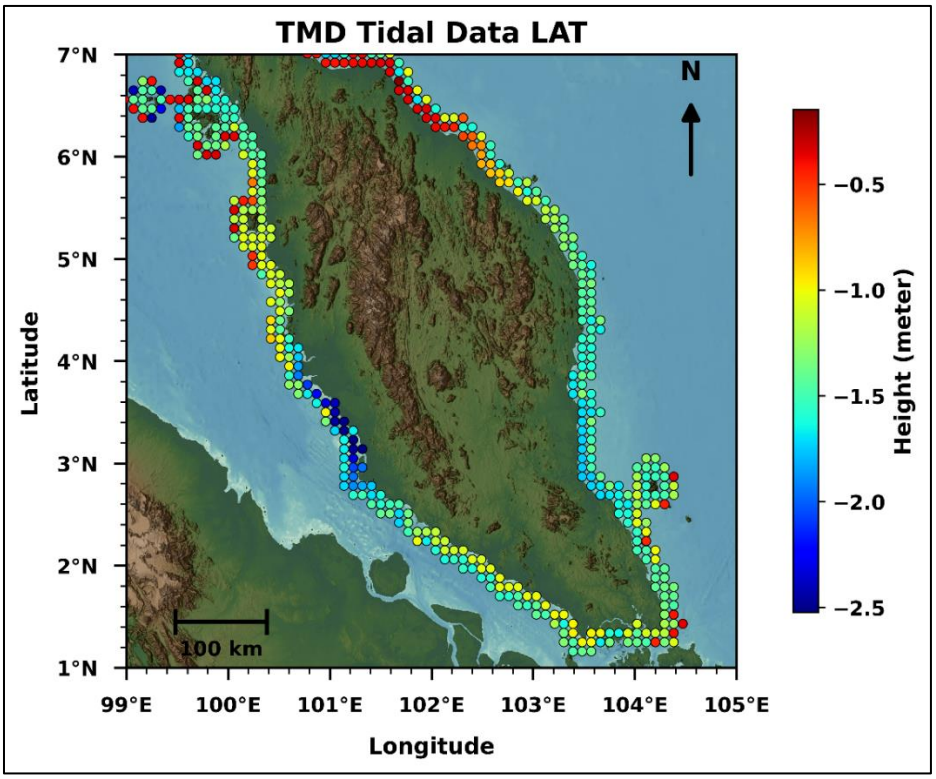
The statistical results of these derived tidal levels are presented in Table 4. 14 and illustrated in Figure 4. 10. Based on table, the LAT data exhibits a minimum, maximum and mean values of -2.523 m, -0.149 m and -1.273 m respectively. In contrast, the HAT values range from 0.149 m to 2.501 m with a mean of 1.271 m. The standard deviations for LAT and HAT are nearly identical at 0.488 m and 0.466 m respectively. This close similarity indicates that the variability of tidal extremes around their mean values is balanced and consistent across the dataset. It also suggests that the tidal model is able to represent both low and high extremes with consistent stability which provides a reliable tidal level for further analysis.

```
Lat:     8.7200, Lon:    98.1700, Parameter: z(m)
Depth (m):      20.48
Constituents included: m2  s2  n2  k2  k1  o1  p1  q1  m4  ms4 mn4
Time start: 00:00,  9.25.1992
Time step (min):      60.00
Time Series length (hours):280320
25-Sep-1992 00:00:00     0.4878
25-Sep-1992 01:00:00     0.9079
25-Sep-1992 02:00:00     1.1084
25-Sep-1992 03:00:00     1.0418
25-Sep-1992 04:00:00     0.7214
25-Sep-1992 05:00:00     0.2165
25-Sep-1992 06:00:00    -0.3572
25-Sep-1992 07:00:00    -0.8586
```

Figure 4. 9 The Sample of TMD Output

Table 4. 14
The Statistical Analysis of Tidal Data Derived From TMD [Unit: Meter]

Tidal Data	No. of Data	Min	Max	Mean	STD
LAT	606	- 2.523	- 0.149	- 1. 273	0.488
HAT	606	0.149	2.501	1.271	0.466



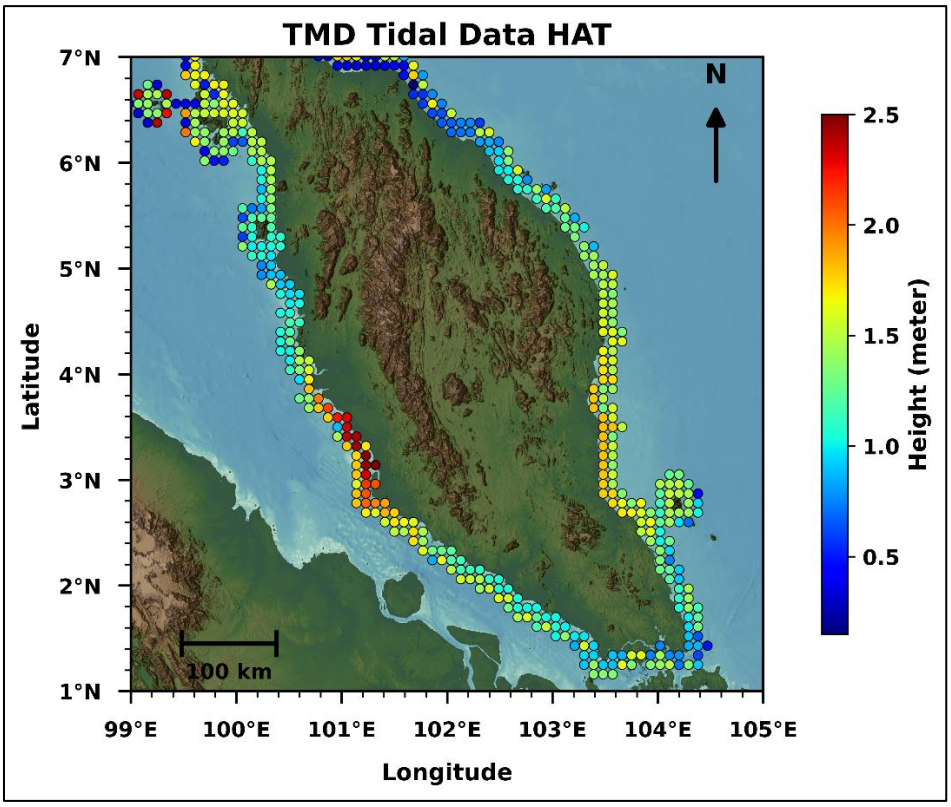


Figure 4. 10 Tidal Data Derived From TMD Encompassed LAT and HAT.

4.3.3.2 Evaluation of Global Mean Sea Surface (MSS) Models

The performance of each MSS models including both direct models and combined (geoid + MDT) models were validated against tidal datums derived at eleven tide gauge stations using UTide processing as previously acquired in 4.3.1. The assessed precision of each global MSS models is listed in Table 4. 15. In this study, the results were analysed in three separate parts which is the (a) direct model, (b) combined global geoid model and MDT, and (c) combined local geoid model and MDT where the summary of the precision are listed in Table 4. 15. Although the main focus of this section is on the MSL performance, the LAT and HAT were also assessed to provide additional insight into the stability and consistency of each model. The spatial patterns of these errors are further illustrated in Figure 4. 11.

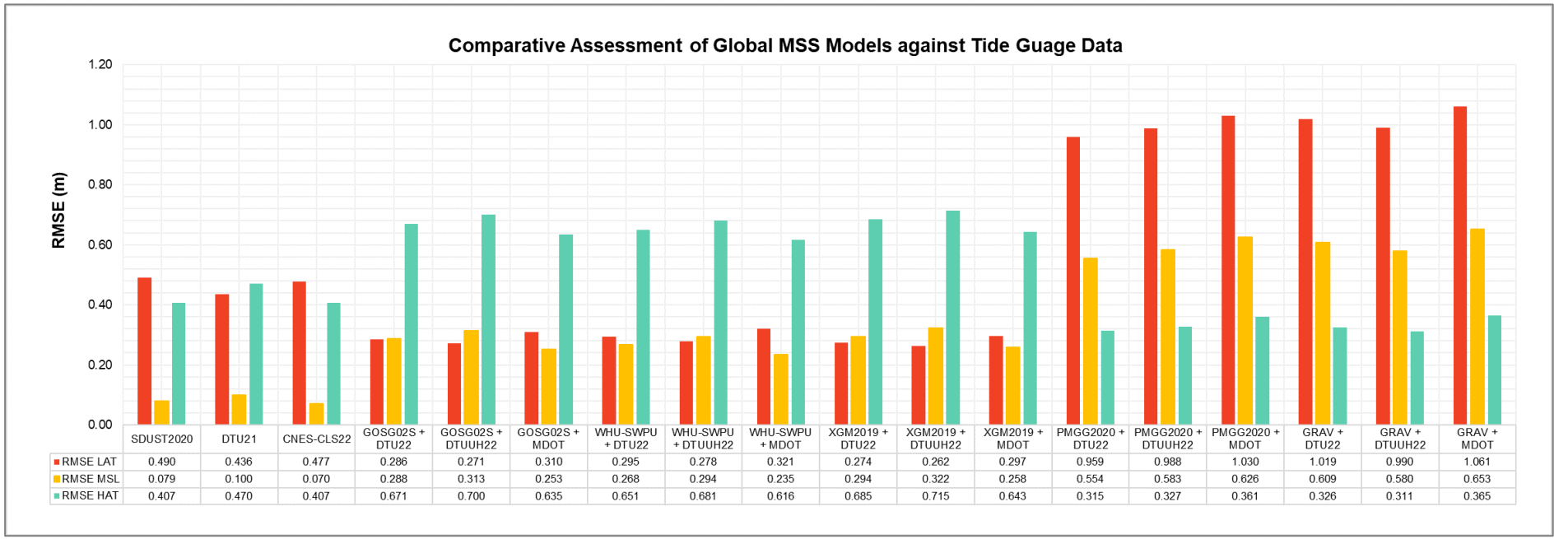
Roughly, the results demonstrated that the direct MSS models indicates a relatively lower RMSE compared to the combined models. The RMSE for MSL of (a) direct models ranging between 0.070 m to 0.100 m, (b) combined global geoid model

and MDT yields ranging from 0.235 m to 0.322 m and the (c) combined local geoid model and MDT indicated the largest RMSE ranging between 0.554 m to 0.653 m. This outcome is expected because direct MSS products such as DTU21 and CNES-CLS22 are explicitly developed through extensive filtering, calibration, and combination of altimetry data to represent sea surface topography as accurately as possible (O. B. Andersen & Knudsen, 2009). Since they are directly derived from satellite altimetry observations, their errors are minimized and no further dataset integration is required. In contrast, the combined models are inherently more complex due to the assimilation of geoid and MDT datasets that may differ in spatial resolution, reference frames or processing standards. Even small inconsistencies in datums, computation strategies, or resolution between geoid and MDT models can introduce systematic and random errors (Filmer et al., 2024). Therefore, achieving consistent results requires rigorous harmonization of metadata which is not always feasible in practice.

Further discussion highlighted where the utilization of global geoids and local geoids indicates two different precisions when validated against the tidal datum at tide gauge locations. The results show evident differences where the RMSE when local geoid models used are three times larger compared to global geoid models. Residual analysis as plotted in Figure 4. 12 shows that local geoids displayed smaller biases relative to MSL at tide gauges but when combined with MDT data they produce less reliable MSS reconstructions than global models. The reason is because global geoid models are purely gravitational derived model which best represents the physical meaning of MSS dataset. In parallel, the local geoid model of PMGG2020 and computed gravimetric geoid in this study were derived from LSMSA or KTH method which known to derive the geoid model closer to the approximate MSL (Sjöberg, 2003b). Although they are useful for national height systems, using them in deriving the MSS can reduce its precision because the physical meaning of the MSS decomposition becomes less clear. In summary, the results highlight that the direct MSS models perform best with CNES-CLS22 achieving the lowest RMSE of 0.070 m, 0.477 m and 0.407 m for MSL, LAT and HAT respectively. Given this performance, CNES-CLS22 was selected for subsequent integration with hydrodynamic modelling as the model demonstrates the highest precision of MSL and stable precision for both tidal extremes of LAT and HAT.

Table 4. 15
The Summary of Assessed Global MSS Models Against Local Tide Gauge Stations

MSS Model	RMSE		
	LAT	MSL	HAT
SDUST2020	0.490	0.079	0.407
DTU21	0.436	0.100	0.470
CNES-CLS22	0.477	0.070	0.407
GOSG02S + DTU22	0.286	0.288	0.671
GOSG02S + DTUUH22	0.271	0.313	0.700
GOSG02S + MDOT	0.310	0.253	0.635
WHU-SWPU-GOGR2022S + DTU22	0.295	0.268	0.651
WHU-SWPU-GOGR2022S + DTUUH22	0.278	0.294	0.681
WHU-SWPU-GOGR2022S + MDOT	0.321	0.235	0.616
XGM2019 + DTU22	0.274	0.294	0.685
XGM2019 + DTUUH22	0.262	0.322	0.715
XGM2019 + MDOT	0.297	0.258	0.643
PMGG2020 + DTU22	0.959	0.554	0.315
PMGG2020 + DTUUH22	0.988	0.583	0.327
PMGG2020 + MDOT	1.030	0.626	0.361
Gravimetric geoid + DTU22	1.019	0.609	0.326
Gravimetric geoid + DTUUH22	0.990	0.580	0.311
Gravimetric geoid + MDOT	1.061	0.653	0.365



	SDUST2020	DTU21	CNES-CLS22	GOSG02S + DTU22	GOSG02S + DTUUH22	GOSG02S + MDOT	WHU-SWPU + DTU22	WHU-SWPU + DTUUH22	WHU-SWPU + MDOT	XGM2019 + DTU22	XGM2019 + DTUUH22	XGM2019 + MDOT	PMGG2020 + DTU22	PMGG2020 + DTUUH22	PMGG2020 + MDOT	GRAV + DTU22	GRAV + DTUUH22	GRAV + MDOT
RMSE LAT	0.490	0.436	0.477	0.286	0.271	0.310	0.295	0.278	0.321	0.274	0.262	0.297	0.959	0.988	1.030	1.019	0.990	1.061
RMSE MSL	0.079	0.100	0.070	0.288	0.313	0.253	0.268	0.294	0.235	0.294	0.322	0.258	0.554	0.583	0.626	0.609	0.580	0.653
RMSE HAT	0.407	0.470	0.407	0.671	0.700	0.635	0.651	0.681	0.616	0.685	0.715	0.643	0.315	0.327	0.361	0.326	0.311	0.365

Figure 4. 11 The Comparative Assessment of Global MSS Models Against Tide Gauges Data

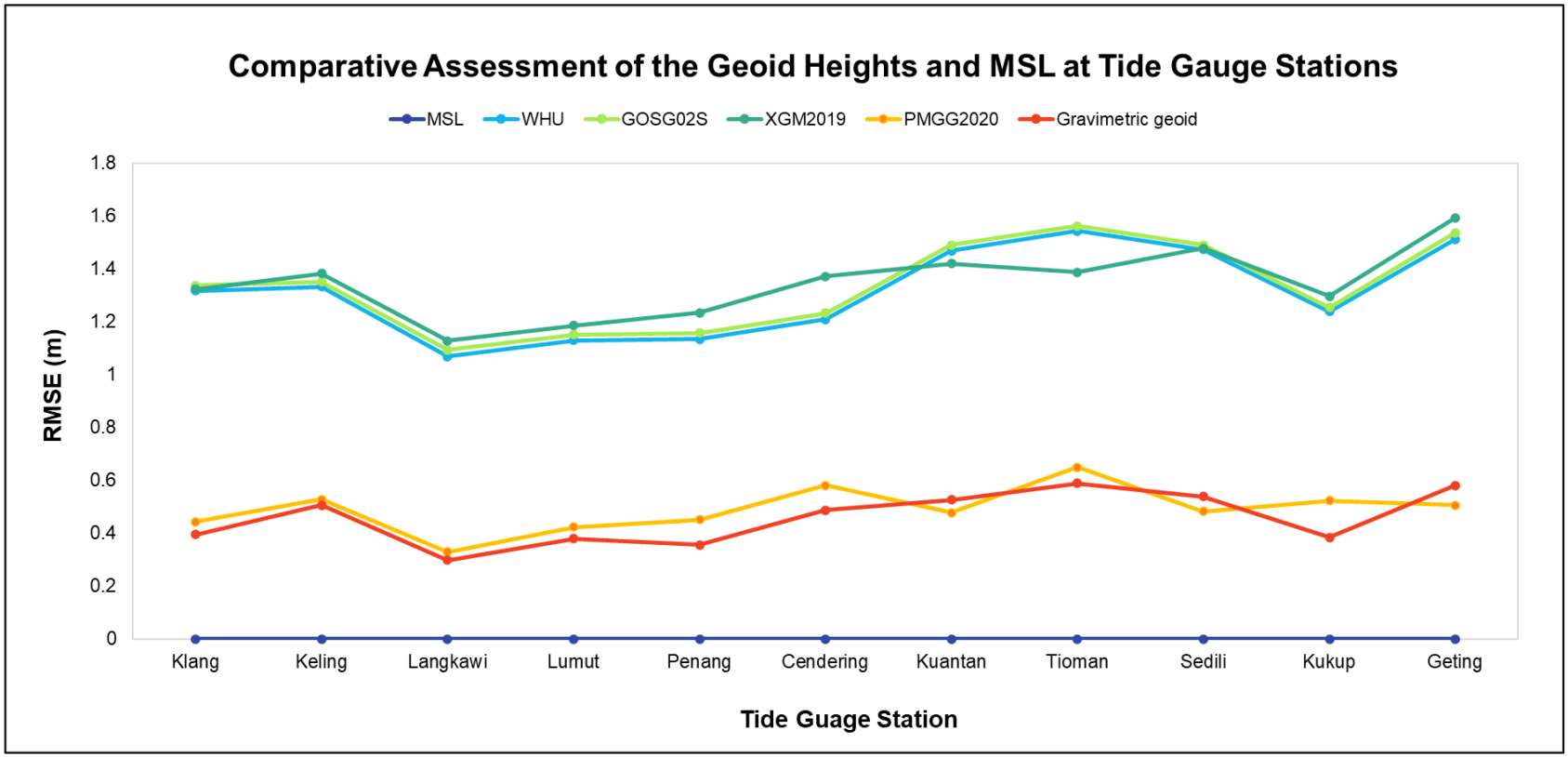


Figure 4. 12 The Comparative Assessment of Geoid Heights and MSL at Tide Gauge Stations

4.3.4 Modelled Tidal Datum

After acquiring tidal datums from satellite altimetry and hydrodynamic process, the datasets were integrated and modelled. As part of this process, global MSS models were incorporated to transform the hydrodynamic outputs into an ellipsoid-based reference system and the datasets were merged and subsequently interpolated into unified grids MSL, LAT and HAT. These modelled surfaces or also called as vertical separation models were then validated against observations from local tide gauge stations to assess their accuracy and reliability.

4.3.4.1 Combine and Gridded Tidal Models

Two independent tidal datum datasets derived from satellite altimetry and the hydrodynamic modelling were integrated and gridded to produce unified surfaces for the MSL, LAT and HAT models. The spatial distribution of each tidal data from hydrodynamic and satellite altimetric dataset is as illustrated in Figure 4. 13. The hydrodynamic outputs (yellow) cover a coastal buffer of approximately 20 km from the shoreline while satellite altimetric data (blue) provide along-track coverage over offshore regions beyond this threshold. This complementary spatial arrangement addresses the limitations of each dataset where hydrodynamic models offer nearshore tidal data and satellite altimetry ensures coverage over open waters where model precision diminishes (Abd Rahman et al., 2024).

Both of the dataset were merged and interpolated into a uniform grid with a resolution of 1 arc-minute (≈ 1.8 km). The gridding process were carried out using kriging interpolation method in Surfer software bounded by the geographic extent of 1˚N < Latitude > 7˚N and 99˚E < Longitude < 105˚E as illustrated in Figure 4. 14. Kriging was selected as it is a reliable and flexible interpolation method that performs well across different types of datasets. A key advantage is its ability to manage unevenly distributed data as it compensates for clustered measurements by assigning them lower weights in the prediction process. This results in a smoother and more realistic surface compared with interpolation techniques such as inverse distance weighting or spline (Golden Software, 2025).

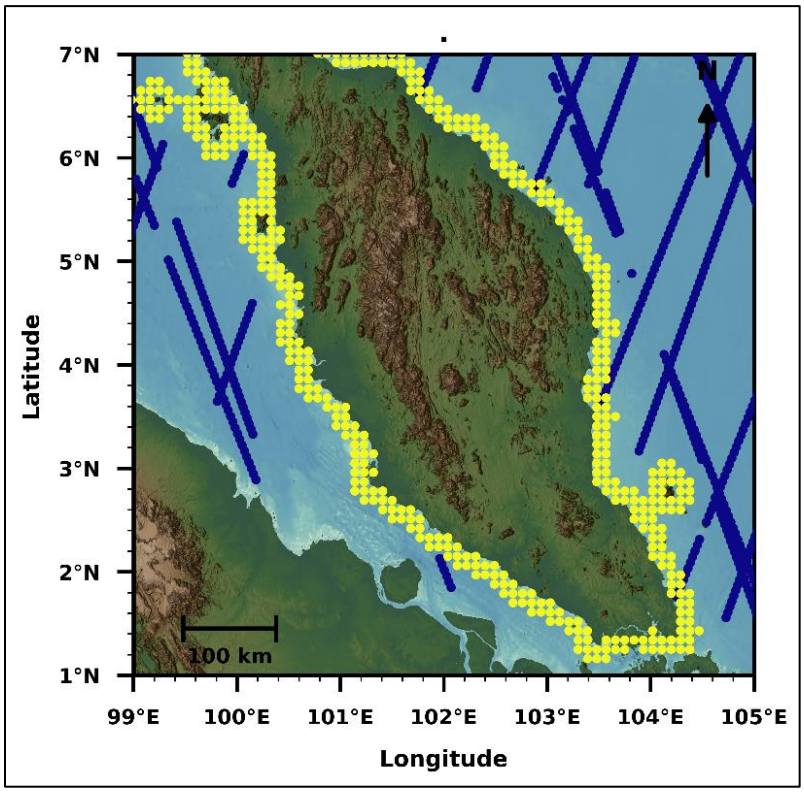


Figure 4. 13 Distribution of Tidal Data From Hydrodynamic (Yellow) and Satellite Altimetric (Blue) Data

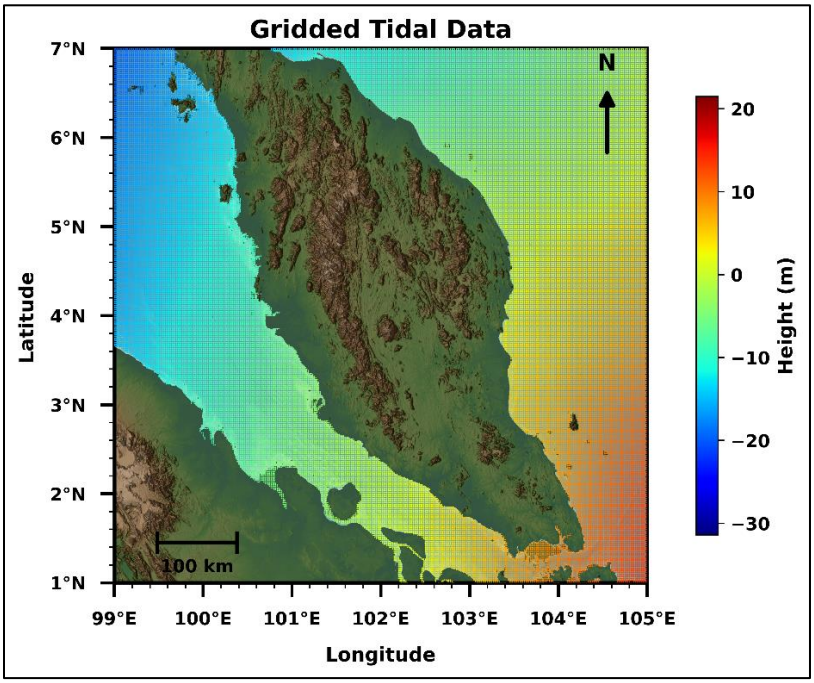


Figure 4. 14 The Gridded Tidal Data From Combined Hydrodynamic and Satellite Altimetric Data

In order to analyse the individual performance of computed tidal models from two different approaches of hydrodynamic and altimetric, these computed models were assessed with local tide gauges data (see Table 4. 11). The comparison outcomes of tidal models using hydrodynamic only and assimilation of hydrodynamic and satellite altimetry approach are as depicted in Table 4. 16 and the residuals were plotted in Figure 4. 15. Based on the results, the RMSE for the MSL increased slightly from 0.070 m to 0.080 m, indicating a deterioration of approximately 14% in accuracy. In contrast, the LAT models benefited from the inclusion of satellite altimetry. The RMSE for LAT improved from 0.477 m to 0.450 m which reflects a reduction of about 6%. Similarly, HAT decreased from 0.407 m to 0.449 m, indicating a deterioration of roughly 10 %.

While the improvement in LAT indicates that altimetry data contributes positively in low tide predictions, the slight degradation in HAT performance suggests limitations in resolving extreme tidal levels through the combined approach. This suggests that the addition of satellite altimetry in this case introduced additional uncertainties rather than improving the model, possibly due to difference in spatial resolutions across the datasets. Additionally, hybrid modelling approaches do not guarantee consistent improvement across all the models. Assimilation may improve overall accuracy in some dimensions yet degrade others depending on data quality and regional variability (Feng et al., 2024). This inconsistency underscores inherent limitations in the method. Although the integrated models differ by only ±1 - 4 cm, the involvement of satellite altimetry data is essential for extending tidal datum estimation into open sea areas where in-situ measurements are absent. Despite slight degradations in MSL and HAT models, the integrated model still provide reliable and acceptable results for the development of vertical transformation models in this study.

Table 4. 16
Comparison of RMSE Values Between Hydrodynamic Only Dataset And Hydrodynamic + Satellite Altimetry Data For Tidal Datums

Tidal Datum	Hydrodynamic	Hydrodynamic + Satellite Altimetry	Δ RMSE Difference	% RMSE Changes
MSL	0.070 m	0.080 m	+ 0.010 m	+ 14.3%
LAT	0.477 m	0.450 m	- 0.027 m	- 5.7 %
HAT	0.407 m	0.449 m	+ 0.042 m	+ 10.3 %

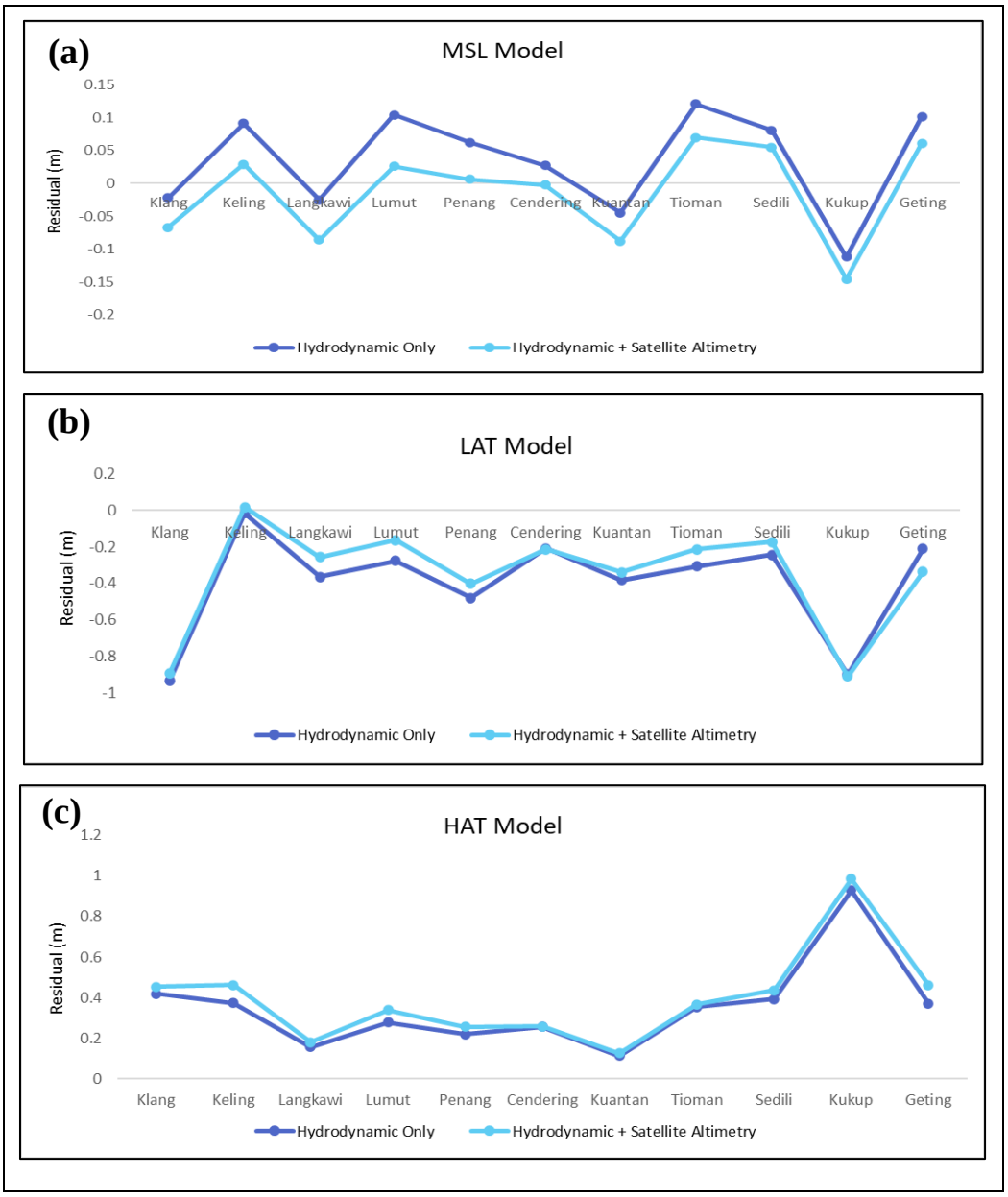


Figure 4. 15 The Residuals of Hydrodynamic Only and Hydrodynamic + Satellite Altimetry Data When Compared With Tide Gauges References for (A) MSL. (B) LAT and (C) HAT Tidal Models

In this study, the tidal models utilized for the computation of vertical transformation model are only the LAT and HAT models. The statistical summary of the final computed tidal model specifically the LAT and HAT models are as presented in Table 4. 17 and plotted in Figure 4. 16 and Figure 4. 17 respectively. Based on the table, the properties of the LAT model indicated that the minimum and maximum value ranging from -21.589 m to 12.779 m. The mean is -4.775 m and the standard deviation

is 7.420 m. In parallel, the minimum and maximum value for HAT model ranging from -18.361 m and 14.717 m. The mean and standard deviation exhibits -2.091 m and 7.548 m consecutively. The similar standard deviations of both models suggest that they achieve a similar level of accuracy in representing tidal extremes. This indicates that the overall variability captured by the LAT and HAT models is consistent, meaning that neither model introduces significantly higher uncertainty than the other. Such consistency is important for vertical transformation applications, as it ensures that both the lowest and highest tidal references can be represented with equivalent reliability.

Table 4. 17
The Statistical Summary of Computed LAT and HAT Models

Tidal Model	Min	Max	Mean	Std
Lowest Astronomical Tide (LAT)	-21.589	12.779	-4.775	7.420
Highest Astronomical Tide (HAT)	-18.361	14.717	-2.091	7.548

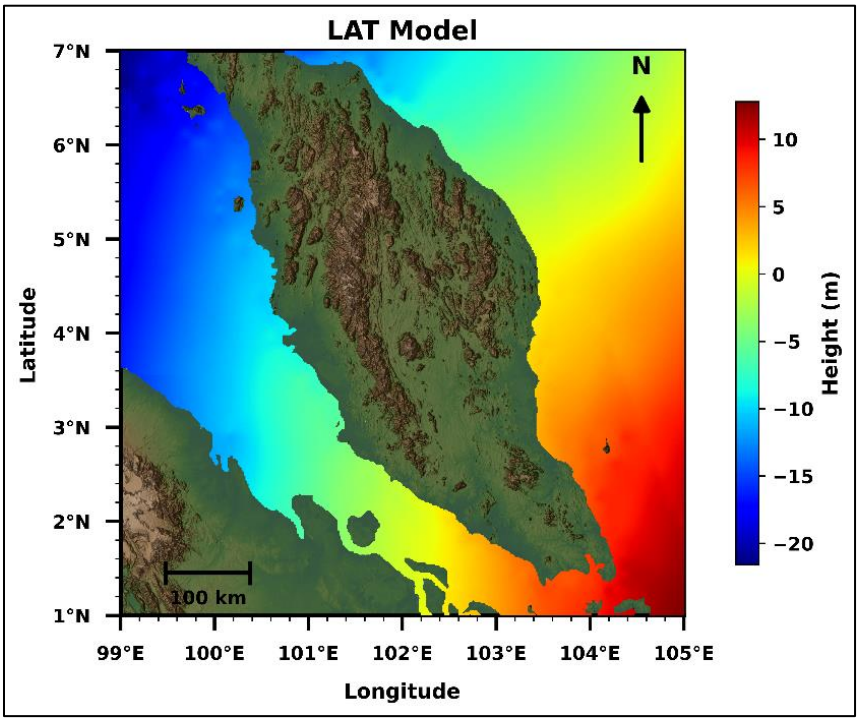


Figure 4. 16 The Computed LAT Tidal Model

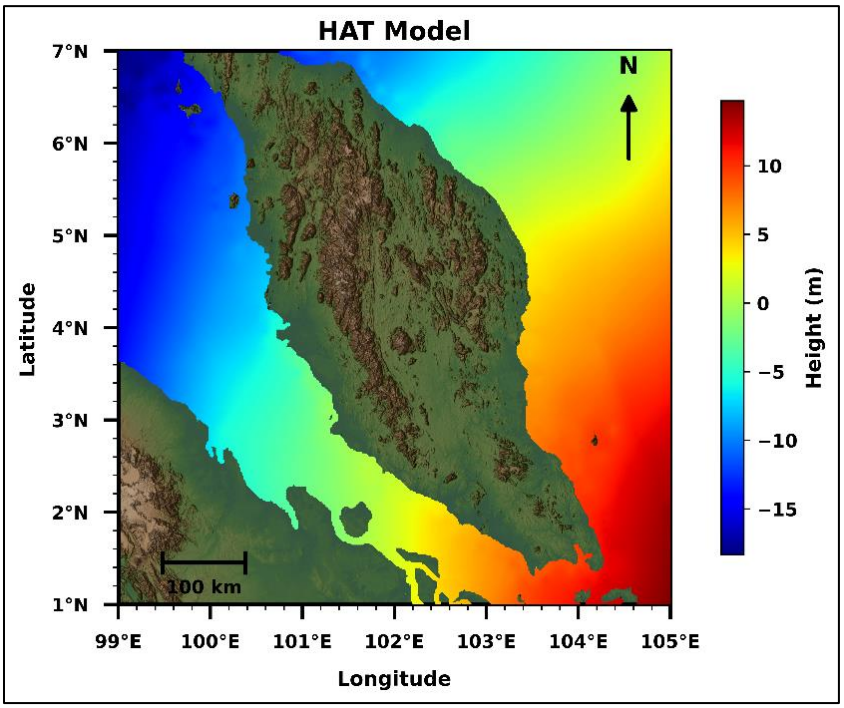


Figure 4. 17 The Computed HAT Tidal Model

4.4 Vertical Transformation Offset

The third objective of this study focused on the computation of vertical transformation offset in the realizing the unified vertical datum across land and marine domains. The procedure involved with the derivation of offset based on the computed hybrid geoid model together with the LAT and HAT tidal models. These offsets represent the vertical differences between the each datums, thereby enabling the transformation of heights from one reference system to another. Following the computation, the offsets were validated against observations obtained from local tide gauge stations to assess the consistency and accuracy of the computed offsets as well identifying potential discrepancies caused by localized oceanographic conditions or limitations within the input datasets or methodologies used.

4.4.1 Computation of Vertical Datum Offset

The analysis of the vertical datum offsets (VDO) from both the statistical results in Table 4. 18. The spatial distribution maps in Figure 4. 18, Figure 4. 19 and Figure 4. 20 provides a consistent picture of the relationship between the hybrid geoid and tidal datums across Peninsular Malaysia. For the hybrid geoid - HAT offsets, the values range from -4.068 m to 2.237 m with a mean of -1.150 m, indicating that the hybrid geoid generally lies below the HAT surface. This is expected since HAT represents the extreme high tide, while the geoid is theoretically closer to mean sea level. In the case of hybrid geoid - LAT, the offsets range from -1.201 m to 4.873 m with a mean of 1.534 m. The model shows that the area around Strait of Malacca records the highest offsets around 2-3 m, whereas the South China Sea area exhibits smaller separations around 0-2 m. Subsequently, the HAT - LAT indicates mean differences of about 2.606 m which match the expected tidal range across Malaysian waters. The offset values vary from near zero to about 5 m is corresponding directly to the difference between the highest and lowest astronomical tides.

Along the northern west coast of Malacca's Straits near Penang and Kedah shows smaller ranges of 2-3 m. However, the offset along southern west coast reaches up to 4-5 m. This happens because the Strait of Malacca becomes shallower and narrower toward the south which works like a funnel that makes the tides rise higher. This pattern is consistent with the findings of the tidal range (Wisha et al., 2023) at the southern reaches is generally lower than in the main strait due to the shallow bottom morphology, highlighting how the shape and depth of the strait amplify the tides. On the east coast facing the South China Sea, the offsets are usually small about 1- 3 m. However, in some places like near offshore islands and shallow coastal areas, the offsets can be higher up to 4 m. This happens because the tides on the South China Sea falls under category of mixed tide (mainly semidiurnal), meaning the tidal pattern changes over time with the occurrence of unequal high and low tides within a day (Alihan et al., 2024). In summary, the small standard deviations of less than 1 m highlight the spatial stability of the offsets. This suggests that the hybrid geoid and tidal datums are well aligned with the tidal conditions in Malaysia.

Table 4. 18
The Spatial Information of Computed Vertical Datum Offset

Vertical Datum Offset (VDO)	Min	Max	Mean	Std
Hybrid geoid – HAT	-4.068	2.237	-1.150	0.723
Hybrid geoid – LAT	-1.201	4.873	1.534	0.797
HAT – LAT	-0.251	5.015	2.606	0.613

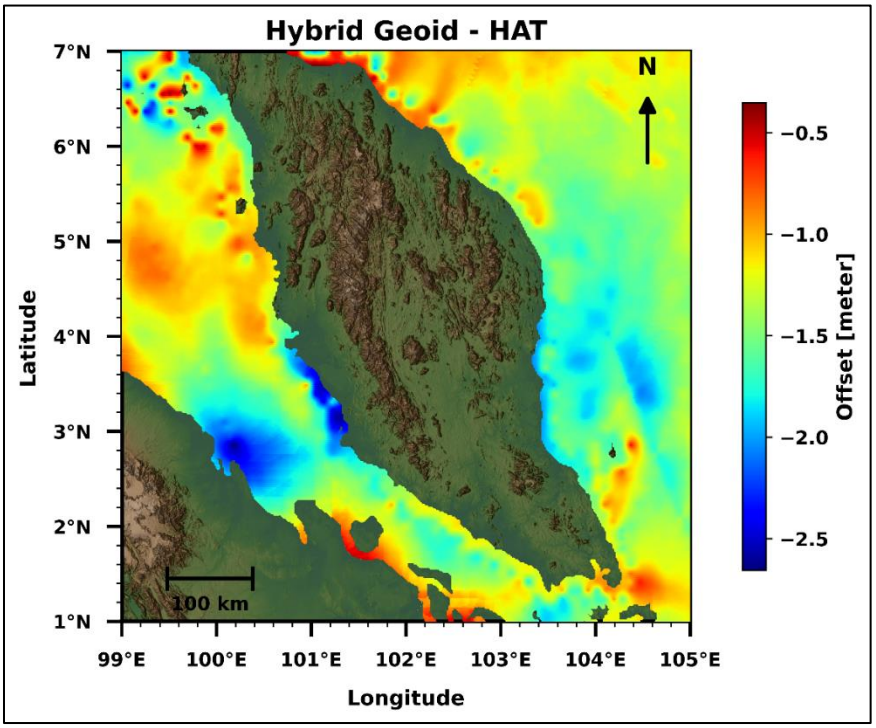


Figure 4. 18 The VDO Model of Hybrid Geoid – HAT

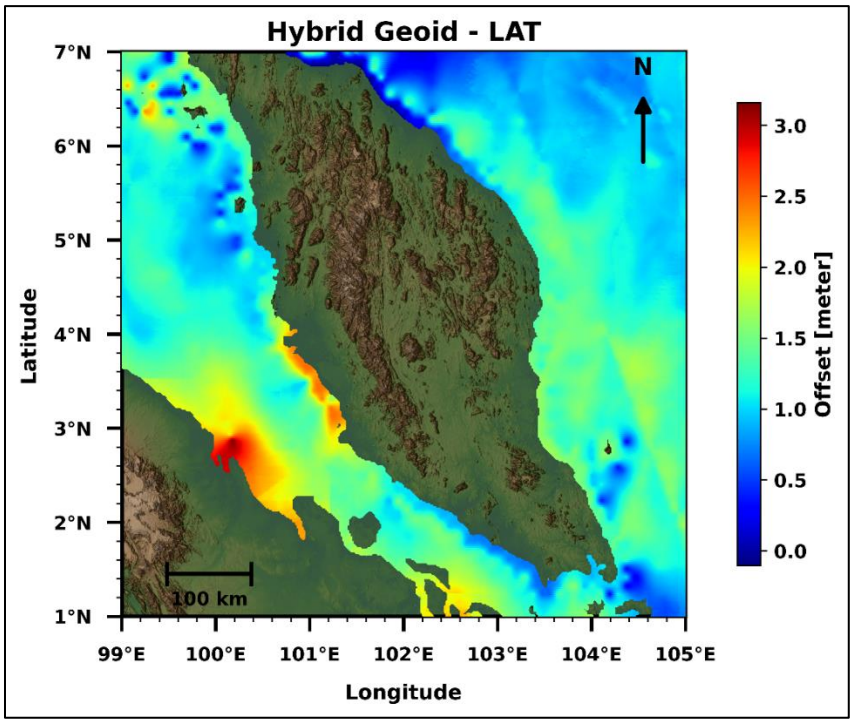


Figure 4. 19 The VDO Model Hybrid Geoid – LAT

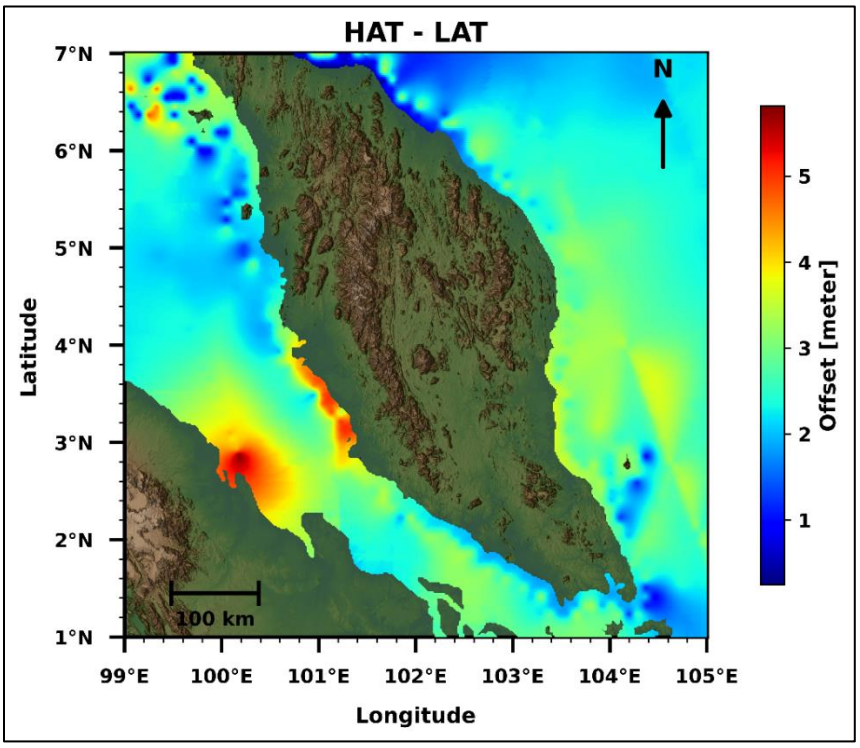


Figure 4. 20 The VDO Model of HAT – LAT

4.4.2 Evaluation of Vertical Datum Offset

After the computation of vertical datum offset, each model was validated using local tidal observations obtained from eleven tide gauge stations. The validation results for the three VDO models are presented in Table 4. 19 (hybrid geoid - HAT), Table 4. 20 (hybrid geoid - LAT), and Table 4. 21 (HAT - LAT). Among the three models, the hybrid geoid–HAT offset achieved the lowest RMSE of 0.353 m, indicating the closest agreement with the tide gauge observations. In comparison, the hybrid geoid - LAT model recorded an RMSE of 0.535 m, while the HAT - LAT model produced the largest RMSE of 0.866 m. The higher RMSE observed for the HAT - LAT model may be attributed to the fact that both surfaces represent tidal extremes, making them more sensitive to local hydrodynamic variations and uncertainties in tidal datum determination. Consequently, larger discrepancies may arise when compared with observed tide gauge values. To further assess the reliability of the results, the residual distributions of each model were examined, as shown in Figure 4. 21, to identify any potential outliers and investigate the stations contributing most significantly to the overall error.

For the hybrid geoid - HAT model, the smallest residual was observed at Kuantan (0.009 m), indicating excellent agreement between the computed and reference offsets. This suggests that the local geoid and tidal datum surfaces are represented consistently in this region, resulting in minimal discrepancies between the modelled and observed values. In contrast, the largest residual was recorded at Kukup (0.835 m), which contributed substantially to the overall RMSE. A similar pattern was observed for the hybrid geoid - LAT model, where Tanjung Keling exhibited the smallest residual (0.132 m) while Kukup again produced the largest residual (1.056 m). For the HAT - LAT model, the smallest residual occurred at Pulau Langkawi (0.435 m), whereas Kukup remained the largest contributor with a residual of 1.891 m.

The consistently large residuals observed at Kukup indicate that the discrepancies are likely associated with local environmental and modelling factors rather than the overall performance of the developed models. Kukup is situated within the southern part of Peninsular Malaysia near the transition between the Straits of Malacca and the Singapore Strait, where tidal propagation, shallow-water effects, and

complex coastal geometry may generate significant spatial variations in sea level characteristics (Rashidi et al., 2021). Coastal geoid determination is generally more challenging because it requires the integration of heterogeneous terrestrial and marine gravity datasets, which often exhibit differences in data coverage, quality, and resolution across the land - sea transition zone (Y. Liu & Lou, 2022). These factors can introduce uncertainties into the geoid surface and subsequently affect the determination of vertical datum offsets. Furthermore, coastal gravity field modelling is known to be more difficult due to limited gravity observations near shorelines and the complexity of representing gravity signals in coastal environments.

Despite the larger residuals observed at Kukup, most stations exhibited considerably smaller discrepancies, particularly for the hybrid geoid - HAT model. This indicates that the developed hybrid geoid provides a reliable representation between the geoid and tidal datums across most coastal regions of Peninsular Malaysia. The HAT surface is more consistently related to the geoid than the LAT surface, while the larger RMSE obtained for the HAT - LAT model reflects the greater sensitivity of tidal extremes to local hydrodynamic conditions and tidal variability.

Table 4. 19
The Validation Result Between Hybrid Geoid – HAT Model Using 11 Tide Gauge Stations

Station	**Latitude**	**Longitude**	**Δ Ref.**	**Δ Comp.**	**Δ**	**Abs**	**Abs^2**
Klang	3.05	101.358	-2.844	-2.406	-0.438	0.438	0.191
T. Keling	2.215	102.153	-1.519	-1.204	-0.315	0.315	0.099
P.Langkawi	6.432	99.765	-1.776	-1.591	-0.185	0.185	0.034
Lumut	4.24	100.613	-1.612	-1.337	-0.275	0.275	0.076
Penang	5.422	100.347	-1.438	-1.254	-0.184	0.184	0.034
Cendering	5.265	103.187	-1.683	-1.457	-0.226	0.226	0.051
Kuantan	3.975	103.43	-1.957	-1.966	0.009	0.009	0.000
P.Tioman	2.807	104.14	-1.811	-1.673	-0.138	0.138	0.019
Sedili	1.932	104.115	-1.529	-1.223	-0.306	0.306	0.094
Kukup	1.325	103.443	-2.054	-1.219	**-0.835**	0.835	0.698
Geting	6.227	102.107	-1.066	-0.789	-0.277	0.277	0.077
						SUM	1.373
						RMSE	0.353

Table 4. 20
The Validation Result Between Hybrid Geoid – LAT Model Using 11 Tide Gauge Stations

Station	**Latitude**	**Longitude**	**Δ Ref.**	**Δ Comp.**	**Δ**	**Abs**	**Abs²**
Klang	3.05	101.358	3.095	2.186	**0.909**	0.909	0.827
T. Keling	2.215	102.153	1.142	1.010	0.132	0.132	0.017
P.Langkawi	6.432	99.765	1.790	1.540	0.250	0.250	0.063
Lumut	4.24	100.613	1.830	1.603	0.227	0.227	0.052
Penang	5.422	100.347	1.658	1.186	0.472	0.472	0.223
Cendering	5.265	103.187	1.364	1.117	0.247	0.247	0.061
Kuantan	3.975	103.43	1.900	1.426	0.474	0.474	0.225
P.Tioman	2.807	104.14	1.922	1.479	0.443	0.443	0.196
Sedili	1.932	104.115	1.640	1.335	0.305	0.305	0.093
Kukup	1.325	103.443	1.751	0.695	**1.056**	1.056	1.115
Geting	6.227	102.107	0.717	0.195	0.522	0.522	0.272
						SUM	3.143
						RMSE	0.535

Table 4. 21
The Validation Result Between HAT – LAT Model Using 11 Tide Gauge Stations

Station	**Latitude**	**Longitude**	**Δ Ref.**	**Δ Comp.**	**Δ**	**Abs.**	**Abs²**
Klang	3.05	101.358	5.939	4.592	**1.347**	1.347	1.814
T. Keling	2.215	102.153	2.661	2.214	0.447	0.447	0.200
P.Langkawi	6.432	99.765	3.566	3.131	0.435	0.435	0.189
Lumut	4.24	100.613	3.442	2.940	0.502	0.502	0.252
Penang	5.422	100.347	3.096	2.440	0.656	0.656	0.430
Cendering	5.265	103.187	3.047	2.574	0.473	0.473	0.224
Kuantan	3.975	103.43	3.857	3.392	0.465	0.465	0.216
P.Tioman	2.807	104.14	3.733	3.152	0.581	0.581	0.338
Sedili	1.932	104.115	3.169	2.558	0.611	0.611	0.373
Kukup	1.325	103.443	3.805	1.914	**1.891**	1.891	3.576
Geting	6.227	102.107	1.783	0.984	0.799	0.799	0.638
						SUM	8.251
						RMSE	0.866

The residuals graph for each result in Figure 4. 21 were plotted to further examine the outliers in the dataset. Based on the pattern of the graph, it can be seen that there are two obvious spikes or unusual high residuals in the dataset which consistent among every model which is at Klang and Kukup. There could be several factors that may cause the high residuals to occur. In this case, the natural conditions of the tide gauge locations for Kukup and Klang could be the main issues.

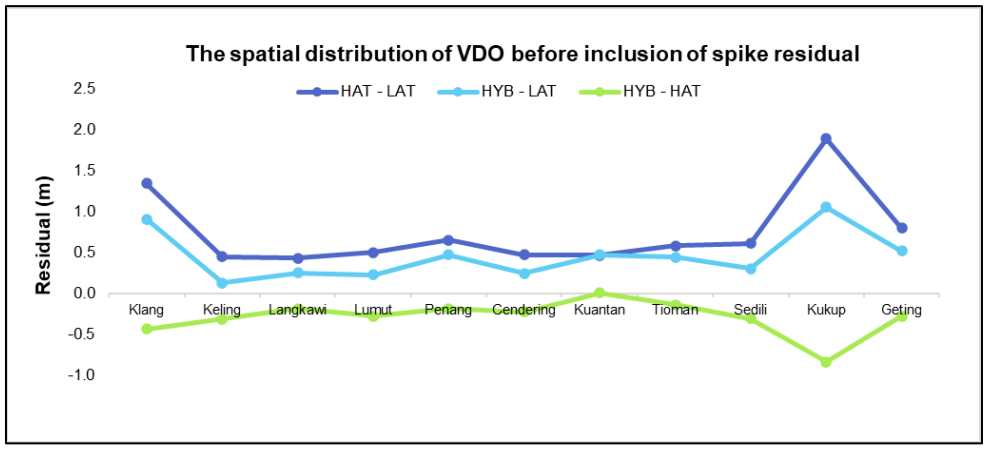


Figure 4. 21 The Trends of Spatial Residuals Before Tide Gauge Exclusion

As for Kukup, it can be seen from the map in Figure 4. 22 that the location sits in a heavily altered coastal setting since the tide gauge area was surrounded with buildings, aquaculture, and dense fish traps (kelong). Those local structures change how water moves near the tide gauge as the fish traps and piers causes the slow flow, reflect waves, and change local currents. Additionally, Kukup was often mentioned as the fastest rate of sea level rise compared to other stations. National reports and regional studies have listed Kukup among the highest trend rates on Peninsular Malaysia's west coast as highlighted in Benson et al. (2017), Ali et al. (2023) and Arif et al. (2023). These local factors can alter tidal amplitude and cause non-tidal residuals which could significantly affects to the inaccurate sea level measurement.

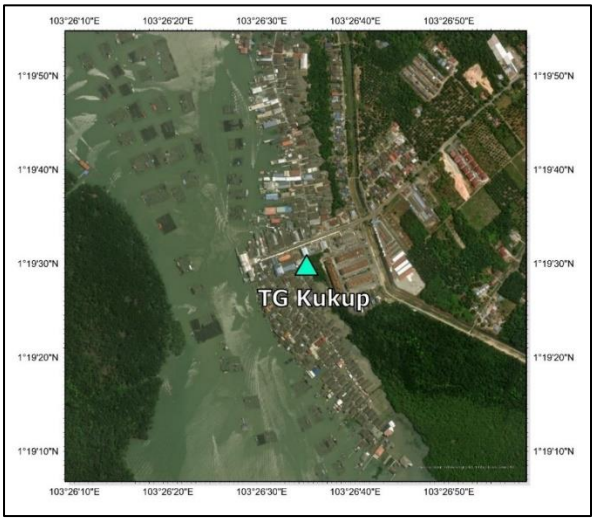


Figure 4. 22 The Location of Tide Gauge Station at Kukup

In the case of Klang, the major issues that may affects an accurate tidal derivation is the location of the tide gauge itself. It can be seen from Figure 4. 23 that the location of the tide gauge sits at the mouth of the Klang River where the area is strongly influenced by the tidal flow of the Strait of Malacca. Two tidal waves that travel along the Straits of Malacca meets the Klang River and creates bigger tidal range where the local tidal signal is more complex (Mustaffa et al., 2024). Additionally, the tide gauge station is located at the Port area where the place of the busiest shipping channel and port works. The movement of ships that pass through may causes the fake or unstable fluctuation of sea level during the measurement is taken. The uncertainties may significantly affected the tidal records at the Klang station which causes the tidal derivation such as LAT and HAT become less accurate.



Figure 4. 23 The Location of Tide Gauge Station at Klang

After examining the conditions at Kukup and Klang tide gauge stations, a second round of validation was carried out by removing these two stations from the dataset. The main purpose of this step was to test whether excluding stations with questionable data quality or strong local influences could change the accuracy of the model. The updated validation was then performed for all three vertical datum offset models. The new validation results of hybrid geoid – HAT are shown in Table 4. 22, while the outcomes for the hybrid geoid – LAT and HAT – LAT model are presented in Table 4. 23 and Table 4. 24 respectively.

Table 4. 22
The Validation Result Between Hybrid Geoid – HAT Model After Exclusion of Kukup and Klang Tide Gauge Stations

Station	**Latitude**	**Longitude**	**Δ Ref**	**Δ Comp**	**Δ**	**Abs**	**Abs²**
T. Keling	2.215	102.153	-1.519	-1.204	-0.315	0.315	0.099
PLangkawi	6.432	99.765	-1.776	-1.591	-0.185	0.185	0.034
Lumut	4.24	100.613	-1.612	-1.337	-0.275	0.275	0.076
Penang	5.422	100.347	-1.438	-1.254	-0.184	0.184	0.034
Cendering	5.265	103.187	-1.683	-1.457	-0.226	0.226	0.051
Kuantan	3.975	103.43	-1.957	-1.966	0.009	0.009	0.000
P. Tioman	2.807	104.14	-1.811	-1.673	-0.138	0.138	0.019
Sedili	1.932	104.115	-1.529	-1.223	-0.306	0.306	0.094
Geting	6.227	102.107	-1.066	-0.789	-0.277	0.277	0.077
						SUM	0.484
						RMSE	0.210

Table 4. 23
The Validation Result Between Hybrid Geoid – LAT Model After Exclusion of Kukup and Klang Tide Gauge Stations

Station	**Latitude**	**Longitude**	**Δ Ref**	**Δ Comp**	**Δ**	**Abs**	**Abs²**
T. Keling	2.215	102.153	2.661	2.214	0.132	0.132	0.017
P.Langkawi	6.432	99.765	3.566	3.131	0.250	0.250	0.063
Lumut	4.24	100.613	3.442	2.940	0.227	0.227	0.052
Penang	5.422	100.347	3.096	2.440	0.472	0.472	0.223
Cendering	5.265	103.187	3.047	2.574	0.247	0.247	0.061
Kuantan	3.975	103.43	3.857	3.392	0.474	0.474	0.225
P. Tioman	2.807	104.14	3.733	3.152	0.443	0.443	0.196
Sedili	1.932	104.115	3.169	2.558	0.305	0.305	0.093
Geting	6.227	102.107	1.783	0.984	0.522	0.522	0.272
						SUM	1.201
						RMSE	0.330

Table 4. 24
The Validation Result Between HAT – LAT Model After Exclusion of Kukup and Klang Tide Gauge Stations

Station	**Latitude**	**Longitude**	**Δ Ref**	**Δ Comp**	**Δ**	**Abs**	**Abs²**
T. Keling	2.215	102.153	2.661	2.214	0.447	0.447	0.200
P.Langkawi	6.432	99.765	3.566	3.131	0.435	0.435	0.189
Lumut	4.24	100.613	3.442	2.940	0.502	0.502	0.252
Penang	5.422	100.347	3.096	2.440	0.656	0.656	0.430
Cendering	5.265	103.187	3.047	2.574	0.473	0.473	0.224
Kuantan	3.975	103.43	3.857	3.392	0.465	0.465	0.216
P. Tioman	2.807	104.14	3.733	3.152	0.581	0.581	0.338
Sedili	1.932	104.115	3.169	2.558	0.611	0.611	0.373
Geting	6.227	102.107	1.783	0.984	0.799	0.799	0.638
						SUM	2.861
						RMSE	0.510

The analysis of the RMSE values before and after adjustment as presented in Table 4. 25 shows clear improvements in the consistency of the vertical datum offsets. For the hybrid geoid - HAT comparison, the RMSE decreased from 0.353 m to 0.210 m, giving a reduction of 0.143 m or about 40%. This means the hybrid geoid and HAT surface are better aligned after adjustment. In the case of hybrid geoid – LAT, the RMSE reduced from 0.535 m to 0.330 m, an improvement of about 38%, showing that the hybrid geoid also matches more closely with the LAT surface. The largest improvement was seen in the HAT – LAT offset, where the RMSE dropped from 0.866 m to 0.510 m, equal to around 41% improvement. This indicates that the adjustment helped capture the tidal range more accurately by reducing the gap between the highest and lowest tidal surfaces. Overall, the consistent decrease in RMSE across all comparisons demonstrates that the adjustment method effectively minimized the vertical separation errors, leading to a more stable and reliable representation of vertical datums across Peninsular Malaysia. This can also be seen from the trends of each model in Figure 4. 24 has become relatively flat and stable compared to the previous graph (see Figure 4. 21).

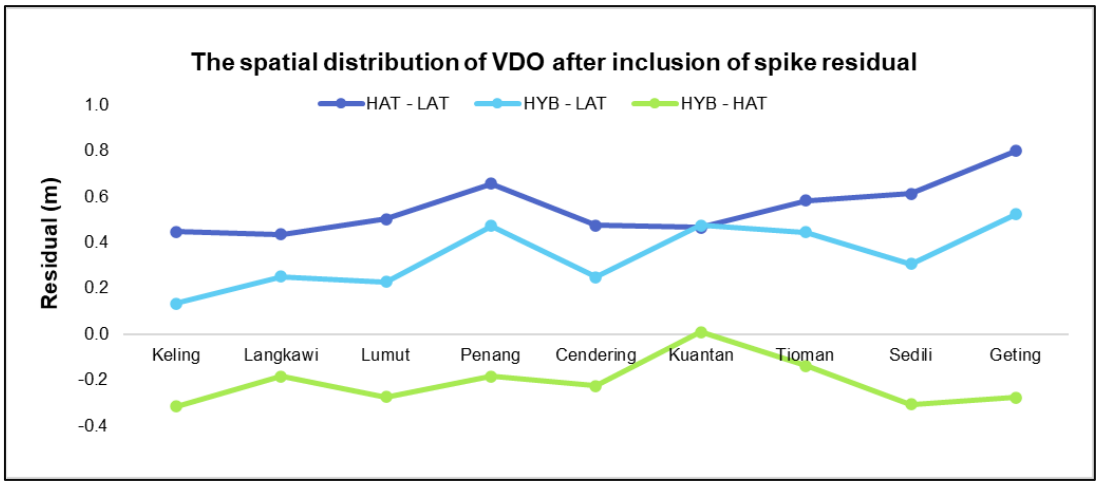


Figure 4. 24 The Trends of Spatial Residuals Before Tide Gauge Exclusion

Table 4. 25
The RMSE of VDO Before and After Tide Gauge Adjustments

Vertical Datum Offset (VDO)	RMSE			
	Before	**After**	**Δ Difference**	**% Changes**
Hybrid geoid – HAT	0.353	0.210	0.143	40 %
Hybrid geoid – LAT	0.535	0.330	0.205	38 %
HAT – LAT	0.866	0.510	0.356	41 %

In summary, the final output of vertical datum offset in this study which fundamentally serves as the input of vertical transformation model managed to provide accuracies that range between ± 21 – 51 cm across Peninsular Malaysia. Regrettably, the accuracies 20 to 50 cm is considered large in the context of vertical transformation models as it significantly exceeds the typical error range of existing models which is approximately 10 to 30 cm. For comparison, the Vdatum (9 – 10 cm), VORF (10 – 15 cm) AUSHDROID (< 20 cm) and CDVCW (10 – 30 cm) (Filmer et al., 2024; Iliffe et al., 2013; Nudds et al., 2016; Nwankwo et al., 2021). Such range of error may not be tolerable for high precision surveying as it exceeds the threshold of acceptability in hydrographic standards such as Special Order or Order 1A but still acceptable for less demanding applications such in Order 1B and Order 2 based on IHO S-44 (International Hydrographic Organization (IHO), 2022).

4.4.3 Discussion on the Outcomes of Computed Vertical Transformation Model

There are several factors that may possibly influence the accuracy of computed transformation models. Among common factors include transformation chain errors, uncertainties in data sources, and interpolation errors (National Oceanic and Atmospheric Administration, 2013a). In this study, transformation chain errors and data uncertainties may arise because the model development process involves combining and merging datasets from different sources. This might occurs specifically during the derivation of tidal datums which adopted the assimilation of hydrodynamic and satellite altimetric dataset that utilized using different methodologies and spatial metadata such as the resolution, reference surface or tidal constituents used. In addition, the conversion between ellipsoid reference surfaces and tide systems is required to achieve a standardized reference before computing offsets between models. This issue strongly emphasized by Filmer et al. (2024) on the importance of careful procedures during reference surface conversion to minimize errors. Although validation is carried out at each stage, every conversion introduces its own uncertainties and these accumulate when models are combined, leading to larger errors than in the initial computations. This effect can be seen in Table 4. 16 where the RMSE increased slightly when hydrodynamic and satellite altimetry data were integrated.

Another factor that may influence the results is the type and availability of validation data. In this study, the validation relies solely on tide gauge stations located along the coastline. Although the spatial distribution of stations is reasonably well spread, the number of available tide gauge records is still too limited to validate the model across the entire Peninsular Malaysia with only nine stations remaining after excluding Klang and Kukup. Previous studies have shown that tidal behaviour can vary within a distance of about 10 km from one location to another (Hamden, 2022). In contrast, the existing tide gauge stations in this study are separated by distances exceeding ±100 km, which weakens the representation of local tidal variations. The number of validation data points has a significant impact on the results. For instance, the AUSHDROID model initially reported comparable accuracy to this study, about 40 - 50 cm when using 25 tide gauges, but the accuracy improved substantially to around 10 - 20 cm after excluding six AHO tide gauges (Filmer et al., 2024). This demonstrates

that both the number and quality of validation data play a critical role in accurately determining the performance of the models.

Conversely, the validation in this study is limited as it relies only on tide gauge stations located near the coast, with no available means to evaluate the transformation models in the open sea. This constraint may cause the validation results to reflect mainly the hydrodynamic accuracy rather than the overall performance of the models. The hydrodynamic approach applied in this study extends up to 20 km from the coastline while tide gauge observations are considered reliable only within about 10 km. This restricts the ability to assess the models with high precision across broader marine areas. Consequently, the tidal datums derived from satellite altimetry could not be fully evaluated under these limitations. This highlights an important research gap, suggesting that the installation of more tide gauge stations across Malaysia would greatly support future studies and contribute to the development of a seamless unified datum bridging land and marine domains.

4.5 Research Summary

This chapter presents several important results in developing the vertical transformation models encompassed the hybrid geoid, LAT, and HAT models. The first part involved with the computation of hybrid geoid model covering the Peninsular Malaysia region. Prior to this, a comprehensive testing and assessment involving varies datasets were conducted as an effort to find the optimal input in the computation of gravimetric geoid model. The testing includes varies geopotential models, least square parameters (correlation length, standard deviation, and maximum degree), and marine gravity models. The testing outcomes shows that GGM = WHU SWPU GOGR2022S, ψ = 0.1°, $\sigma_{\Delta g}$= 1.0 mGal, M = L = 240 and Sandwell gravity model shows the best fit parameters in this study. During this phase, different GNSS levelling data were tested to examine the stability and precision of the computed models. Through this process, the final gravimetric model was developed with the accuracy of ± 3 – 6 cm across Peninsular Malaysia. The model was then fitted with 153 GNSS levelling data to develop the hybrid geoid. The fitting process was compute using 4-parameter datum shift and kriging interpolation method. In this study, the prediction variable of correlation distance and RMSE of data noise was included to effectively capture the

local spatial correlation of the geoid surface without introducing excessive smoothing and balanced representation of the random errors inherent in the GNSS levelling data. Then, the hybrid model was validated with 20 GNSS levelling data which indicates accuracy of 0.045 m.

The needs of validation data are one of the crucial parts in this study to accessed the performance of each computed data throughout this study. In this study, local tide gauge records were acquired from DSMM via University of Hawaii Sea Level Centre (UHSLC) data repository. The data were then processed using UTide Tools in MATLAB. Prior to that, the raw time series over 18 years observational data were filtered and converted into the UTide format first. Subsequently, the tidal datums for each tide gauge stations were derived from using harmonic analysis based on tidal constituents mounted in the UTide system. This study standardized the reference surface to GRS80 ellipsoid for effective data integration across the computed models. Therefore, the outputs from UTide were converted into GRS80 ellipsoid since the data were initially referenced to the zero tide gauge. This process which also called as tide reduction were made possible through the in-situ GNSS observation data at tide gauge benchmarks to acquire the ellipsoidal heights (h_{GNSS}) at each station. This study adopted the observation data from the 2019 GNSS Campaign carried out from joint collaboration between UiTM and UTM in 2019. The data were utilized together with other height reference which is the H_{ZTG} and from DSMM to produce an ellipsoidal-based tidal datums of LAT and HAT for each tide gauge locations.

In parallel, another datums that has been computed are the tidal datums specifically the LAT and HAT. The tidal datums were dervied through the assimilation of hydrodynamic model and satellite altimetry. In this study, the hydrodynamic approach was taken to provide tidal data within 20 km from the shoreline to the open sea where the satellite altimetry data are less reliable due to the land contamination of the radar footprint. The hydrodynamic data were derived using TMD software which managed to acquire the tidal data based on the selected global tide model which in this case is using the Indian Ocean model. The TMD provide output in form of time series amplitude measurement with respect to the MSL surface. From the output, the lowest and highest amplitude within specified duration of 32 years were determined specifically to acquire the LAT and HAT values respectively. As this study adopted an

ellipsoid-based reference as standard reference, these datasets were converted through an additional computation utilizing the MSS model data. Prior to this, a series of global MSS models which is not only direct model, but also combined data using Geoid + MDT models were evaluated using processed tide gauge stations data. Findings in this study indicated that the direct model of CNES-CLS22 provide the best accuracy that fit the area of Peninsular Malaysia the most compared to other model. Therefore, this model was adopted to convert the hydrodynamic data into ellipsoid reference surface.

As for tidal data beyond 20 km from shoreline and extending towards the open sea, the data were derived using multi-mission satellite altimetry data. This study utilized the combined dataset from TOPEX/Poseidon A/B, Jason-1 A/B, Jason-2 A/B, Jason-3A, GEOSAT Follow-On (GFO), and Sentinel-6A for over 32 years observational period. In order to generate the tidal datums, harmonic tidal analysis was applied based on 12 principal tidal constituents (M2, S2, N2, K2, K1, O1, P1, Q1, MF, MM, SSA, SA). These constituents were then used to reconstruct tidal elevations along satellite ground tracks, enabling the prediction of the full tidal cycle at each observation point. To ensure consistency between missions, a crossover adjustment was implemented using nearest-neighbour analysis. This method compared mean sea level values at locations where ground tracks from different satellites intersected. Outliers exceeding three standard deviations from the mean were removed through statistical filtering, leaving only valid data pairs. The remaining residual differences were averaged to determine systematic offsets, which were then applied to refine the initial LAT and HAT estimates. This adjustment step is essential for harmonizing datasets from multiple missions with varying orbits and instrumentation. Through discrepancies reduction at crossover points and aligning measurements across satellites, the integrated dataset achieves improved vertical consistency, spatial continuity, and accuracy in representing the tidal datums.

Following the derivation of tidal datums from both approaches, the dataset was validated in two parts which is the pure hydrodynamic data and assimilation of hydrodynamic and satellite altimetry data. As for the assimilation model, both tidal data for hydrodynamic and satellite altimetry were merged and gridded into a unified model of LAT and HAT models. Subsequently, the models were validated against processed data from tide gauge stations to access the accuracy of the computed models. Findings

in this study indicate that the accuracy of the model deteriorates by mere ± 1- 4 cm across the tidal models. However, since the changes in accuracy were not too great, the assimilation data were still be implemented in this study mainly to provide tidal data in open sea region. Subsequently, these computed tidal data were integrated with the hybrid geoid that has been computed to calculate the vertical datum offset between each model. The calculated offsets were once again validated against the reference offset at tide gauge stations. The final assessment indicated that the accuracy of vertical datum offset varies from ± 21 – 51 cm which serve as the dataset for developing a vertical transformation model in future studies.

CHAPTER 5
CONCLUSION AND RECOMMENDATION

5.1 Introduction

This chapter concludes the study by presenting the overall summary of the research outcomes. It brings together the key findings obtained from the analysis and relates them back to the research objectives. The discussion highlights what has been achieved throughout the study and how the results contribute to the existing knowledge in the field. This chapter presents the research conclusion where the main findings are summarised and discussed, addresses the limitations of the study, and provides recommendations for future work, suggesting possible improvements and directions for further research. Overall, this chapter provides a final reflection of the research work. It summarises the key outcomes, acknowledges the limitations encountered, and suggests areas that can be explored in future studies.

5.2 Research Conclusion

The rapid development of technologies in multiple field has led to the increasing recognition in driving the economic development that integrated across land and marine region such as overwater structures, oil reservoirs and natural gas deposits. These development of properties on/in water brings the cons in managing the spatial metadata in terms of its cadastral land position that become complex as it involves not only the horizontal (x, y) elements, but also the elevation (z) elements. A lot of studies particularly in Malaysia has highlighted the needs for unifed vertical datum across land and marine region, mainly for the purpose of realizing the 3D marine cadastre to effectively manage the marine properties. Apparently, a unified vertical datum or vertical transformation is not new globally but still understudies especially in Asia. There are several countries such as the United States of America, United Kingdom, Canada, Australia that has been working towards the unified datum since 2003 until now. Therefore, this study seeks to investigate and develop a framework for a unified vertical datum in Peninsular Malaysia.

This study has formed three core objectives focused on developing a unified vertical datum across Peninsular Malaysia land and marine region. The first objective involved with the computation of the first datum that can provide a seamless height across both domains which is the hybrid geoid model. The development of the hybrid geoid model was preceded by comprehensive evaluation of various input datasets to identify the most suitable parameters for the study region. Several global geopotential models were tested to determine their reliability and accuracy when applied locally. In addition, different least-squares collocation parameters, such as correlation length, standard deviation, and maximum degree, were examined to assess their impact on the overall precision of the computed geoid. Marine gravity models were also included in the testing to account for variations in gravity across offshore areas. The outcomes of these assessments identified the best-fit parameter set which was then applied in developing the final gravimetric geoid. Subsequently, the final gravimetric geoid was fitted to GNSS levelling data to derived a hybrid geoid. In this study, hybrid geoid was utilized instead of gravimetric geoid was mainly to account the standard practical of height reference in Malaysia that still adopt the MSL of PMGVD that tied to the 18 years observation of tidal datum at Port Klang.

The second objective involved with the development of tidal datums. Generally, the tidal datums in this study can be separated into three parts. The first part is the derivation of tidal datums at tide gauge stations using UTide tools. This tidal data were reserved for the use of validation of computed tidal models from the second and third parts later on. On the second part, the tidal datums were derived using hydrodynamic approach to acquire the tidal data within 20 km from the shoreline. The data were acquired from Indian Ocean tide model through the TMD software. The last part which is the third part involved the multi-mission satellite altimetry dataset. This approach was taken as the satellite altimetry not only capable to provide a stable observation of MSS but also offers a good coverage of data in the open sea area. Prior to further computation, all dataset underwent a tide reduction process to transform each datatset into an ellipsoid-based reference specifically the GRS80. Subsequently, the data from hydrodynamic and satellite altimetry were combine and gridded before validated against the tide gauge data acquired during the first part.

The third and final objective focused on the development of vertical transformation models. In this phase, the models derived from the first and second objectives were integrated to determine their vertical datum offsets. Three offsets were computed, representing the separations between (a) the hybrid geoid and HAT, (b) the hybrid geoid and LAT, and (c) HAT and LAT models. These offsets were then validated against tide gauge observations. The results revealed varying accuracies for each vertical datum offset, ranging from ±21 cm to ±51 cm. Although the final outcomes of this study did not achieve highly precise models, the findings provide valuable insights and serve as important references for future research. This is particularly significant given that this field remains relatively understudies not only in Malaysia but also across Asia. Therefore, the study establishes a foundation for advancing research on vertical datums in the region and highlights the need for more comprehensive datasets and refined methodologies to achieve a seamless and accurate unified height reference system.

In summary, this study has provided an initial but significant step toward the realization of a seamless unified vertical datum for Peninsular Malaysia. Although the accuracy of the results can still be improved, the work shows the possibility of combining geoid models, tidal datums, and vertical transformations within a single framework. More importantly, the findings underscore the main challenges that remain particularly the need for better datasets, improved methods, and more extensive validation. As Malaysia progresses towards a 3D marine cadastre and stronger integration of land and marine management, the establishment of a reliable unified vertical datum will be an essential foundation for supporting sustainable development, effective governance and regional collaboration.

5.3 Limitation

This study is subject to several limitations that should be acknowledged when interpreting the results. These constraints mainly arise from data availability, spatial coverage, and methodological considerations, which collectively influence the accuracy and reliability of the outcomes.

5.3.1 Temporal Mismatch Between Datasets

A notable limitation of this study is related to inconsistencies in both temporal coverage and spatial resolution among the datasets used. Hydrodynamic model outputs, satellite altimetry observations, tide gauge records, and geoid models are not always consistent in terms of time period and spatial scale, which introduces uncertainty during data integration and model development. Temporal mismatch occurs because each dataset represents different observation periods and averaging strategies. Tide gauge records provide continuous in-situ measurements, while satellite altimetry data are typically derived from mission-specific repeat cycles and processed into time-averaged products. On the other hand, hydrodynamic models are based on global tide model which derived from assimilated satellite altimetry and tide gauge data over long-term climatological periods (Egbert & Erofeeva, 2002). This limitation is directly reflected in the results of this study, where a slight increase in RMSE is observed in Table 4. 16 after integrating hydrodynamic outputs with satellite altimetry and geoid datasets. The increase suggests that while individual datasets perform well independently, inconsistencies in temporal alignment introduce additional uncertainty when they are combined. Consequently, the integration of multi-resolution datasets may reduce the sensitivity of the transformation model to local variations, thereby influencing the accuracy of the derived vertical datum offsets and overall transformation results. This highlights that data integration, although essential for developing a unified vertical transformation model, remains a key source of error propagation in multi-source geodetic frameworks

5.3.2 Limitations of validation data availability and distribution

The reliability of the results is also affected by the limited availability of tide gauge data. Validation in this study relies solely on coastal tide gauge stations. After excluding Klang and Kukup due to data issues, only nine stations were available for analysis. Although these stations are geographically distributed, their spacing exceeds 100 km in many cases. Previous studies have shown that tidal behaviour can vary significantly within distances of approximately 10 km (Hamden, 2022). Therefore, the available tide gauge network is too sparse to fully capture local tidal variability across Peninsular Malaysia. The influence of validation data quantity has also been highlighted in previous research. Filmer et al. (2024) demonstrated that model accuracy can improve significantly when unreliable stations are excluded, showing that both the number and quality of tide gauges strongly affect validation outcomes.

5.3.3 Lack of offshore validation capability

Another important limitation is the absence of offshore validation data. In this study, all validation is restricted to coastal tide gauge stations, meaning that model performance in open sea conditions cannot be directly assessed. The hydrodynamic model extends approximately 20 km offshore, while tide gauge observations are generally considered reliable within about 10 km of the coastline. This mismatch limits the ability to evaluate model performance in deeper marine environments. As a result, the accuracy of tidal datums derived from satellite altimetry in offshore regions remains uncertain. This highlights a clear research gap and indicates the need for additional observational infrastructure such as offshore platforms, shipborne surveys, or expanded tide gauge networks to support more comprehensive validation and improve the development of a seamless land - sea vertical datum.

5.4 Recommendations for Future Research

Several recommendations can be put forward to improve and strengthen future studies related to this research. These recommendations aim to address the limitations encountered in this study and to provide guidance for developing more accurate and comprehensive outcomes. The suggested directions for future work are outlined as follows:

i) Improved approaches to enhance the accuracy of hydrodynamic model

Future studies should consider adopting more advanced modelling techniques beyond the TMD approach used in this study. One possible alternative is the OTIS (Ocean Tidal Inversion Software) system, which may provide improved flexibility for regional tidal modelling compared to pre-computed global solutions such as TPXO accessed through TMD. Unlike TMD, which applies fixed global tidal constituents, OTIS allows regional refinement of tidal parameters through inverse modelling and the incorporation of local observational constraints (Egbert & Erofeeva, 2002). This improvement could also involve the use of higher-resolution tidal modelling setups supported by more detailed bathymetric data, improved boundary forcing, and the assimilation of additional oceanographic observations such as tide gauges and satellite altimetry. The ability to adjust tidal constituents at regional scale in OTIS can help reduce spatial smoothing effects and improve agreement between modelled and observed tides. A more refined representation of tidal dynamics will directly enhance the reliability of tidal datum estimation, consistency with other integrated models, and essential to reduce uncertainties in vertical transformations in this study.

ii) Utilization of denser satellite altimetry datasets

The incorporation of denser and more recent satellite altimetry datasets would enhance spatial coverage, particularly in regions where tide gauge observations are sparse, as encountered in this study. The limited number and uneven distribution of tide gauges restricted the ability to comprehensively validate the computed models across Peninsular Malaysia. Future studies should therefore consider extending the altimetry database through the integration of additional multi-mission datasets with longer temporal records and improved coastal observation capabilities. Besides the satellite missions utilised in this study, datasets from ERS-2, Envisat, CryoSat-2, and SARAL/AltiKa could be incorporated. ERS-2 and Envisat provide longer historical records that can improve the representation of long-term tidal and sea level variability (Dubock et al., 2001), while CryoSat-2 and SARAL/AltiKa offer enhanced coastal observation capabilities and denser spatial coverage (Francis et al., 2010; Verron et al., 2015). The integration of these datasets would reduce data gaps, improve model validation, and provide a more detailed representation of tidal variability across both coastal and offshore regions. Consequently, the accuracy and reliability of vertical transformation models could be further enhanced.

iii) Refinement of methodologies to integrate diverse datasets

Future research should focus on improving the integration framework used to combine geoid models, hydrodynamic outputs, and satellite altimetry datasets. In this study, the integration process involved multiple transformations between reference surfaces and datasets of different spatial resolutions, which may have contributed to error propagation and reduced model accuracy. A potential improvement is the implementation of weighted adjustment, where weights are assigned according to the accuracy and uncertainty of each dataset. This approach would allow more reliable datasets to have a greater influence on the final solution while minimizing the impact of less accurate observations. Developing more rigorous statistical frameworks or advanced data fusion

techniques would help minimize such inconsistencies and reduce the propagation of errors across datasets. A more robust integration process would ensure that the resulting models are not only more consistent and accurate but also more reliable when applied across both coastal and offshore domains.

iv) Expansion of tide gauge station networks

Expanding the number of tide gauge stations across Malaysia, particularly in regions with wide spatial gaps would provide more comprehensive and reliable validation data. In this study, only nine tide gauge stations were available after the exclusion of Klang and Kukup, with distances between stations often exceeding 100 km. Such limitations restricted the ability to capture local tidal variability and reduced the reliability of model validation. Considering that tidal characteristics may vary significantly over much shorter distances, additional stations should be established between existing observation sites, particularly along the west coast of Peninsular Malaysia where complex coastal geometry and shallow waters influence tidal behaviour (Wisha et al., 2023). Establishing a denser tide gauge network would allow local tidal characteristics to be represented more accurately, minimize interpolation errors, and enable more precise assessments of vertical transformation model performance. Strengthening this observational network is therefore essential, as the current distribution of tide gauges is too sparse to adequately validate models on a regional scale.

v) Acquisition of validation data in offshore regions

Validation of the transformation models in this study was restricted to tide gauges located along the coastline, as no validation data were available for offshore regions. This limitation meant that the models could only be assessed within nearshore zones, leaving uncertainties in their performance further out at sea. Future research should therefore prioritize the acquisition of offshore datasets to overcome this gap. Potential approaches include deploying oceanographic instruments, conducting shipborne GPS campaigns or utilizing

tidal observations from offshore oil platforms. In addition, validation through comparisons with global tide models may also serve as a complementary alternative. Access to such datasets would enable validation beyond the coastal zone, leading to a more accurate assessment of model performance in open waters and strengthening efforts toward the development of a seamless land–sea unified vertical datum.

REFERENCES

Abbak, R. A., Erol, B., & Ustun, A. (2012). Comparison of the KTH and Remove-Compute-Restore Techniques to Geoid Modelling in a Mountainous Area. *Computers and Geosciences*, *48*, 31–40. https://doi.org/10.1016/j.cageo.2012.05.019

Abd Rahman, M. F., Md Din, A. H., Mahmud, M. R., & Hamden, M. H. (2024). Quasi-Continuous Tidal Datum for Peninsular Malaysia using Tide Gauge, Satellite Altimetry, and Tide Model Driver (TMD) Data. *Engineering, Technology and Applied Science Research*, *14*(3), 14428–14436. https://doi.org/10.48084/etasr.6810

Abdalla, A., & Tenzer, R. (2011). The Evaluation of the New Zealand's Geoid Model Using the KTH Method. *Geodesy and Cartography*, *37*, 5–14. https://doi.org/10.3846/13921541.2011.558326

Abdallah, M., Abd El Ghany, R., Rabah, M., & Zaki, A. (2022a). Assessments of recently released global geopotential models along the Red Sea with shipborne gravity data. *Egyptian Journal of Remote Sensing and Space Science*, *25*(1), 125–133. https://doi.org/10.1016/j.ejrs.2022.01.005

Abdallah, M., Abd El Ghany, R., Rabah, M., & Zaki, A. (2022b). Comparison of Recently Released Satellite Altimetric Gravity Models with Shipborne Gravity Over the Red Sea. *Egyptian Journal of Remote Sensing and Space Science*, *25*(2), 579–592. https://doi.org/10.1016/j.ejrs.2022.03.016

Abdullah, M. A., & Omar, A. H. (2011). Geoid Based Seamless Vertical Height Datum for Marine Cadastre Application. *Geoinformation Science Journal*, 1–16.

Adebisi, N., Balogun, A. L., Min, T. H., & Tella, A. (2021). Advances in estimating Sea Level Rise: A review of tide gauge, satellite altimetry and spatial data science approaches. In *Ocean and Coastal Management* (Vol. 208). Elsevier Ltd. https://doi.org/10.1016/j.ocecoaman.2021.105632

Al-Ajami, H., Zaki, A., Rabah, M., & El-Ashquer, M. (2022). A High-Resolution Gravimetric Geoid Model for Kuwait Using the Least-Squares Collocation. *Frontiers in Earth Science*, *9*. https://doi.org/10.3389/feart.2021.753269

Ali, Z. M., Tan, L. W., Ahmad, N. A., & Musa, S. (2023). Trend Analysis of Tides

Level and Projection Sea Level Rise on the West Coast of Peninsular Malaysia. *International Journal of Integrated Engineering*, *15*(4), 322–328. https://doi.org/10.30880/ijie.2023.15.04.028

Alihan, N. S. A., Din, A. H. M., Hamden, M. H., & Wijaya, D. D. (2024). Classification of Tidal Patterns in Malaysian Maritime Regions: Integrating from Multi-Mission Satellite Altimeter, Tidal Data and Hydrodynamic Model. *IOP Conference Series: Earth and Environmental Science*, *1412*(1). https://doi.org/10.1088/1755-1315/1412/1/012007

Amjadiparvar, B., Rangelova, E., & Sideris, M. G. (2016). The GBVP approach for vertical datum unification: recent results in North America. *Journal of Geodesy*, *90*(1), 45–63. https://doi.org/10.1007/s00190-015-0855-8

Andersen, O. B., & Knudsen, P. (2009). DNSC08 Mean Sea Surface and Mean Dynamic Topography Models. *Journal of Geophysical Research: Oceans*, *114*(11). https://doi.org/10.1029/2008JC005179

Andersen, O. B., & Knudsen, P. (2016). Deriving the DTU15 Global high resolution marine gravity field from satellite altimetry. *ESA Living Planet Symposium 2016*. http://lps16.esa.int/

Andersen, O. B., & Knudsen, P. (2020). The DTU17 Global Marine Gravity Field: First Validation Results. *International Association of Geodesy Symposia, 150*, 83–87. https://doi.org/https://doi.org/10.1007/1345_2019_65

Andersen, O. B., Knudsen, P., & Berry, P. A. M. (2010). The DNSC08GRA Global Marine Gravity Field From Double Retracked Satellite Altimetry. *Journal of Geodesy*, *84*(3), 191–199. https://doi.org/10.1007/s00190-009-0355-9

Andersen, O. B., Knudsen, P., & Trimmer, R. (2005). Improved High Resolution Altimetric Gravity Field Mapping (KMS2002 Global Marine Gravity Field). *International Association of Geodesy Symposia, (V28)*, 326–331. https://doi.org/10.1007/3-540-27432-4_56

Andersen, O. B., Nielsen, K., Hughes, C. W., Bingham, R., Fenoglio-Marc, L., Gravelle, M., Kern, M., & Padilla Polo, S. (2018). Improving the Coastal Mean Dynamic Topography by Geodetic Combination of Tide Gauge and Satellite Altimetry. *Marine Geodesy*. https://doi.org/https://doi.org/10.1080/01490419.2018.1530320

Andersen, O. B., Rose, S. K., Abulaitijiang, A., Zhang, S., & Fleury, S. (2023). The DTU21 Global Mean Sea Surface and First Evaluation. *Earth System Science Data*, *15*(9), 4065–4075. https://doi.org/10.5194/essd-15-4065-2023

Andersen, O., Knudsen, P., & Stenseng, L. (2015). The DTU13 MSS (Mean Sea Surface) and MDT (Mean Dynamic Topography) from 20 Years of Satellite Altimetry. *International Association of Geodesy Symposia (Vol 144)*, 111–121. https://doi.org/https://doi.org/10.1007/1345_2015_182

Annunziato, Alessandro., & Probst, P. (2016). *Continuous Harmonics Analysis of Sea Level Measurements : Description of a New Method to Determine Sea Level Measurement Tidal Component*. European Union. https://doi.org/10.2788/4295

Ardalan, A. A., & Hashemifaraz, A. (2024). Tidal Modeling Based on Satellite Altimetry Observations of TOPEX/Poseidon, Jason1, Jason2, and Jason3 with High Prediction Capability: A Case Study of the Baltic Sea. *Geodesy and Geodynamics*. https://doi.org/10.1016/j.geog.2024.04.010

Ardalan, & Grafarend. (2001). Ellipsoidal Geoidal Undulations (Ellipsoidal Bruns formula): Case Studies. *Journal of Geodesy*, *75*, 544–552. https://doi.org/10.1007/s001900100212

Arif, M. I., Din, A. H. M., Zulkifli, N. A., Hamden, M. H., Omar, A. H., & Adzmi, N. H. M. (2023). Assessment of Sea Level Rise Impact on Peninsular Malaysia Geodetic Vertical Datum. *International Archives of the Photogrammetry, Remote Sensing and Spatial Information Sciences - ISPRS Archives*, *48*(4/W6-2022), 25–32. https://doi.org/10.5194/isprs-archives-XLVIII-4-W6-2022-25-2023

AVISO+. (2024). *CNES-CLS2022 Mean Sea Surface*. AVISO+ Portal. https://doi.org/10.24400/527896/a01-2022.017

Azmin, N. S. H. N., Pa'Suya, M. F., Din, A. H. M., Talib, N., Othman, N. A., & Zamri, A. N. M. (2024). Development of Gravimetric Geoid over Peninsular Malaysia using the Most Recent Global Geopotential Model. *2024 20th IEEE International Colloquium on Signal Processing & Its Applications (CSPA)*, 47–52. https://doi.org/10.1109/CSPA60979.2024.10525401

Bingham, R., & Haines, K. (2006). Mean dynamic topography: Intercomparisons and errors. *Philosophical Transactions. Series A, Mathematical, Physical, and Engineering Sciences*, *364*, 903–916. https://doi.org/10.1098/rsta.2006.1745

Binns, A., Rajabifard, A., Collier, P. A., & Williamson, I. P. (2004). Developing the Concept of a Marine Cadastre: An Australian Case Study. *The Australian Surveyor*, *6*, 1–12.

Boon, J. D., & Kiley, K. P. (1978). *Harmonic Analysis and Tidal Prediction by the Method of Least Squares : A User's Manual*. https://doi.org/10.21220/V5PF2T

Chen, J., Zhang, X., Chen, Q., Shen, Y., & Nie, Y. (2022). Static Gravity Field Recovery and Accuracy Analysis Based on Reprocessed GOCE Level 1b Gravity Gradient Observations. In *EGU General Assembly 2022*. https://doi.org/https://doi.org/10.5194/egusphere-egu22-6771

Chen, X., Kong, X., Zhou, R., & Zhang, S. (2024). Fusion of Altimetry-Derived Model and Ship-Borne Data in Preparation of High-Resolution Marine Gravity Determination. *Geophysical Journal International*, *236*(3), 1262–1274. https://doi.org/10.1093/gji/ggad471

Cipollini, P., Calafat, F. M., Jevrejeva, S., Melet, A., & Prandi, P. (2017). Monitoring Sea Level in the Coastal Zone with Satellite Altimetry and Tide Gauges. *Surveys in Geophysics*, *38*(1), 33–57. https://doi.org/10.1007/s10712-016-9392-0

Cob, S., Kadir, M., Forsberg, R., Simons, W., Naeije, M., Din, A. H., Yacob, H., Amat, A., Mahdzur, D., Ibrahim, Z., Aziz, K., Yaacob, N., Johann, F., Jensen, T., Teitsson, H., Ses, S., Yahaya, A., Nordin, S., & Majid, F. (2022). Epoch-Based Height Reference System for Sea Level Rise Impact Assessment on the Coast of Peninsular Malaysia. *Remote Sensing*, *14*(23). https://doi.org/10.3390/rs14236179

Codiga, D. L. (2011). *Unified Tidal Analysis and Prediction using the UTide MATLAB Functions* (1.0; pp. 4–8). Graduate School of Oceanography University of Rhode Island. https://doi.org/10.13140/RG.2.1.3761.2008

Cui, Y., Jin, S., Chen, N., Chen, S., & Bao, J. (2019). On the establishment method of marine vertical datum seamless system. *IOP Conference Series: Earth and Environmental Science*, *237*(3). https://doi.org/10.1088/1755-1315/237/3/032031

Danila, U. (2012). *Mold2012: A New Gravimetric Quasi-Geoid Model over Moldova (Master's Thesis)*. KTH Royal Institute of Technology, Stockholm, Sweden.

Dubock, P. A., Spoto, F., Simpson, J., Spencer, D., Schutte, E., & Sontag, H. (2001). The Envisat Satellite and Its Integration. *ESA Bulletin*, 26–45.

Earth Resources Observation and Science (EROS). (2019, July 30). *USGS EROS Archive - Digital Elevation - Shuttle Radar Topography Mission (SRTM) 1 Arc-Second Global*. U.S Geological Survey. https://www.unavco.org/education/education-resources/tutorials/the-shape-of-earth-and-reference-ellipsoids/

EarthScope Consortium. (2011, February 11). *The Shape of Earth and Reference Ellipsoids*. https://www.unavco.org/education/education-resources/tutorials/the-shape-of-earth-and-reference-ellipsoids/

Egbert, G. D., & Erofeeva, S. Y. (2002). Efficient Inverse Modeling of Barotropic Ocean Tides. *Journal of Atmospheric and Oceanic Technology*, *19*, 183–204. https://doi.org/https://doi.org/10.1175/1520-0426(2002)019<0183:EIMOBO>2.0.CO;2

Fan, X., Guo, J., Zhang, H., Jia, Y., & Liu, X. (2025). A Two-Step Method of Crossover Adjustment for Satellite Altimeter Data. *Advances in Space Research*, *75*(1), 219–232. https://doi.org/10.1016/j.asr.2024.09.024

Featherstone, W. E., & Kirby, J. F. (2000). The Reduction of Aliasing in Gravity Anomalies and Geoid Heights using Digital Terrain Data. *Geophysics Journal International*, *141*, 204–212. https://doi.org/https://doi.org/10.1046/j.1365-246X.2000.00082.x

Featherstone, W. E., Kirby, J. F., Hirt, C., Filmer, M. S., Claessens, S. J., Brown, N. J., Hu, G., & Johnston, G. M. (2011). The AUSGeoid09 model of the Australian Height Datum. *Journal of Geodesy*, *85*(3), 133–150. https://doi.org/10.1007/s00190-010-0422-2

Feng, X., Widlansky, M. J., Balmaseda, M. A., Zuo, H., Spillman, C. M., Smith, G., Long, X., Thompson, P., Kumar, A., Dusek, G., & Sweet, W. (2024). Improved capabilities of global ocean reanalyses for analysing sea level variability near the Atlantic and Gulf of Mexico Coastal U.S. *Frontiers in Marine Science*, *11*. https://doi.org/10.3389/fmars.2024.1338626

FIG. (2006). *FIG guide on the development of a vertical reference suface for hydrography* (Vol. 37). International Federation of Surveyors.

Filmer, M. S., Johnston, P. J., Jayaswal, Z., Taylor, A., Chittleborough, J., Claessens, S. J., Seifi, F., Kuhn, M., McCubbine, J., & Entel, M. (2024). Connecting land

and sea vertical datums: A data evaluation for developing Australia's AUSHYDROID model. *Marine Geodesy*. https://doi.org/10.1080/01490419.2024.2305898

Fok, H. S. (2012). *Ocean Tides Modeling using Satellite Altimetry* [Doctoral Dissertation, The Ohio State University, Columbus, Ohio]. https://earthsciences.osu.edu/sites/earthsciences.osu.edu/files/report-501.pdf

Forsberg, R. (1987). A New Covariance Model for Inertial Gravimetry and Gradiometry. *Journal of Geophysics Research*, *92*(B2), 1305–1310. https://doi.org/10.1029/JB092iB02p01305

Forsberg, R. (1991). A New High-Resolution Geoid of the Nordic Area. In R. H. Rapp & F. Sansò (Eds.), *Determination of the Geoid* (pp. 241–250). Springer New York.

Forsberg, R. (2005). *Towards a cm-geoid for Malaysia*. www.nga.mil.

Fotopoulos, G., Kotsakis, C., & Sideris, M. G. (1999). A New Canadian Geoid Model in Support of Levelling by GPS. *Geomatica*, *53*(4), 53–62.

Francis, R. ., Drinkwater, M. ., & Davidson, M. . (2010). *ESA's Ice Mission* (2nd ed.). European Space Agency.

G. S. Brown. (1977). SKYLAB S-193 Radar Altimeter Experiment Analysis and Results. In *National Aeronautics and Space Administration*.

Geisser, S., & Eddy, W. F. (1979). A Predictive Approach to Model Selection. *Journal of the American Statistical Association*, *74*(365), 153–160. https://doi.org/10.2307/2286745

Gesch, D., & Wilson, R. (2001). Development of a seamless multisource topographic/bathymetric elevation model of Tampa Bay. *Marine Technology Society Journal*, *35*(4), 58–64. https://doi.org/10.4031/002533201788058062

Golden Software. (2025, June). *Understanding Surfer gridding methods*. Golden Software .

Gommenginger, C., Thibaut, P., Fenoglio-Marc, L., Quartly, G., Deng, X., Gómez-Enri, J., Challenor, P., & Gao, Y. (2011). Retracking Altimeter Waveforms Near The Coasts a Review of Retracking Methods and Some Applications to Coastal Waveforms. In *Coastal Altimetry* (pp. 61–101). Springer Berlin Heidelberg. https://doi.org/10.1007/978-3-642-12796-0_4

Goyal, R., Featherstone, W., Claessens, S., Dikshit, O., & Balasubramanian, N. (2021). The Indian Gravimetric Geoid Model Based on The KTH method of Least Squares Modification of the Stokes Formula with Additive Corrections: IndGG-LSMSA2021. *International Services of Geoid*.

Grgić, M., & Bašić, T. (2021). Radar Satellite Altimetry in Geodesy - Theory, Applications and Recent Developments. In *Geodetic Sciences - Theory, Applications and Recent Developments*. IntechOpen. https://doi.org/10.5772/intechopen.97349

Gunathilaka, M. D. E. K., & Mahmud, M. R. (2016). *Modelling the Tidal Datum Variability at the Strait of Malacca*.

Guo, J., Hwang, C., & Deng, X. (2022). Editorial: Application of Satellite Altimetry in Marine Geodesy and Geophysics. *Frontiers in Earth Science, 10*. https://doi.org/10.3389/feart.2022.910562

Hamden, M. H. (2022). *Development of Quasi-Seamless Hydrographic Separation Models Based on Satellite Altimetry and Coastal Tide Gauges in Malaysia* [Doctoral Dissertation]. Universiti Teknologi Malaysia.

Hamden, M. H., Md Din, A., Wijaya, D. D., & Pa'suya, M. F. (2021). Deriving offshore tidal datums using satellite altimetry around Malaysian seas. *IOP Conference Series: Earth and Environmental Science*, *880*(1). https://doi.org/10.1088/1755-1315/880/1/012011

Hart-Davis, M. G., Laan, S., Schwatke, C., Backeberg, B., Dettmering, D., Zijl, F., Verlaan, M., Passaro, M., & Seitz, F. (2023). Altimetry-Derived Tide Model for Improved Tide and Water Level Forecasting Along the European Continental Shelf. *Ocean Dynamics*, *73*(8), 475–491. https://doi.org/10.1007/s10236-023-01560-0

Heiskanen, W. A., & Moritz, H. (1967). *Physical geodesy*. Library of Congress Catalogue Card Number : 66-24950.

Higginson, S., Thompson, K. R., Woodworth, P. L., & Hughes, C. W. (2015). The tilt of mean sea level along the east coast of North America. *Geophysical Research Letters*, *42*(5), 1471–1479. https://doi.org/10.1002/2015GL063186

Hofmann-Wellenhof, B., & Moritz, H. (2006). Gravity reduction. In B. Hofmann-Wellenhof & H. Moritz (Eds.), *Physical Geodesy* (pp. 129–155). Springer

Vienna. https://doi.org/10.1007/978-3-211-33545-1_4

Huang, J. (2017). Determining Coastal Mean Dynamic Topography by Geodetic Methods. In *Geophysical Research Letters* (Vol. 44, Number 21, pp. 11,125-11,128). Blackwell Publishing Ltd. https://doi.org/10.1002/2017GL076020

Huismain, O., & de By, R. A. (2009). *Principles of Geographic Information Systems : An Introductory Textbook* (R. A. de By, Ed.; 4th ed.). The International Institute for Geo-Information Science and Earth Observation (ITC).

Hwang, C., Hsu, H. Y., & Jang, R. J. (2002). Global mean sea surface and marine gravity anomaly from multi-satellite altimetry: Applications of deflection-geoid and inverse Vening Meinesz formulae. *Journal of Geodesy*, *76*(8), 407–418. https://doi.org/10.1007/s00190-002-0265-6

Iliffe, J. C., Turner, J., & Oliveira, J. F. (2007). VORF-The UK Vertical Offshore Reference Frame: Enabling Real-Time Hydrographic Surveying. *20th International Technical Meeting of the Satellite Division of The Institute of Navigation (ION GNSS 2007)*, 1943–1949. https://www.researchgate.net/publication/260767251

Iliffe, J. C., Ziebart, M. K., Turner, J. F., Talbot, A. J., & Lessnoff, A. P. (2013). Accuracy of Vertical Datum Surfaces in Coastal and Offshore Zones. *Survey Review*, *45*(331), 254–262. https://doi.org/10.1179/1752270613Y.0000000040

International Federation of Surveyors. (2006). *FIG guide on the development of a vertical reference suface for hydrography* (Vol. 37). International Federation of Surveyors.

International Hydrographic Organization (IHO). (2006). *Harmonic Constants Product Specification : Harmonic Constituents with Nodal Corrections* (1st ed.). https://legacy.iho.int/mtg_docs/com_wg/IHOTC/IHOTC8/Product_Spec_for_Exchange_of_HCs.pdf

International Hydrographic Organization (IHO). (2020). *IHO Standards for Hydrographic Surveys*. www.iho.int

International Hydrographic Organization (IHO). (2022). *International Hydrographic Organization Standards for Hydrographic Surveys: S-44* (6.1.0). International hydrographic Organization. www.iho.int

Jabatan Ukur dan Pemetaan Malaysia. (2005). *Garis panduan penggunaan model*

geoid Malaysia (MyGEOID). Pekeliling Ketua Pengarah Ukur dan Pemetaan.

Jabatan Ukur dan Pemetaan Malaysia. (2021). *Garis panduan teknikal pengukuran graviti*. Pekeliling Ketua Pengarah Ukur dan Pemetaan.

Jabatan Ukur dan Pemetaan Malaysia. (2024, February 16). *Geoidal height computation*. Pekeliling Ketua Pengarah Ukur Dan Pemetaan.

Jamil, H. (2011). *GNSS heighting and its potential use in Malaysia*.

Jamil, H., Kadir, M., Forsberg, R., Olesen, A., Isa, M. N., Rasidi, S., Mohamed, A., Chihat, Z., Nielsen, E., Majid, F., Talib, K., & Aman, S. (2017). Airborne geoid mapping of land and sea areas of East Malaysia. *Journal of Geodetic Science*, *7*(1), 84–93. https://doi.org/10.1515/jogs-2017-0010

Janpaule, I. (2014). Application of KTH Method for Determination of Latvian Geoid Model. *International Conference - Innovative Materials, Structure and Technologies*, 64. https://doi.org/10.7250/iscconstrs.2014.11

Jones, C. (2007). *Vertical Offshore Reference Frame (VORF)*. https://docs.iho.int/mtg_docs/com_wg/IHOTC/IHOTC8/UK_VORF.pdf

Kaula, W. M. (1966). Global Harmonic and Statistical Analysis of Gravimetry. In *Gravity Anomalies: Unsurveyed Areas* (pp. 58–67). American Geophysical Union (AGU). https://doi.org/https://doi.org/10.1029/GM009p0058

Keysers, J. H., Quadros, N. D., & Collier, P. A. (2013). Vertical Datum Transformations Across the Littoral Zone : Developing a Method to Establish a Common Vertical Datum Before Integrating Land Height Data with Near-Shore Seafloor Depth Data. In *Journal Of Coastal Research*. https://www.crcsi.com.au/assets/Uploads/Files/ Vertical-Datum-Transformations-Across-the-Littoral-Zone-v1-3.pdf.

Keysers, J. H., Quadros, N. D., & Collier, P. A. (2015). Vertical datum transformations across the Australian littoral zone. *Journal of Coastal Research*, *31*(1), 119–128. https://doi.org/10.2112/JCOASTRES-D-12-00228.1

Kiamehr, R. (2007). Qualification and Refinement of the Gravity Database Based on Cross-Validation Approach — A Case Study of Iran. *Acta Geodaetica Et Geophysica Hungarica*, *42*, 285–295. https://doi.org/10.1556/AGeod.42.2007.3.3

Kiamehr, R., & Sjöberg. (2005). Effect of The SRTM Global DEM in the Determination of a High-Resolution Geoid Model of Iran. *Journal of Geodesy*,

79, 540–551. https://doi.org/10.1007/s00190-005-0006-8

Knudsen, P., Andersen, O. B., Maximenko, N., & Hafner, J. (2024). The DTU 2022 Mean Dynamic Topography models. In *Technical University of Denmark*. https://doi.org/https://doi.org/10.11583/DTU.26947894.v1

Knudsen, P., Andersen, O., Maximenko, N., Hafner, J., & Hawaii, U. (2022). The New Combined Mean Dynamic Topography Model - DTUUH22MDT. *Living Planet Symposium*. https://doi.org/10.24400/527896/a03-2022.3613

Kotsakis, C., & Sideris, M. (1999). On the Adjustment of Combined GPS/Levelling/Geoid Networks. *Journal of Geodesy*, *73*, 412–421. https://doi.org/10.1007/s001900050261

Lee, J., & Kwon, J. H. (2022). Review the Status of Korean Geoid Model Development Since 2000s and Future Improvement Plan. *Terrestrial, Atmospheric and Oceanic Sciences*, *33*(12). https://doi.org/10.1007/S44195-022-00013-3

Li, Z., Guo, J., Zhu, C., Liu, X., Hwang, C., Lebedev, S., Chang, X., Soloviev, A., & Sun, H. (2024). The SDUST2022GRA global marine gravity anomalies recovered from radar and laser altimeter data: Contribution of ICESat-2 laser altimetry. *Earth System Science Data*, *16*(9), 4119–4135. https://doi.org/10.5194/essd-16-4119-2024

Liang, W., Li, J., Xu, X., Zhang, S., & Zhao, Y. (2020). A High-Resolution Earth's Gravity Field Model SGG-UGM-2 from GOCE, GRACE, Satellite Altimetry, and EGM2008. *Engineering*, *6*(8), 860–878. https://doi.org/https://doi.org/10.1016/j.eng.2020.05.008

Liu, Q., Schmidt, M., Sánchez, L., Moisés, L., & Cortez, D. (2024). High-resolution regional gravity field modeling in data-challenging regions for the realization of geopotential-based height systems. *Earth, Planets and Space*, *76*(1). https://doi.org/10.1186/s40623-024-01981-1

Liu, Y., Guo, J., Guan, B., Bian, S., Sun, H., & Liu, X. (2026). Refining Gravity Anomaly Data of Coastal Areas by Combining XGM2019e-2159 and SRTM/GEBCO_2024 Residual Terrain Model with Forward Modeling Method. *Geoscientific Model Development*, *19*(8), 3361–3374. https://doi.org/10.5194/gmd-19-3361-2026

Liu, Y., & Lou, L. (2022). Unified Land–Ocean Quasi-Geoid Computation from Heterogeneous Data Sets Based on Radial Basis Functions. *Remote Sensing*, *14*(13). https://doi.org/10.3390/rs14133015

Lorell, J., Colquitt, E., & Anderle, R. ~J. (1982). Ionospheric Correction for SEASAT Altimeter Height Measurement. *Journal of Geophysical Research*, *87*(C5), 3207–3212. https://doi.org/https://doi.org/10.1029/JC087iC05p03207

Maximenko, N. (2006). Mean Surface Circulation of the Global Ocean Inferred from Satellite Altimeter and Drifter Data. *European Space Agency, (Special Publication) ESA SP*. https://www.researchgate.net/publication/253210861

Maximenko, N., Niiler, P., Rio, M. H., Melnichenko, O., Centurioni, L., Chambers, D., Zlotnicki, V., & Galperin, B. (2009). Mean dynamic topography of the ocean derived from satellite and drifting buoy data using three different techniques. *Journal of Atmospheric and Oceanic Technology*, *26*(9), 1910–1919. https://doi.org/10.1175/2009JTECHO672.1

McCubbine, J. C., Amos, M. J., Tontini, F. C., Smith, E., Winefied, R., Stagpoole, V., & Featherstone, W. E. (2018). The New Zealand gravimetric quasigeoid model 2017 that incorporates nationwide airborne gravimetry. *Journal of Geodesy*, *92*(8), 923–937. https://doi.org/10.1007/s00190-017-1103-1

Mills, Jerry., & Dodd, David. (2014). *Ellipsoidally Referenced Surveying for Hydrography* (FIG, Ed.; Vol. 62). The International Federation of Surveyors (FIG).

Ming, T. K., Amin, Z. M., & Din, A. H. M. (2021). Least Square Modification of Stokes Formulae with Additive Corrections Estimator for Klang Valley Geoid Modeling. *IOP Conference Series: Earth and Environmental Science*, *620*(1). https://doi.org/10.1088/1755-1315/620/1/012016

Miyahara, B., Kodama, T., & Kuroishi, Y. (2014). Development of new hybrid geoid model for Japan, "GSIGEO2011." *Bulletin of the Geospatial Information Authority of Japan*, *62*, 11–20.

Montgomery, D. C., & Runger, G. C. (2018). *Applied Statistics and Probability for Engineers, 7th Edition* (7th ed.). John Wiley & Sons.

Moritz, H. (1980). Geodetic reference system 1980. *Bulletin Géodésique*, *54*(3), 395–405. https://doi.org/10.1007/BF02521480

Moritz, H. (2000). Geodetic Reference System 1980. *Journal of Geodesy, 74*(1), 128–133. https://doi.org/10.1007/s001900050278

Mphuthi, M. S. (2025). Evaluation of recent Global Geopotential Models over South Africa. *South African Journal of Geomatics, 14*(1), 57–68. https://doi.org/10.4314/sajg.v14i1.5

Munk, W. H., & MacDonald, G. J. F. (1961). The Rotation of the Earth: A Geophysical Discussion. *American Journal Research, 29*(8), 559–560.

Mustaffa, M., Amirah, E. N., Ahmad, S., Aini, N. A., & Ghazali, R. (2024). Tidal of Malacca Straits From AIS Data. *Journal of Maritime Research, 21*(1), 120–125. www.jmr.unican.es

NAHRIM. (2017). *Impact of Climate Change : Sea Level Rise Projections for Malaysia*. National Water Research Institute of Malaysia (NAHRIM).

National Oceanic and Atmospheric Administration. (2000a). *Tidal datum and their applications*.

National Oceanic and Atmospheric Administration. (2000b). *Tide and Current Glossary*. Retrieved from https://tidesandcurrents.noaa.gov/publications/glossary2.pdf

National Oceanic and Atmospheric Administration. (2004). *North Carolina Sea Level Rise Project : Interim Technical Report*. Retrieved from https://vdatum.noaa.gov/download/publications/TM_NOS-CS05_FY04_Hess_NCSeaLevelRise.pdf

National Oceanic and Atmospheric Administration. (2013a). *Estimation of Vertical Uncertainties in VDatum*. Retrieved from, https://vdatum.noaa.gov/download/publications/Estimation_of_Vertical_Uncertainties_in_VDatum_Dec2013.pdf (Accessed on 8 May 2025)

National Oceanic and Atmospheric Administration. (2013b). *VDatum for the Coastal Waters of Texas and Western Louisiana: Tidal Datums and Topography of the Sea Surface*. Retrieved from https://vdatum.noaa.gov/download/publications/TM_NOS-CS29_FY13_Xu_TexasWesternLouisiana.pdf

National Oceanic and Atmospheric Administration (NOAA). (2021). *What is a datum?* National Ocean Services. Retrieved from

https://oceanservice.noaa.gov/facts/datum.html (Accessed on 14 February 2024)

Natsiopoulos, D. A., Vergos, G. S., Qirko, K., Balliu, O., Qershija, E., Kasnec, L., & Ndoj, P. (2026). *A New Gravimetric and Hybrid Geoid Model in Albania*. https://doi.org/10.1007/1345_2026_337

Natural Resources Canada. (2025). *Canadian Spatial Reference System (CSRS)*. Government of Canada. Retrieved from https://natural-resources.canada.ca/science-data/science-research/geomatics/geodetic-reference-systems/canadian-spatial -reference-system-csrs (Assessed on 14 February 2026)

Nudds, S., Robin, C., & Macaulay, P. (2016). Continuous Vertical Datum Separations for Canadian Waters : Creating Canada's First Hydrographic Vertical Separation Surfaces. *Sea Technology*, 38–42.

Nwankwo, U. C., Howden, S., Wells, D., & Connon, B. (2021). Validation of VDatum in Southeastern Louisiana and Western Coastal Mississippi. *Marine Geodesy*, *44*(1), 1–25. https://doi.org/10.1080/01490419.2020.1846644

Oktavia, S. N., & Heliani, L. S. (2026). Modelling the Local Geoid of East Kalimantan from Combination of Airborne and Terrestrial Gravity Data Using KTH Method. *Geodesy and Cartography (Vilnius)*, *52*(1), 33–41. https://doi.org/10.3846/gac.2026.21948

Osman, A. S. M., & Anjasmara, I. M. (2023). Determination of a new gravimetric geoid modelling for Sudan using the least-squares collocation technique. *IOP Conference Series: Earth and Environmental Science*, *1127*(1). https://doi.org/10.1088/1755-1315/1127/1/012014

Othman, N. A., Pa'suya, M. F., Din, A. H. M., Aziz, M. A. C., Azmin, N. S. H. N., & Zamri, A. N. M. (2024). Gravimetric Geoid Modeling for East Malaysia using the LSMSA Method. *2024 20th IEEE International Colloquium on Signal Processing and Its Applications, CSPA 2024 - Conference Proceedings*, 213–218. https://doi.org/10.1109/CSPA60979.2024.10525484

Padman, L., Howard, L., & Erofeeva. (2015). *Tide Model Driver (TMD) Manual : Version 2.5* (2.5). Oregon State University (OSU). Retrieved from https://arcticdata.io/data/10.18739/A24Q7QR39/TMD_toolbox_v2_5/TMD/UserManual_TMD2.5.pdf (Accessed on 10 September 2024)

Palmer, K., Watson, C. S., Hunter, J. R., Hague, B. S., & Power, H. E. (2023). An

improved method for computing tidal datums. *Coastal Engineering*, *184*. https://doi.org/10.1016/j.coastaleng.2023.104354

Pa'suya, M. F. (2020). *New modern height reference system for Peninsular Malaysia using Least Square Modification of Stroke's Formula* [Doctoral Dissertation]. Universiti Teknologi Malaysia.

Pa'suya, M. F., Md Din, A. H., Abbak, R. A., Hamden, M. H., Yazid, N. M., Aziz, M. A. C., & Samad, M. A. A. (2022). Hybrid geoid model over peninsular Malaysia (PMHG2020) using two approaches. *Studia Geophysica et Geodaetica*, *66*(3–4), 98–123. https://doi.org/10.1007/s11200-021-0769-2

Pa'suya, M. F., Md Din, A. H., Alpay Abbak, R., Talib, N., Che Aziz, M. A., Ramli, M. Z., Hamden, M. H., & Mohammad Yazid, N. (2019). *Integration of local mean sea level and land vertical datum over Peninsular Malaysia via transformation model*.

Pa'suya, M. F., Md Din, A. H., McCubbine, J. C., Omar, A. H., Amin, Z. M., & Yahaya, N. A. Z. (2019). Gravimetric geoid modelling over Peninsular Malaysia using two different gridding approaches for combining free air anomaly. *International Archives of the Photogrammetry, Remote Sensing and Spatial Information Sciences - ISPRS Archives*, *42*(4/W16), 515–522. https://doi.org/10.5194/isprs-archives-XLII-4-W16-515-2019

Pa'suya, M. F., Md Din, A. H., Mohammad Yazid, N., & Hisham Omar, A. (2023). Improving the accuracy of marine gravity anomaly data from the combination of shipborne gravity and global marine gravity derived from satellite altimetry. *Journal of Sustainability Science and Management*, *18*(12), 111–122. https://doi.org/10.46754/jssm.2023.12.010

Pa'Suya, M. F., Yusof, N. N. M., Din, A. H. M., Othman, A. H., Som, Z. A. A., Amin, Z. M., Aziz, M. A. C., & Samad, M. A. A. (2018). Gravimetric geoid modeling in the northern region of Peninsular Malaysia (NGM17) using KTH method. *IOP Conference Series: Earth and Environmental Science*, *169*(1). https://doi.org/10.1088/1755-1315/169/1/012089

Pavlis, N. K., Holmes, S. A., Kenyon, S. C., & Factor, J. K. (2012). The Development and Evaluation of the Earth Gravitational Model 2008 (EGM2008). *Journal of Geophysical Research: Solid Earth*, *117*(4).

https://doi.org/10.1029/2011JB008916

Petit, G., & Luzum, B. (2010). IERS conventions (2010). *Tech. Rep. DTIC Document*, *36*, 180.

Ponte, R. (2006). Low-Frequency Sea Level Variability and the Inverted Barometer Effect. *Journal of Atmospheric and Oceanic Technology*, *23*(4), 619–629. https://doi.org/10.1175/JTECH1864.1

Prijatna, K., Lestari, R., Bramanto, B., Pahlevi, A. M., & Wijaya, D. D. (2024). Assessing the Impact of Methodological Differences on Geoid Model Performance. *Geographia Technica*, *19*(2), 124–138. https://doi.org/10.21163/GT_2024.192.10

Pugh, D., Woodworth, P., & Vogel, M. (2015). Sea-level Science: Understanding Tides, Surges, Tsunamis and Mean Sea-level Changes. In *Contemporary Physics* (Number 3). Cambridge University Press. https://doi.org/10.1080/00107514.2015.1005682

Pujol, M., Schaeffer, P., Faugère, Y., Raynal, M., Dibarboure, G., & Picot, N. (2018). Gauging the Improvement of Recent Mean Sea Surface Models: A New Approach for Identifying and Quantifying Their Errors. *Journal of Geophysical Research: Oceans*, *123*(8), 5889–5911. https://doi.org/10.1029/2017JC013503

Rashidi, A. H. M., Jamal, M. H., Hassan, M. Z., Sendek, S. S. M., Sopie, S. L. M., & Hamid, M. R. A. (2021). Coastal structures as beach erosion control and sea level rise adaptation in malaysia: A review. *Water (Switzerland)*, *13*(13). https://doi.org/10.3390/w13131741

Rio, M. H., & Hernandez, F. (2004). A mean dynamic topography computed over the world ocean from altimetry, in situ measurements, and a geoid model. *Journal of Geophysical Research: Oceans*, *109*(12), 1–19. https://doi.org/10.1029/2003JC002226

Robin, C., Nudds, S., Macaulay, P., Boom, B. D. L., Bartlett, J., Maltais, L., Herron, T., Fadaie, K., Craymer, M., Veronneau, M., & Hains, D. (2014). The Continuous Vertical Datum for Canadian Waters Project: Overview and Status Report. *Canadian Hydrographic Conference*. https://www.researchgate.net/publication/278036789

Robin, C., Nudds, S., MacAulay, P., Godin, A., De Lange Boom, B., & Bartlett, J.

(2016). Hydrographic Vertical Separation Surfaces (HyVSEPs) for the Tidal Waters of Canada. *Marine Geodesy*, *39*(2), 195–222. https://doi.org/10.1080/01490419.2016.1160011

Roman, D. R. (2007). *Datum, Height and Geodesy [Presentation Slides]*. Retrieved from https://www.ngs.noaa.gov/GEOID/PRESENTATIONS /2007_02_24_CCPS/Roman_A_PLSC2007notes.pdf

Saastamoinen, J. (1972). Atmospheric Correction for the Troposphere and Stratosphere in Radio Ranging Satellites. In *The Use of Artificial Satellites for Geodesy* (pp. 247–251). American Geophysical Union (AGU). https://doi.org/https://doi.org/10.1029/GM015p0247

Sánchez, L., & Sideris, M. G. (2017). Vertical datum unification for the International Height Reference System (IHRS). *Geophysical Journal International*, *209*(2), 570–586. https://doi.org/10.1093/gji/ggx025

Sandwell, D., Müller, D., Smith, W., Garcia, E., & Francis, R. (2014). New global marine gravity from CryoSat-2 and Jason-1 reveals buried tectonic structure. *Science*, *346*, 65–67. https://doi.org/10.1126/science.1258213

Sandwell, D., & Smith, W. H. F. (1997). Marine Gravity Anomaly from Geosat and ERS-1 Satellite Altimetry. *Journal of Geophysical Reseacrh B : Solid Earth*, *102*(B5), 10039–10054. https://doi.org/https://doi.org/10.1029/96JB03223

Sandwell, D. T., & Smith, W. H. F. (2009). Global marine gravity from retracked Geosat and ERS-1 altimetry: Ridge segmentation versus spreading rate. *Journal of Geophysical Research: Solid Earth*, *114*(1). https://doi.org/10.1029/2008JB006008

Sansò, F., & Sideris, M. G. (Eds.). (2013). *Geoid Determination: Theory and Methods*. Springer Berlin Heidelberg. https://doi.org/10.1007/978-3-540-74700-0

Sarsito, D. A., Syahrullah, M., Wijaya, D. D., Pradipta, D., & Andreas, H. (2021). Studying Dynamic Ocean Topography in Indonesia Sea Based on Satellite Altimetry. *IOP Conference Series: Earth and Environmental Science*, *925*(1). https://doi.org/10.1088/1755-1315/925/1/012062

Schaeffer, P., Faugére, Y., Legeais, J. F., Ollivier, A., Guinle, T., & Picot, N. (2012). The CNES_CLS11 Global Mean Sea Surface Computed from 16 Years of Satellite Altimeter Data. *Marine Geodesy*, *35*(sup1), 3–19.

https://doi.org/10.1080/01490419.2012.718231

Schaeffer, P., Pujol, M.-I., Veillard, P., Faugere, Y., Dagneaux, Q., Dibarboure, G., & Picot, N. (2023). The CNES CLS 2022 Mean Sea Surface: Short Wavelength Improvements from CryoSat-2 and SARAL/AltiKa High-Sampled Altimeter Data. *Remote Sensing*, *15*(11), 2910. https://doi.org/10.3390/rs15112910

Schureman, P. (1994). *Manual of Harmonic Analysis and Prediction of Tides* (Vol. 98). U.S Department of Commerce (Special Publication No.98). Retrieved from https://scispace.com/pdf/manual-of-harmonic-analysis-and-prediction-of-tides-by-paul-4uzh0tk6ws.pdf

Shoganbekova, D., Urazaliyev, A., Nurakynov, S., Kozhakhmetov, M., Zhaksygul, N., & Sermiagin, R. (2025). Combination of Soviet-Era Surface Gravity and Modern Satellite Data for Geoid Model Computation: A Case Study for Kazakhstan. *Computation*, *13*(11). https://doi.org/10.3390/computation13110260

Shum, C. K., Tapley, B. D., & Ries, J. C. (1993). Satellite altimetry: Its applications and accuracy assessment. *Advances in Space Research*, *13*(11), 315–324. https://doi.org/https://doi.org/10.1016/0273-1177(93)90234-3

Sjöberg. (1991). Refined Least Squares Modification of Stokes' Formula. *Manuscr Geod*, *16*, 367–375. https://doi.org/10.1007/s00190-020-01405-4

Sjöberg. (2003a). A computational scheme to model the geoid by the modified Stokes formula without gravity reductions. *Journal of Geodesy*, *77*, 423–432. https://doi.org/10.1007/s00190-003-0338-1

Sjöberg. (2003b). A general model for modifying Stokes' formula and its least-squares solution. *Journal of Geodesy*, *77*, 459–464. https://doi.org/10.1007/s00190-003-0346-1

Sjöberg. (2003c). Ellipsoidal corrections to order e 2 of geopotential coefficients and Stokes' formula. *Journal of Geodesy*, *77*, 139–147. https://doi.org/10.1007/s00190-003-0321-x

Sjöberg. (2005). A Local Least-Squares Modification of Stokes' Formula. *Studia Geophysica et Geodaetica*, *49*, 23–30. https://doi.org/10.1007/s11200-005-1623-7

Sjöberg. (2020). Unbiased Least-Squares Modification of Stokes' Formula. *Journal of Geodesy*, *94*(9). https://doi.org/10.1007/s00190-020-01405-4

Sjöberg, Gidudu, & Ssengendo. (2015a). The Uganda gravimetric geoid model 2014 computed by the KTH method. *Journal of Geodetic Science*, *5*(1), 35–46. https://doi.org/10.1515/jogs-2015-0007

Sjöberg, L. E., Gidudu, A., & Ssengendo, R. (2015b). The Uganda gravimetric geoid model 2014 computed by the KTH method. *Journal of Geodetic Science*, *5*(1), 35–46. https://doi.org/10.1515/jogs-2015-0007

Ssengendo, R. (2015). *A height datum for Uganda based on a gravimetric quasigeoid model and GNSS/levelling* [Doctoral Dissertation]. KTH Royal Institute of Technology.

Stanley, H. R. (1979). The Geos 3 Project. *Journal of Geophysical Research: Solid Earth*, *84*(B8), 3779–3783. https://doi.org/https://doi.org/10.1029/JB084iB08p03779

Steudler, D. (2014). Cadastre 2014 and beyond. *FIG Publication No.61*.

Sukma, N. O., & Leni, S. H. (2024). *Evaluasi Meteode KTH dan RCR dalam Pemodelan Geoid Lokal berdasarkan Data Gayaberat Airborne dan Teretris (Studi kasus: kalimantan Timur)* [Master's Thesis]. Universitas Gadjah Mada.

Sulaiman, S. A. (2016). *Gravimetric Geoid Model Determination for Peninsular Malaysia using Least Squares Modification of Strokes* [Doctoral Dissertation]. Universiti Teknologi MARA.

Sulaiman, S. A., Talib, K., Md Wazir, M. akhir, Mohd Yusof, O., & Zalil, S. A. (2012). Height Discrepancies Based on Various Vertical Datum. *2012 IEEE Control and System Graduate Research Colloquium (ICSGRC 2012)*, 253–256. https://doi.org/https://doi.org/10.1109/ICSGRC.2012.6287171

Talib, K., & Sulaiman, S. (2016). Geological Mapping of Sabah, Malaysia, Using Airborne Gravity Survey. Borneo Science. In *The Journal of Science and Technology* (Vol. 37, Number 2).

Tapley, B. D., & Rosborough, G. W. (1985). Geographically correlated orbit error and its effect on satellite altimetry missions. *Journal of Geophysical Research: Oceans*, *90*(C6), 11817–11831. https://doi.org/https://doi.org/10.1029/JC090iC06p11817

Till, G., & Tsjeng, H. (2017). Naval Development in Malaysia. In *Naval Modernisation in Southeast Asia: Problems and Prospects for Small and Medium*

Navies (pp. 77–92). https://doi.org/10.1007/978-3-319-58406-5_6

Tscherning, C. C., Forsberg, R., & Knudsen, P. (1992). The GRAVSOFT package for geoid determination. *Continued Workshop on the European Geoid.*

Turner, J. F., Iliffe, J. C., Ziebart, M. K., Wilson, C., & Horsburgh, K. J. (2010). Interpolation of tidal levels in the coastal zone for the creation of a hydrographic datum. *Journal of Atmospheric and Oceanic Technology*, *27*(3), 605–613. https://doi.org/10.1175/2009JTECHO645.1

Varga, M., Zurich, E., Oršulić, O. B., & Bašić, T. (2018). *Investigation and comparison of RCR and LSMSA regional geoid modelling approaches*. https://doi.org/10.13140/RG.2.2.35079.04008

Vergos, G. S., Grigoriadis, V. N., Tziavos, I. N., & Kotsakis, C. (2014). Evaluation of GOCE/GRACE Global Geopotential Models over Greece with Collocated GPS/Levelling Observations and Local Gravity Data. In *International Association of Geodesy Symposia* (Vol. 141, pp. 85–92). Springer Verlag. https://doi.org/https://doi.org/10.1007/978-3-319-10837-7_11

Véronneau, M., Duval, R., & Huang, J. (2006). A Gravimetric Geoid Model as a Vertical Datum in Canada. *Geomatica*, *60*(2), 165–172.

Verron, J., Sengenes, P., Lambin, J., Noubel, J., Steunou, N., Guillot, A., Picot, N., Coutin-Faye, S., Sharma, R., Gairola, R. M., Murthy, D. V. A. R., Richman, J. G., Griffin, D., Pascual, A., Rémy, F., & Gupta, P. K. (2015). The SARAL/AltiKa Altimetry Satellite Mission. *Marine Geodesy*, *38*, 2–21. https://doi.org/10.1080/01490419.2014.1000471

Vestøl, O., Breili, K., & Taskjelle, T. (2025). Common adjustment of geoid and mean sea level with least squares collocation. *Journal of Geodesy*, *99*(5). https://doi.org/10.1007/s00190-025-01961-7

Vignudelli, S., Birol, F., Benveniste, J., Fu, L. L., Picot, N., Raynal, M., & Roinard, H. (2019). Satellite Altimetry Measurements of Sea Level in the Coastal Zone. In *Surveys in Geophysics* (Vol. 40, Number 6, pp. 1319–1349). Springer Netherlands. https://doi.org/10.1007/s10712-019-09569-1

Wisha, U. J., Wijaya, Y. J., & Hisaki, Y. (2023). Sea Level Variability in the Equatorial Malacca Strait: The Influence of Climatic –Oceanographic Factors and Its Implications for Tidal Properties in the Estuarine Zone. *Climate*, *11*(3).

https://doi.org/10.3390/cli11030070

Wu, Q., Wang, H., Wang, B., Chen, S., & Li, H. (2020). Performance comparison of geoid refinement between XGM2016 and EGM2008 based on the KTH and RCR Methods: Jilin Province, China. *Remote Sensing*, *12*(2). https://doi.org/10.3390/rs12020324

Wu, Y., Wang, J., Abulaitijiang, A., He, X., Luo, Z., Shi, H., Wang, H., & Ding, Y. (2022). Local Enhancement of Marine Gravity Field over the Spratly Islands by Combining Satellite SAR Altimeter-Derived Gravity Data. *Remote Sensing*, *14*(3), 474. https://doi.org/10.3390/rs14030474

Xu, X., Li, J., Zhao, Y., & Wei, H. (2023). A GOCE only gravity model GOSG02S based on the SGG and SST observations. *Chinese Journal of Geophysics*, *66*(6).

Yang, H. J. (2013). *Geoid determination based on a combination of terrestrial and airborne gravity data in South Korea* [Doctoral Dissertation]. Ohio State University.

Yildiz, H., Forsberg, R., Ågren, J., Tscherning, C., & Sjöberg, L. (2012). Comparison of Remove-Compute-Restore and Least Squares Modification of Stokes' Formula Techniques to Quasi-Geoid Determination Over the Auvergne Test Area. *Journal of Geodetic Science*, *2*(1), 53–64. https://doi.org/10.2478/v10156-011-0024-9

Yuan, J., Guo, J., Zhu, C., Li, Z., Liu, X., & Gao, J. (2023). SDUST2020 MSS: a global 1' 1' mean sea surface model determined from multi-satellite altimetry data. *Earth System Science Data*, *15*(1), 155–169. https://doi.org/10.5194/essd-15-155-2023

Yusof Hussaini, atulukwu, & Alias, A. R. (2023). Marine cadastre data models with temporal aspect - Review. *International Archives of the Photogrammetry, Remote Sensing and Spatial Information Sciences - ISPRS Archives*, *48*(4/W6-2022), 159–166. https://doi.org/10.5194/isprs-archives-XLVIII-4-W6-2022-159-2023

Zamri, A. N. M., Pa'suya, M. F., Din, A. H. M., Abbak, R. A., Ali, T. A. T., Talib, N., Azmin, N. S. H. N., & Othman, N. A. (2025). Airborne Gravity Data Reconstruction Strategies for Geoid Optimization in Peninsular Malaysia. *International Journal of Geoinformatics*, *21*(6), 90–104.

https://doi.org/10.52939/ijg.v21i6.4239

Zamri, A. N. M., Pa'suya, M. F., Din, A. H. M., Samad, A. M., Azmin, N. S. H. N., & Othman, N. A. (2024). Optimizing the Integration of Gravity Data Inputs for Geoid Modelling over Peninsular Malaysia. *2024 20th IEEE International Colloquium on Signal Processing and Its Applications, CSPA 2024 - Conference Proceedings*, 41–46. https://doi.org/10.1109/CSPA60979.2024.10525293

Zamzuri, N. A. A., & Hassan, M. I. (2021). 3D marine cadastre within land administration. *IOP Conference Series: Earth and Environmental Science*, *767*(1). https://doi.org/10.1088/1755-1315/767/1/012039

Zamzuri, N. A. A., Hassan, M. I., & Abdul Rahman, A. (2021). *Developing 3D marine cadastre data model within Malaysian LADM country profile-preliminary result*. https://www.researchgate.net/publication/353152159

Zhang, S., Chen, X., Zhou, R., & Jia, Y. (2025). NSOAS24: a new global marine gravity model derived from multi-satellite sea surface slopes. *Geoscientific Model Development*, *18*(4), 1221–1239. https://doi.org/10.5194/gmd-18-1221-2025

Zhao, Y., Li, J., Xu, X., & Su, Y. (2023). WHU-SWPU-GOGR2022S: A combined gravity model of GOCE and GRACE. *Chinese Journal of Geophysics*, *66*(6). https://doi.org/https://doi.org/10.5880/icgem.2023.003

Zhong, L., Li, H., Wang, B., Liu, S., & Wu, Q. (2024). A General Model of RCR Modification and its Geoid Determination. *Survey Review*, *56*(395), 200–210. https://doi.org/10.1080/00396265.2023.2218682

Zingerle, P., Pail, R., Gruber, T., & Oikonomidou, X. (2020). The combined global gravity field model XGM2019e. *Journal of Geodesy*, *94*(7). https://doi.org/10.1007/s00190-020-01398-0

APPENDICES

APPENDIX 1

Evaluation of CNES-CLS22 Global Mean Sea Surface (MSS), Lowest Astronomical Tide (LAT) and Highest Astronomical Tide (HAT) Models against Local Tide Gauges Dataset Processed using UTide

Evaluation of CNES-CLS22 : MSS

Station	Lat	Long	UTIDE	CNES-CLS22	Δ	Δ ABS	ABS²
Klang	3.050	101.358	-3.213	-3.146	-0.067	0.067	0.004
Keling	2.215	102.153	0.794	0.765	0.029	0.029	0.001
Langkawi	6.432	99.765	-15.952	-15.866	-0.086	0.086	0.007
Lumut	4.240	100.613	-8.348	-8.374	0.026	0.026	0.001
Penang	5.422	100.347	-11.460	-11.466	0.006	0.006	0.000
Cendering	5.265	103.187	-0.479	-0.477	-0.002	0.002	0.000
Kuantan	3.975	103.430	3.132	3.220	-0.088	0.088	0.008
Tioman	2.807	104.140	8.116	8.046	0.070	0.070	0.005
Sedili	1.932	104.115	9.378	9.323	0.055	0.055	0.003
Kukup	1.325	103.443	7.371	7.517	-0.146	0.146	0.021
Geting	6.227	102.107	-6.851	-6.912	0.061	0.061	0.004
						SUM	0.054
						RMSE	0.070

Evaluation of CNES-CLS22 : LAT

Station	Lat	Long	UTIDE	CNES-CLS22	Δ	Δ ABS	ABS²
Klang	3.050	101.358	-6.357	-5.423	-0.934	0.934	0.872
Keling	2.215	102.153	-0.366	-0.351	-0.015	0.015	0.000
Langkawi	6.432	99.765	-17.759	-17.394	-0.365	0.365	0.133
Lumut	4.240	100.613	-10.179	-9.904	-0.275	0.275	0.076
Penang	5.422	100.347	-13.141	-12.661	-0.479	0.479	0.230
Cendering	5.265	103.187	-1.930	-1.721	-0.209	0.209	0.044
Kuantan	3.975	103.430	1.212	1.594	-0.382	0.382	0.146
Tioman	2.807	104.140	6.179	6.486	-0.307	0.307	0.094
Sedili	1.932	104.115	7.661	7.904	-0.243	0.243	0.059
Kukup	1.325	103.443	5.601	6.500	-0.899	0.899	0.808
Geting	6.227	102.107	-7.580	-7.368	-0.212	0.212	0.045
						SUM	2.507
						RMSE	0.477

Evaluation of CNES-CLS22 : HAT

Station	**Lat**	**Long**	**UTIDE**	**CNES-CLS22**	**Δ**	**Δ ABS**	**ABS^2**
Klang	3.050	101.358	-0.418	-0.837	0.419	0.419	0.176
Keling	2.215	102.153	2.295	1.922	0.373	0.373	0.139
Langkawi	6.432	99.765	-14.193	-14.350	0.157	0.157	0.025
Lumut	4.240	100.613	-6.737	-7.014	0.277	0.277	0.077
Penang	5.422	100.347	-10.045	-10.264	0.219	0.219	0.048
Cendering	5.265	103.187	1.117	0.862	0.255	0.255	0.065
Kuantan	3.975	103.430	5.069	4.957	0.112	0.112	0.013
Tioman	2.807	104.140	9.912	9.559	0.353	0.353	0.125
Sedili	1.932	104.115	10.830	10.438	0.392	0.392	0.154
Kukup	1.325	103.443	9.406	8.477	0.929	0.929	0.863
Geting	6.227	102.107	-5.797	-6.169	0.372	0.372	0.138
						SUM	1.822
						RMSE	0.407

AUTHOR'S PROFILE



Afreena Nisha Mohd Zamri obtained her Bachelor in Surveying Science and Geomatics (Hons) and MSc in Science (Built Environment) in 2026 from Universiti Teknologi MARA, Perlis. Her MSc thesis involves the research on Integration of Land and Marine Vertical Datums for a Unified Height Reference System in Peninsular Malaysia. This research focusing on finding the optimum datasets and methodologies to address the discontinuity between land and marine vertical datums.

LIST OF JOURNAL

Zamri, A. N. M., Pa'suya, M. F., Din, A. H. M., Abbak, R. A., Ali, T. A. T., Talib, N., Azmin, N. S. H. N., & Othman, N. A. (2025). Airborne Gravity Data Reconstruction Strategies for Geoid Optimization in Peninsular Malaysia. *International Journal of Geoinformatics*, *21*(6), 90–104. https://doi.org/10.52939/ijg.v21i6.4239

Sibaruddin, H. I., Pa'suya, M. F., Talib, N., Md Din, A. H., Yong, C. Z., & Mohd Zamri, A. N. (2026). Comparative Accuracy Assessment of Shuttle Radar Topography Mission, NASA Digital Elevation Model, and Copernicus Digital Elevation Model in Perlis, Malaysia. *Built Environment Journal*, *23*(1), 215–229. https://doi.org/10.24191/bej.v23i1.8308

Othman, N. A., Pa'suya, M. F., Din, A. H. M., Abbak, R. A., Aziz, M. A. C., Nyoka, C. J., Azmin, N. S. H. N., & Zamri, A. N. M. (2026). Impact of Various Global Digital Elevation and Crustal Density Models on Accurate Topographic Correction for Geoid Modelling Over East Malaysia. *Pure and Applied Geophysics*. https://doi.org/10.1007/s00024-026-03999-w

CONFERENCE PROCEEDINGS

Zamri, A. N. M., Pa'suya, M. F., Din, A. H. M., Samad, A. M., Azmin, N. S. H. N., & Othman, N. A. (2024). Optimizing the Integration of Gravity Data Inputs for Geoid Modelling over Peninsular Malaysia. *2024 20th IEEE International Colloquium on Signal Processing and Its Applications, CSPA 2024 - Conference Proceedings*, 41–46. https://doi.org/10.1109/CSPA60979.2024.10525293

Azmin, N. S. H. N., Pa'Suya, M. F., Din, A. H. M., Talib, N., Othman, N. A., & Zamri, A. N. M. (2024). Development of Gravimetric Geoid over Peninsular Malaysia using the Most Recent Global Geopotential Model. *2024 20th IEEE International Colloquium on Signal Processing & Its Applications (CSPA)*, 47–52. https://doi.org/10.1109/CSPA60979.2024.10525401

Othman, N. A., Pa'suya, M. F., Din, A. H. M., Aziz, M. A. C., Azmin, N. S. H. N., & Zamri, A. N. M. (2024). Gravimetric Geoid Modeling for East Malaysia using the LSMSA Method. *2024 20th IEEE International Colloquium on Signal Processing and Its Applications, CSPA 2024 - Conference Proceedings*, 213–218. https://doi.org/10.1109/CSPA60979.2024.10525484